Project funded by the European Commission under the 6th (EC) RTD Framework Programme (2002- 2006) within the framework of the specific research and technological development programme "Integrating and strengthening the European Research Area"

Project UpWind

Contract No.: 019945 (SES6)

"Integrated Wind Turbine Design"

TEST RESULTS OF IN-PLANE MECHANICAL PROPERTIES FOR MODELING COMPLEX STRESS STATES

AUTHOR:	T. P. Philippidis
AFFILIATION:	University of Patras, Dept. of Mech. Engng & Aeronautics, Section of Applied Mechanics
ADDRESS:	P. O. Box 1401, Panepistimioupolis Rio, GR 265 04, Greece
TEL.:	+30 2610 969450, 997235
EMAIL:	philippidis@mech.upatras.gr
FURTHER AUTHORS:	E. N. Eliopoulos, K. Bacharoudis, I. Masmanidis, T. T. Assimakopoulou
REVIEWER:	
APPROVER:	

Document Information

DOCUMENT TYPE	Deliverable
DOCUMENT NAME:	Test results of in-plane mechanical properties for modeling complex stress states
REVISION:	0
REV.DATE:	
CLASSIFICATION:	R3: Restricted to WP3 members + PL
STATUS:	S3: Draft for comments

Abstract: Work described in this technical report was performed in the frame of Task 3.3 “Damage Tolerant Design Concept” of Work-Package WP3 “Rotor Structure and Materials” of the UPWIND project. 128 axial static tests were performed for characterization of in-plane mechanical properties of the Gl/ep UD UPWIND reference material. Not only the engineering constants necessary in design calculations but the entire stress-strain curves, especially the non-linear ones, in the various material anisotropy directions were monitored. They will be eventually implemented in the FADAS routine for laminate strength prediction under either static or cyclic loading. At least 25 tests for each one out of 10 mechanical properties were used to derive statistical characteristics, i.e. probability distributions and other descriptive statistics. These results will be valuable for reliability analyses performed in the same work-package. Finally, a comparative study of the statistical features of OPTIMAT and UPWIND UD materials was presented.

Table of Contents

STATUS, CONFIDENTIALITY AND ACCESSIBILITY										
Status				**Confidentiality**				**Accessibility**	
S0	Approved/Released			**R0**	General public			Private web site	
S1	Reviewed			**R1**	Restricted to project members			Public web site	
S2	Pending for review			**R2**	Restricted to European. Commission			Paper copy	
S3	Draft for commends	**X**		**R3**	Restricted to WP members + PL	**X**			
S4	Under preparation			**R4**	Restricted to Task members +WPL+PL				

PL: *Project leader* **WPL:** *Work package leader* **TL:** *Task leader*

1. Introduction

In this technical report, axial tests performed in the frame of WP 3.3 of UPWIND project were described. The purpose of the experimental work was the characterization of in-plane mechanical properties of the Gl/Ep UD reference material [1] of the UPWIND project. The geometry of coupons tested was the UPWIND R08 for axial tests along the fibres and in the transverse direction (R089) while the standard ISO 14129 $[\pm 45]_S$ geometry was used for in-plane shear characterization. In total, 128 static tests, 25 UD tensile and 25 UD compressive along the fibres, 25 UD tensile and 25 UD compressive in the transverse direction as well as 28 tensile axial tests on $[\pm 45]_S$ were conducted.

Static tests were performed for the determination of the elastic properties and strengths of the UD ply in the lamina principal plane. According to the test plan, 25 coupons were tested for each case to define the respective elastic property and static strength distribution characteristics. Test data were used for the determination of the tensile and compressive modulus of elasticity E_{1T}, E_{1C} parallel to the fibres and in the transverse direction E_{2T}, E_{2C}, major v_{12} and minor v_{21} Poisson ratios, in-plane shear modulus G_{12}, tensile X and compressive X' strength along the fibres as well as tensile Y and compressive Y' strength in the transverse direction, in-plane shear strength S.

A detailed statistical treatment for all mechanical property samples was performed by means of STATREL (RCP, GmbH) [2], including calculation of descriptive statistics, parameter estimation of three standard distribution functions, goodness-of-fit tests and theoretical CDF plots vs. experimental data. Finally, a comparison of the statistical features of OPTIMAT and UPWIND databases was presented.

2. Test coupons

Coupons of the R08 UPWIND geometry and the standard ISO 14129, designated as "I10" were used for the static tests, see Fig. 1 and 2. All coupons were made of four layers of the UD material and were trimmed with sandpaper to smooth appropriately the faces for efficient bonding of the strain gauges. WMC manufactured and delivered all coupons cut from various plates. Coupons were identified as 'XXYYzzz', with 'XX' denoting the plate, 'YY' the specimen number and 'zzz' the geometry.

Coupon dimensions for the I10 geometry, i.e. thickness and width, were measured using a digital caliper (0.01 mm precision), as received from WMC and prior to all surface treatments for strain gauge bonding. Three measurements were performed: one in the middle of the specimen and one near each tab. Cross sectional areas were calculated using the average of these three measurements. Dimensions for all coupons of the R08 geometry were provided by WMC. Several measurements were conducted at UP in a sample randomly selected yielding negligible differences. Actual sectional data for all tested coupons were presented in Tables 1 to 5.

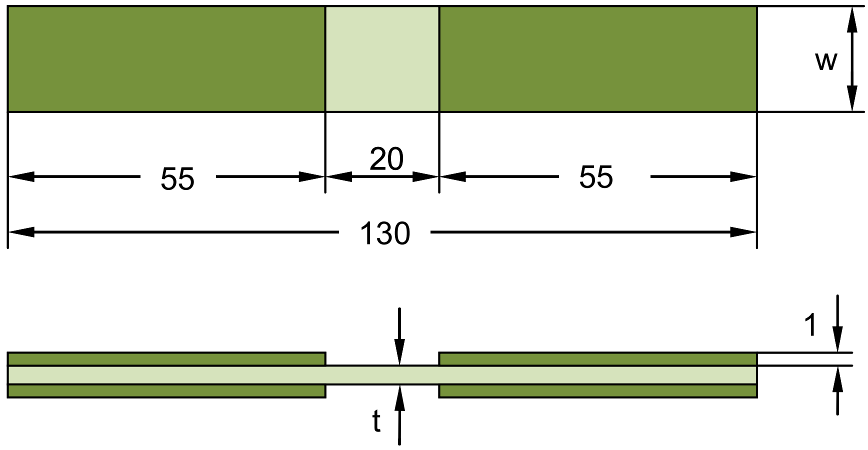

Fig. 1 R08 & R089 UPWIND coupon geometry

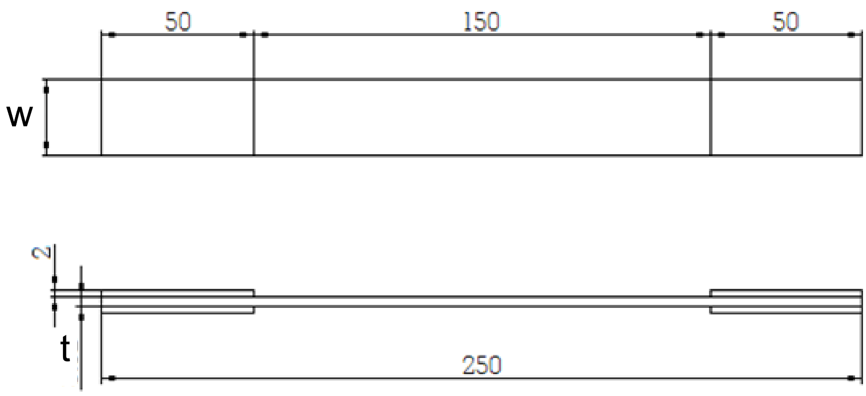

Fig. 2 The standard ISO 14129 $[\pm 45]_S$ test specimen

Table 1 Dimensions of the coupons tested in tension along the fibres

Coupon ID	w (mm)	t (mm)	area (mm^2)
BV03R08	20.02	3.02	60.36
BV09R08	20.02	2.99	59.76
BV10R08	20.05	2.98	59.65
BV11R08	19.93	2.99	59.49
BV13R08	20.86	2.98	62.16
BW01R08	19.64	2.91	57.05
BW05R08	19.90	2.91	57.91
BW07R08	19.96	2.88	57.39
BW11R08	19.85	2.88	57.17
BW03R08	19.83	2.92	57.80
BW09R08	20.01	2.88	57.63
BW15R08	19.96	2.89	57.58
BW17R08	19.98	2.86	57.14
BW19R08	20.00	2.88	57.50
BW21R08	20.04	2.89	57.92
BW22R08	19.94	2.88	57.33
BW23R08	20.04	2.86	57.31
BW25R08	20.07	2.87	57.60
BW27R08	20.03	2.89	57.79
BX20R08	20.08	2.96	59.44
BX24R08	20.15	2.90	58.44
BX26R08	20.13	2.93	58.98
BX28R08	20.13	2.93	58.98
BX30R08	20.09	2.91	58.36
BX18R08	20.09	3.03	60.77

Note: Dimensions were measured at WMC

Table 2 Dimensions of the coupons tested in compression along the fibres

Coupon ID	w (mm)	t (mm)	area (mm^2)
BV01R08	20.05	2.99	59.85
BV05R08	19.98	3.02	60.24
BV07R08	20.04	3.02	60.42
BV15R08	20.00	2.97	59.40
BV17R08	20.01	3.00	59.93
BV19R08	20.03	2.99	59.89
BV21R08	20.03	2.99	59.79
BV23R08	20.04	2.95	59.12
BV25R08	20.12	2.93	58.85
BV27R08	20.03	2.93	58.69
BW13R08	19.91	2.90	57.64
BX02R08	20.16	3.00	60.48
BX04R08	20.13	3.00	60.29
BX06R08	20.11	2.93	58.92
BX08R08	20.08	2.90	58.13
BX10R08	20.10	2.93	58.89
BX12R08	20.10	2.95	59.19
BX14R08	20.09	2.90	58.26
BX16R08	19.99	3.00	59.87
CB08R08	20.13	3.05	61.30
CB10R08	20.12	3.04	61.06
CB12R08	20.13	2.99	60.09
CB26R08	20.12	3.03	60.86
CB28R08	20.10	3.00	60.30
CB30R08	19.87	2.97	59.01

Note: Dimensions were measured at WMC

Table 3 Dimensions of the coupons tested in tension in the transverse to the fibres direction

Coupon ID	w (mm)	t (mm)	area (mm^2)
BJ27R089	19.92	3.02	60.16
BY07R089	20.10	3.02	60.70
BY08R089	20.09	3.02	60.67
BY09R089	20.14	3.02	60.72
BY10R089	20.06	3.02	60.58
BY23R089	20.07	3.01	60.31
BY24R089	20.10	3.00	60.30
BY25R089	20.06	3.00	60.08
BY27R089	20.09	2.97	59.57
BY21R089	20.03	3.03	60.59
BY26R089	20.10	2.99	60.00
CC01R089	19.89	3.01	59.77
CC02R089	19.92	3.01	59.96
CC04R089	20.05	3.00	60.05
CC05R089	20.09	2.98	59.77
CC07R089	20.05	2.97	59.45
CC08R089	20.09	2.97	59.57
CC11R089	20.13	2.94	59.08
CC12R089	19.95	2.94	58.65
CC03R089	20.00	3.00	60.00
CC09R089	20.09	2.96	59.37
CC13R089	19.99	2.92	58.37
CC15R089	19.98	3.05	60.94
CC16R089	19.96	3.04	60.68
CC17R089	20.05	3.06	61.25

Note: Dimensions were measured at WMC

Table 4 Dimensions of the coupons tested in compression in the transverse direction

Coupon ID	w (mm)	t (mm)	area (mm^2)
BJ26R089	19.94	3.02	60.22
BJ29R089	19.81	3.01	59.53
BY01R089	19.84	2.97	58.83
BY03R089	19.91	3.00	59.73
BY11R089	20.10	3.01	60.40
BY13R089	20.08	3.01	60.34
BY15R089	19.86	2.94	58.39
BY17R089	20.11	2.97	59.73
BY18R089	20.12	2.99	60.16
BY19R089	20.09	3.00	60.27
BZ01R089	20.03	2.86	57.19
BZ03R089	19.87	2.86	56.73
BZ05R089	20.06	2.87	57.47
BZ07R089	20.12	2.89	58.05
BZ08R089	20.04	2.88	57.72
BZ09R089	19.99	2.90	57.97
BZ11R089	20.01	2.90	57.93
BZ13R089	20.04	2.90	58.02
BZ14R089	19.94	2.86	56.93
BZ15R089	19.90	2.85	56.72
CC19R089	20.07	3.06	61.31
CC21R089	20.03	3.04	60.89
CC23R089	20.13	3.04	61.20
CC25R089	20.08	3.03	60.74
CC27R089	20.05	3.03	60.65

Note: Dimensions were measured at WMC

Table 5 Dimensions of the ISO 14129 [±45]$_S$ coupons tested in axial tension

Coupon ID	w (mm)	t (mm)	area (mm^2)
KH01I10	25.10	3.07	77.15
KH02I10	25.42	3.08	78.28
KH03I10	25.27	3.08	77.83
KH04I10	25.31	3.08	78.04
KH05I10	24.89	3.09	76.90
KH06I10	25.30	3.08	78.01
KH07I10	25.27	3.09	78.17
KH08I10	25.23	3.07	77.53
KH09I10	25.19	3.07	77.33
KH10I10	25.23	3.06	77.19
KH11I10	25.20	3.04	76.70
KJ01I10	25.19	3.02	76.08
KJ02I10	25.23	3.02	76.29
KJ03I10	25.23	3.03	76.35
KJ04I10	25.22	3.03	76.43
KJ05I10	25.24	3.04	76.73
KJ06I10	25.28	3.04	76.84
KJ07I10	25.22	3.04	76.75
KJ08I10	25.25	3.04	76.83
KJ09I10	25.25	3.04	76.84
KJ10I10	25.23	3.05	76.88
KK01I10	25.05	2.96	74.22
KK02I10	24.97	2.95	73.67
KK03I10	24.98	2.95	73.77
KK04I10	25.00	2.96	73.93
KK05I10	24.98	2.98	74.44
KK06I10	24.96	2.96	73.89
KK07I10	24.97	2.96	73.92

3. Experimental

3.1. Equipment

A MAYES DH 100S of 100kN capacity equipped with a 407 MTS controller and hydraulic MTS 647 wedge grips was used for the static tests, see Fig. 3. A rosette, consisting of two perpendicular strain gauges and a single strain gauge were placed back-to-back in all coupons used for the tensile tests. A single strain gauge was placed on both sides of all coupons tested in compression. For axial tests on R08 and R089 coupons, strains were measured using HBM 3/350LY11 single strain gauges and HBM 3/350XY11 rosette strain gauges with a nominal electrical resistance of 350 Ohms and gauge length of 3 mm. For the static tensile tests of the I10 coupons, HBM 6/350LY11 single strain gauges and HBM 6/350XY11 rosettes of 6 mm gauge length were used respectively. Strain gauge, load and displacement signals were acquired using an HBM Spider 8 data acquisition unit.

3.2. Testing procedure

Coupons were aligned in the grips of the test rig using the special metal guides of the wedges. At first, the coupon was mounted on the lower grips. Gripping pressure was set at 10 MPa for all tests in the fibre direction, either tensile or compressive, and at 5 MPa for all tests in the transverse direction and for the $[\pm45]_S$ coupons. Strain gauge readings were then zeroed and the upper grips were closed. Loading caused from gripping was removed to start the test from zero load. All tests on coupons of R08 geometry were performed under displacement control at a crosshead speed of 1 mm/min, resulting at an ISO comparable strain rate of 8.33 10^{-4} s^{-1}. The tests on the ISO 14129 standard coupons of I10 geometry as well as those on the R089 geometry, in tension and compression, were performed on the 25 kN setup of the test rig. Tensile tests for the I10 coupons were performed at a crosshead speed of 2 mm/min.

Fig. 3 Set-up for the static tests of R08 coupons

4. Test results and discussion

Concerning the I10 coupons, the axial normal stress, σ_x, was calculated as the ratio of the applied force, over the measured average cross sectional area of the coupons. The strain was measured using strain gauges. The shear stress, τ_{12}, was derived as $\sigma_x/2$ and the shear strain, γ_{12}, as (ε_x-ε_y). The Young modulus E_x was determined as the slope of the linear fit of the axial stress vs. axial strain curve, for strain between 500 and 2500 με, according to EN ISO 527-5:1997 [3]. The same holds for the major Poisson ratio, v_{xy}, derived from the transverse strain vs. axial strain curve. The shear modulus, G_{12}, was determined from the slope of the linear fit of the shear stress vs. shear strain curve, for shear strain between 1000 and 5000 με, in accordance with ISO 14129:1997(E) [4].

In a similar way for the R08 and R089 coupons, normal axial stress was calculated as the ratio of the applied force over the cross sectional area of the coupon while strain was measured directly using the strain gauges. Stress-strain curves for all coupons tested were presented in the appendix. Axial strain shown in these figures is the average of axial strain values measured by strain gauges bonded on both sides of the coupon. Elastic moduli E_1 and E_2, parallel and transverse to the fibres respectively, were determined by linear interpolation of the axial stress vs. axial strain curves. Major and minor Poisson ratios v_{12} and v_{21}, were determined by linear interpolation of the transverse vs. axial strain curves. For these calculations axial strains were considered between 500 and 2500 με [3]. For the coupons tested in compression, the bending strain, ε_b was calculated as the absolute ratio of the difference of the two axial gauge readings over their sum [5].

$$\varepsilon_{\mathrm{b}} = \left| \frac{\varepsilon_{x_b} - \varepsilon_{x_a}}{\varepsilon_{x_b} + \varepsilon_{x_a}} \right| \leq 0.1 \tag{1}$$

It was considered that the coupon does not fail in buckling if the bending strain value was less than 0.1 at 80% of the Ultimate Compressive Stress (UCS).

Since strain in all tests was measured using two axial strain gauges, Young modulus values were calculated using the average of the two axial measurements, provided that no significant discrepancies were observed. Poisson ratios and G_{12} values were calculated using solely the strain-gauge rosette readings. Calculated values for E-modulus, Poisson ratio, stress and strain at failure were presented in Tables 6-10, where average values and coefficients of variation (COV) of the sample set were also shown.

Graphs of stress-strain curves for all coupons were presented in the Appendix. Axial strain shown in the figures is the average of the axial strain values measured with the two axial strain gauges mounted on each side of the coupon. Characteristic photographs of failed coupons were also presented for every loading case highlighting the various failure modes.

Table 6 Tensile test results for the UPWIND Gl/Ep UD parallel to the fibres

Coupon ID	Maximum force F_{max} (kN)	Tensile strength X (MPa)	E_1 (GPa)	v_{12}	Strain at failure ε_{1f} (x10[6])
BV03R08[1]	52.692	872.96	37.85	0.2288	-
BV09R08[1]	54.704	915.40	39.23	0.2501	-
BV10R08[2,4]	53.904	903.69	37.89	-	-
BV11R08[1]	54.76	920.47	38.14	0.261	-
BV13R08[3]	51.632	830.59	36.06	0.2418	24456.60
BW01R08[4]	54.696	958.67	44.50	0.2953	22825.92
BW05R08[1]	52.62	908.67	38.93	0.2762	-
BW07R08[1]	56.028	976.35	40.68	0.2326	-
BW11R08[3]	52.38	916.25	38.44	0.2399	25498.75
BW03R08[3]	50.292	870.04	38.84	0.2656	24062.09
BW09R08[1]	55.776	967.85	41.00	0.2988	-
BW15R08[3]	57.152	992.49	44.16	0.2963	24612.30
BW17R08[3]	51.904	908.32	41.04	0.2545	24008.60
BW19R08[4,5]	54.044	939.90	40.04	0.2456	22882.56
BW21R08[1]	56.768	980.18	40.98	0.2933	-
BW22R08[1]	56.216	980.61	41.59	0.2762	-
BW23R08[1]	52.736	920.12	40.44	0.2783	-
BW25R08[3]	53.916	936.03	40.60	0.2386	24363.94
BW27R08[3]	52.796	913.64	40.08	0.2243	23660.90
BX20R08[1]	54.928	924.14	37.48	0.2336	-
BX24R08[1]	53.276	911.71	40.46	0.2687	-
BX26R08[1]	56.684	961.06	39.49	0.2206	-
BX28R08[4]	52.256	885.98	39.76	0.2602	21693.12
BX30R08[1]	54.116	927.26	40.54	0.2732	-
BX18R08[3,6]	52.8	868.82	39.31	0.3046	23245.37
Mean	53.96	923.65	39.90	0.26	23755.47
COV	0.033	0.043	0.047	0.098	0.044

[1] Both axial strain gauges failed before maximum load was reached
[2] No axial strain gauge of rosette reading
[3] Axial strain gauge of rosette failed before maximum load was reached
[4] Single strain gauge failed before maximum load was reached
[5] Coupon loaded until about 30 kN and unloaded due to a DAQ problem. Test repeated
[6] Coupon loaded until about 20 kN and unloaded due to a servo-valve problem. Test repeated

Table 7 Compressive test results for the UPWIND Gl/Ep UD parallel to the fibres

Coupon ID	Maximum force F_{max} (kN)	Compressive strength X' (MPa)	E_{1C} (GPa)	Strain at failure ε_{1f} (x10^6)
BV01R08	-28.288	-472.65	39.99	-12443.70
BV05R08	-27.596	-458.10	37.66	-12665.79
BV07R08	-30.976	-512.67	37.81	-14672.24
BV15R08	-29.652	-499.19	38.79	-13308.66
BV17R08	-28.796	-480.49	37.39	-13139.58
BV19R08	-27.528	-459.64	37.49	-12391.64
BV21R08	-30.496	-510.06	39.35	-13494.45
BV23R08	-28.716	-485.74	38.93	-12838.21
BV25R08[1]	-31.208	-530.29	37.84	-14824.12
BV27R08	-27.28	-464.83	37.59	-12832.96
BW13R08	-24.524	-425.47	39.50	-11151.76
BX02R08	-29.516	-488.03	38.86	-13405.13
BX04R08[1]	-29.324	-486.39	40.23	-11515.22
BX06R08[1]	-29.372	-498.49	39.63	-13431.40
BX08R08	-28.832	-495.98	40.00	-12758.45
BX10R08	-28.312	-480.74	38.81	-12957.61
BX12R08	-28.784	-486.26	38.35	-13316.30
BX14R08	-29.728	-510.26	39.04	-14316.42
BX16R08	-31.612	-528.01	41.24	-13316.78
CB08R08	-30.22	-493.02	38.78	-13238.93
CB10R08[1]	-29.16	-477.53	37.46	-13633.43
CB12R08	-28.396	-472.57	38.13	-12993.91
CB26R08	-27.016	-443.88	37.62	-12492.42
CB28R08	-28.776	-477.21	38.32	-12884.06
CB30R08	-28.328	-480.02	40.75	-12227.34
Mean	-28.73	-482.14	38.78	-12992.68
COV	-0.053	-0.049	0.028	-0.056

[1] Not used in mean values evaluation because of high bending strain

Table 8 Tensile test results for the UPWIND Gl/Ep UD transversely to the fibres

Coupon ID	Maximum force F_{max} (kN)	Tensile strength Y (MPa)	E_2 (GPa)	ν_{21}	Strain at failure ε_{2f} (x10^6)
BJ27R089[1]	5.089	84.59	12.98	0.0804	-
BY07R089[2]	5.446	89.72	12.73	0.0676	18482.63
BY08R089[2]	4.799	79.10	12.32	0.0801	17915.22
BY09R089	6.222	102.47	13.40	0.0772	20759.31
BY10R089[3,4]	5.346	88.25	12.65	0.1373	19097.28
BY23R089[1,4]	5.539	91.84	13.82	0.0902	-
BY24R089[4]	4.97	82.42	14.59	0.1057	15922.82
BY25R089[4]	5.325	88.63	13.51	0.1058	19530.82
BY27R089[4]	5.487	92.11	13.75	0.124	17892.12
BY21R089[2]	5.202	85.85	13.17	0.0877	15723.94
BY26R089[2,4]	4.994	83.24	13.80	0.0957	17715.58
CC01R089[5]	5.752	96.24	13.69	0.074	23490.24
CC02R089[6]	4.417	73.67	12.77	-	16864.49
CC04R089	5.274	87.83	12.47	0.0645	18556.69
CC05R089[2]	4.582	76.66	12.53	0.0739	14618.75
CC07R089[5]	5.156	86.73	13.26	0.0765	18301.44
CC08R089	4.749	79.73	13.27	0.083	16874.09
CC11R089[2]	4.988	84.43	13.38	0.0758	16916.06
CC12R089[1]	5.437	92.70	13.72	0.0838	-
CC03R089	4.472	74.53	12.58	0.095	15990.93
CC09R089	5.315	89.53	13.88	0.1088	18869.11
CC13R089	5.124	87.78	12.42	0.0556	17409.98
CC15R089[2]	4.879	80.06	12.67	0.0804	16787.11
CC16R089[2]	5.359	88.32	13.45	0.0841	18468.30
CC17R089[2]	4.762	77.74	12.91	0.0868	15379.11
Mean	5.15	85.77	13.19	0.08	17798.46
COV	0.079	0.080	0.044	0.150	0.110

[1] Both axial strain gauges failed before maximum load was reached
[2] Axial strain gauge of rosette failed before maximum load was reached
[3] No single strain gauge reading
[4] Invalid Poisson's ratio measurement caused by irregularities in ε_1-ε_2 graph. Not used for the evaluation of the average Poisson's ratio
[5] Single strain gauge failed before maximum load was reached
[6] Transverse strain gauge failed

Table 9 Compressive test results for the UPWIND Gl/Ep UD transversely to the fibres

Coupon ID	Maximum force F_{max} (kN)	Compressive strength Y' (MPa)	E_{2C} (GPa)	Strain at failure ε_{2f} (x10^6)
BJ26R089	-9.096	-151.05	14.54	-14308.78
BJ29R089	-10.073	-169.21	14.38	-17290.99
BY01R089[1]	-9.317	-158.38	14.66	-12811.46
BY03R089[2]	-9.175	-153.61	13.25	-13187.34
BY11R089	-9.198	-152.28	13.88	-17090.39
BY13R089	-9.473	-156.99	14.42	-15192.84
BY15R089	-9.15	-156.71	14.33	-15773.13
BY17R089	-9.047	-151.47	14.29	-13781.97
BY18R089	-8.712	-144.82	14.14	-13675.46
BY19R089	-8.959	-148.65	14.72	-13348.78
BZ01R089	-8.482	-148.32	15.24	-13424.24
BZ03R089[3]	-7.814	-137.74	14.69	-12089.31
BZ05R089	-8.383	-145.86	14.39	-12960.96
BZ07R089[4]	-8.008	-137.96	14.18	-
BZ08R089	-8.007	-138.73	14.52	-12342.93
BZ09R089	-8.002	-138.03	14.55	-12482.87
BZ11R089	-8.099	-139.81	14.46	-12455.64
BZ13R089	-8.153	-140.53	14.28	-13255.64
BZ14R089	-8.803	-154.63	14.42	-14491.70
BZ15R089	-8.539	-150.56	14.17	-15074.39
CC19R089	-8.715	-142.14	13.13	-14769.67
CC21R089	-8.739	-143.52	13.68	-13905.67
CC23R089	-8.499	-138.88	13.98	-13384.12
CC25R089	-8.853	-145.75	13.75	-14451.58
CC27R089	-8.513	-140.36	13.65	-13047.88
Mean	-8.73	-147.49	14.24	-14107.43
COV	-0.060	-0.053	0.032	-0.099

[1] One strain gauge damaged. Not used in mean values evaluation
[2] Coupon was loaded until about -8.9 kN and unloaded due to a servo-valve problem. Test repeated. Not used in mean values evaluation
[3] Not used in mean values evaluation because of high bending strain
[4] No reading from one strain gauge. Not used in mean values evaluation. The other strain gauge failed before maximum force was applied

Table 10 Tensile test results for the UPWIND Gl/Ep ISO 14129 $[\pm 45]_S$ coupons

Coupon ID	F_{max} **[kN]**	**UTS [MPa]**	τ_{max} **[MPa]**	τ_{max} **at** γ_{12}**=5% [MPa]**	G_{12} **[GPa]**	E_x **[GPa]**	ν_{xy}
KH01I10	8.74	113.28	56.64	45.72	3.283	11.03	0.570
KH02I10[3]	9.799	125.18	62.59	45.05	3.53	12.04	0.570
KH03I10[4a]	9.35	120.14	60.07	44.02	3.465	11.84	0.602
KH04I10	9.187	117.72	58.86	42.92	3.478	11.52	0.553
KH05I10	8.659	112.60	56.30	42.11	3.537	11.88	0.563
KH06I10	8.863	113.62	56.81	41.78	3.469	11.83	0.609
KH07I10	8.625	110.34	55.17	42.19	3.479	11.65	0.514
KH08I10	8.609	111.04	55.52	43.09	3.602	11.97	0.576
KH09I10[1]	8.904	115.14	57.57	46.96	3.526	11.54	0.518
KH10I10	8.669	112.30	56.15	43.14	3.527	12.25	0.571
KH11I10	8.892	115.92	57.96	42.78	3.501	11.5	0.547
KJ01I10	9.124	119.92	59.96	45.91	3.619	11.88	0.533
KJ02I10	9.603	125.88	62.94	44.05	3.573	11.73	0.508
KJ03I10	9.477	124.12	62.06	43.85	3.475	12.03	0.548
KJ04I10[1,4b]	9.248	121.00	60.50	43.77	3.512	12.5	0.590
KJ05I10	9.053	117.98	58.99	41.89	3.548	12.23	0.577
KJ06I10[2]	8.998	117.10	58.55	42.79	3.651	12.44	0.589
KJ07I10	9.302	121.20	60.60	42.79	3.552	11.92	0.541
KJ08I10	9.172	119.38	59.69	43.93	3.569	11.84	0.570
KJ09I10	9.414	122.50	61.25	42.9	3.421	11.47	0.576
KJ10I10	9.656	125.60	62.80	44.66	3.531	11.77	0.523
KK01I10	8.888	119.74	59.87	43.81	3.599	11.94	0.531
KK02I10[4c]	9.237	125.38	62.69	44.34	3.63	12.54	0.643
KK03I10	9.03	122.40	61.20	44.23	3.663	12.48	0.565
KK04I10	9.009	121.86	60.93	43.33	3.587	12.12	0.565
KK05I10	8.753	117.58	58.79	42.63	3.486	11.86	0.556
KK06I10	8.387	113.50	56.75	42.05	3.589	12.21	0.481
KK07I10	8.515	115.20	57.60	41.57	3.605	12.18	0.584
Mean	9.041	118.486	59.243	43.509	3.535	11.935	0.559
COV	0.039	0.039	0.039	0.030	0.022	0.029	0.060

[1]The transverse gauge of the rosette was damaged (above a load value)
[2]The axial gauge of the rosette was short-circuited (above a load value)
[3]The axial gauge was short-circuited (above a load value)
[4]Some problems with the DAQ resulted in loss of some measurements during the experiment. The acquisition was restarted. The load in the second part of the acquisition was approximated by adding values read on the display of the controller the moment of collapse: a) 8.0 kN, b) 7.8 kN, c) 9.1 kN

5. Statistical Analysis of test data

A detailed statistical treatment for all mechanical property samples was performed by using STATREL (RCP, GmbH) [2]. The analysis consists of calculations for descriptive statistics, parameter estimation of three standard distribution functions, goodness-of-fit tests and theoretical CDF plots vs. experimental data. Finally, a comparison of the statistical features of OPTIMAT and UPWIND databases was presented. 12 samples from the following stochastic variables were considered: E_{1T}, E_{1C}, E_{2T}, E_{2C}, v_{12}, v_{21}, X_T, X_C, Y_T, Y_C, S, and G_{12}. For the in-plane shear properties two additional samples from tests performed at WMC [6] were analyzed. To avoid any confusion, shear data S, and G_{12} from Table 10 of the present report, will be referred to as the ISO data while those of ref. [6] as VARIOUS (they were derived using 5 different test methods).

5.1. Descriptive statistics

Some data were removed from the samples of Tables 7 to 9 due to various undesired situations in the process of the experiments, e.g. strain gauge failures, servo-valve problems etc.. In Table 11 below the footnote numbers from each separate table that were excluded were shown.

Table 11 Footnote cases for which the data were not considered in the statistical analysis

Sample	Footnote #	Sample	Footnote #
$\mathbf{E_{1T}}$	2, 5, 6	$\mathbf{v_{21}}$	3, 4, 6,
$\mathbf{E_{1C}}$	1	$\mathbf{X_T}$	5, 6
$\mathbf{E_{2T}}$	3	$\mathbf{X_C}$	1
$\mathbf{E_{2C}}$	1, 2, 3, 4	$\mathbf{Y_T}$	-
$\mathbf{v_{12}}$	2, 5, 6	$\mathbf{Y_C}$	2, 3

For completeness, the data sets considered are given in the following tables. The data samples for S, and G_{12} from [6] were also shown while those for the ISO data were not repeated here; all entries of Table 10 were used.

Table 12 Data for E_{1T}, E_{1C} and v_{12}

Coupon ID	**E_{1T} [GPa]**	**Coupon ID**	**E_{1C} [GPa]**	**Coupon ID**	**v_{12}**
BV03R08	37.85	BV01R08	39.99	BV03R08	0.2288
BV09R08	39.23	BV05R08	37.66	BV09R08	0.2501
BV11R08	38.14	BV07R08	37.81	BV11R08	0.261
BV13R08	36.06	BV15R08	38.79	BV13R08	0.2418
BW01R08	44.50	BV17R08	37.39	BW01R08	0.2953
BW05R08	38.93	BV19R08	37.49	BW05R08	0.2762
BW07R08	40.68	BV21R08	39.35	BW07R08	0.2326
BW11R08	38.44	BV23R08	38.93	BW11R08	0.2399
BW03R08	38.84	BV27R08	37.59	BW03R08	0.2656
BW09R08	41.00	BW13R08	39.50	BW09R08	0.2988
BW15R08	44.16	BX02R08	38.86	BW15R08	0.2963
BW17R08	41.04	BX08R08	40.00	BW17R08	0.2545
BW21R08	40.98	BX10R08	38.81	BW21R08	0.2933
BW22R08	41.59	BX12R08	38.35	BW22R08	0.2762
BW23R08	40.44	BX14R08	39.04	BW23R08	0.2783
BW25R08	40.60	BX16R08	41.24	BW25R08	0.2386
BW27R08	40.08	CB08R08	38.78	BW27R08	0.2243
BX20R08	37.48	CB12R08	38.13	BX20R08	0.2336
BX24R08	40.46	CB26R08	37.62	BX24R08	0.2687
BX26R08	39.49	CB28R08	38.32	BX26R08	0.2206
BX28R08	39.76	CB30R08	40.75	BX28R08	0.2602
BX30R08	40.54			BX30R08	0.2732

Table 13 Data for E_{2T}, E_{2C} and v_{21}

Coupon ID	**E_{2T} [GPa]**	**Coupon ID**	**E_{2C} [GPa]**	**Coupon ID**	**v_{21}**
BJ27R089	12.98	BJ26R089	14.54	BJ27R089	0.0804
BY07R089	12.73	BJ29R089	14.38	BY07R089	0.0676
BY08R089	12.32	BY11R089	13.88	BY08R089	0.0801
BY09R089	13.40	BY13R089	14.42	BY09R089	0.0772
BY23R089	13.82	BY15R089	14.33	BY21R089	0.0877
BY24R089	14.59	BY17R089	14.29	CC01R089	0.074
BY25R089	13.51	BY18R089	14.14	CC04R089	0.0645
BY27R089	13.75	BY19R089	14.72	CC05R089	0.0739
BY21R089	13.17	BZ01R089	15.24	CC07R089	0.0765
BY26R089	13.80	BZ05R089	14.39	CC08R089	0.083
CC01R089	13.69	BZ08R089	14.52	CC11R089	0.0758
CC02R089	12.77	BZ09R089	14.55	CC12R089	0.0838
CC04R089	12.47	BZ11R089	14.46	CC03R089	0.095
CC05R089	12.53	BZ13R089	14.28	CC09R089	0.1088
CC07R089	13.26	BZ14R089	14.42	CC13R089	0.0556
CC08R089	13.27	BZ15R089	14.17	CC15R089	0.0804
CC11R089	13.38	CC19R089	13.13	CC16R089	0.0841
CC12R089	13.72	CC21R089	13.68	CC17R089	0.0868
CC03R089	12.58	CC23R089	13.98		
CC09R089	13.88	CC25R089	13.75		
CC13R089	12.42	CC27R089	13.65		
CC15R089	12.67				
CC16R089	13.45				
CC17R089	12.91				

Table 14 Data for X_T, X_C, Y_T and Y_C

Coupon ID	**X_T [MPa]**	**Coupon ID**	**X_C [MPa]**	**Coupon ID**	**Y_T [MPa]**
BV03R08	872.96	BV01R08	-472.65	BJ27R089	84.59
BV09R08	915.40	BV05R08	-458.10	BY07R089	89.72
BV10R08	903.69	BV07R08	-512.67	BY08R089	79.10
BV11R08	920.47	BV15R08	-499.19	BY09R089	102.47
BV13R08	830.59	BV17R08	-480.49	BY10R089	88.25
BW01R08	958.67	BV19R08	-459.64	BY23R089	91.84
BW05R08	908.67	BV21R08	-510.06	BY24R089	82.42
BW07R08	976.35	BV23R08	-485.74	BY25R089	88.63
BW11R08	916.25	BV27R08	-464.83	BY27R089	92.11
BW03R08	870.04	BW13R08	-425.47	BY21R089	85.85
BW09R08	967.85	BX02R08	-488.03	BY26R089	83.24
BW15R08	992.49	BX08R08	-495.98	CC01R089	96.24
BW17R08	908.32	BX10R08	-480.74	CC02R089	73.67
BW21R08	980.18	BX12R08	-486.26	CC04R089	87.83
BW22R08	980.61	BX14R08	-510.26	CC05R089	76.66
BW23R08	920.12	BX16R08	-528.01	CC07R089	86.73
BW25R08	936.03	CB08R08	-493.02	CC08R089	79.73
BW27R08	913.64	CB12R08	-472.57	CC11R089	84.43
BX20R08	924.14	CB26R08	-443.88	CC12R089	92.70
BX24R08	911.71	CB28R08	-477.21	CC03R089	74.53
BX26R08	961.06	CB30R08	-480.02	CC09R089	89.53
BX28R08	885.98			CC13R089	87.78
BX30R08	927.26			CC15R089	80.06
				CC16R089	88.32
				CC17R089	77.74

Coupon ID	**Y_C [MPa]**
BJ26R089	-151.05
BJ29R089	-169.21
BY01R089	-158.38
BY11R089	-152.28
BY13R089	-156.99
BY15R089	-156.71
BY17R089	-151.47
BY18R089	-144.82
BY19R089	-148.65
BZ01R089	-148.32
BZ05R089	-145.86
BZ07R089	-137.96
BZ08R089	-138.73
BZ09R089	-138.03
BZ11R089	-139.81
BZ13R089	-140.53
BZ14R089	-154.63
BZ15R089	-150.56
CC19R089	-142.14
CC21R089	-143.52
CC23R089	-138.88
CC25R089	-145.75
CC27R089	-140.36

Table 15 Data for S, G_{12} (VARIOUS) [6]

S [MPa]		**G_{12}** [GPa]	
76.73	71.23	4.76	3.42
78.57	72.66	4.20	3.42
80.79	63.74	4.18	3.24
78.28	62.60	4.28	3.51
78.38	64.46	3.91	3.45
76.19	39.27	3.41	3.64
77.91	39.94	4.15	3.47
75.76	43.13	3.97	3.21
73.80	42.18	3.59	3.78
74.85	41.96	4.22	3.62
78.00	43.66	3.50	3.28
76.10	66.24	4.25	3.07
67.50	64.84	3.32	3.03
63.02	54.78	3.60	3.56
66.23	65.32	3.25	3.51
66.46	61.29	3.56	2.99
63.49	52.39	3.90	3.27
54.09	56.74	3.13	3.34
58.10	58.18	4.01	
54.72	54.35	3.05	
55.58		3.32	
62.73		2.46	
55.92		2.85	
62.60		3.47	
74.44		3.51	

Definitions and notation used for the descriptive statistics were presented in Table 16. Results were displayed in Tables 17 to 21.

Table 16 Definitions and notation for the descriptive statistics [2]

Valid observations	n
Minimum	$\hat{x}_1 = \min\{x_i\}$
Maximum	$\hat{x}_n = \max\{x_i\}$
Range	$d_n = \left\lvert \hat{x}_1 - \hat{x}_n \right\rvert$
Median	$\hat{x} = H^{-1}(p = 0.50) \quad , where\ H(\hat{x}_i) = \frac{i}{n+1}$
Arithmetic mean	$\bar{x} = \frac{\sum_{i=1}^{n} x_i}{n}$
Geometric mean	$\tilde{x} = \left(\prod_{i=1}^{n} x_i \right)^{1/n}$
Mean square	$s'^2 = \hat{\mu}_2 = \frac{1}{n} \sum_{i=1}^{n} (x_i - \bar{x})^2$
Variance	$s^2 = \frac{1}{n-1} \sum_{i=1}^{n} (x_i - \bar{x})^2$
Stand. Deviation	$s = \sqrt{s^2}$
Coef. of variation	$v = s / \bar{x}$
Third moment	$\hat{\mu}_3 = \varepsilon = \frac{1}{n} \sum_{i=1}^{n} (x_i - \bar{x})^3$
Stand. skewness	$\varepsilon' = \varepsilon / \left(\sqrt{\hat{\mu}_2} \right)^3$
Fourth moment	$\hat{\mu}_4 = \gamma = \frac{1}{n} \sum_{i=1}^{n} (x_i - \bar{x})^4$
Stand. Kurtosis	$\gamma' = \gamma / \left(\sqrt{\hat{\mu}_2} \right)^4$
Variance of mean	$s_{\bar{x}}^2 = \hat{\mu}_2 / n$
Var. of variance	$s_{s^2}^2 = \left(\hat{\mu}_4 - \hat{\mu}_2^2 \right) / n$

Table 17 Descriptive statistics for E_{1T}, E_{1C} and v_{12}

Sample	E_{1T}	E_{1C}	v_{12}
Valid observations	22	21	22
Minimum	36.06	37.39	0.2206
Maximum	44.5	41.24	0.2988
Range	8.44	3.85	0.782e-1
Median	40.260	38.79	0.2606
Arithmetic mean	40.013	38.781	0.25945
Geometric mean	39.968	38.767	0.25832
Mean square	3.6563	1.1047	0.58559e-3
Variance	3.8304	1.1599	0.61348e-3
Stand. Deviation	1.9571	1.077	0.24768e-1
Coef. of variation	0.48912e-1	0.27771e-1	0.95465e-1
Third moment	3.0531	0.75171	0.11406e-5
Stand. Skewness	0.43669	0.64745	0.8049e-1
Fourth moment	47.274	3.3046	0.61946e-6
Stand. Kurtosis	3.5362	2.708	1.8064
Variance of mean	0.16619	0.52603e-1	0.26618e-4
Var. of variance	86.477	0.23045	0.15554e-7

Table 18 Descriptive statistics for E_{2T}, E_{2C} and v_{21}

Sample	E_{2T}	E_{2C}	v_{21}
Valid observations	24	21	18
Minimum	12.320	13.13	0.556e-1
Maximum	14.590	15.24	0.1088
Range	2.27	2.11	0.532e-1
Median	13.265	14.33	0.8025e-1
Arithmetic mean	13.211	14.234	0.79733e-1
Geometric mean	13.199	14.228	0.78932e-1
Mean square	0.32323	0.19084	0.12775e-3
Variance	0.33728	0.20039	0.13527e-3
Stand. Deviation	0.58076	0.44764	0.11631e-1
Coef. of variation	0.43959e-1	0.31448e-1	0.14587
Third moment	0.51065e-1	-0.30688e-1	0.51587e-6
Stand. Skewness	0.27788	-0.36809	0.35725
Fourth moment	0.25732	0.13729	0.66265e-7
Stand. Kurtosis	2.4629	3.7696	4.06
Variance of mean	0.13468e-1	0.90878e-2	0.70978e-5
Var. of variance	0.181e-3	0.13655e-3	0.90579e-9

Table 19 Descriptive statistics for X_T, X_C, Y_T and Y_C

Sample	X_T	X_C	Y_T	Y_C
Valid observations	23	21	25	23
Minimum	830.59	425.47	73.67	137.96
Maximum	992.49	528.01	102.47	169.21
Range	161.9	102.54	28.8	31.250
Median	920.12	480.74	86.73	145.86
Arithmetic mean	925.33	482.13	85.767	147.59
Geometric mean	925.49	481.56	85.505	147.39
Mean square	1539.4	549.8	45.119	63.996
Variance	1609.4	577.29	46.999	64.814
Stand. Deviation	40.117	24.027	6.8556	8.0507
Coef. of variation	0.43355e-1	0.4983e-1	0.7993e-1	0.54547e-1
Third moment	-13859	-4378.8	63.542	388.35
Stand. Skewness	-0.22946	-0.33966	0.20967	0.79557
Fourth moment	0.66056e7	0.9436e6	5948.4	12567
Stand. Kurtosis	2.7874	3.1218	2.922	3.2696
Variance of mean	66.931	26.181	1.8047	2.6955
Var. of variance	0.18963e3	0.42359e11	0.1393e7	0.6798e7

Table 20 Descriptive statistics for S and G_{12} (VARIOUS)

Sample	S	G_{12}
Valid observations	45	43
Minimum	39.27	2.46
Maximum	80.79	4.76
Range	41.52	2.3
Median	63.74	3.5
Arithmetic mean	63.316	3.5502
Geometric mean	62.143	3.5229
Mean square	136	0.19607
Variance	139.10	0.20074
Stand. Deviation	11.794	0.44804
Coef. of variation	0.18627	0.1262
Third moment	-692.06	0.31832e-1
Stand. Skewness	-0.43633	0.36665
Fourth moment	42511	0.12709
Stand. Kurtosis	2.2982	3.3060
Variance of mean	3.0223	0.45597e-2
Var. of variance	0.39903e8	0.11065e-3

Table 21 Descriptive statistics for S (τ_{max} at γ_{12}=50000 με) and G_{12} (ISO)

Sample	S	G_{12}
Valid observations	28	28
Minimum	41.57	3.283
Maximum	46.96	3.663
Range	5.39	0.38
Median	43.235	3.534
Arithmetic mean	43.509	3.536
Geometric mean	43.490	3.5351
Mean square	1.6812	0.0060027
Variance	1.7435	0.006225
Stand. Deviation	1.3204	0.078899
Coef. of variation	0.030348	0.022313
Third moment	1.6101	-0.00046197
Stand. Skewness	0.7386	-0.99334
Fourth moment	8.94	0.00017841
Stand. Kurtosis	3.1629	4.9513
Variance of mean	0.060044	0.00021438
Var. of variance	1.8818	0.12115e-5

5.2. Parameter estimation–Goodness of fit tests-CDF plots

Definitions and notation used for parameter estimation of three standard distribution functions was presented in Table 22. Two methods of parameter estimation, i.e. the method of moments and the maximum likelihood estimation were used. Also, two tests were considered for the adequacy of the fitted distributions to the data, namely Smirnov-Kolmogorov (S-K) and Anderson-Darling (A-D). As it can be seen in the respective tables, all three distributions were accepted (Non Rejected, NR) to represent the data of every sample. Results were displayed in Tables 23 to 50. All goodness of fit tests were performed at a significance level of 0.05. The plots of probability distribution (CDF) compared with the experimental data (empirical distribution) for the different distributions were those for which the test distributions indicated better fits. The italic format in the entries of Tables 23-50 correspond to the distributions plotted in the graphs and the bold and italic format of the same tables corresponds to the optimum distribution.

Table 22 Definitions and notation for standard distribution functions [5]

Name	Density/Distribution Function	Range	Mean	Standard Deviation
Normal	$f_x(x)=\frac{1}{\sqrt{2\pi}\sigma}\exp\left[-\frac{1}{2}\left(\frac{x-m}{\sigma}\right)^2\right]$ $=\frac{1}{\sigma}\varphi\left(\frac{x-m}{\sigma}\right)$ $F_x(x)=\Phi\left(\frac{x-m}{\sigma}\right)$	$-\infty < x < +\infty$	m	σ
Lognormal	$f_x(x)=\frac{1}{x\delta\sqrt{2\pi}}\exp\left[-\frac{1}{2}\left(\frac{\ln(x/\xi)}{\delta}\right)^2\right]$ $=\frac{1}{x\delta}\varphi\left(\frac{\ln(x/\xi)}{\delta}\right)$ $F_x(x)=\Phi\left(\frac{\ln(x/\xi)}{\delta}\right)$	$0 \le x < +\infty$	$\xi e^{\frac{\delta^2}{2}}$	$\xi e^{\frac{\delta^2}{2}}\sqrt{e^{\frac{\delta^2}{2}}-1}$
Weibull	$f_x(x)=\frac{k}{(w-\tau)}\left(\frac{x-\tau}{w-\tau}\right)^{k-1}\exp\left[-\left(\frac{x-\tau}{w-\tau}\right)^k\right]$ $F_x(x)=1-\exp\left[-\left(\frac{x-\tau}{w-\tau}\right)^k\right]$	$\tau \le x < +\infty$	m_w	$s.d._w$*

$$m_w=(w-\tau)\Gamma\left(1+\frac{1}{k}\right)+\tau$$

$$s.d._w=(w-\tau)\sqrt{\Gamma\left(1+\frac{2}{k}\right)-\Gamma^2\left(1+\frac{1}{k}\right)}$$

Sample E_{1T}

Table 23 Values of the estimated parameters for different distributions

	Method of Moments (MM)			Maximum Likelihood (ML) Or ML-opt		
Normal (m,σ)	40.0132	1.95714	-	*40.0132*	*1.95714*	---
Lognormal(ξ,δ)	39.9654	0.488831e-1	-	***39.968***	***0.474456e-1***	**---**
Weibull (w,κ,τ)	*40.8778*	*25.5195*	*0*	40.9564	19.8612	0

Table 24 Test statistic values for the three tested distributions

	MM		ML or ML-opt	
	S-K	A-D	S-K	A-D
Normal	0.59845 (NR)	0.15> (NR)	*0.59845 (NR)*	*0.15> (NR)*
Lognormal	0.64792 (NR)	0.15> (NR)	***0.6888 (NR)***	***0.15> (NR)***
Weibull	*0.37655 (NR)*	*0.15> (NR)*	0.25319 (NR)	0.15> (NR)

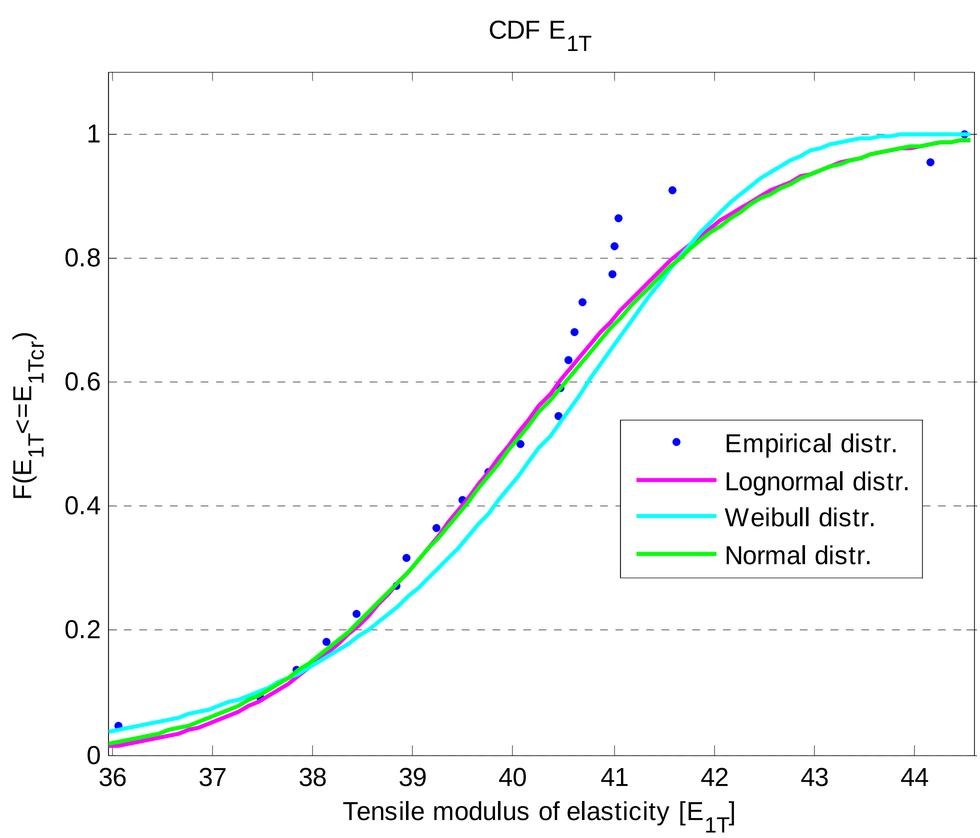

Sample E_{1C}

Table 25 Values of the estimated parameters for different distributions

	Method of Moments (MM)			Maximum Likelihood (ML) Or ML-opt		
Normal (m, σ)	38.781	1.07699	--	*38.781*	*1.07699*	--
Lognormal(ξ, δ)	38.766	0.277657e-1	--	***38.7669***	***0.268845e-1***	**--**
Weibull (w, κ, τ)	39.2609	45.4687	0	*39.3185*	*34.7174*	*0*

Table 26 Test statistic values for the three tested distributions

	MM		ML or ML-opt	
	S-K	A-D	S-K	A-D
Normal	0.92634 (NR)	0.15> (NR)	*0.92634 (NR)*	*0.15> (NR)*
Lognormal	0.94717 (NR)	0.15> (NR)	***0.95724 (NR)***	***0.15 > (NR)***
Weibull	0.5365 (NR)	0.15> (NR)	*0.56269 (NR)*	*0.15> (NR)*

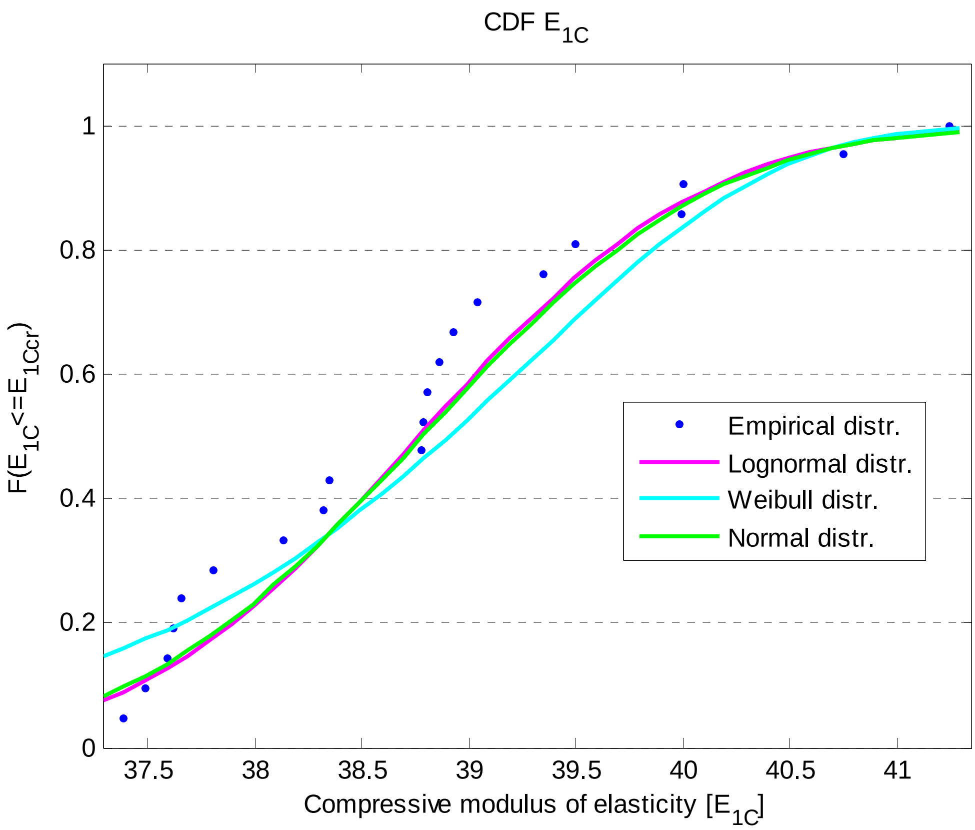

Sample v_{12}

Table 27 Values of the estimated parameters for different distributions

	Method of Moments (MM)			Maximum Likelihood (ML) Or ML-opt		
Normal (m, σ)	0.25945	0.247685e-1	--	*0.25945*	*0.247685e-1*	--
Lognormal(ξ, δ)	***0.258276***	***0.952489e-1***	**--**	0.25832	0.934883e-1	--
Weibull (w, κ, τ)	0.270138	12.76	0	*0.270583*	*11.9183*	*0*

Table 28 Test statistic values for the three tested distributions

	MM		ML or ML-opt	
	S-K	A-D	S-K	A-D
Normal	0.87842 (NR)	0.15 > (NR)	*0.87842 (NR)*	*0.15 > (NR)*
Lognormal	***0.91347 (NR)***	***0.15> (NR)***	0.88859 (NR)	0.15 (NR)
Weibull	0.72252 (NR)	0.15> (NR)	*0.82889 (NR)*	*0.15> (NR)*

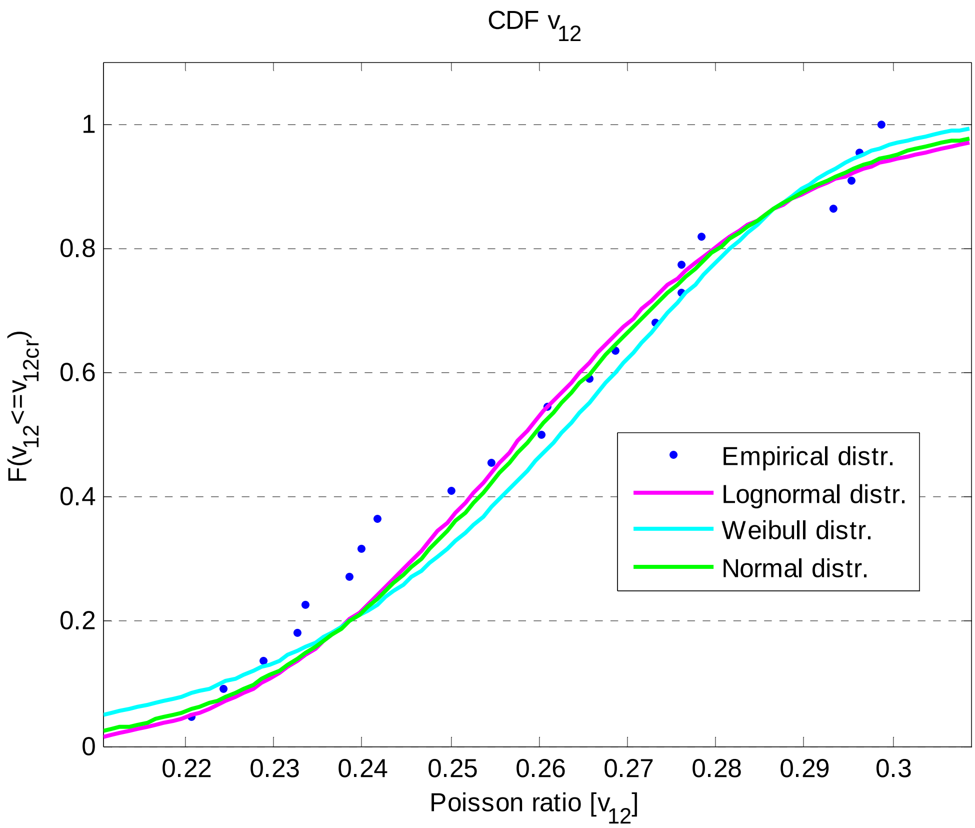

Sample E_{2T}

Table 29 Values of the estimated parameters for different distributions

	Method of Moments (MM)			Maximum Likelihood (ML) Or ML-opt		
Normal (m, σ)	13.211 3	0.580759	--	*13.211 3*	*0.580759*	--
Lognormal(ξ, δ)	***13.198 5***	***0.439382e-1***	**--**	13.199 1	0.428529e-1	--
Weibull (w, κ, τ)	13.468 4	28.471	0	*13.488 7*	*23.2464*	*0*

Table 30 Test statistic values for the three tested distributions

	MM		ML or ML-opt	
	S-K	A-D	S-K	A-D
Normal	0.93515 (NR)	0.15> (NR)	*0.93515 (NR)*	*0.15> (NR)*
Lognormal	***0.94611 (NR)***	***0.15> (NR)***	0.91893 (NR)	0.15> (NR)
Weibull	0.76502 (NR)	0.15> (NR)	*0.91126 (NR)*	*0.15> (NR)*

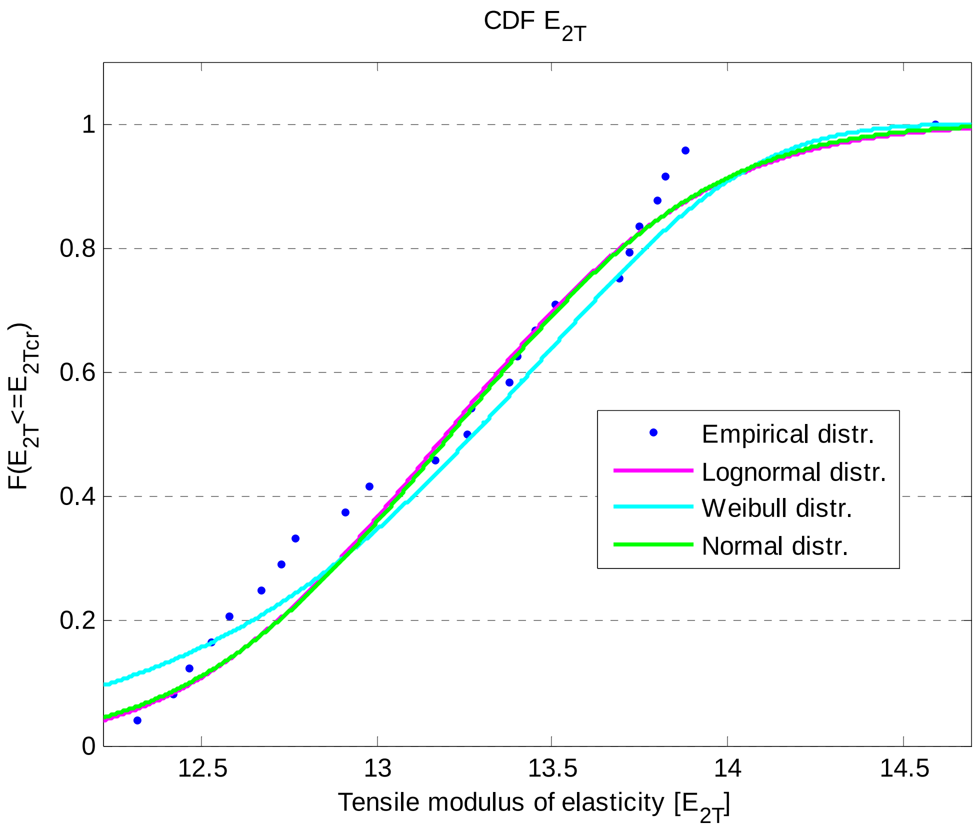

Sample E_{2C}

Table 31 Values of the estimated parameters for different distributions

	Method of Moments (MM)			Maximum Likelihood (ML) Or ML-opt		
Normal (m, σ)	14.2343	0.447645	--	*14.2343*	*0.447645*	--
Lognormal(ξ, δ)	*14.2273*	*0.314406e-1*	--	14.2275	0.309103e-1	--
Weibull (w, κ, τ)	***14.4335***	***40.0706***	***0***	14.4399	34.1858	0

Table 32 Test statistic values for the three tested distributions

	MM		ML or ML-opt	
	S-K	A-D	S-K	A-D
Normal	0.65765 (NR)	0.15> (NR)	*0.65765 (NR)*	*0.15> (NR)*
Lognormal	*0.60997 (NR)*	*0.15> (NR)*	0.60569 (NR)	0.15 (NR)
Weibull	***0.68379 (NR)***	***0.15> (NR)***	0.51714 (NR)	0.15 (NR)

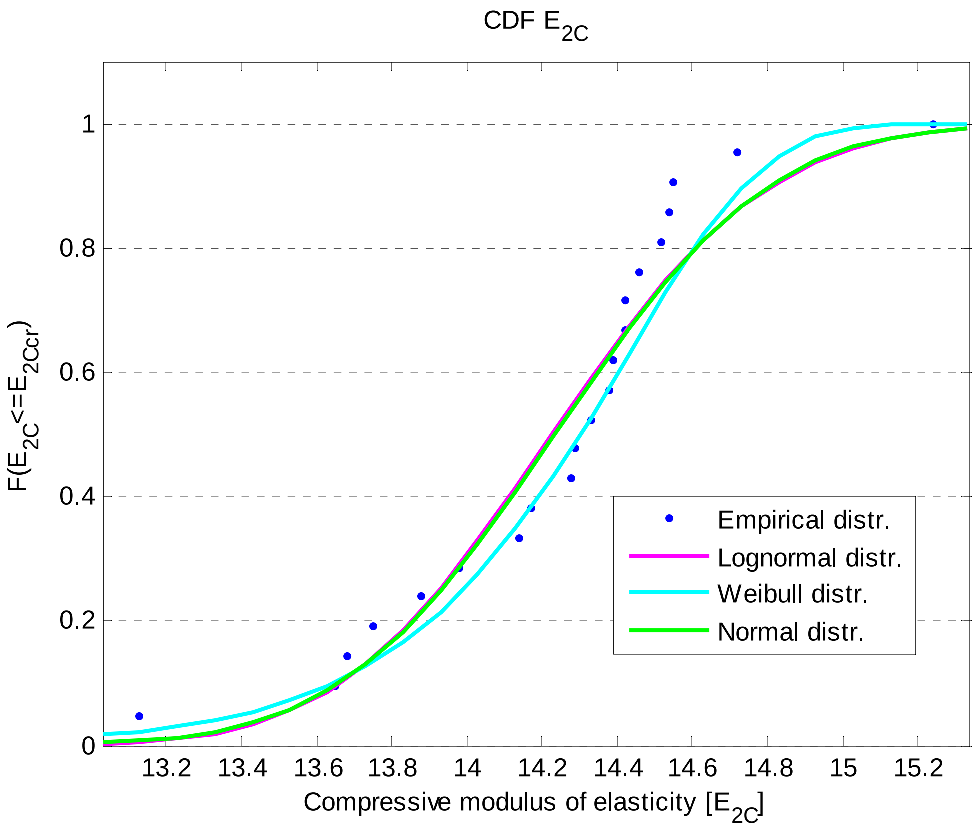

Sample v_{21}

Table 33 Values of the estimated parameters for different distributions

	Method of Moments (MM)			Maximum Likelihood (ML) Or ML-opt		
Normal (m, σ)	0.79733e-1	0.116305e-1	--	***0.79733e-1***	***0.116305e-1***	**--**
Lognormal(ξ, δ)	0.78898e-1	0.145101	--	*0.789318e-1*	*0.142918*	--
Weibull (w, κ, τ)	*0.84591e-1*	*8.14679*	*0*	0.846989e-1	7.05012	0

Table 34 Test statistic values for the three tested distributions

	MM		ML or ML-opt	
	S-K	A-D	S-K	A-D
Normal	0.86483 (NR)	0.15> (NR)	***0.86483 (NR)***	***0.15> (NR)***
Lognormal	0.7509 (NR)	0.15> (NR)	*0.775 (NR)*	*0.15> (NR)*
Weibull	*0.72447 (NR)*	*0.15> (NR)*	0.69404 (NR)	0.15> (NR)

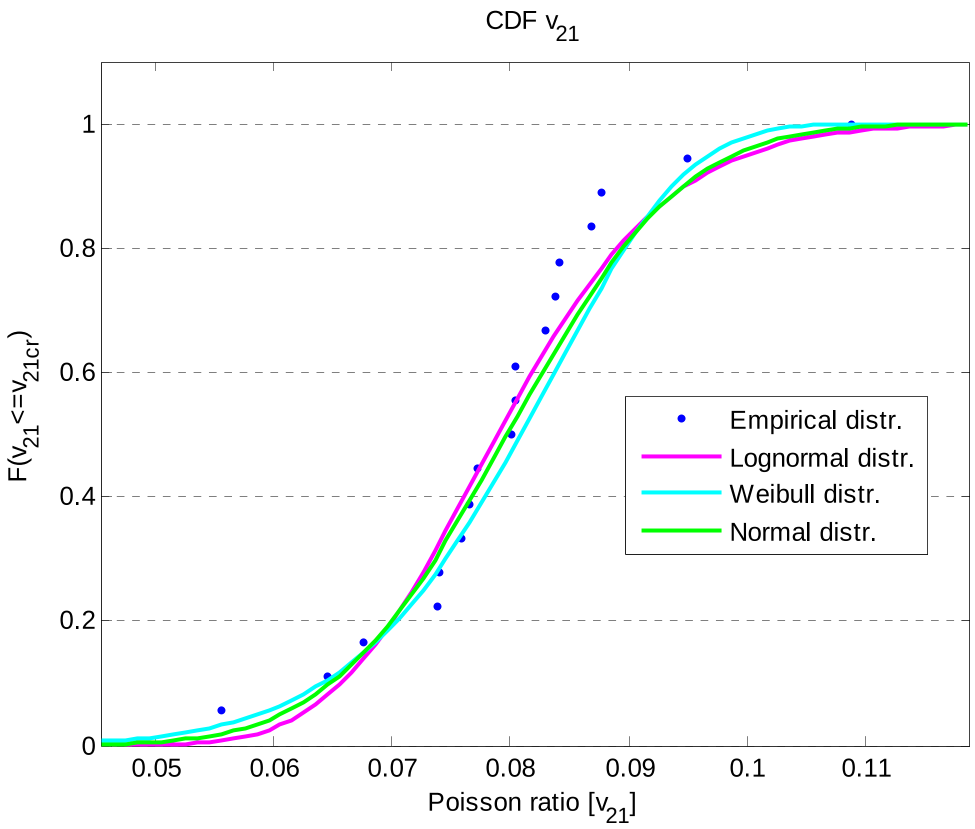

Sample G_{12} (ISO)

Table 35 Values of the estimated parameters for different distributions

	Method of Moments (MM)			Maximum Likelihood (ML) Or ML-opt		
Normal (m, σ)	3.5359 6	0.788987e-1	--	3.5359 6	0.788987e-1	--
Lognormal(ξ, δ)	3.5350 8	0.223104e-1	--	*3.5351*	*0.221718e-1*	--
Weibull (w, κ, τ)	***3.5712***	***56.7619***	***0***	3.5708 9	56.1397	0

Table 36 Test statistic values for the three tested distributions

	MM		ML or ML-opt	
	S-K	A-D	S-K	A-D
Normal	0.86851	(NR)>0.15	0.86851	(NR)>0.15
Lognormal	0.865	(NR)>0.15	*0.87567*	*(NR)>0.15*
Weibull	***0.95824***	***(NR)>0.15***	0.95455	(NR)>0.15

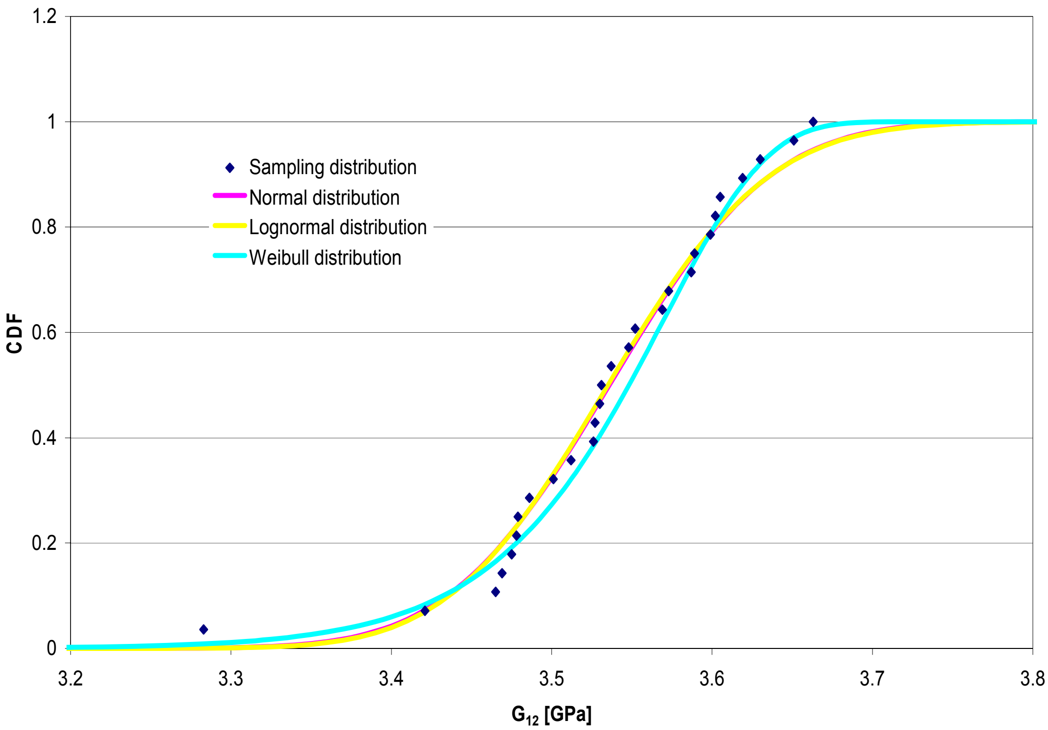

Sample G_{12} (VARIOUS)

Table 37 Values of the estimated parameters for different distributions

	Method of Moments (MM)			Maximum Likelihood (ML) Or ML-opt		
Normal (m,σ)	3.55023	0.448035	---	*3.55023*	*0.448035*	---
Lognormal(ξ,δ)	3.5223	0.125701	---	***3.52287***	***0.12455***	**---**
Weibull (w,κ,τ)	3.73994	9.50595	0	*3.74938*	*8.11428*	*0*

Table 38 Test statistic values for the three tested distributions

	MM		ML or ML-opt	
	S-K	A-D	S-K	A-D
Normal	0.35515 (NR)	0.15> (NR)	*0.35515 (NR)*	*0.15> (NR)*
Lognormal	0.5897 (NR)	0.15 (NR)	***0.5944 (NR)***	***0.15> (NR)***
Weibull	0.11383 (NR)	0.15> (NR)	*0.13766 (NR)*	*0.15> (NR)*

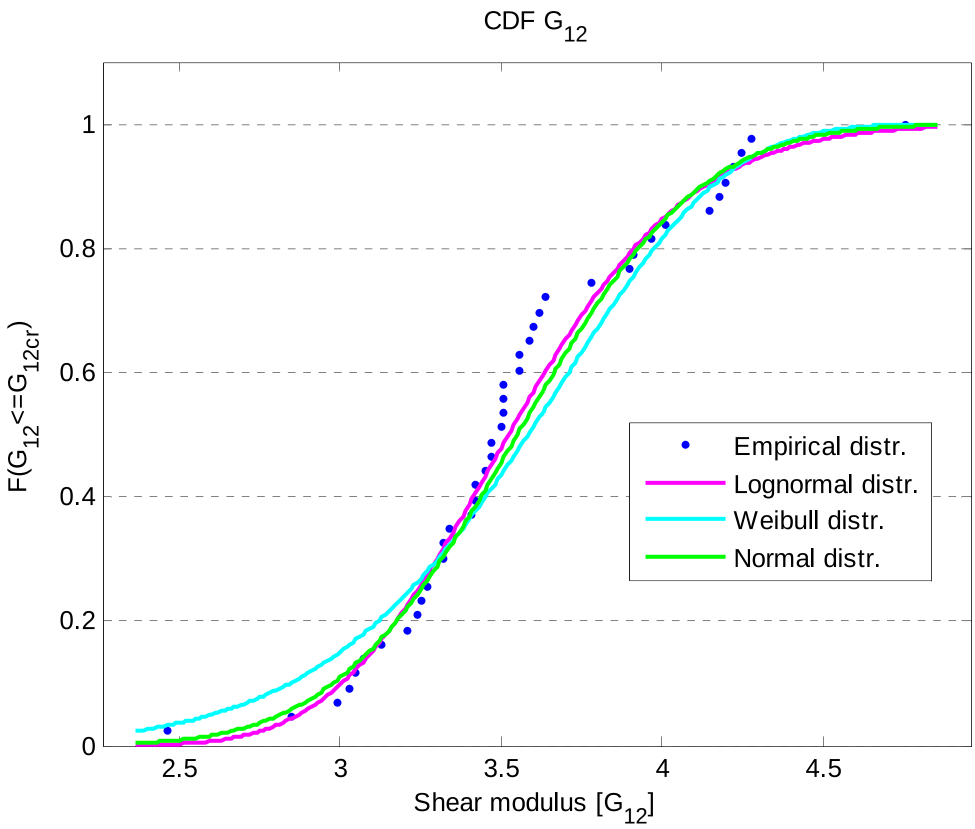

Sample X_T

Table 39 Values of the estimated parameters for different distributions

	Method of Moments (MM)			Maximum Likelihood (ML) Or ML-opt		
Normal (m,σ)	925.325	40.1172	--	*925.325*	*40.1172*	--
Lognormal(ξ,δ)	924.457	0.43334e-1	--	***924.486***	***0.42698e-1***	--
Weibull (w,κ,τ)	943.092	28.8776	0	*943.86*	*26.4322*	*0*

Table 40 Test statistic values for the three tested distributions

	MM		ML or ML-opt	
	S-K	A-D	S-K	A-D
Normal	0.811 (NR)	0.15> (NR)	*0.811 (NR)*	*0.15> (NR)*
Lognormal	0.85777 (NR)	0.15> (NR)	***0.86996 (NR)***	***0.15> (NR)***
Weibull	0.353383 (NR)	0.15> (NR)	*0.39645 (NR)*	*0.15> (NR)*

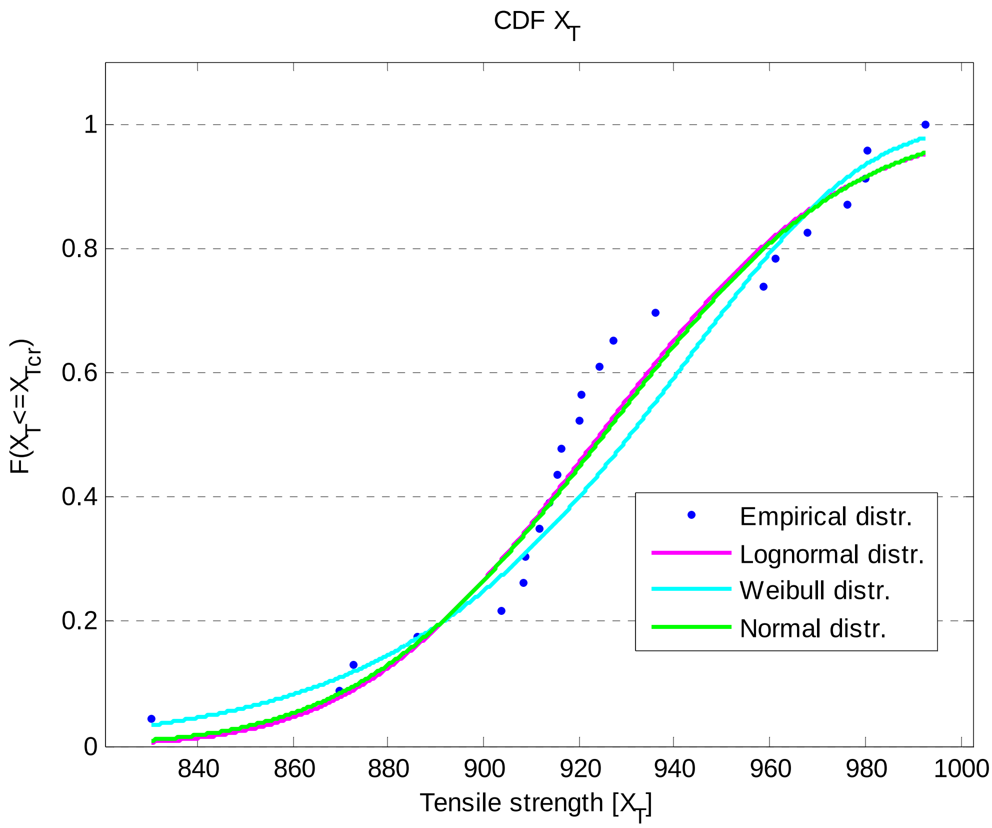

Sample X_C

Table 41 Values of the estimated parameters for different distributions

	Method of Moments (MM)			Maximum Likelihood (ML) Or ML-opt		
Normal (m,σ)	482.134	24.027	--	***482.134***	***24.027***	**--**
Lognormal(ξ,δ)	481.537	0.498037e-1	--	*481.556*	*0.491899e-1*	--
Weibull (w,κ,τ)	*429.745*	*25.0348*	*0*	492.983	22.9163	0

Table 42 Test statistic values for the three tested distributions

	MM		ML or ML-opt	
	S-K	A-D	S-K	A-D
Normal	0.96928 (NR)	0.15 (NR)	***0.96928 (NR)***	***0.15 (NR)***
Lognormal	0.94463 (NR)	0.15 (NR)	*0.95213 (NR)*	*0.15> (NR)*
Weibull	*0.91195 (NR)*	*0.15> (NR)*	0.9276 (NR)	0.15> (NR)

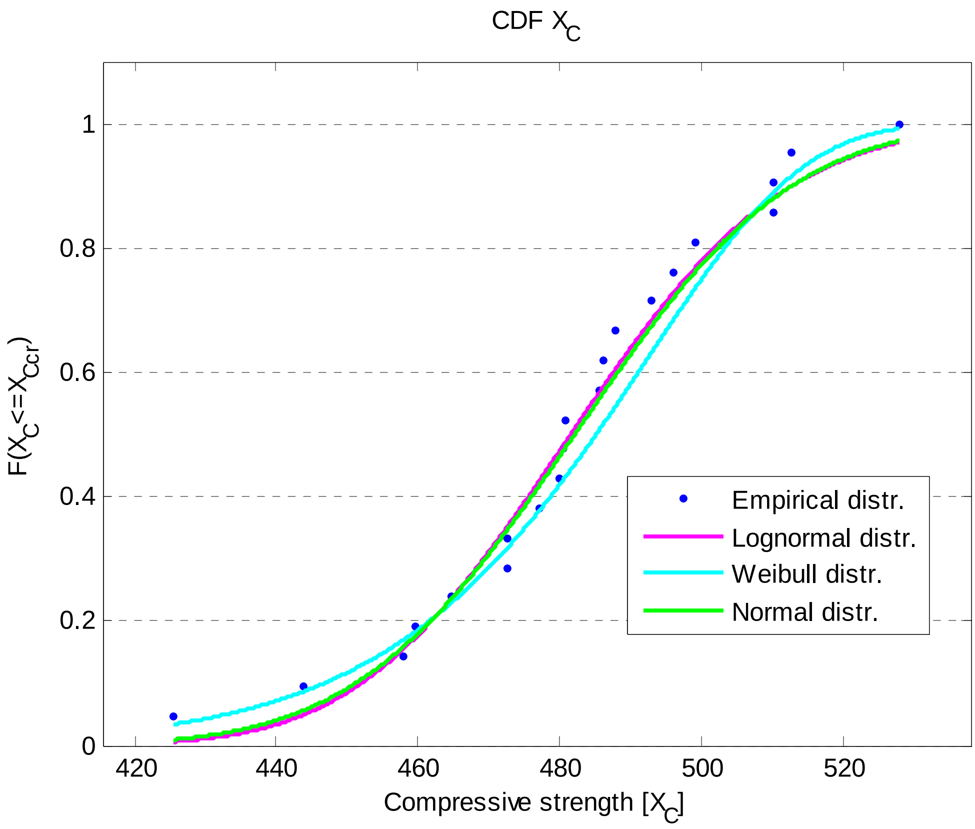

Sample Y_T

Table 43 Values of the estimated parameters for different distributions

	Method of Moments (MM)			Maximum Likelihood (ML) Or ML-opt		
Normal (m,σ)	85.7668	6.85555	--	***85.7668***	***6.85555***	**--**
Lognormal(ξ,δ)	*85.4941*	*0.798053e-1*	--	85.5048	0.782298e-1	--
Weibull (w,κ,τ)	*88.7504*	*15.3617*	*0*	88.9135	12.9219	--

Table 44 Test statistic values for the three tested distributions

	MM		ML or ML-opt	
	S-K	A-D	S-K	A-D
Normal	0.97657 (NR)	0.15> (NR)	***0.97657 (NR)***	***0.15> (NR)***
Lognormal	*0.92512 (NR)*	*0.15> (NR)*	0.91535 (NR)	0.15> (NR)
Weibull	*0.93811 (NR)*	*0.15> (NR)*	0.82916 (NR)	0.15> (NR)

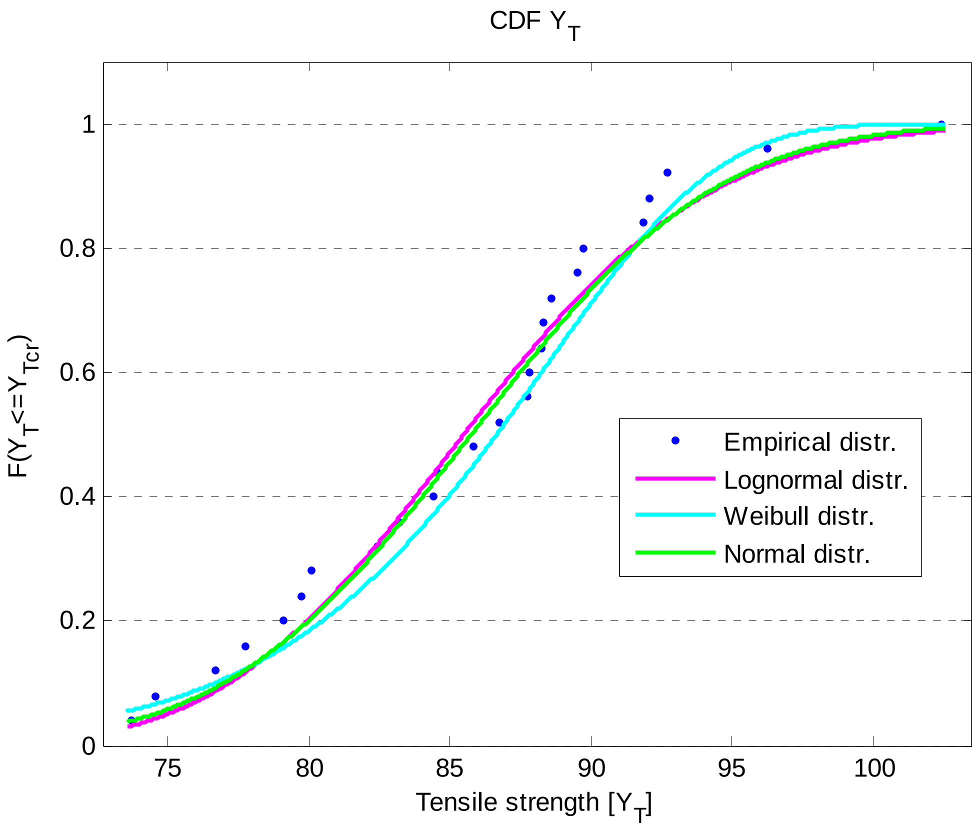

Sample Y_C

Table 45 Values of the estimated parameters for different distributions

	Method of Moments (MM)			Maximum Likelihood (ML) Or ML-opt		
Normal (m,σ)	147.593	8.0507	--	*147.593*	*8.0507*	--
Lognormal(ξ,δ)	***147.374***	***0.545061e-1***	**--**	147.388	0.523967e-1	--
Weibull (w,κ,τ)	*151.141*	*22.8144*	*0*	151.526	17.1163	0

Table 46 Test statistic values for the three tested distributions

	MM		ML or ML-opt	
	S-K	A-D	S-K	A-D
Normal	0.91763 (NR)	0.15> (NR)	*0.91763 (NR)*	*0.15> (NR)*
Lognormal	***0.93097 (NR)***	***0.15> (NR)***	0.87874 (NR)	0.15> (NR)
Weibull	*0.57376 (NR)*	*0.001 (R)*	0.43176 (NR)	0.15> (NR)

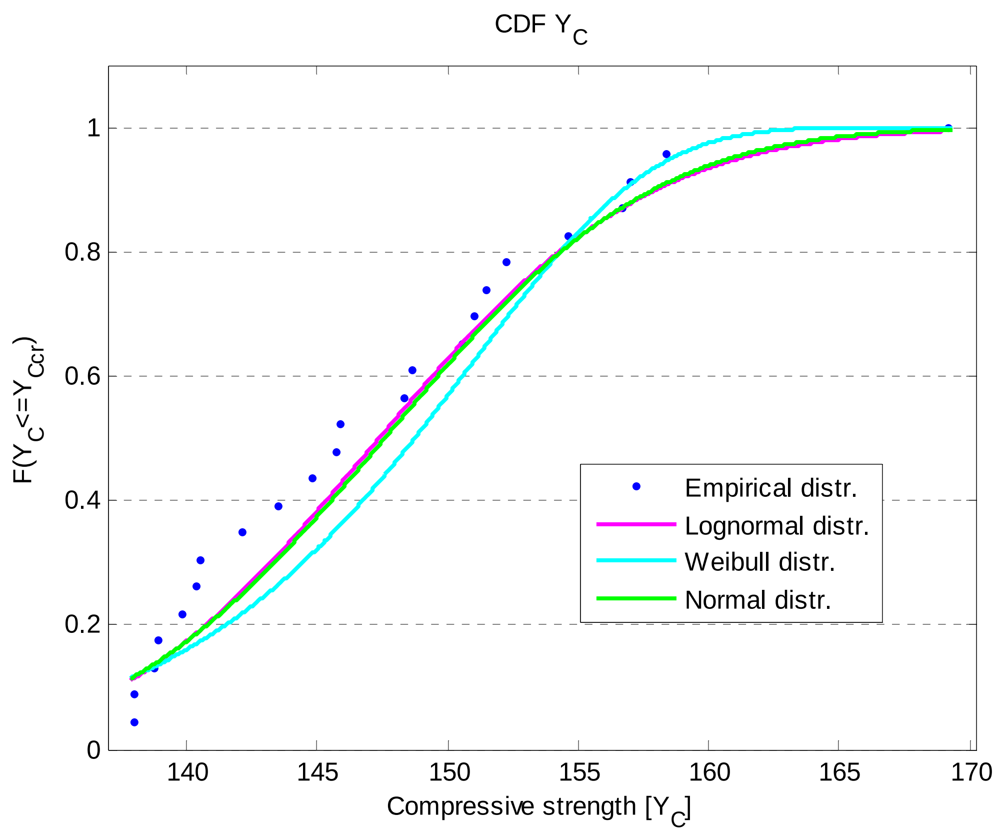

Sample S (τ_{max} at γ_{12}=50000 με) (ISO)

Table 47 Values of the estimated parameters for different distributions

	Method of Moments (MM)			Maximum Likelihood (ML) Or ML-opt		
Normal (m, σ)	43.5093	1.32041	--	43.5093	1.32041	--
Lognormal(ξ, δ)	***43.4893***	***0.303408e-1***	**--**	43.4902	0.29505e-1	--
Weibull (w, κ, τ)	44.0972	41.5489	0	*44.1745*	*30.5859*	*0*

Table 48 Test statistic values for the three tested distributions

	MM		ML or ML-opt	
	S-K	A-D	S-K	A-D
Normal	0.88622	(NR)>0.15	0.88622	(NR)>0.15
Lognormal	***0.91824***	***(NR)>0.15***	0.8998	(NR)>0.15
Weibull	0.39985	(NR)>0.15	*0.55791*	*(NR)>0.15*

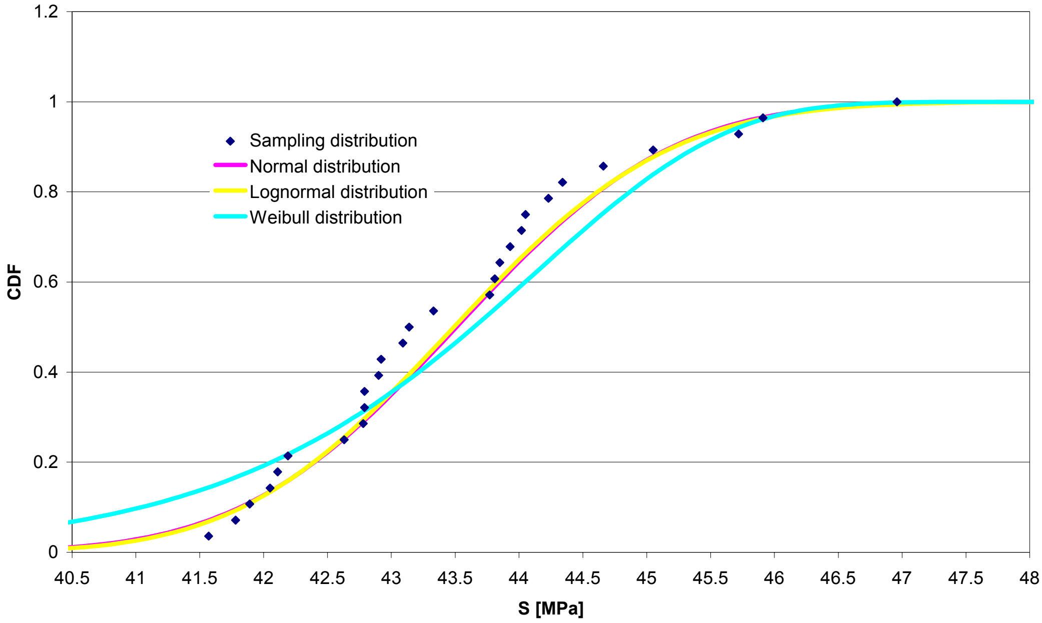

Sample S (VARIOUS)

Table 49 Values of the estimated parameters for different distributions

	Method of Moments (MM)			Maximum Likelihood (ML) Or ML-opt		
Normal (m,σ)	63.3156	11.7939	---	*63.3156*	*11.7939*	---
Lognormal(ξ,δ)	*62.2449*	*0.184686*	---	62.1429	0.198573	---
Weibull (w,κ,τ)	***68.0883***	***6.26239***	***0***	68.0634	6.60207	0

Table 50 Test statistic values for the three tested distributions

	MM		ML or ML-opt	
	S-K	A-D	S-K	A-D
Normal	0.73861 (NR)	0.15> (NR)	*0.73861 (NR)*	*0.15> (NR)*
Lognormal	*0.38955 (NR)*	*0.15> (NR)*	0.36752 (NR)	0.15> (NR)
Weibull	***0.78042 (NR)***	***0.15> (NR)***	0.67781 (NR)	0.15> (NR)

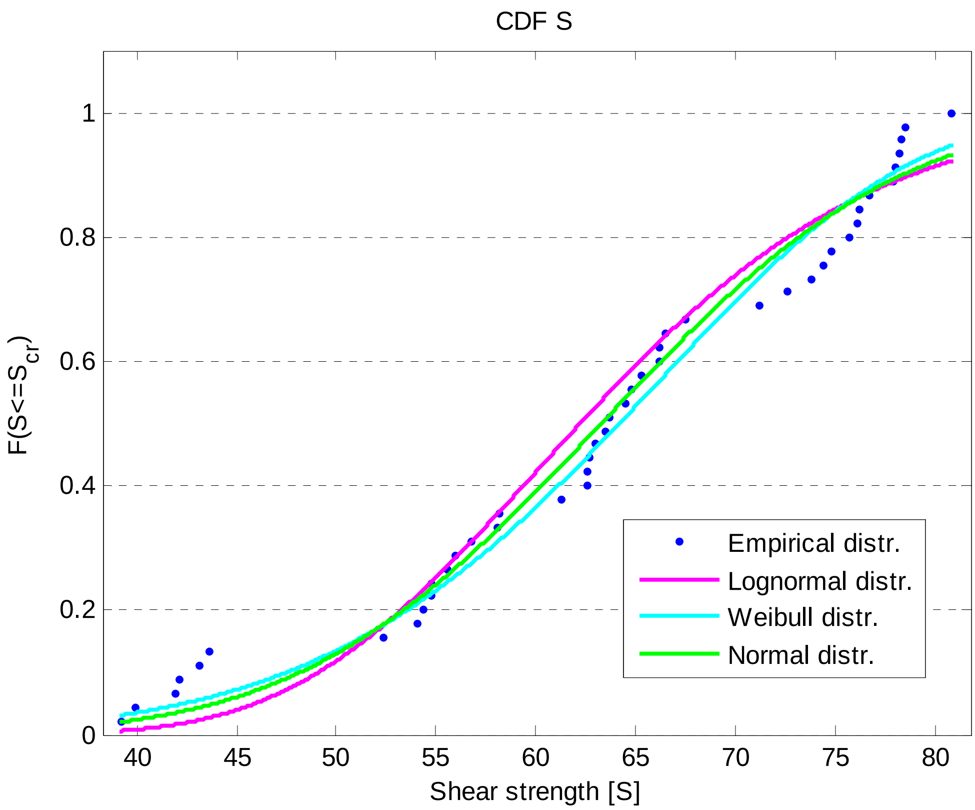

5.3. Comparison between OPTIMAT-UPWIND

A comparison of most important descriptive statistics for the basic stochastic variables of OPTIMAT and UPWIND was presented in Table 51. Graphs comparing the optimum distributions and experimental data follow.

Table 51 Comparison of some descriptive statistics of OPTIMAT and UPWIND

	Arithmetic mean	Variance	Coef. Of variation
Sample $\mathbf{E_{1T}}$ **(UPWIND)** [GPa]	40.013	3.8304	0.48912e-1
Sample $\mathbf{E_{1T}}$ **(OPTIMAT)** [GPa]	39.042	1.0657	0.26442e-1
Sample $\mathbf{E_{1C}}$ **(UPWIND)** [GPa]	38.781	1.1599	0.27771e-1
Sample $\mathbf{E_{1C}}$ **(OPTIMAT)** [GPa]	38.91	0.26888	0.13327e-1
Sample $\mathbf{v_{12}}$ **(UPWIND)**	0.25945	0.61348e-3	0.95465e-1
Sample $\mathbf{v_{12}}$ **(OPTIMAT)**	0.29058	0.73642e-3	0.93391e-1
Sample $\mathbf{E_{2T}}$ **(UPWIND)** [GPa]	13.211	0.33728	0.43959e-1
Sample $\mathbf{E_{2T}}$ **(OPTIMAT)** [GPa]	14.077	0.10549	0.23072e-1
Sample $\mathbf{E_{2C}}$ **(UPWIND)** [GPa]	14.234	0.20039	0.31448e-1
Sample $\mathbf{E_{2C}}$ **(OPTIMAT)** [GPa]	14.997	0.6534e-1	0.17044e-1
Sample $\mathbf{v_{21}}$ **(UPWIND)**	0.79733e-1	0.13527e-3	0.14587
Sample $\mathbf{v_{21}}$ **(OPTIMAT)**	0.95036e-1	0.4168e-4	0.67932e-1
Sample $\mathbf{G_{12}}$ **(UPWIND-VARIOUS)**	3.5502	0.20074	0.1262
Sample $\mathbf{G_{12}}$ **(OPTIMAT)**	4.2388	0.98352e-2	0.23396e-1
Sample $\mathbf{G_{12}}$ **(UPWIND-ISO)**	3.5360	0.006225	0.22313e-1
Sample $\mathbf{X_T}$ **(UPWIND)** [MPa]	925.33	1609.4	0.43355e-1
Sample $\mathbf{X_T}$ **(OPTIMAT)** [MPa]	776.5	1306.3	0.46546e-1
Sample $\mathbf{X_C}$ **(UPWIND)**	482.13	577.29	0.49835e-1
Sample $\mathbf{X_C}$ **(OPTIMAT)**	521.82	272.28	0.31622e-1
Sample $\mathbf{Y_T}$ **(UPWIND)**	85.767	46.999	0.79932e-1
Sample $\mathbf{Y_T}$ **(OPTIMAT)**	53.865	6.5628	0.4756e-1
Sample $\mathbf{Y_C}$ **(UPWIND)**	147.59	64.814	0.54547e-1
Sample $\mathbf{Y_C}$ **(OPTIMAT)**	165	23.512	0.29386e-1
Sample **S (UPWIND-VARIOUS)**	63.316	139.10	0.18627
Sample **S (OPTIMAT)**	56.071	1.2084	0.19605e-1
Sample **S (UPWIND-ISO)**	43.509	1.7435	0.30348e-1

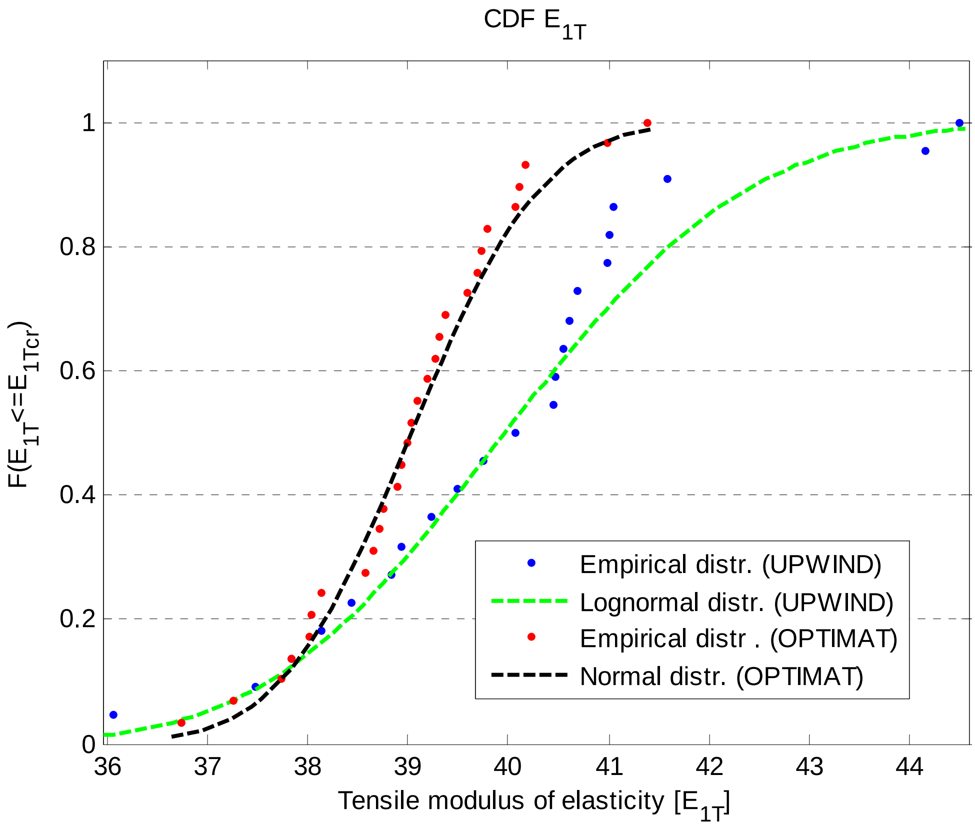
CDF E1T
F(E1T<=E1Tcr)
1
0.8
0.6
0.4
0.2
0
36
37
38
39
40
41
42
43
44
Tensile modulus of elasticity [E1T]
Empirical distr. (UPWIND)
Lognormal distr. (UPWIND)
Empirical distr . (OPTIMAT)
Normal distr. (OPTIMAT)

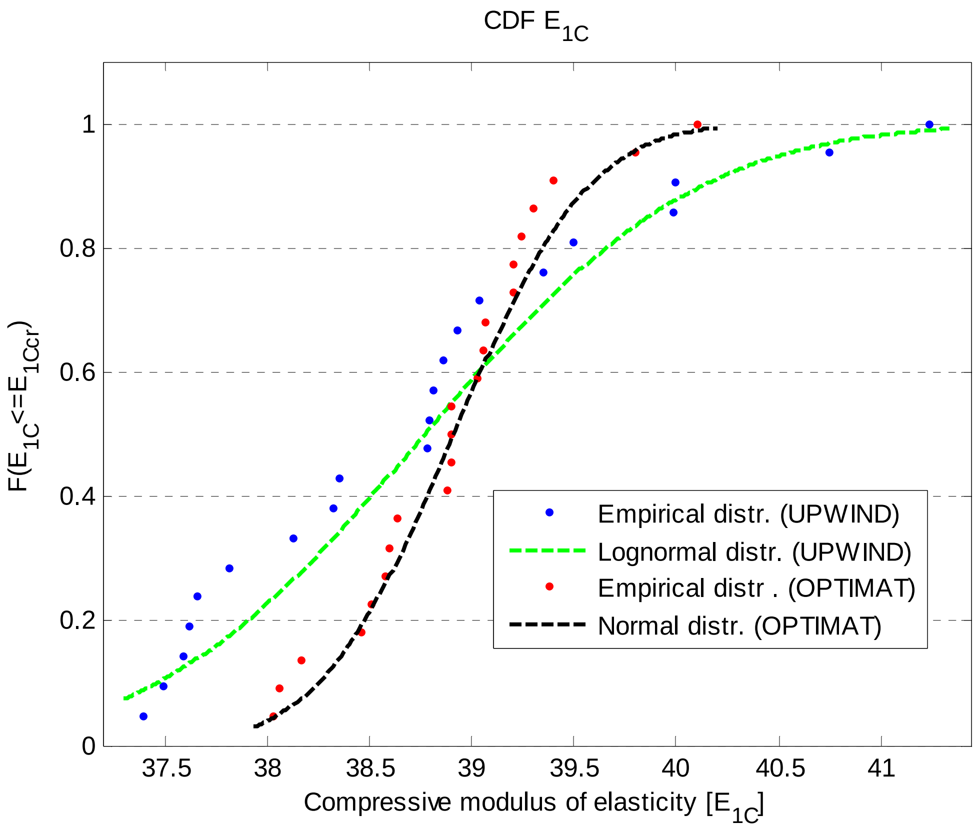
CDF E1C
F(E1C<=E1Ccr)
1
0.8
0.6
0.4
0.2
0
37.5
38
38.5
39
39.5
40
40.5
41
Compressive modulus of elasticity [E1C]
Empirical distr. (UPWIND)
Lognormal distr. (UPWIND)
Empirical distr . (OPTIMAT)
Normal distr. (OPTIMAT)

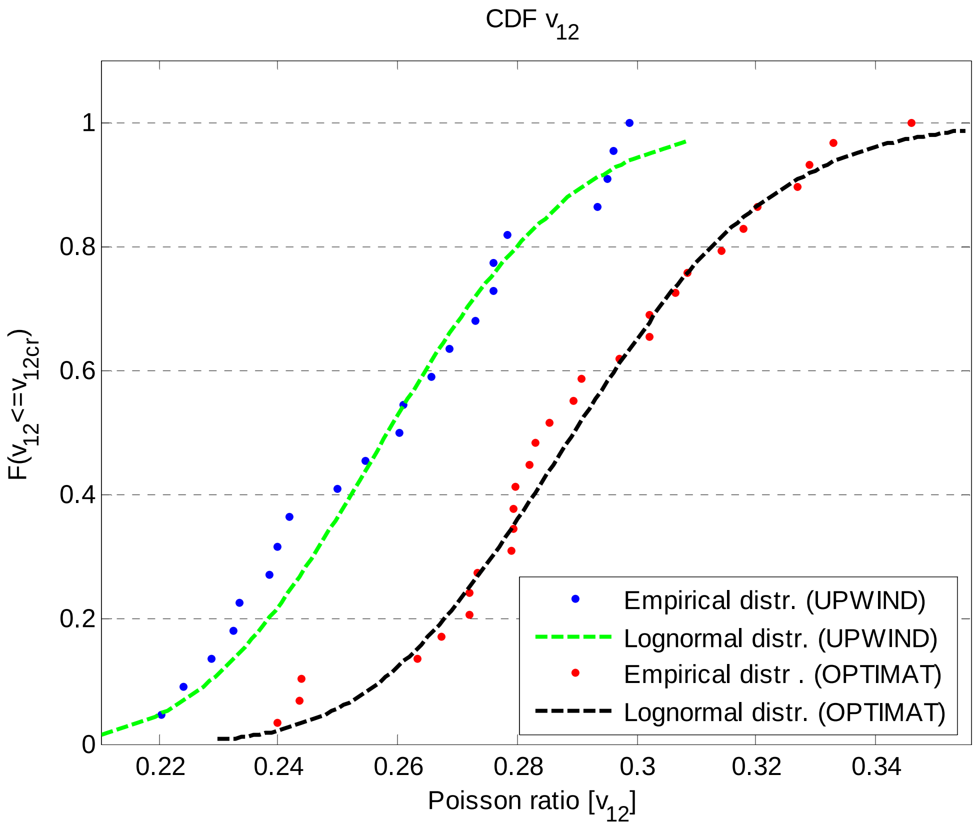
CDF v_{12}
F(v_{12}<=v_{12cr})
1
0.8
0.6
0.4
0.2
0
0.22
0.24
0.26
0.28
0.3
0.32
0.34
Poisson ratio [v_{12}]
Empirical distr. (UPWIND)
Lognormal distr. (UPWIND)
Empirical distr . (OPTIMAT)
Lognormal distr. (OPTIMAT)

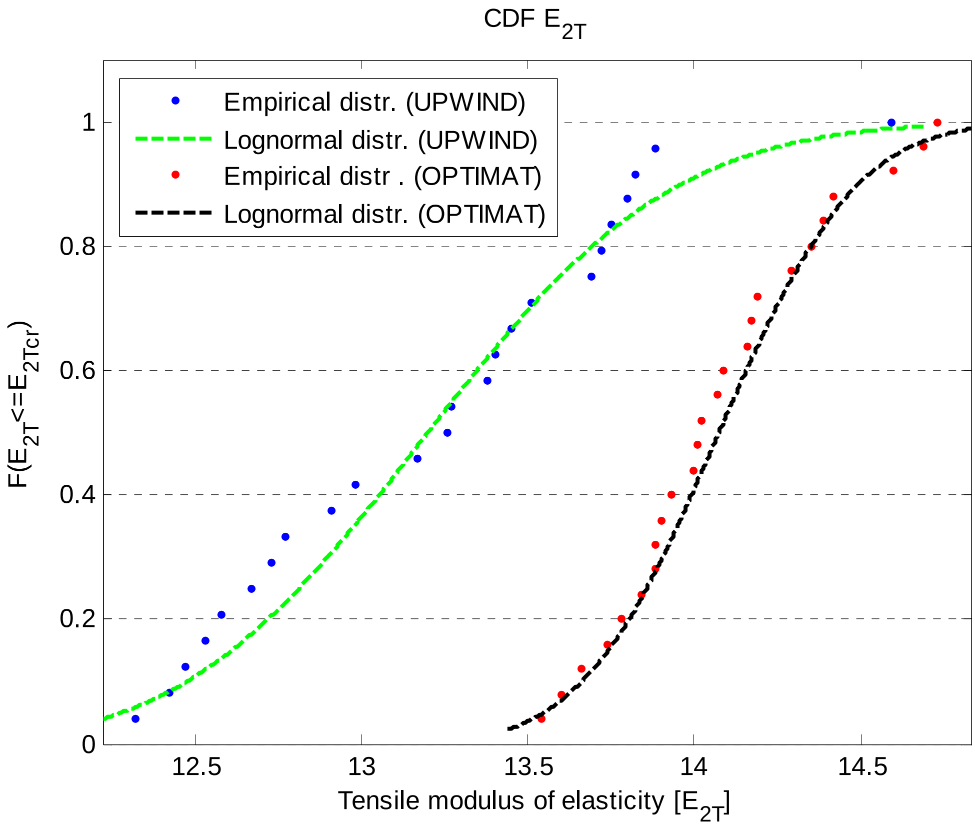
CDF E_{2T}
F(E_{2T}<=E_{2Tcr})
1
0.8
0.6
0.4
0.2
0
12.5
13
13.5
14
14.5
Tensile modulus of elasticity [E_{2T}]
Empirical distr. (UPWIND)
Lognormal distr. (UPWIND)
Empirical distr . (OPTIMAT)
Lognormal distr. (OPTIMAT)

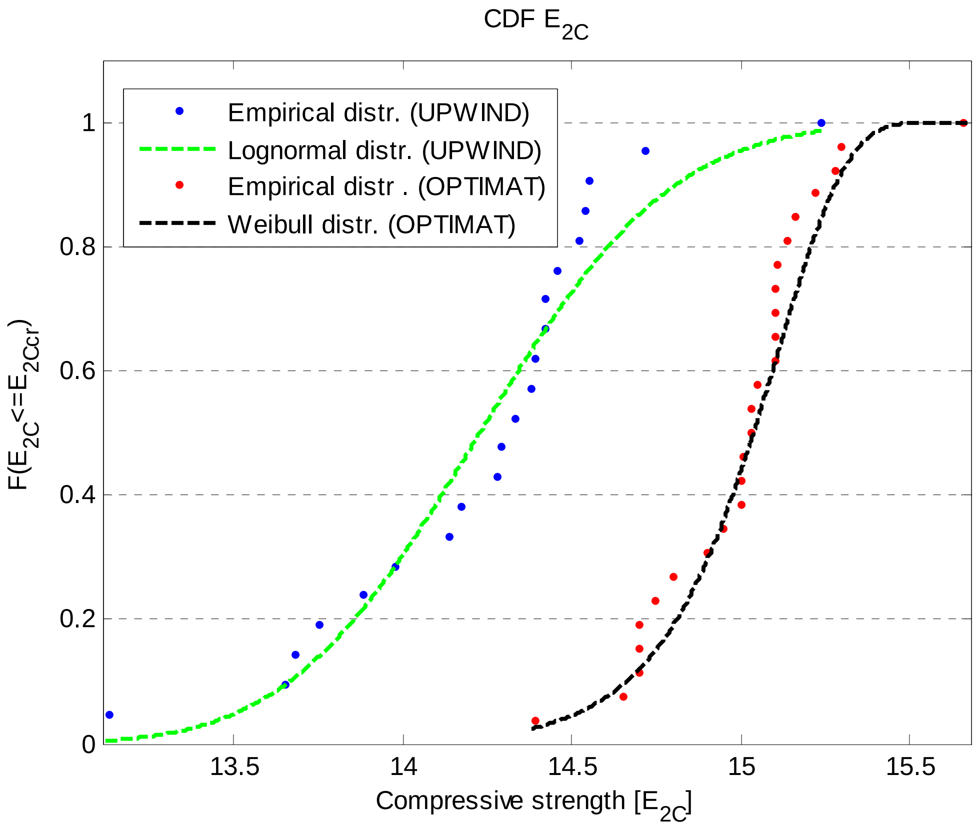
CDF E2C
Empirical distr. (UPWIND)
Lognormal distr. (UPWIND)
Empirical distr . (OPTIMAT)
Weibull distr. (OPTIMAT)
F(E2C<=E2Ccr)
Compressive strength [E2C]
0
0.2
0.4
0.6
0.8
1
13.5
14
14.5
15
15.5

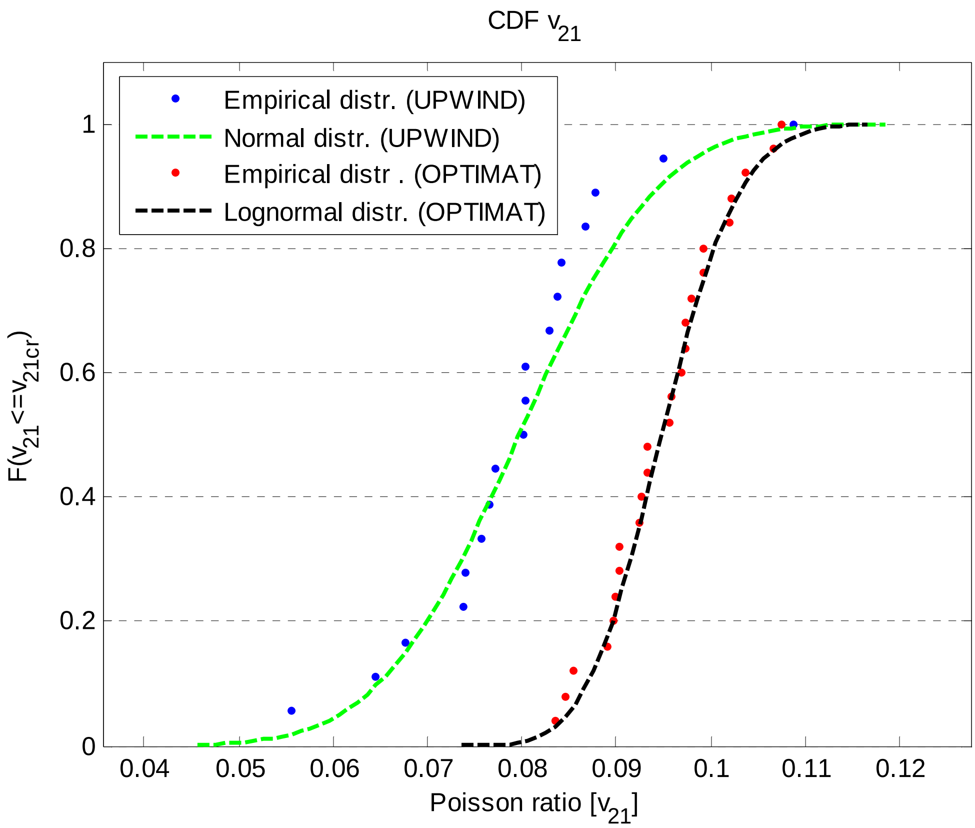
CDF v21
Empirical distr. (UPWIND)
Normal distr. (UPWIND)
Empirical distr . (OPTIMAT)
Lognormal distr. (OPTIMAT)
F(v21<=v21cr)
Poisson ratio [v21]
0
0.2
0.4
0.6
0.8
1
0.04
0.05
0.06
0.07
0.08
0.09
0.1
0.11
0.12

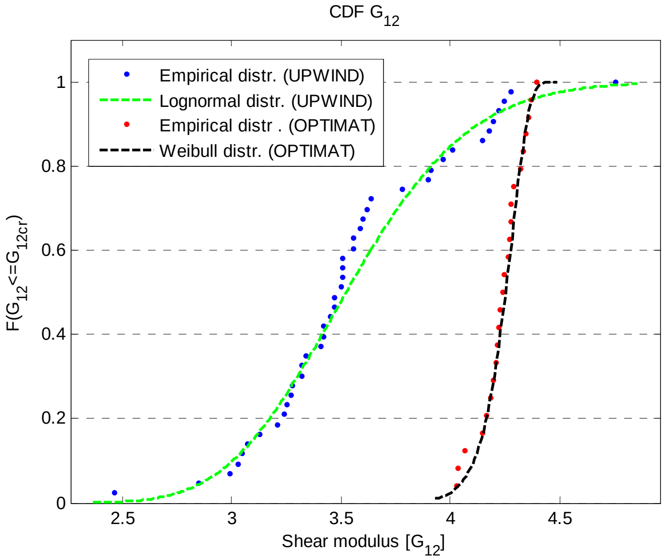
CDF G12
Empirical distr. (UPWIND)
Lognormal distr. (UPWIND)
Empirical distr . (OPTIMAT)
Weibull distr. (OPTIMAT)
F(G12<=G12cr)
Shear modulus [G12]
0
0.2
0.4
0.6
0.8
1
2.5
3
3.5
4
4.5

VARIOUS

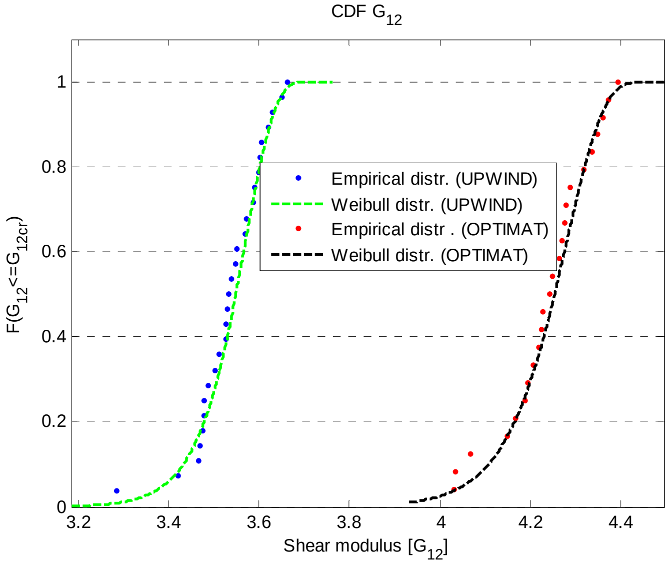
CDF G12
Empirical distr. (UPWIND)
Weibull distr. (UPWIND)
Empirical distr . (OPTIMAT)
Weibull distr. (OPTIMAT)
F(G12<=G12cr)
Shear modulus [G12]
0
0.2
0.4
0.6
0.8
1
3.2
3.4
3.6
3.8
4
4.2
4.4

ISO

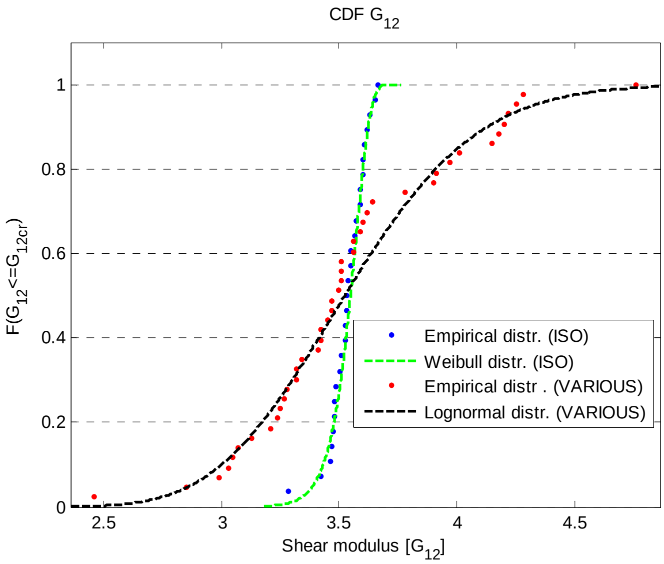
CDF G12
Empirical distr. (ISO)
Weibull distr. (ISO)
Empirical distr . (VARIOUS)
Lognormal distr. (VARIOUS)
F(G12<=G12cr)
Shear modulus [G12]
0
0.2
0.4
0.6
0.8
1
2.5
3
3.5
4
4.5

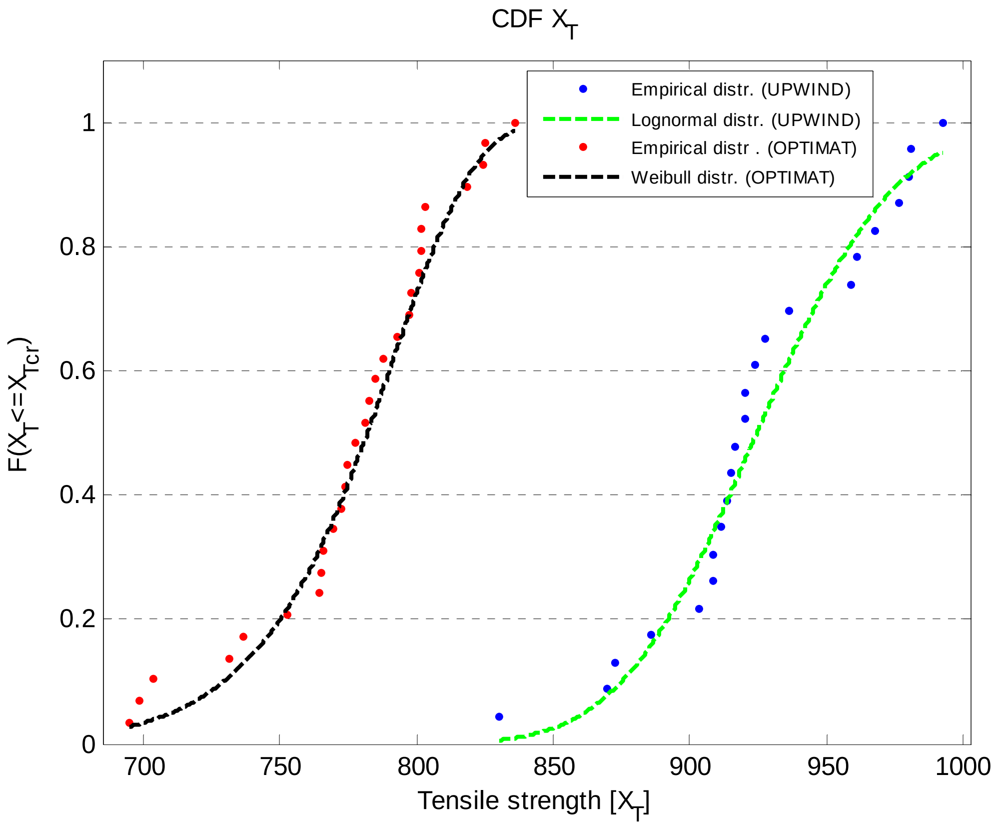

CDF X_T
Empirical distr. (UPWIND)
Lognormal distr. (UPWIND)
Empirical distr . (OPTIMAT)
Weibull distr. (OPTIMAT)
$F(X_T<=X_{Tcr})$
0
0.2
0.4
0.6
0.8
1
700
750
800
850
900
950
1000
Tensile strength $[X_T]$

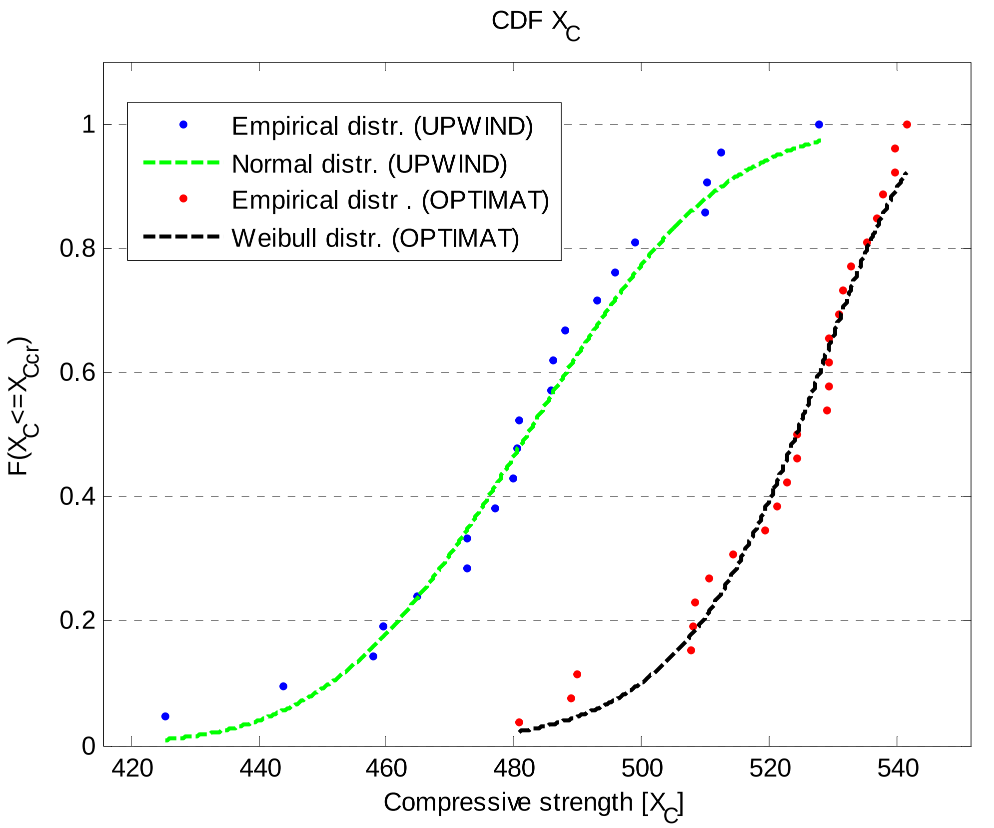

CDF X_C
Empirical distr. (UPWIND)
Normal distr. (UPWIND)
Empirical distr . (OPTIMAT)
Weibull distr. (OPTIMAT)
$F(X_C<=X_{Ccr})$
0
0.2
0.4
0.6
0.8
1
420
440
460
480
500
520
540
Compressive strength $[X_C]$

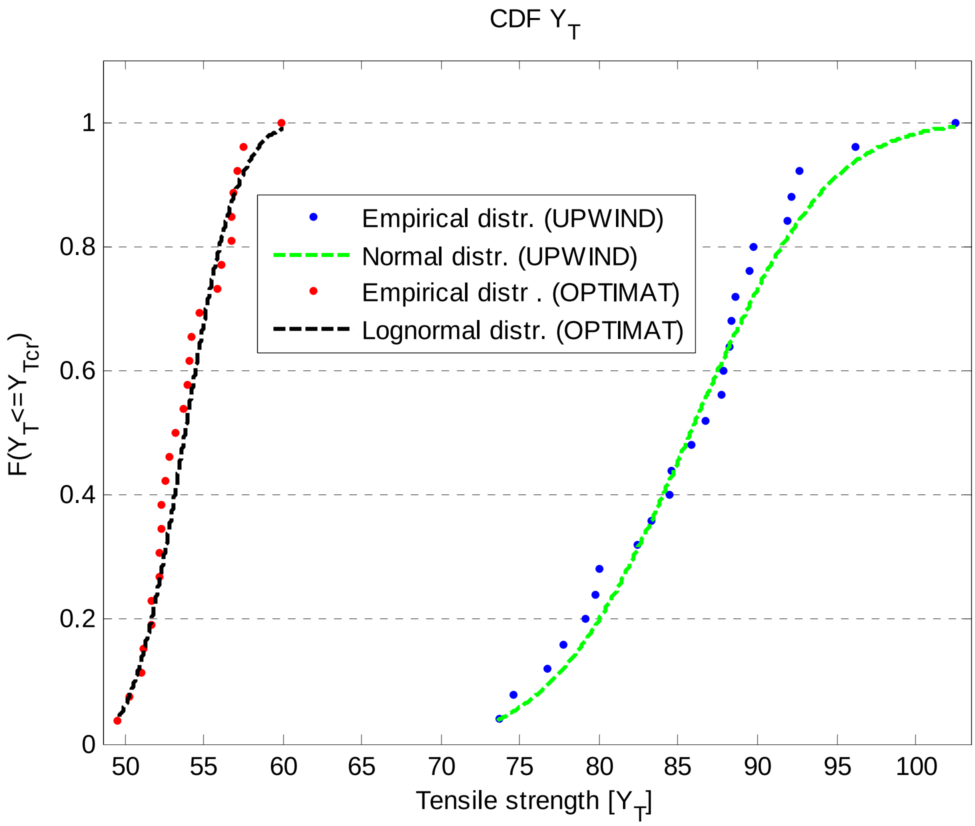
CDF Y_T
Empirical distr. (UPWIND)
Normal distr. (UPWIND)
Empirical distr . (OPTIMAT)
Lognormal distr. (OPTIMAT)
$F(Y_T<=Y_{Tcr})$
Tensile strength [Y_T]
0
0.2
0.4
0.6
0.8
1
50
55
60
65
70
75
80
85
90
95
100

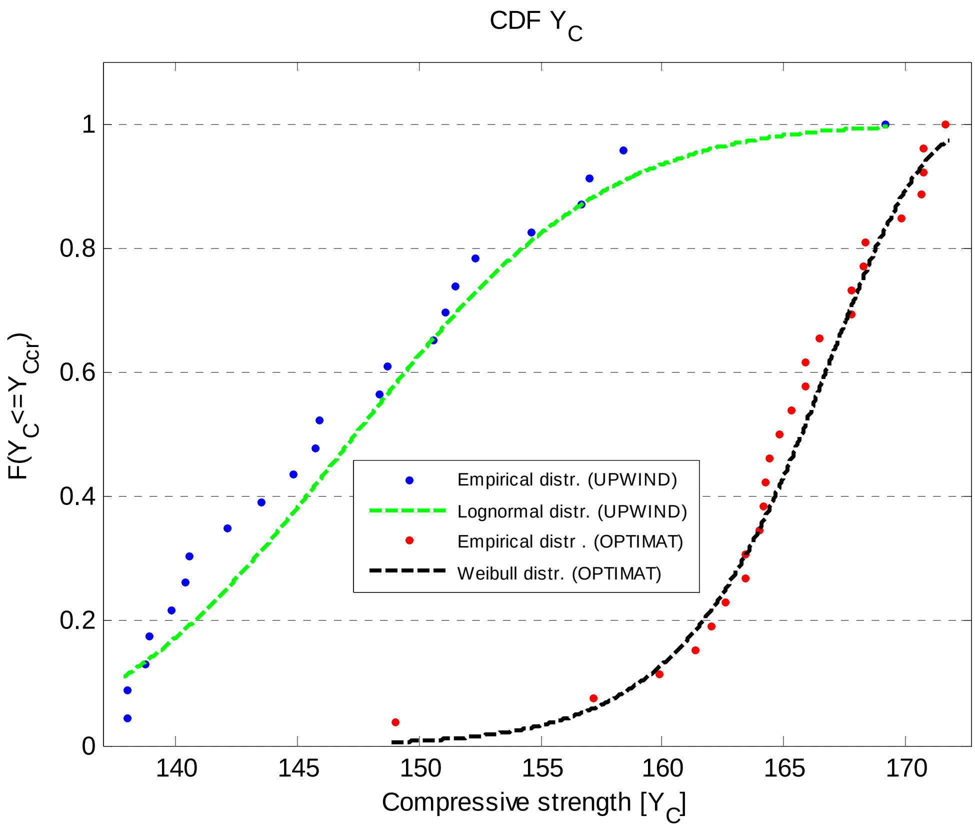
CDF Y_C
Empirical distr. (UPWIND)
Lognormal distr. (UPWIND)
Empirical distr . (OPTIMAT)
Weibull distr. (OPTIMAT)
$F(Y_C<=Y_{Ccr})$
Compressive strength [Y_C]
0
0.2
0.4
0.6
0.8
1
140
145
150
155
160
165
170

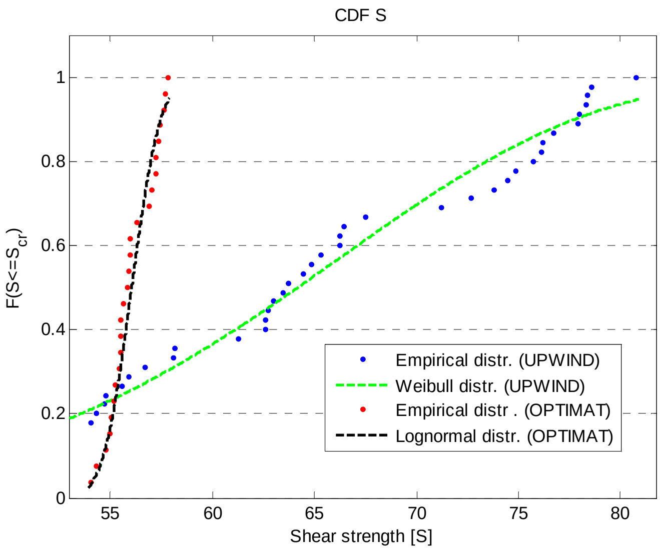
CDF S
F(S<=S_cr)
Shear strength [S]
Empirical distr. (UPWIND)
Weibull distr. (UPWIND)
Empirical distr . (OPTIMAT)
Lognormal distr. (OPTIMAT)

VARIOUS

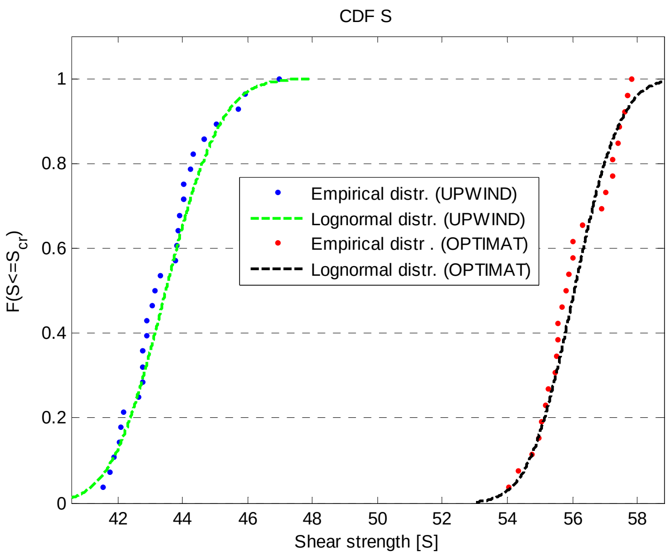
CDF S
F(S<=S_cr)
Shear strength [S]
Empirical distr. (UPWIND)
Lognormal distr. (UPWIND)
Empirical distr . (OPTIMAT)
Lognormal distr. (OPTIMAT)

ISO

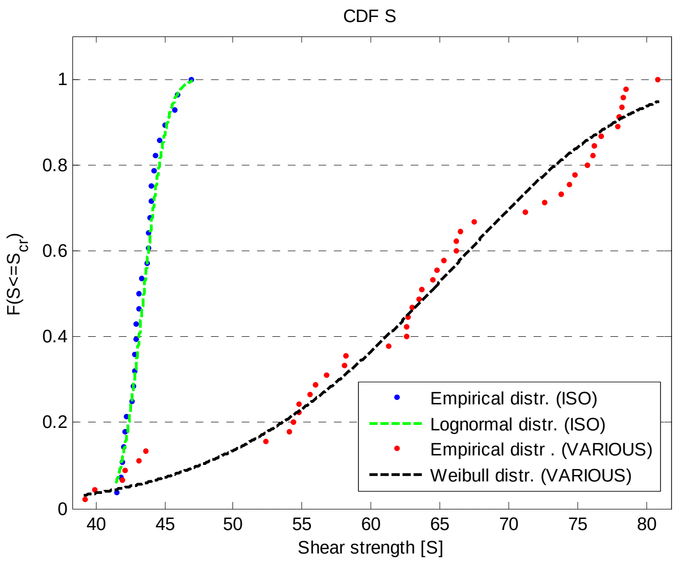
CDF S
F(S<=S_cr)
Shear strength [S]
Empirical distr. (ISO)
Lognormal distr. (ISO)
Empirical distr . (VARIOUS)
Weibull distr. (VARIOUS)

6. Conclusions

For the characterization of in-plane mechanical properties of the UPWIND Gl/Ep UD 128 axial static tests were performed at UP in the frame of WP 3.3. Concerning the static tensile tests parallel to the fibres, average values of UTS, E_1 and v_{12} were found equal to 923.65 MPa, 39.90 GPa and 0.26 respectively. Failure was located in the gauge length region. Coefficients of variation were relatively low, verifying the consistency of the experiments.

For the static compressive tests parallel to the fibres, average values of UCS and E_1 were found equal to -482.14 MPa and 38.78 GPa respectively. Considerable bending was observed in four (4/25) coupons. Failure modes were almost the same for all coupons. Coefficients of variation verify the consistency of the experiments.

In the static tensile tests transverse to the fibres, average values of UTS, E_2 and v_{21} were found equal to 85.77 MPa, 13.19 GPa and 0.08 respectively. Failure was always located in the tab region. Coefficients of variation were relatively low. For the respective compressive tests, average values of UCS and E_2 were found equal to -147.49 MPa and 14.24 GPa respectively. Considerable bending was observed in one (1/25) coupon. Failure modes were in all cases acceptable. Coefficients of variation verify the consistency of the experiments.

In the tensile tests of the ISO 14129 $[\pm45]_S$ coupons for shear properties characterization, average values of G_{12} and S were found equal to 3.53 GPa, and 43.509 MPa respectively. Failure was located always in the gauge length region and the failure mode was the same. Coefficients of variation were low verifying the consistency of the experiments.

In a detailed statistical analysis of the test data, three different distributions were considered to fit the samples, namely normal, lognormal and weibull. Two methods of parameter estimation, i.e. the method of moments and the maximum likelihood estimation were used. Finally, two hypothesis tests were considered for the adequacy of the fitted distributions to the data, Smirnov-Kolmogorov and Anderson-Darling. As presented, all three distributions are accepted to represent the data of every sample.

From the comparison of the basic statistical features of OPTIMAT and UPWIND databases it was derived that the samples E_{1T}, X_T, Y_T and S (VARIOUS) from UPWIND exhibit greater mean values. It must be said that the differences in mean values of samples E_{1T}, E_{1C}, v_{12}, E_{2T}, E_{2C}, v_{21} were not significant. It seems that the new material is stiffer in the fibre direction and has greater tensile strength in both directions (parallel and transverse to the fibres) and shear strength (according to the VARIOUS data set). The opposite was valid for the compressive strengths.

From the results it can be derived that the OPTIMAT database has less variability in the data than the UPWIND. All the OPTIMAT samples have smaller coefficients of variation except for X_T. This lower variability is explained by the fact that the OPTIMAT experiments were conducted for coupons cut out of a few only plates.

7. References

1. R. Nijssen et al., “UPWIND material tests; Programme, methods, results and analysis”, Technical Report WMC-2007-36
2. STATREL, v. 3.12, Users Manual, 1999
3. EN ISO 527-5:1997 “Plastics – Determination of tensile properties, Part 5: Test conditions for unidirectional fibre-reinforced plastic composites”
4. ISO 14129:1997(E) “Fibre-reinforced plastic composites – Determination of the in-plane shear stress/shear strain response, including the in-plane shear modulus and strength, by the $\pm 45^0$ tension test method”
5. EN ISO 14126:1999(E) “Fiber-reinforced plastic composites-Determination of compressive properties in the in-plane direction”
6. D.A. Leeuwen, R.P.L. Nijssen, T. Westphal, E. Stammes, “Comparison of static shear test methodologies; test results and analysis”, 2008

8. Appendix

8.1. Tensile UD tests parallel to the fibres

8.1.1. Stress-strain graphs

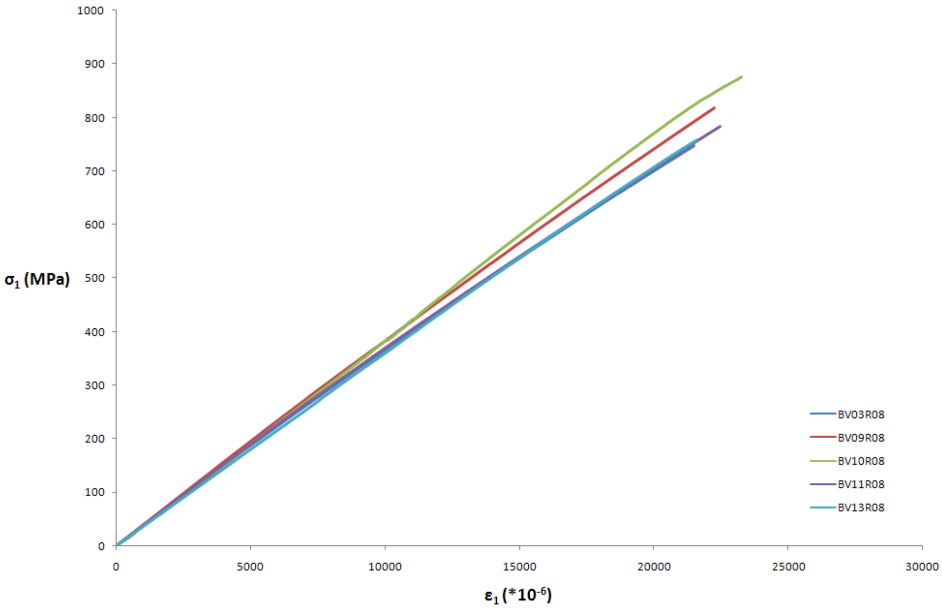

Fig. 4: Stress-strain curve of 5 coupons tested in tension in the fibres direction: BV03R08, BV09R08, BV10R08, BV11R08 and BV13R08

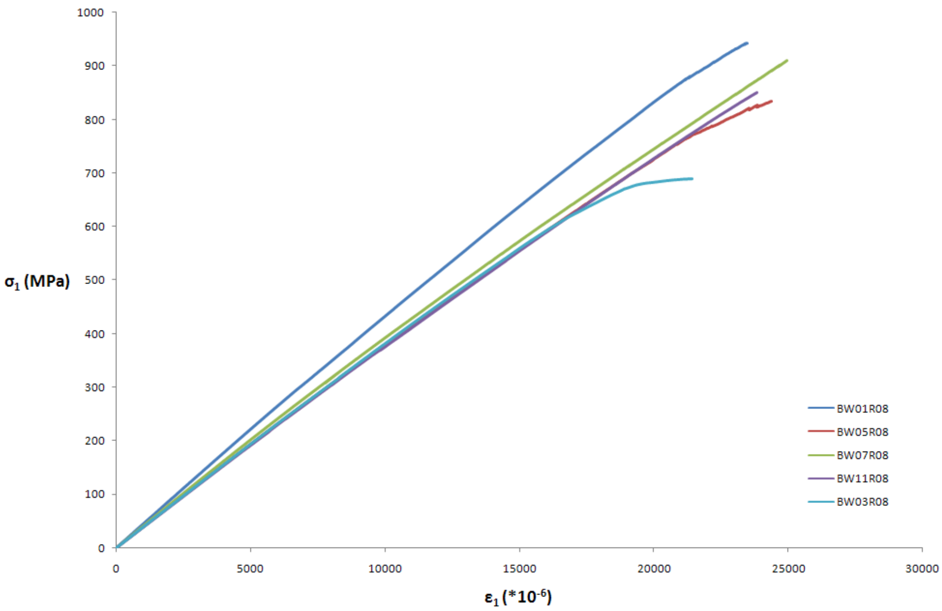

Fig. 5: Stress-strain curve of 5 coupons tested in tension in the fibres direction: BW01R08, BW05R08, BW07R08, BW11R08 and BW03R08

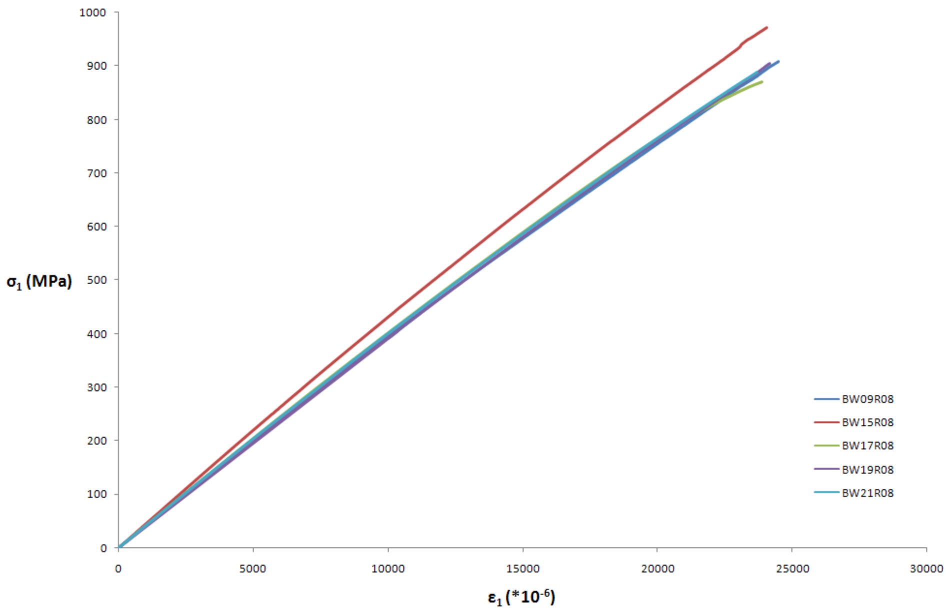

Fig. 6: Stress-strain curve of 5 coupons tested in tension in the fibres direction: BW09R08, BW15R08, BW17R08, BW19R08 and BW21R08

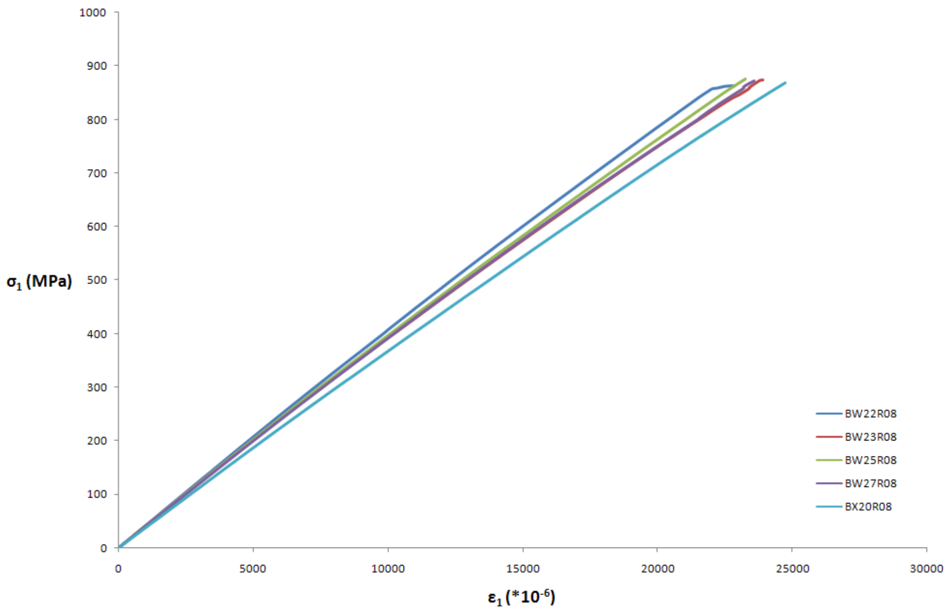

Fig. 7: Stress-strain curve of 5 coupons tested in tension in the fibres direction: BW22R08, BW23R08, BW25R08, BW27R08 and BX20R08

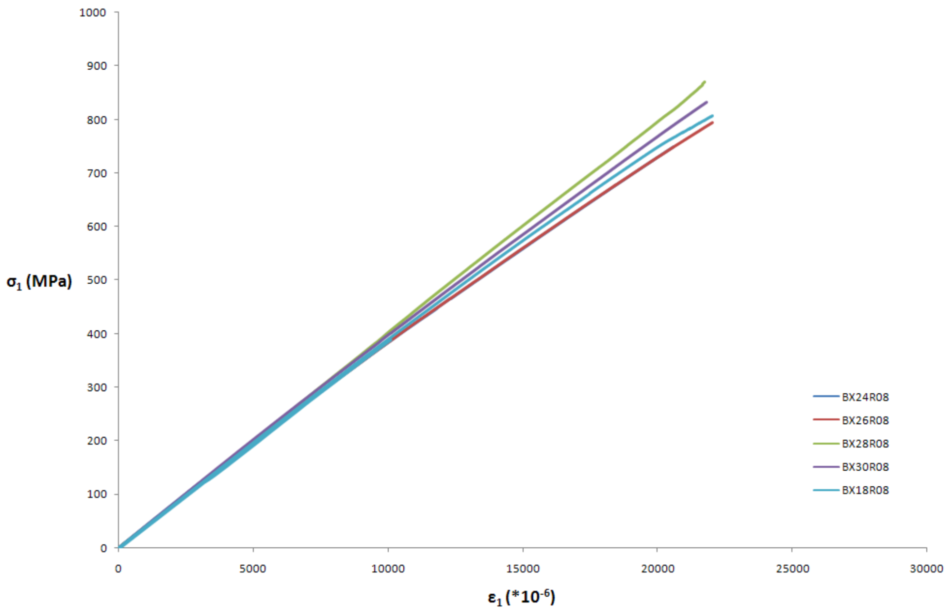

Fig. 8: Stress-strain curve of 5 coupons tested in tension in the fibres direction: BX24R08, BX26R08, BX28R08, BX30R08 and BX18R08

8.1.2. Stress-strain graphs (500-2500 με)

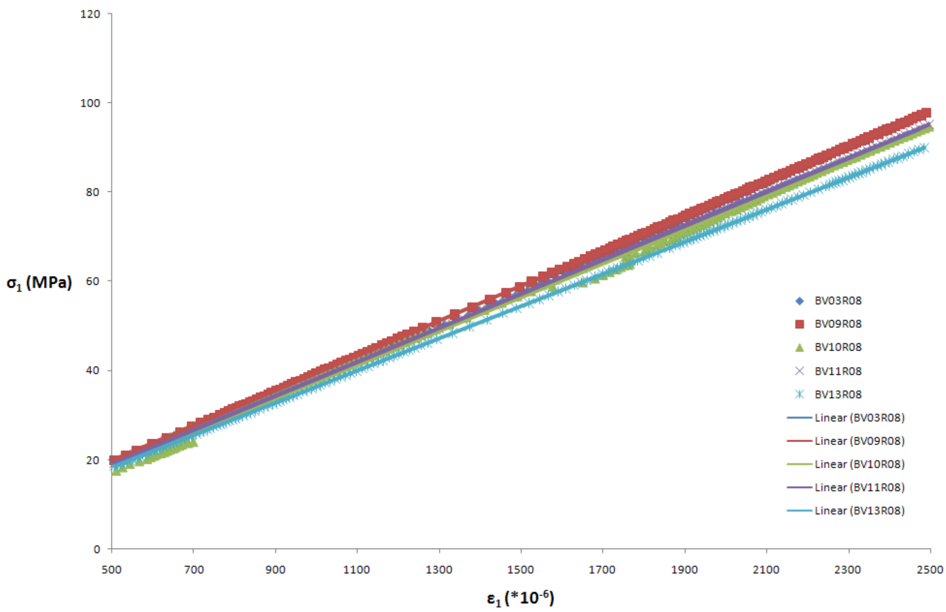

Fig. 9: Stress-strain curve of 5 coupons tested in tension in the fibres direction and linear curve fit: BV03R08, BV09R08, BV10R08, BV11R08 and BV13R08

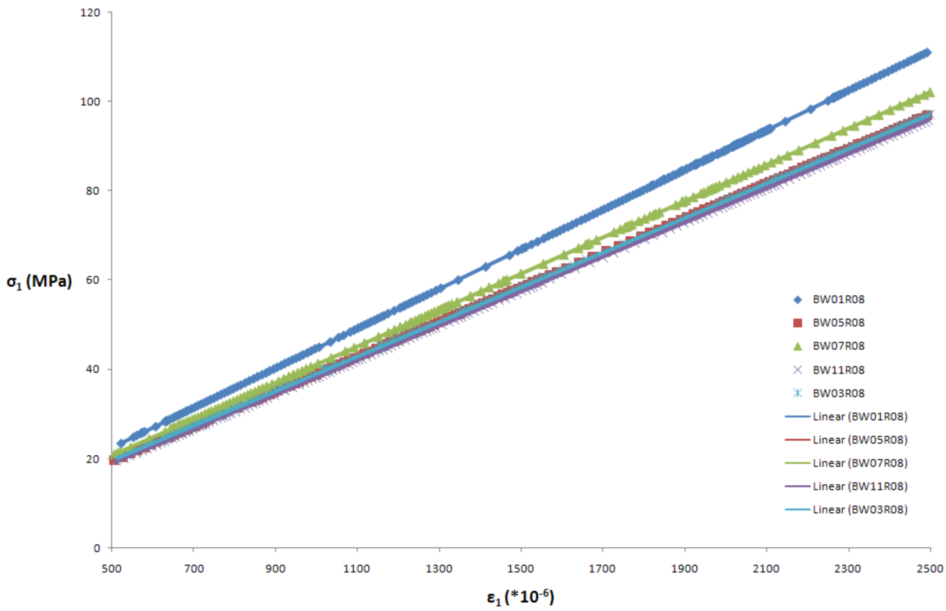

Fig. 10: Stress-strain curve of 5 coupons tested in tension in the fibres direction and linear curve fit: BW01R08, BW05R08, BW07R08, BW11R08 and BW03R08

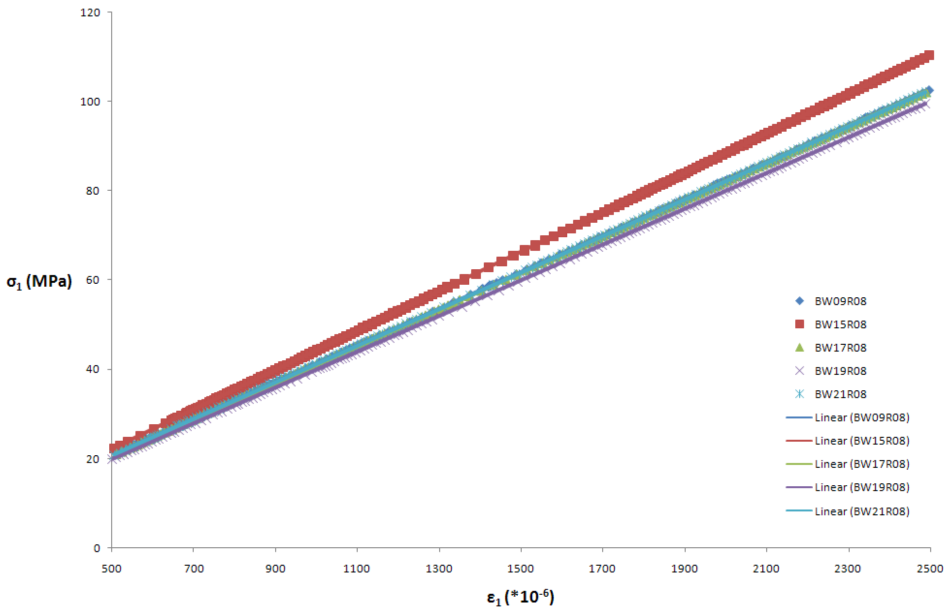

Fig. 11: Stress-strain curve of 5 coupons tested in tension in the fibres direction and linear curve fit: BW09R08, BW15R08, BW17R08, BW19R08 and BW21R08

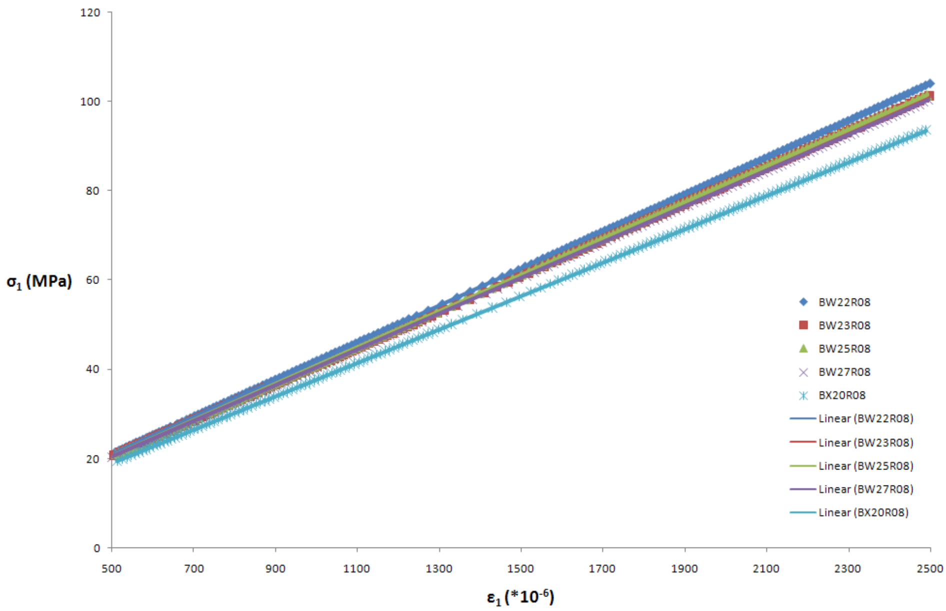

Fig. 12: Stress-strain curve of 5 coupons tested in tension in the fibres direction and linear curve fit: BW22R08, BW23R08, BW25R08, BW27R08 and BX20R08

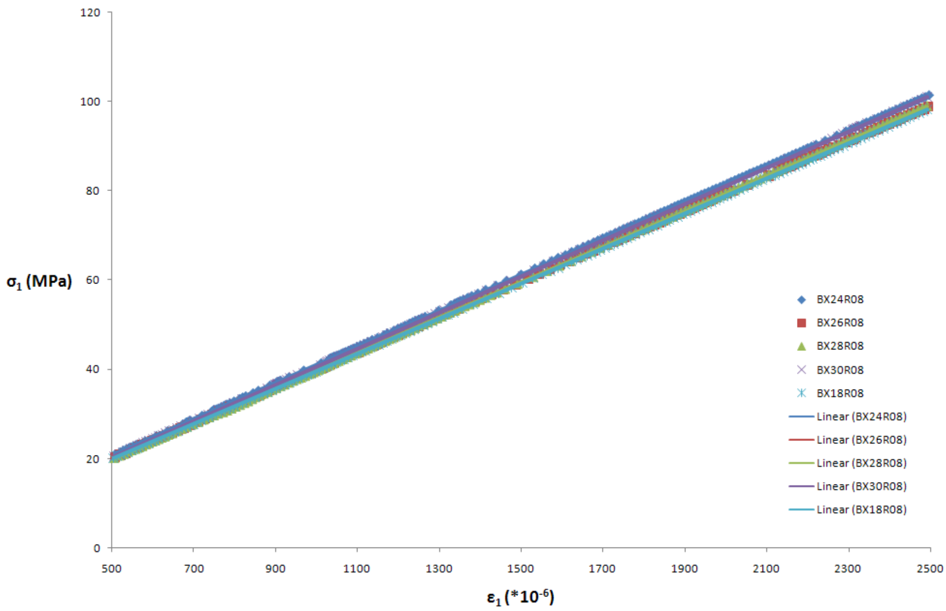

Fig. 13: Stress-strain curve of 5 coupons tested in tension in the fibres direction and linear curve fit: BX24R08, BX26R08, BX28R08, BX30R08 and BX18R08

8.1.3. Transverse strain-Axial strain graphs (500-2500 με)

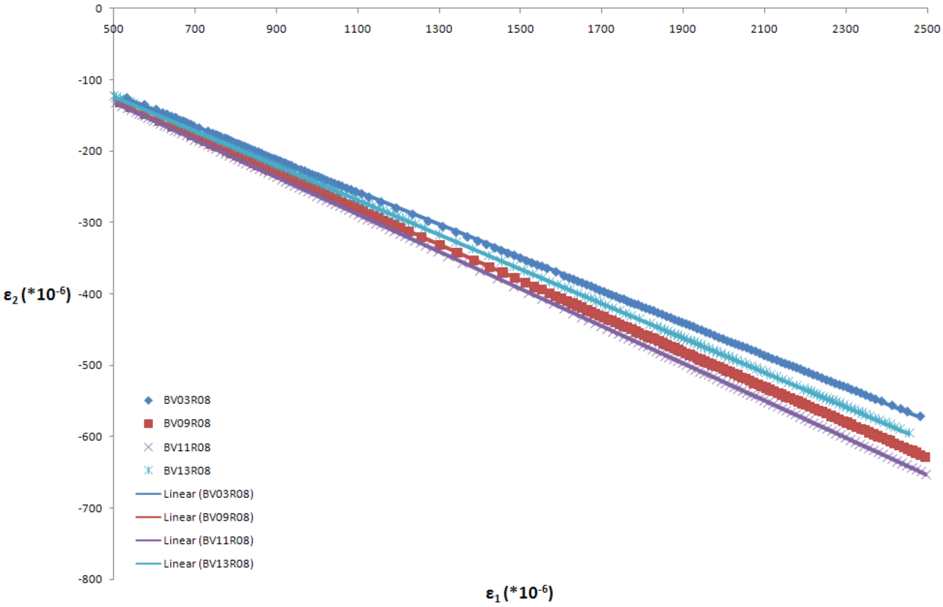

Fig. 14: Transverse strain-Axial strain curve of 4 coupons tested in tension in the fibres direction and linear curve fit: BV03R08, BV09R08, BV11R08 and BV13R08

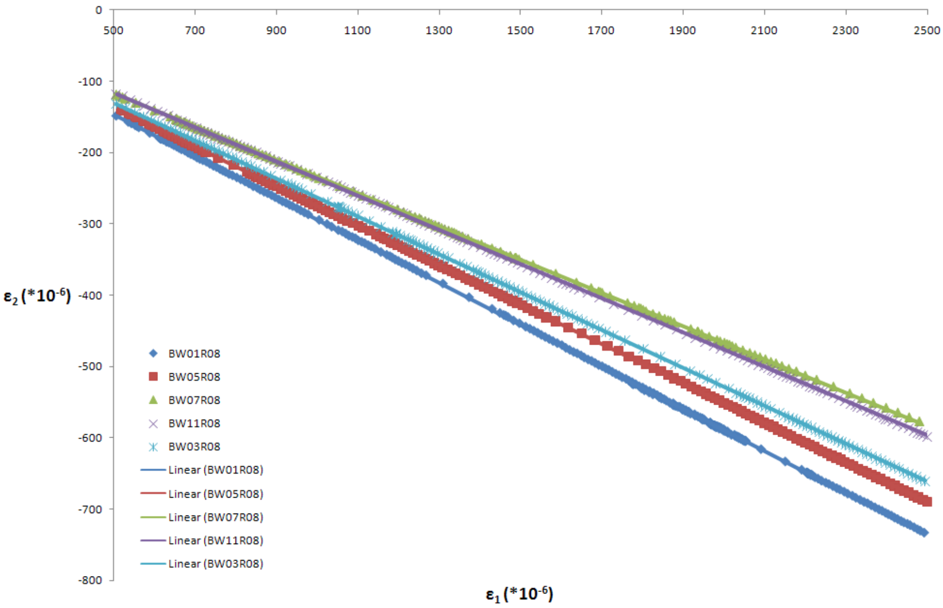

Fig. 15: Transverse strain-Axial strain curve of 5 coupons tested in tension in the fibres direction and linear curve fit: BW01R08, BW05R08, BW07R08, BW11R08 and BW03R08

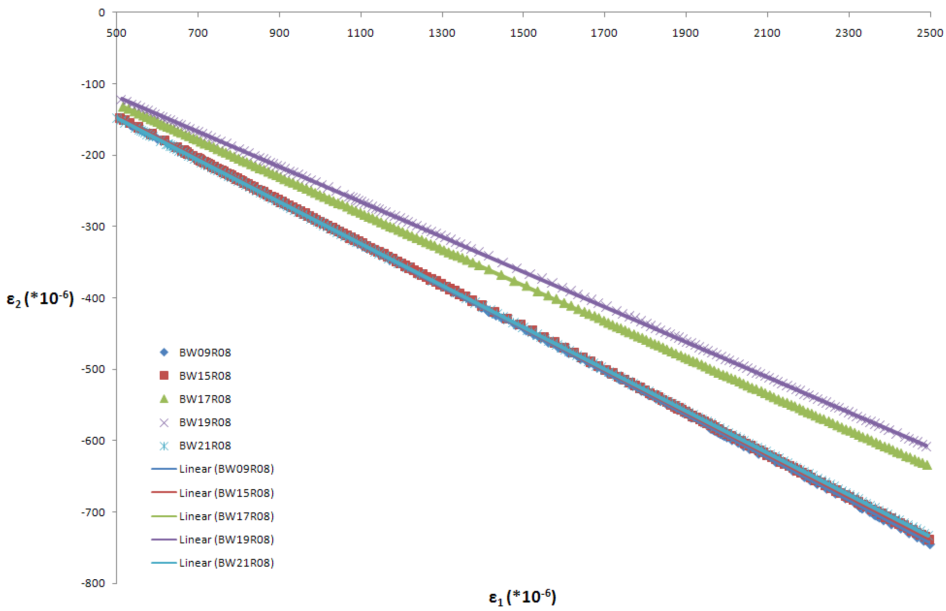

Fig. 16: Transverse strain-Axial strain curve of 5 coupons tested in tension in the fibres direction and linear curve fit: BW09R08, BW15R08, BW17R08, BW19R08 and BW21R08

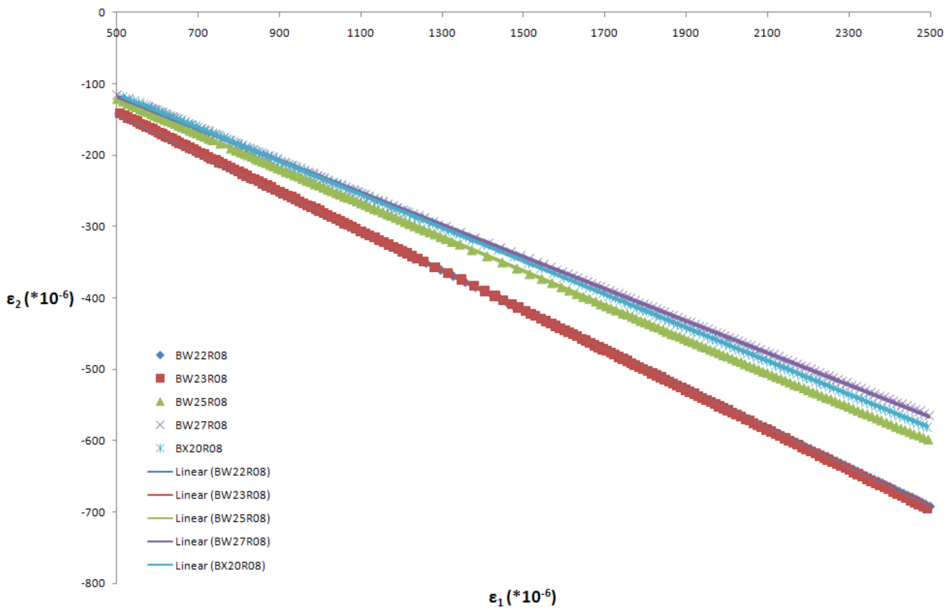

Fig. 17: Transverse strain-Axial strain curve of 5 coupons tested in tension in the fibres direction and linear curve fit: BW22R08, BW23R08, BW25R08, BW27R08 and BX20R08

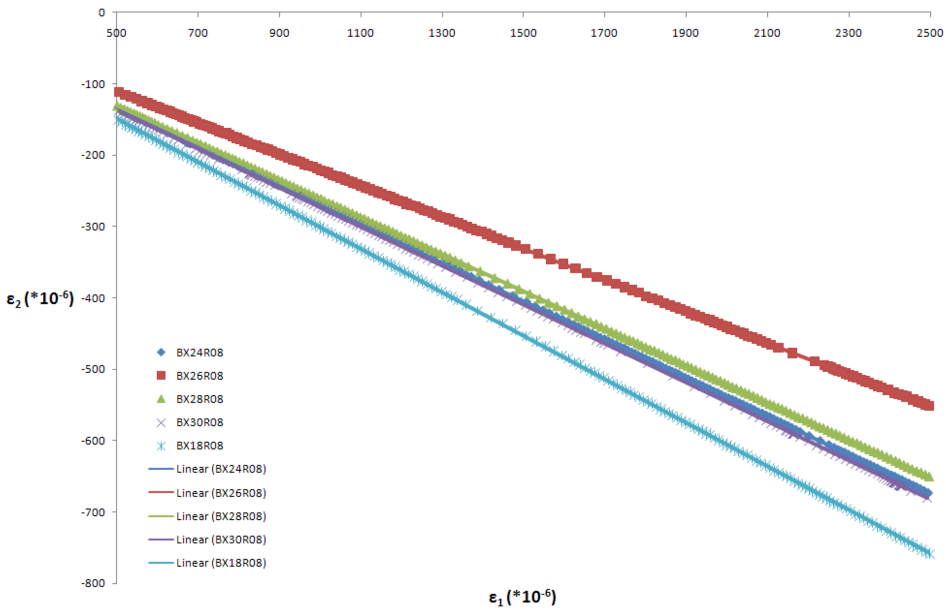

Fig. 18: Transverse strain-Axial strain curve of 5 coupons tested in tension in the fibres direction and linear curve fit: BX24R08, BX26R08, BX28R08, BX30R08 and BX18R08

8.1.4. Photographs of tested coupons

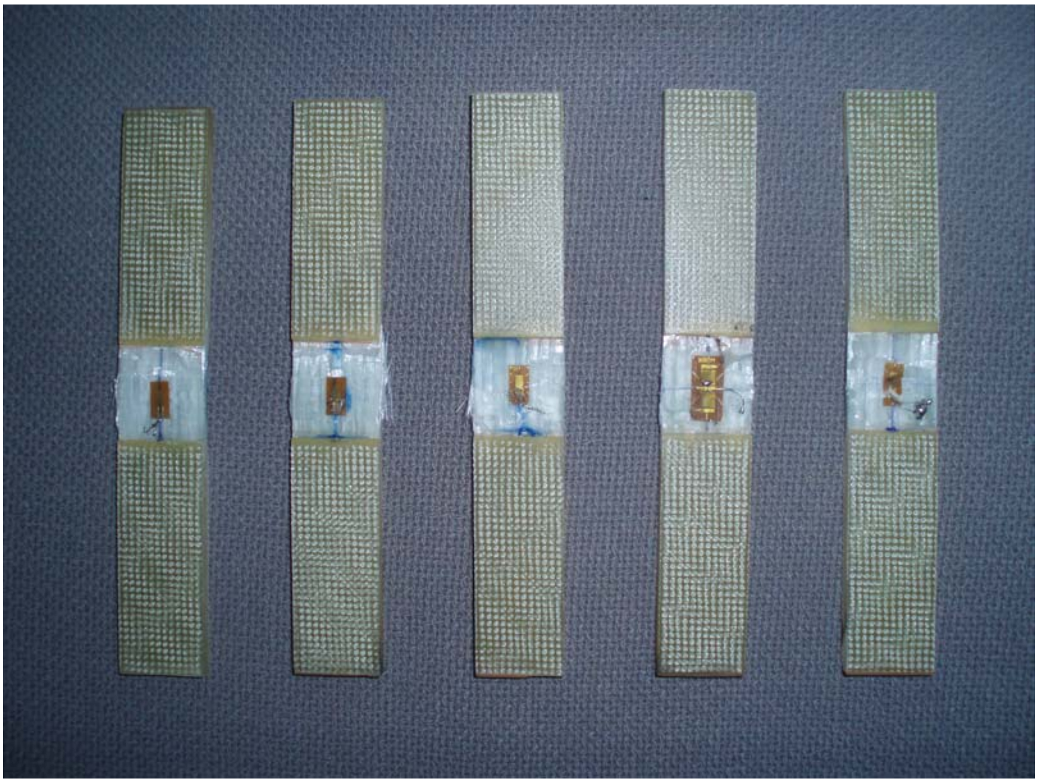

Fig. 19: Photo of the tested coupons BV03R08, BV09R08, BV10R08, BV11R08 and BV13R08 (from left to right)

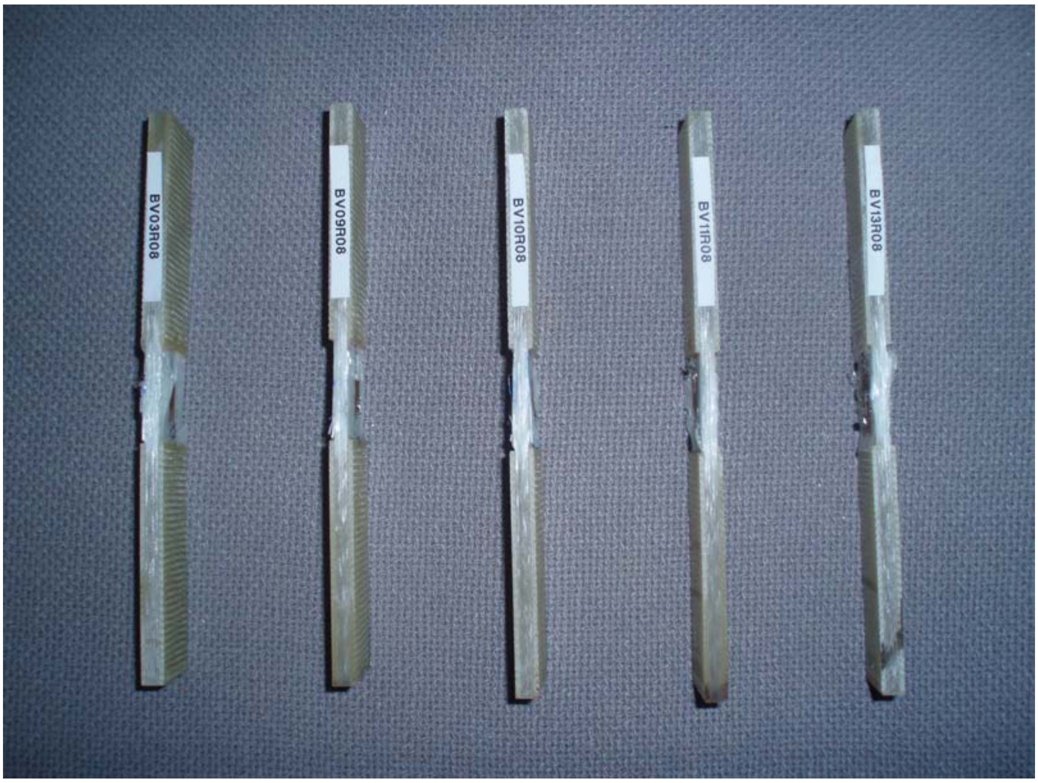

Fig. 20: Photo of the tested coupons BV03R08, BV09R08, BV10R08, BV11R08 and BV13R08 (from left to right)

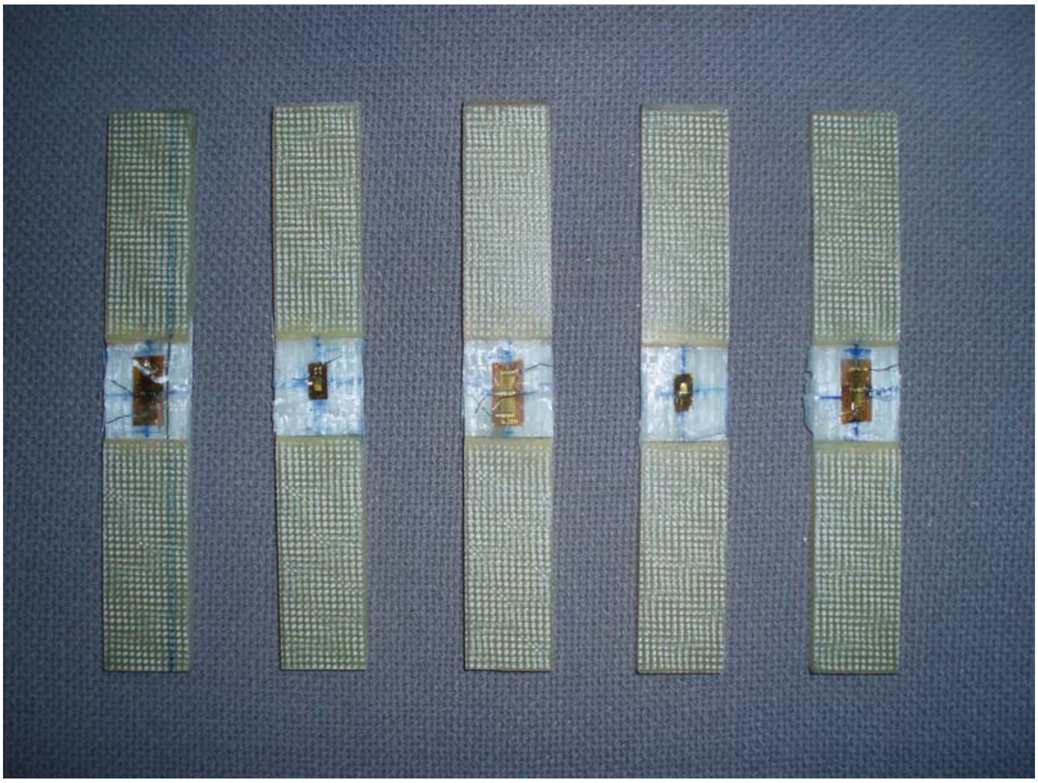

Fig. 21: Photo of the tested coupons BW01R08, BW05R08, BW07R08, BW11R08 and BW03R08 (from left to right)

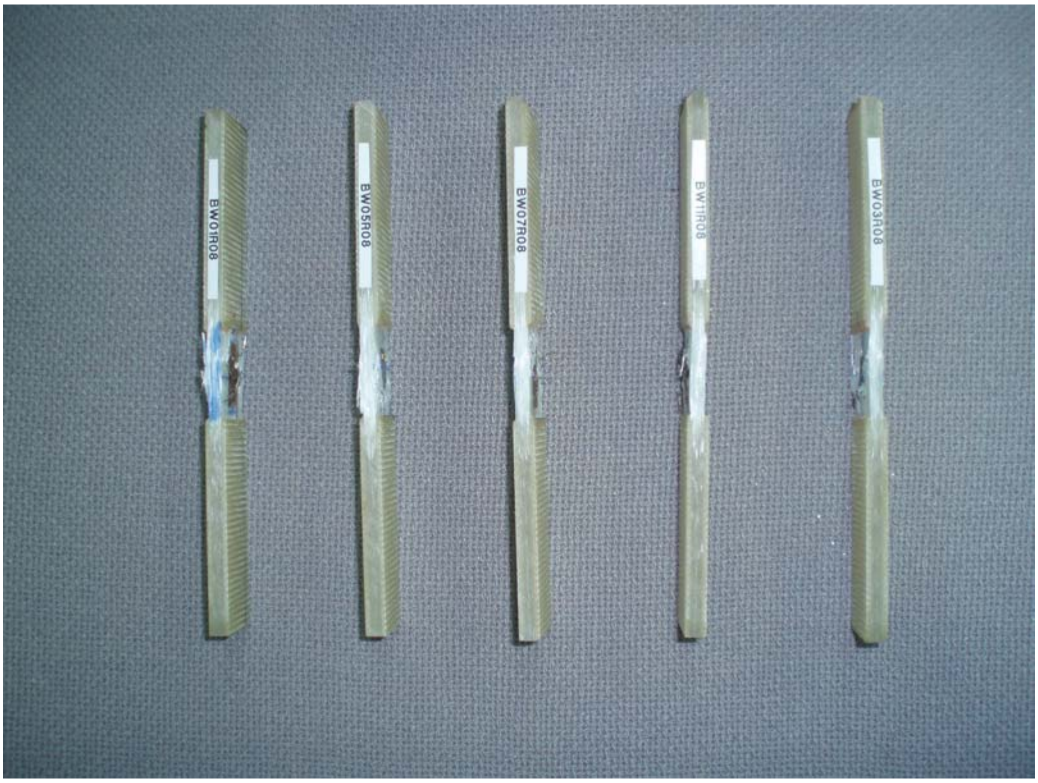

Fig. 22: Photo of the tested coupons BW01R08, BW05R08, BW07R08, BW11R08 and BW03R08 (from left to right)

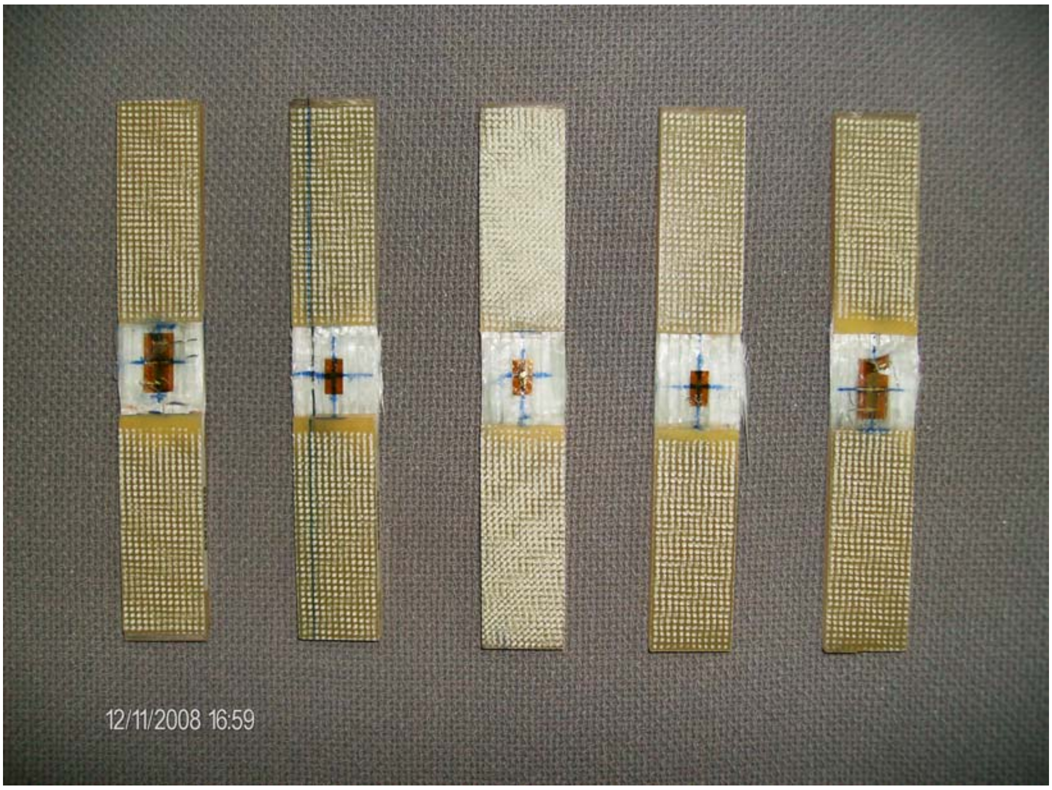

Fig. 23: Photo of the tested coupons BW09R08, BW15R08, BW17R08, BW19R08 and BW21R08 (from left to right)

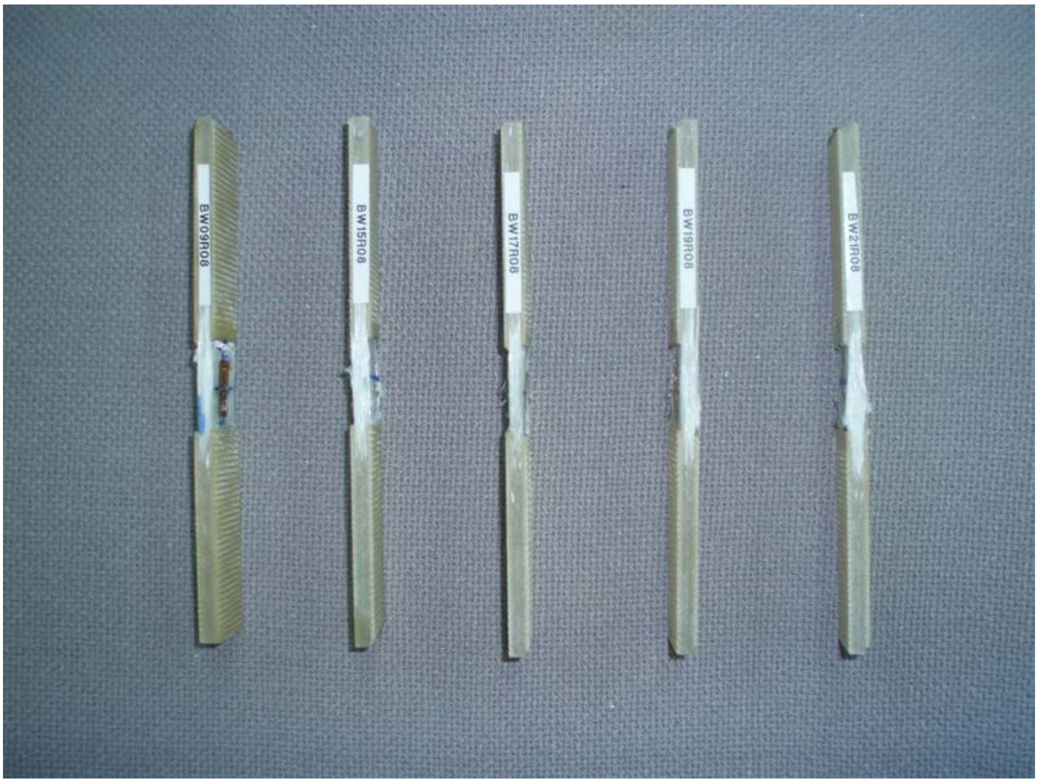

Fig. 24: Photo of the tested coupons BW09R08, BW15R08, BW17R08, BW19R08 and BW21R08 (from left to right)

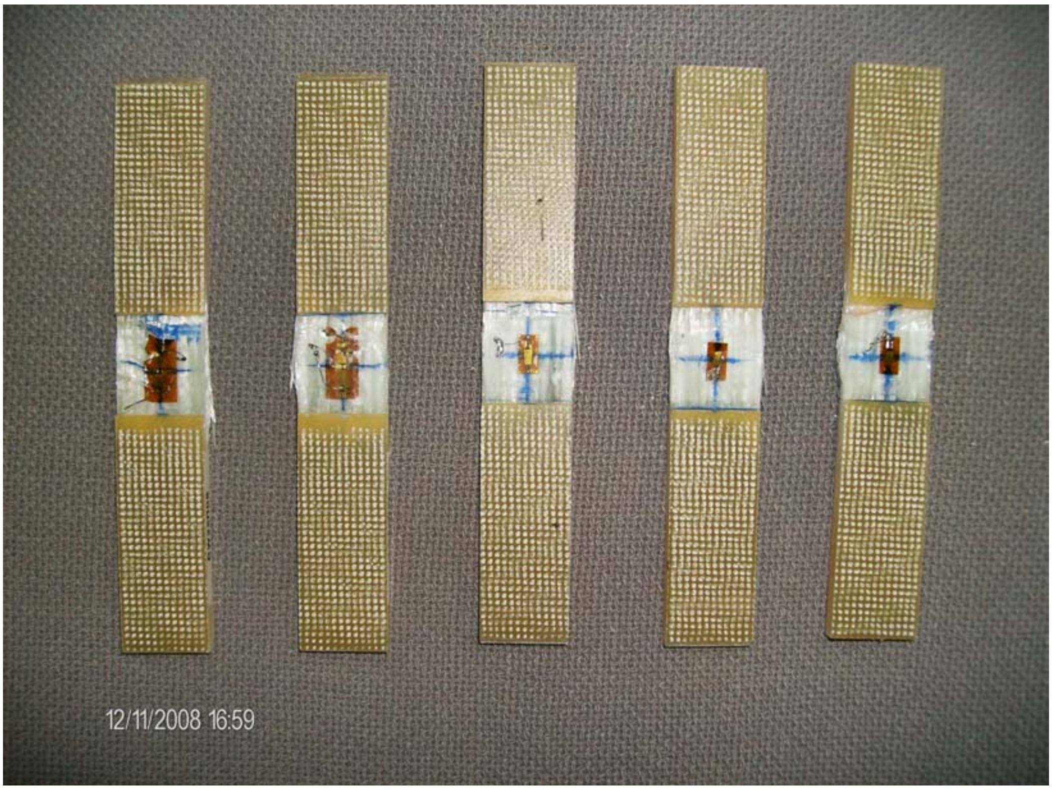

Fig. 25: Photo of the tested coupons BW22R08, BW23R08, BW25R08, BW27R08 and BX20R08 (from left to right)

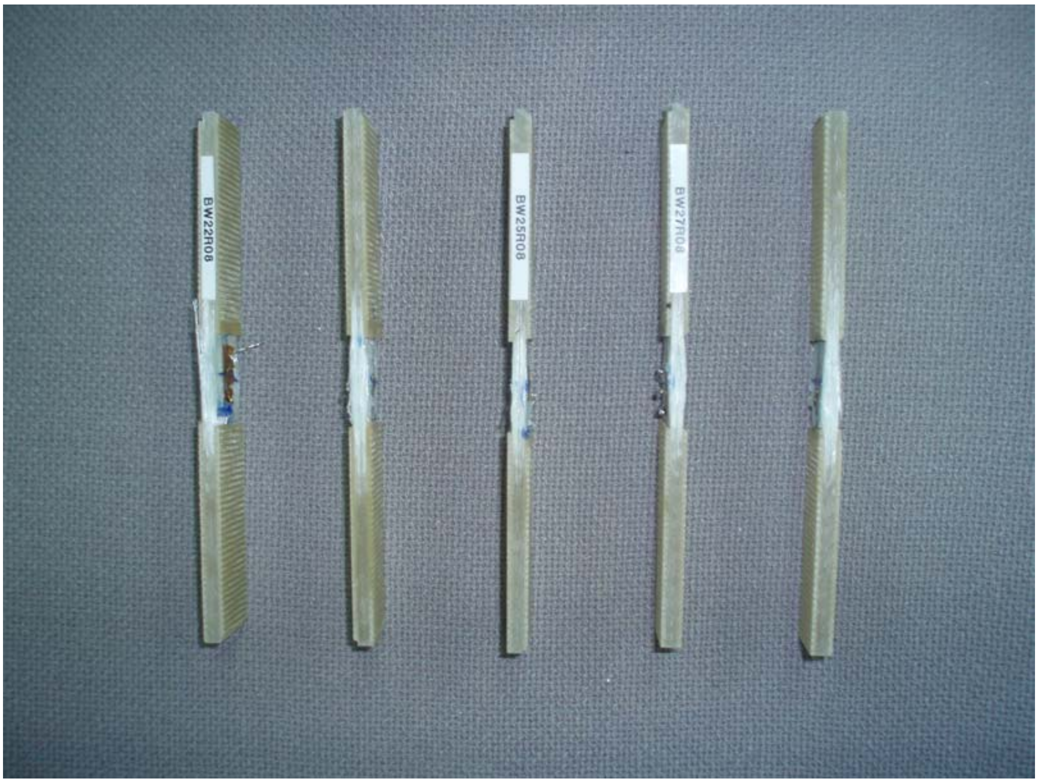

Fig. 26: Photo of the tested coupons BW22R08, BW23R08, BW25R08, BW27R08 and BX20R08 (from left to right)

Fig. 27: Photo of the tested coupons BX24R08, BX26R08, BX28R08, BX30R08 and BX18R08 (from left to right)

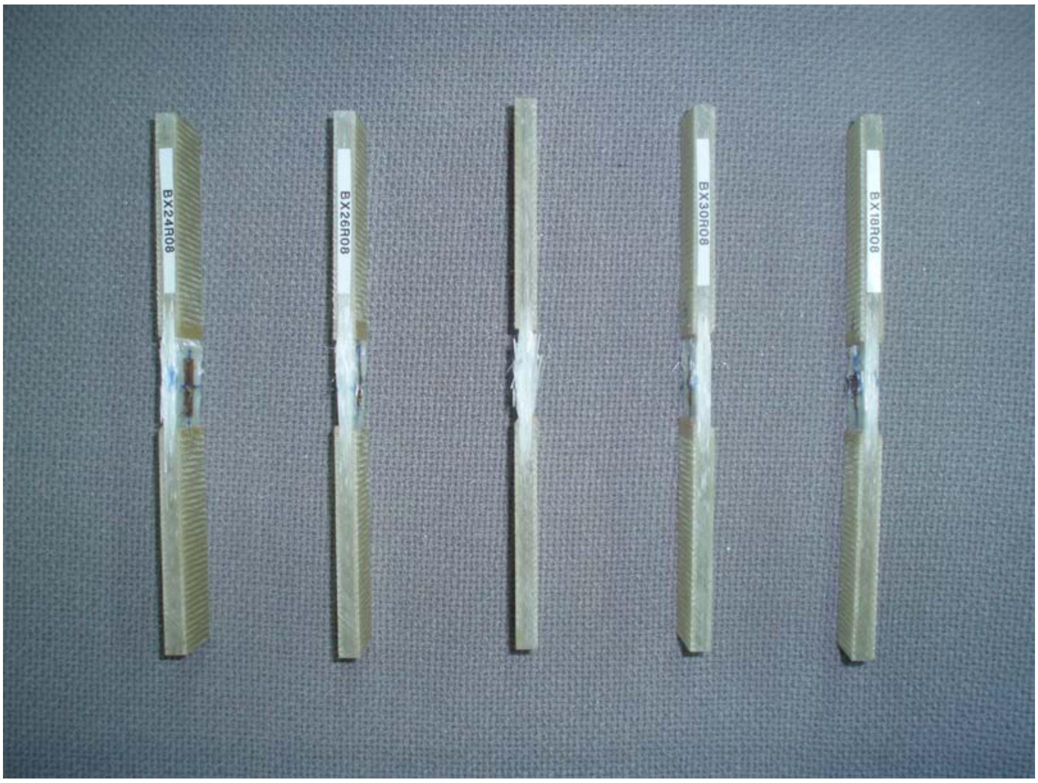

Fig. 28: Photo of the tested coupons BX24R08, BX26R08, BX28R08, BX30R08 and BX18R08 (from left to right)

8.2. Compressive UD tests parallel to the fibres

8.2.1. Stress-strain graphs

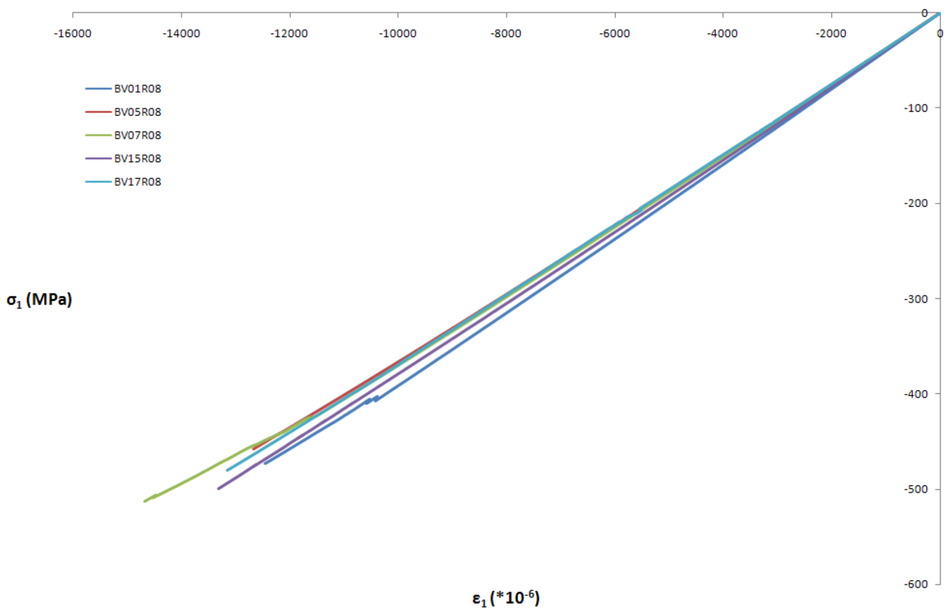

Fig. 29: Stress-strain curve of 5 coupons tested in compression in the fibres direction: BV01R08, BV05R08, BV07R08, BV15R08 and BV17R08

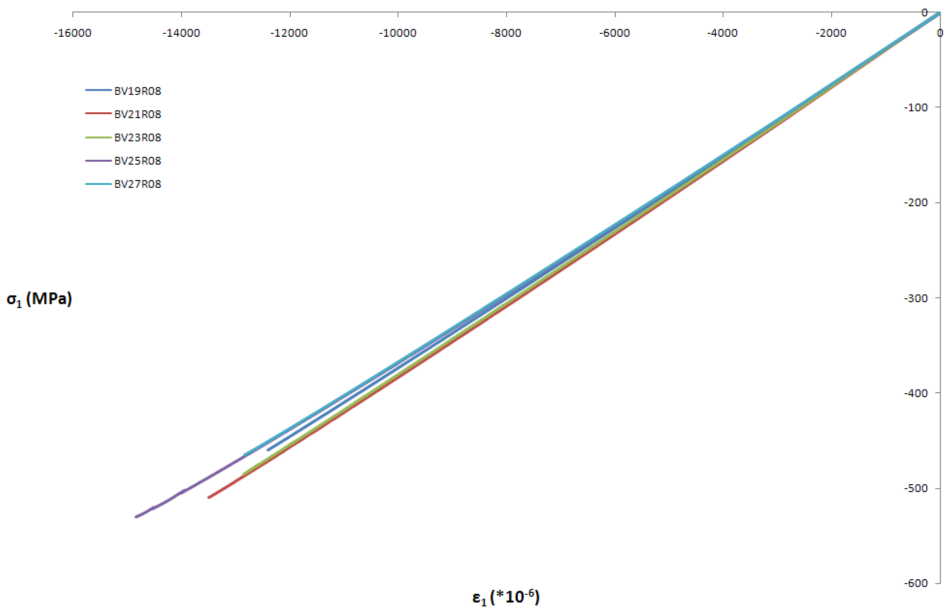

Fig. 30: Stress-strain curve of 5 coupons tested in compression in the fibres direction: BV19R08, BV21R08, BV23R08, BV25R08 and BV27R08

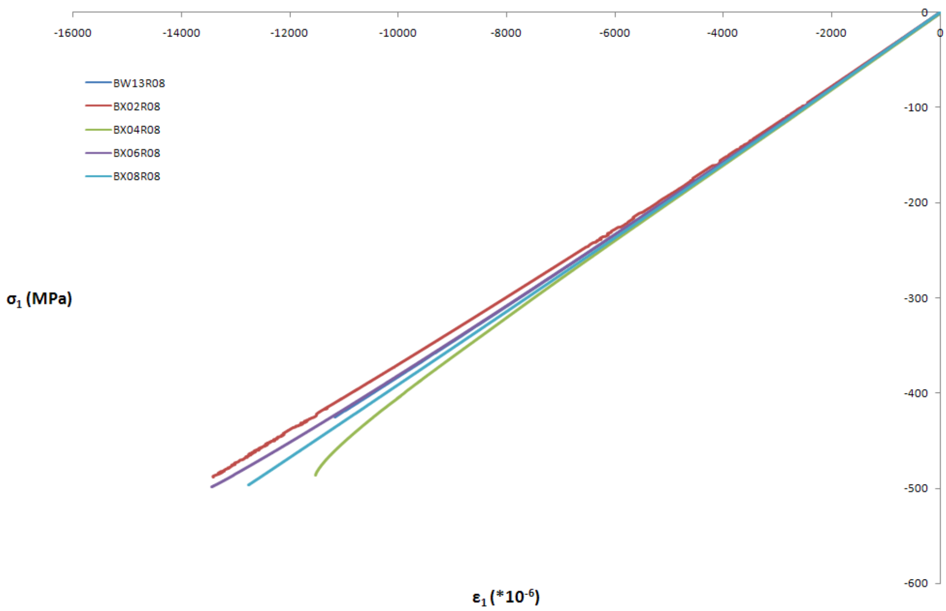

Fig. 31: Stress-strain curve of 5 coupons tested in compression in the fibres direction: BW13R08, BX02R08, BX04R08, BX06R08 and BX08R08

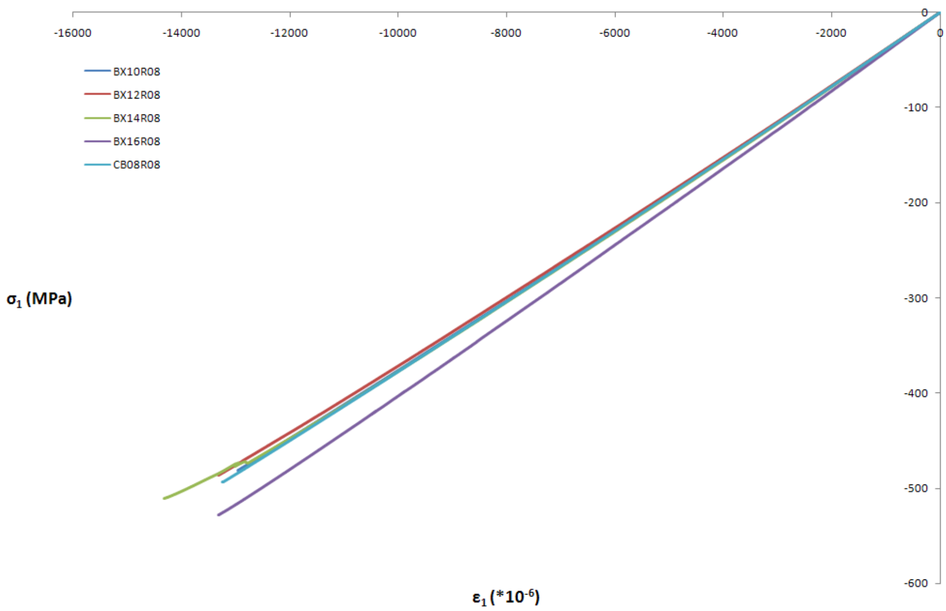

Fig. 32: Stress-strain curve of 5 coupons tested in compression in the fibres direction: BX10R08, BX12R08, BX14R08, BX16R08 and CB08R08

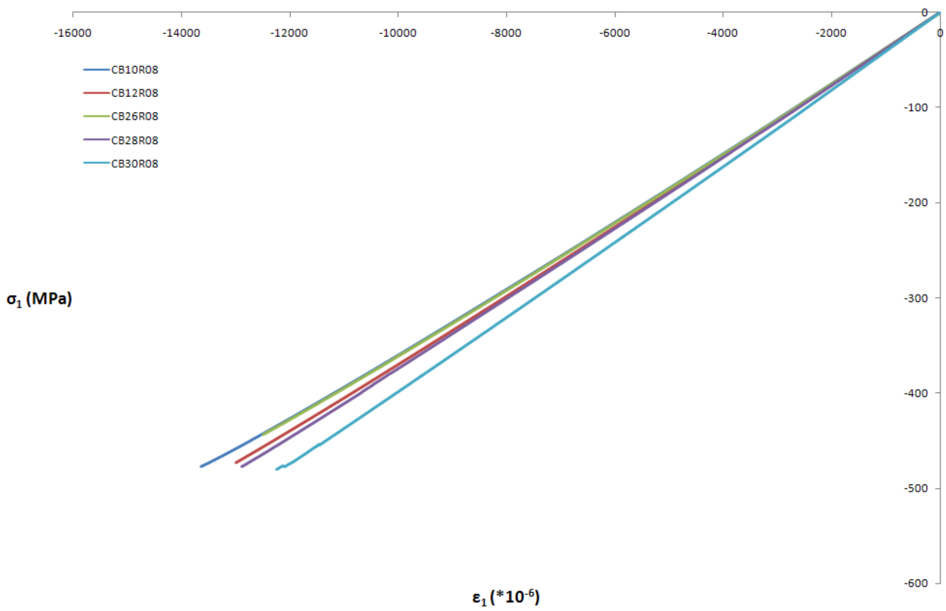

Fig. 33: Stress-strain curve of 5 coupons tested in compression in the fibres direction: CB10R08, CB12R08, CB26R08, CB28R08 and CB30R08

8.2.2. Stress-strain graphs (500-2500 με)

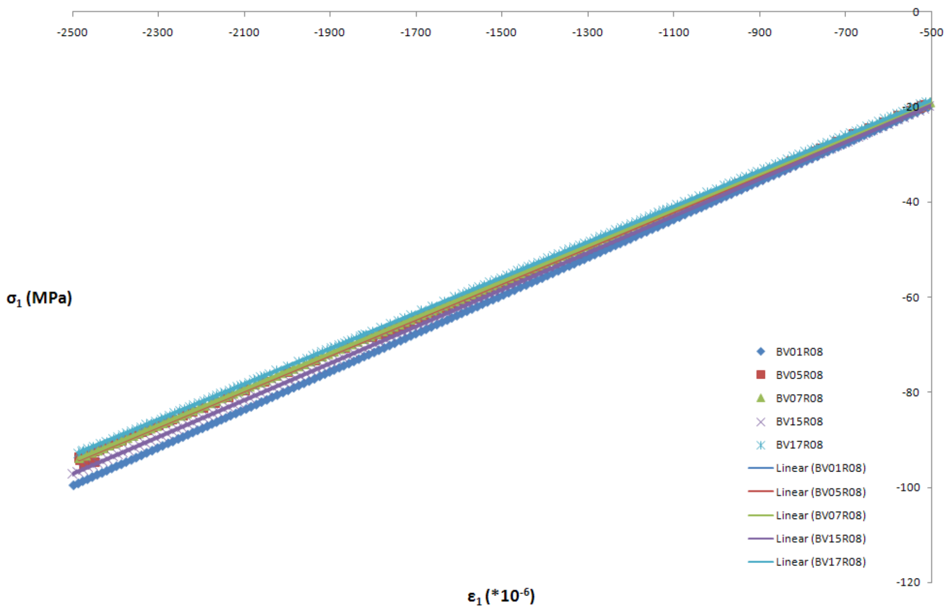

Fig. 34: Stress-strain curve of 5 coupons tested in compression in the fibres direction and linear curve fit: BV01R08, BV05R08, BV07R08, BV15R08 and BV17R08

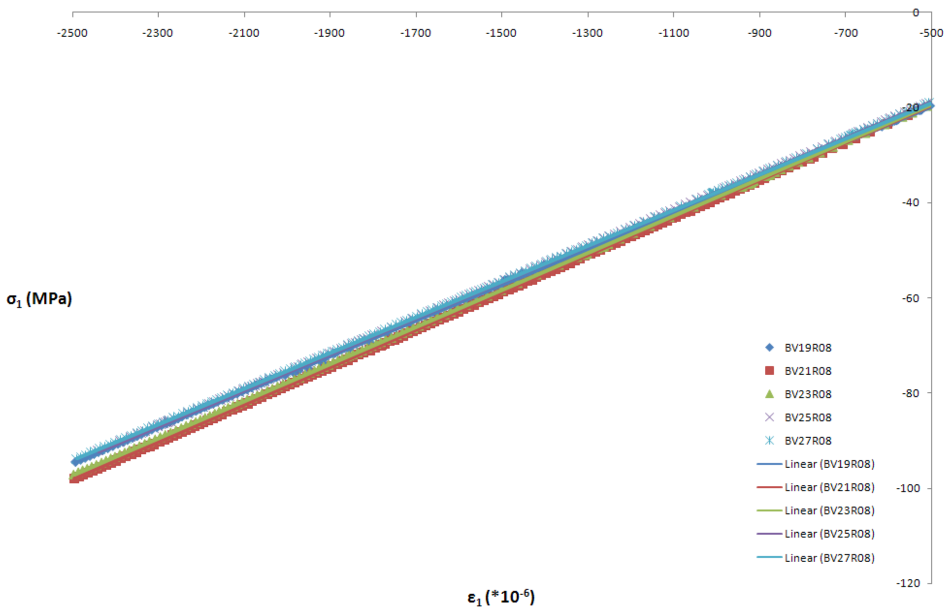

Fig. 35: Stress-strain curve of 5 coupons tested in compression in the fibres direction and linear curve fit: BV19R08, BV21R08, BV23R08, BV25R08 and BV27R08

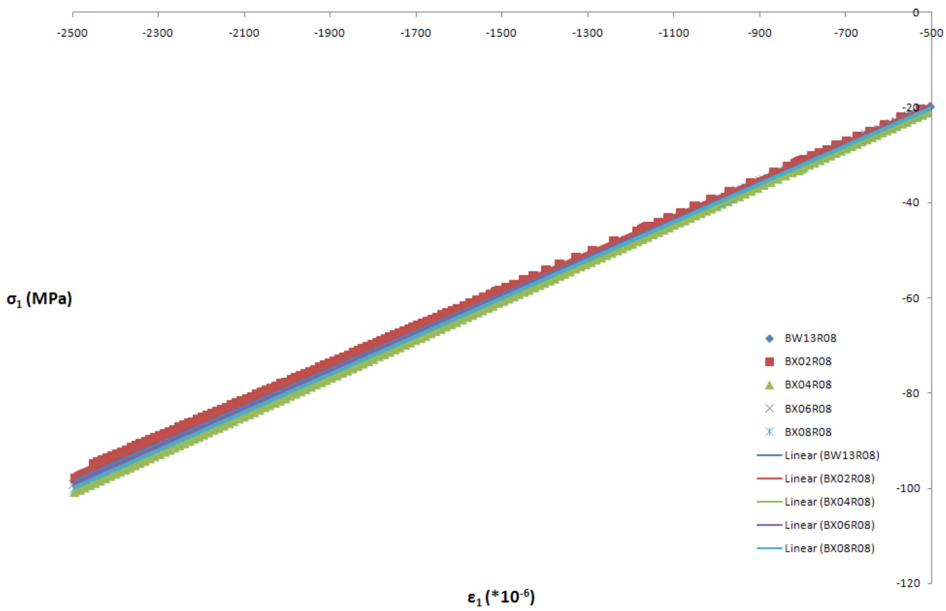

Fig. 36: Stress-strain curve of 5 coupons tested in compression in the fibres direction and linear curve fit: BW13R08, BX02R08, BX04R08, BX06R08 and BX08R08

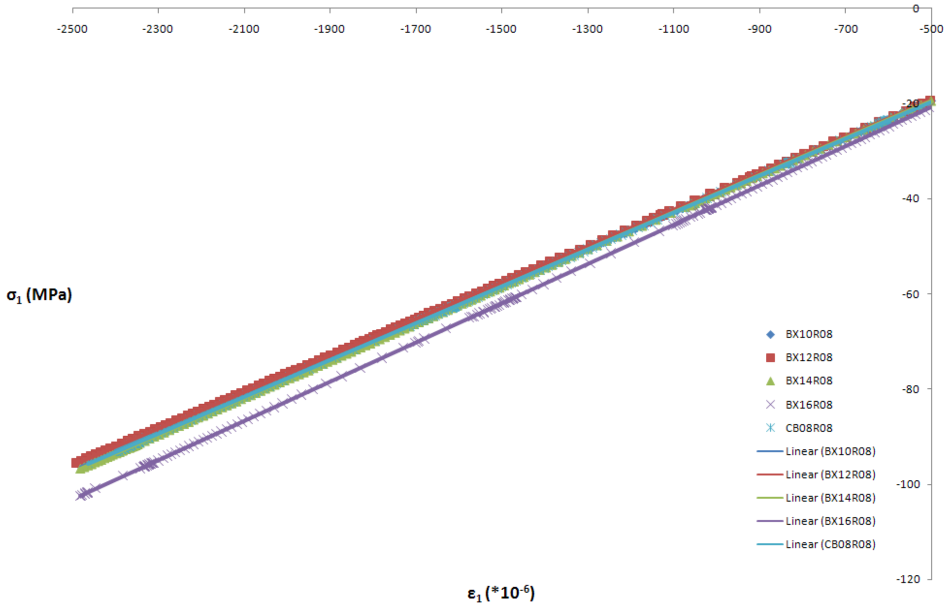

Fig. 37: Stress-strain curve of 5 coupons tested in compression in the fibres direction and linear curve fit: BX10R08, BX12R08, BX14R08, BX16R08 and CB08R08

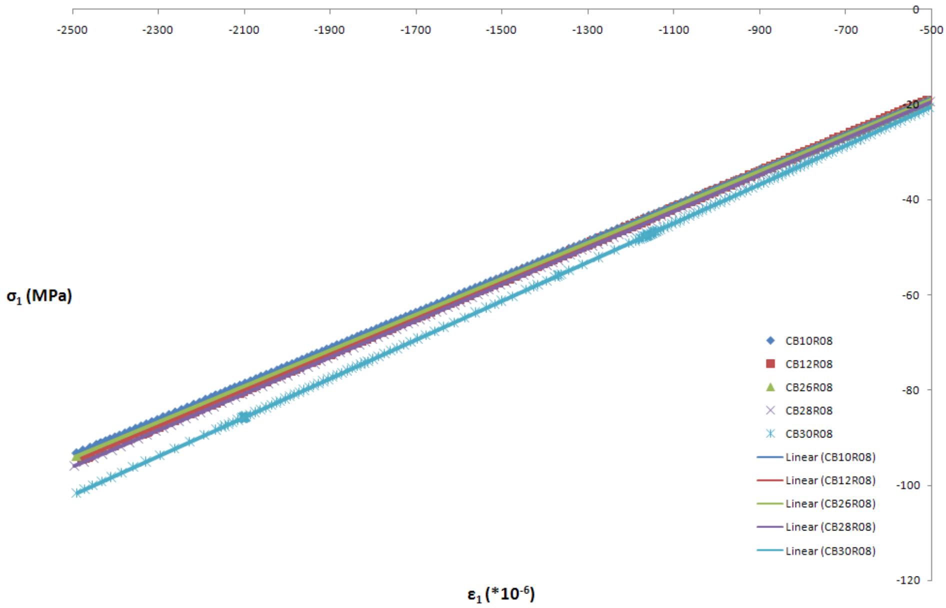

Fig. 38: Stress-strain curve of 5 coupons tested in compression in the fibres direction and linear curve fit: CB10R08, CB12R08, CB26R08, CB28R08 and CB30R08

8.2.3. Bending strain-Axial stress graphs

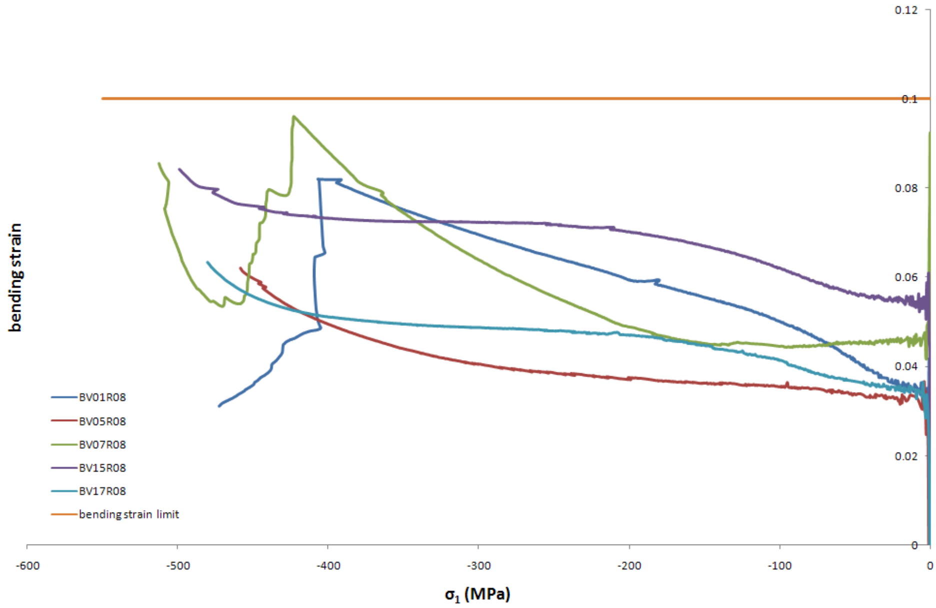

Fig. 39: Bending strain-Axial stress curve of 5 coupons tested in compression in the fibres direction: BV01R08, BV05R08, BV07R08, BV15R08 and BV17R08

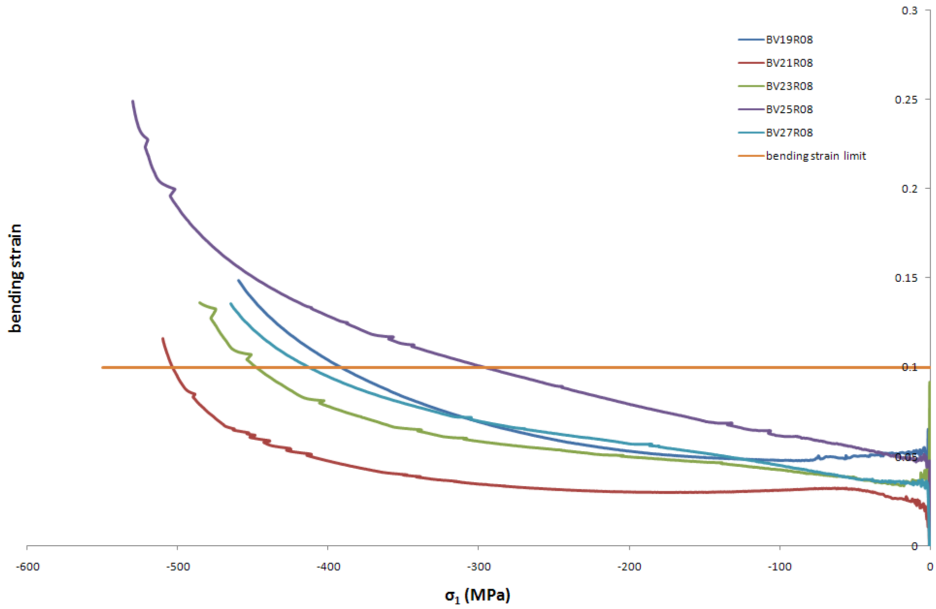

Fig. 40: Bending strain-Axial stress curve of 5 coupons tested in compression in the fibres direction: BV19R08, BV21R08, BV23R08, BV25R08 and BV27R08

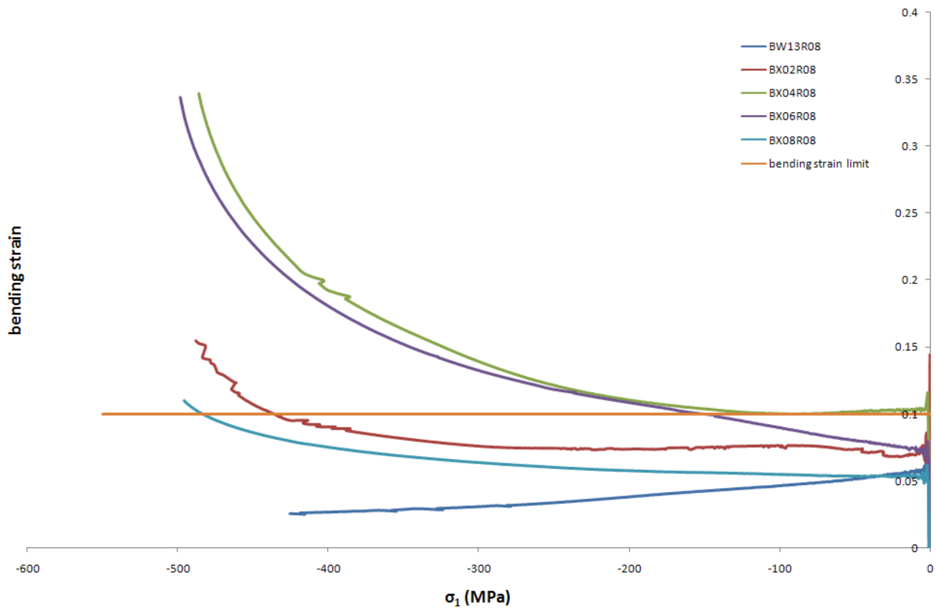

Fig. 41: Bending strain-Axial stress curve of 5 coupons tested in compression in the fibres direction: BW13R08, BX02R08, BX04R08, BX06R08 and BX08R08

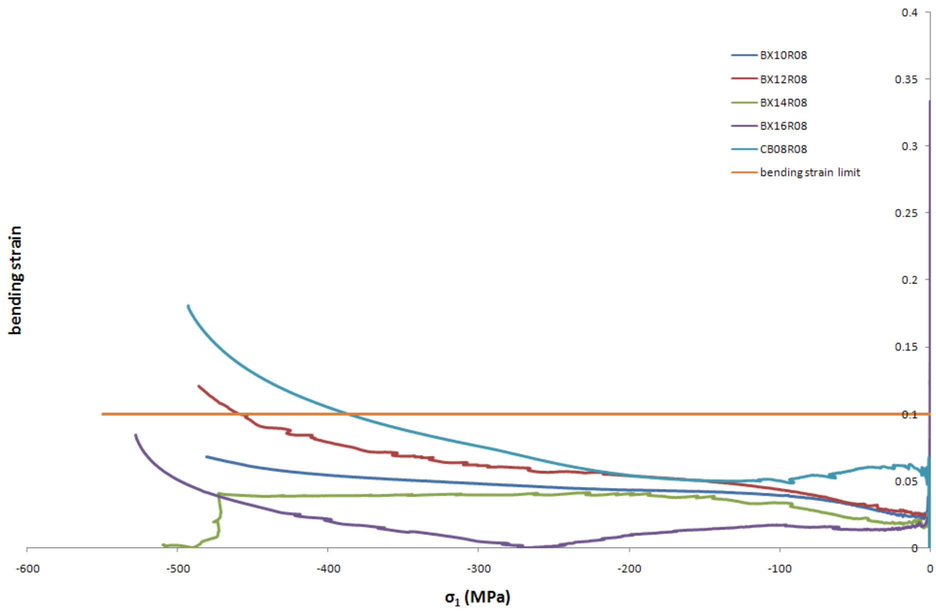

Fig. 42: Bending strain-Axial stress curve of 5 coupons tested in compression in the fibres direction: BX10R08, BX12R08, BX14R08, BX16R08 and CB08R08

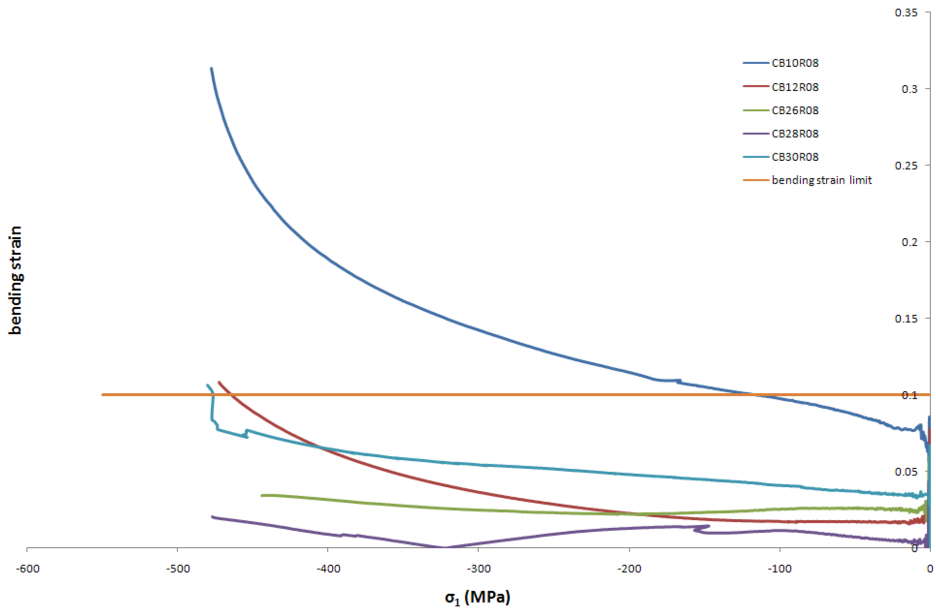

Fig. 43: Bending strain-Axial stress curve of 5 coupons tested in compression in the fibres direction: CB10R08, CB12R08, CB26R08, CB28R08 and CB30R08

8.2.4. Photographs of tested coupons

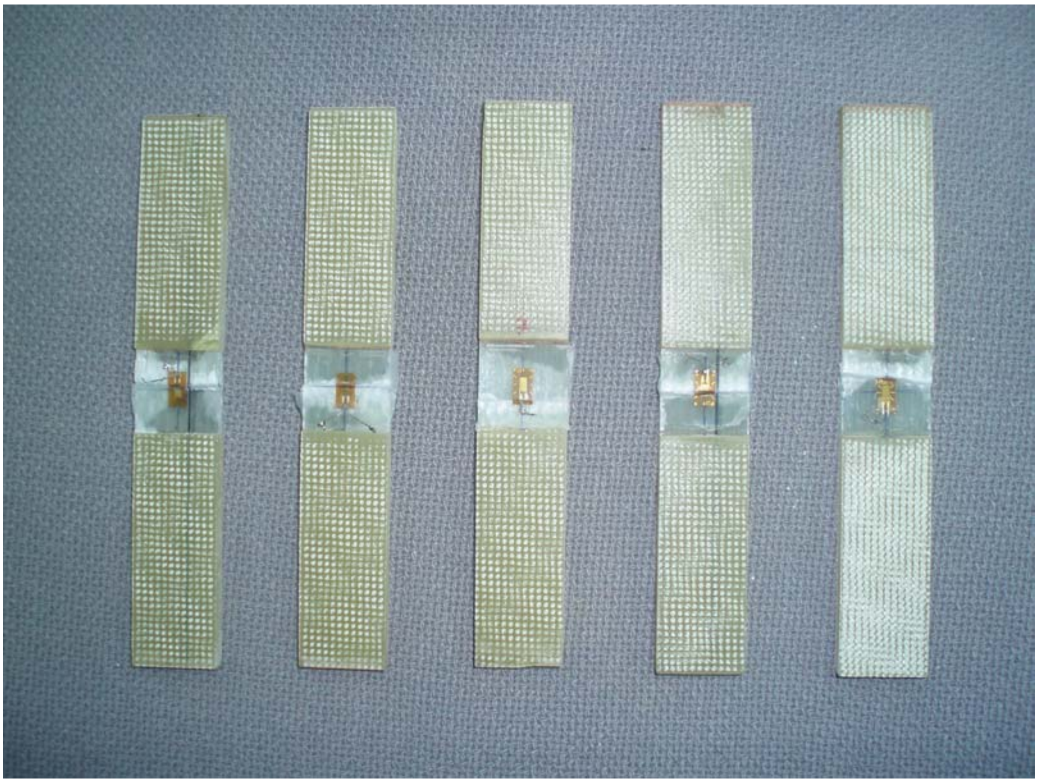

Fig. 44: Photo of the tested coupons BV01R08, BV05R08, BV07R08, BV15R08 and BV17R08 (from left to right)

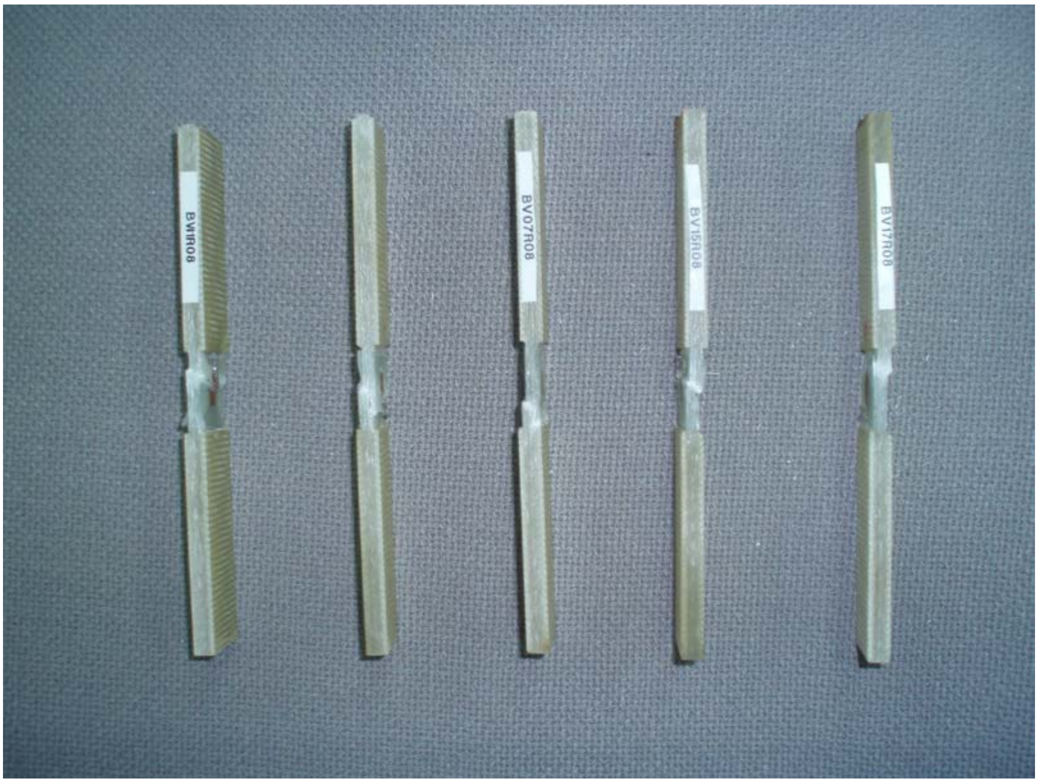

Fig. 45: Photo of the tested coupons BV01R08, BV05R08, BV07R08, BV15R08 and BV17R08 (from left to right)

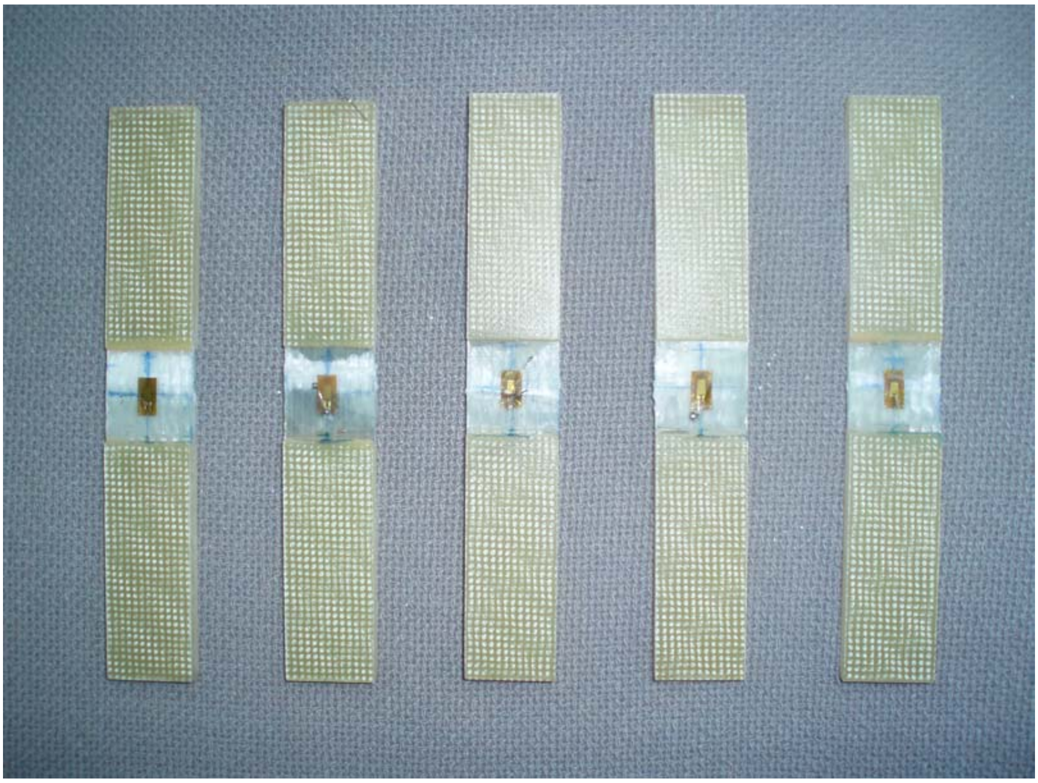

Fig. 46: Photo of the tested coupons BV19R08, BV21R08, BV23R08, BV25R08 and BV27R08 (from left to right)

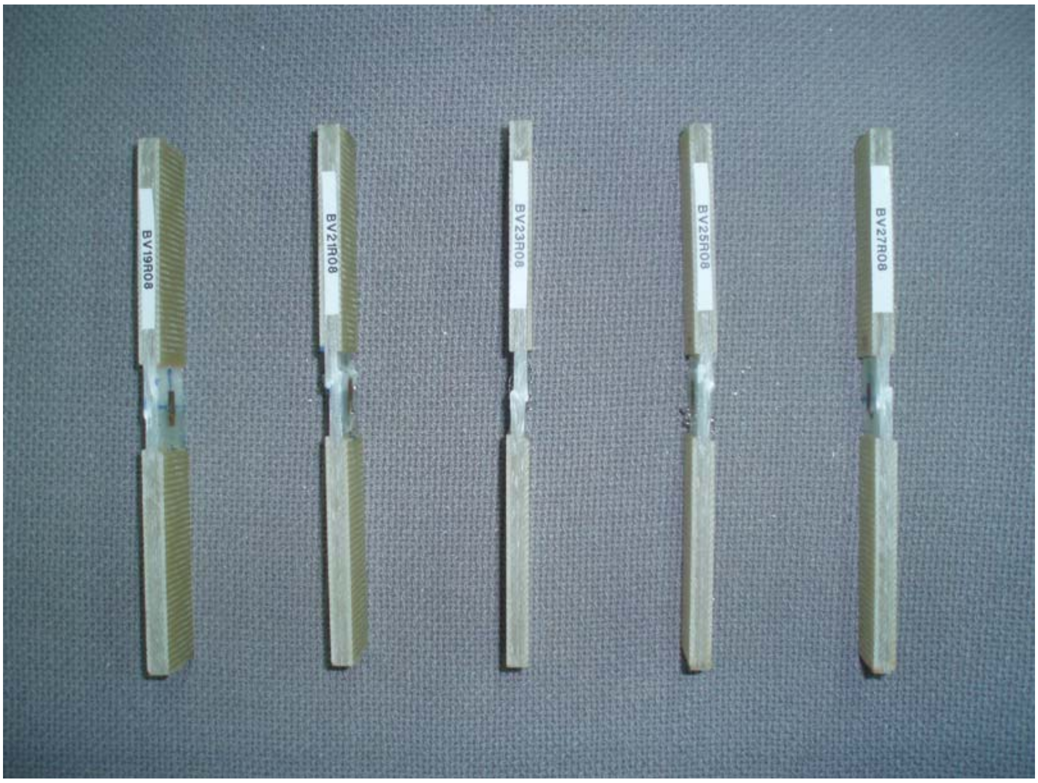

Fig. 47: Photo of the tested coupons BV19R08, BV21R08, BV23R08, BV25R08 and BV27R08 (from left to right)

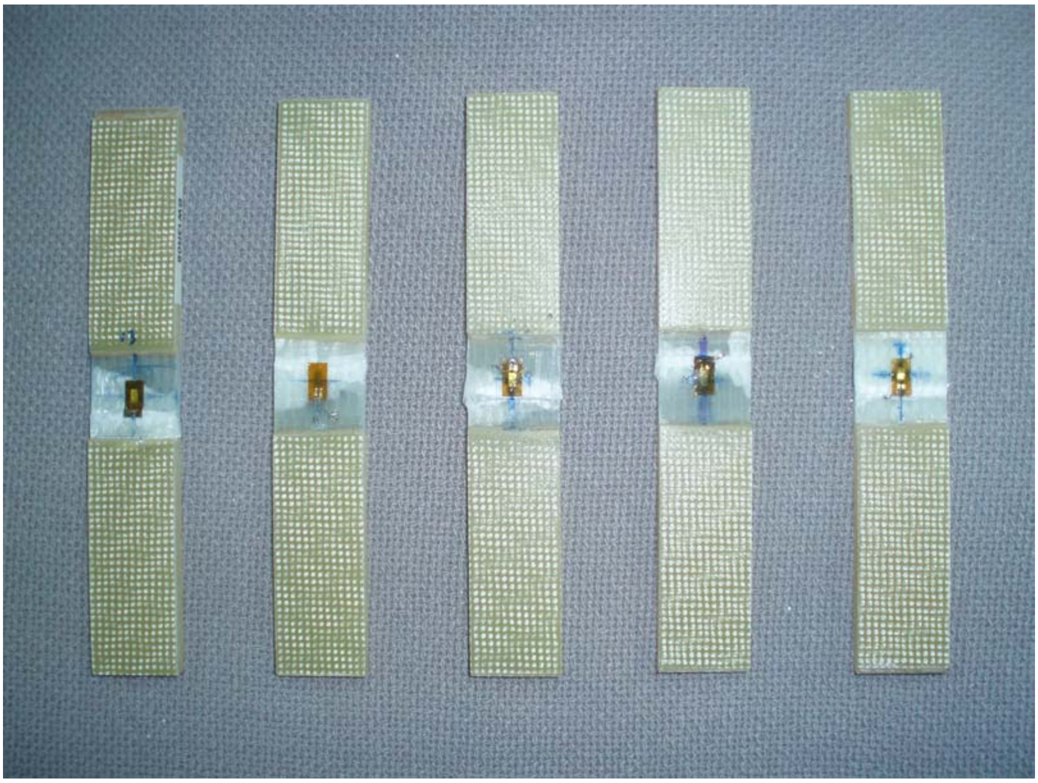

Fig. 48: Photo of the tested coupons BW13R08, BX02R08, BX04R08, BX06R08 and BX08R08 (from left to right)

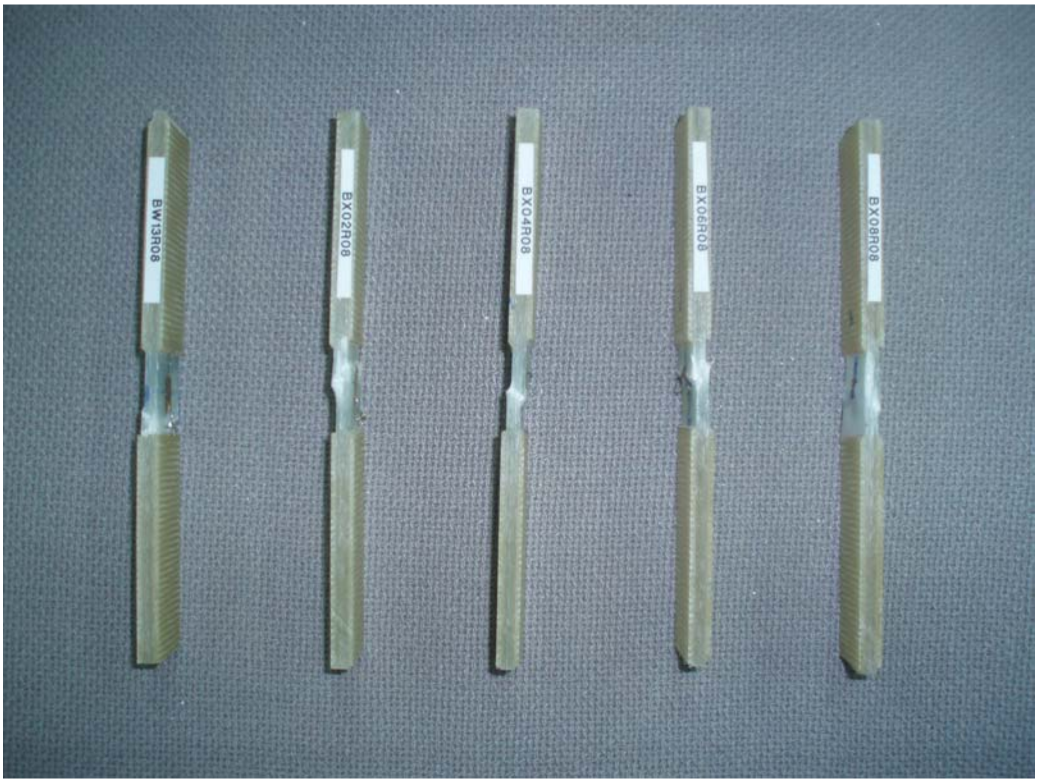

Fig. 49: Photo of the tested coupons BW13R08, BX02R08, BX04R08, BX06R08 and BX08R08 (from left to right)

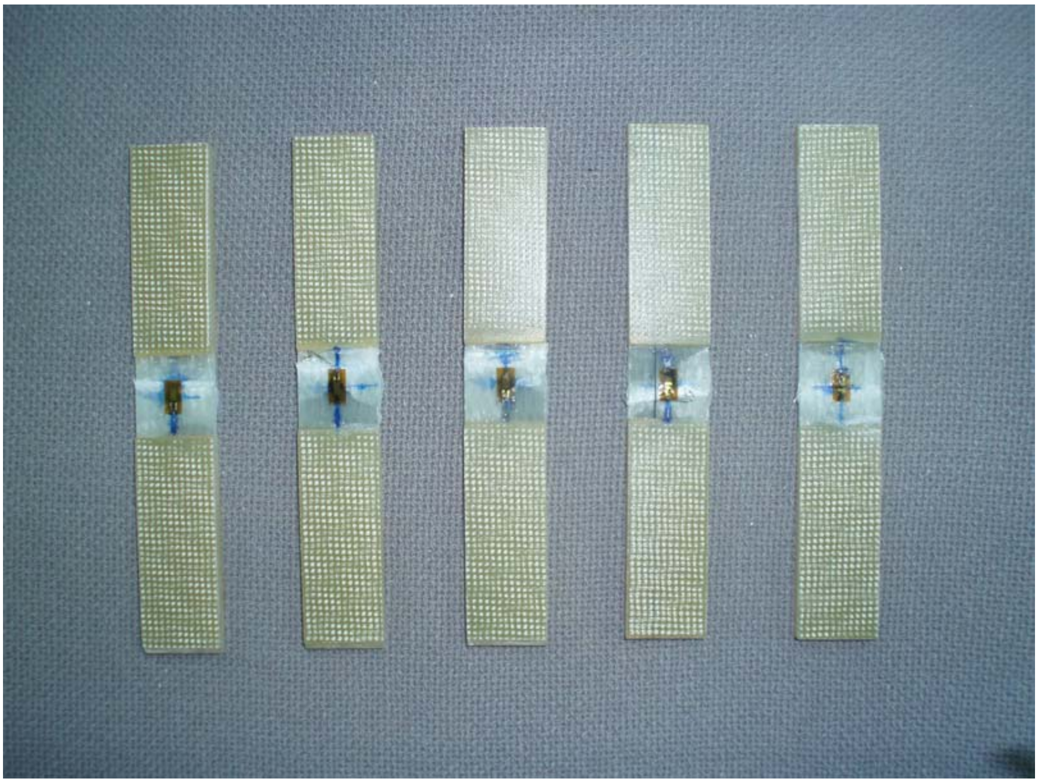

Fig. 50: Photo of the tested coupons BX10R08, BX12R08, BX14R08, BX16R08 and CB08R08 (from left to right)

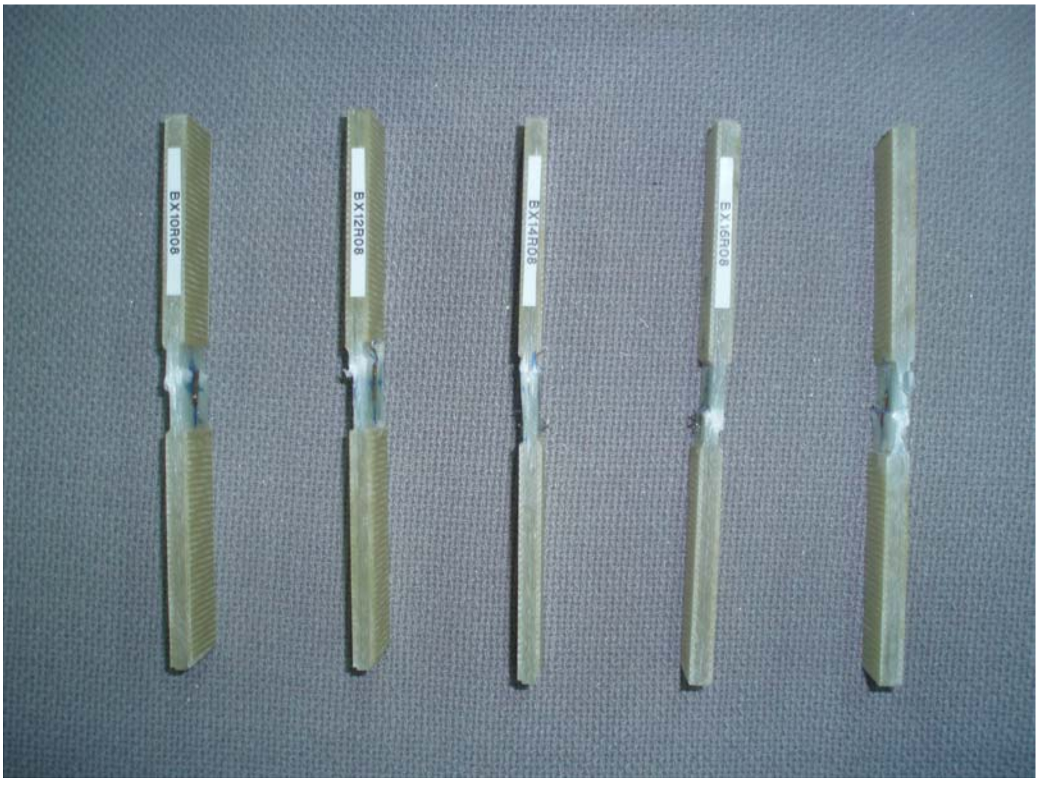

Fig. 51: Photo of the tested coupons BX10R08, BX12R08, BX14R08, BX16R08 and CB08R08 (from left to right)

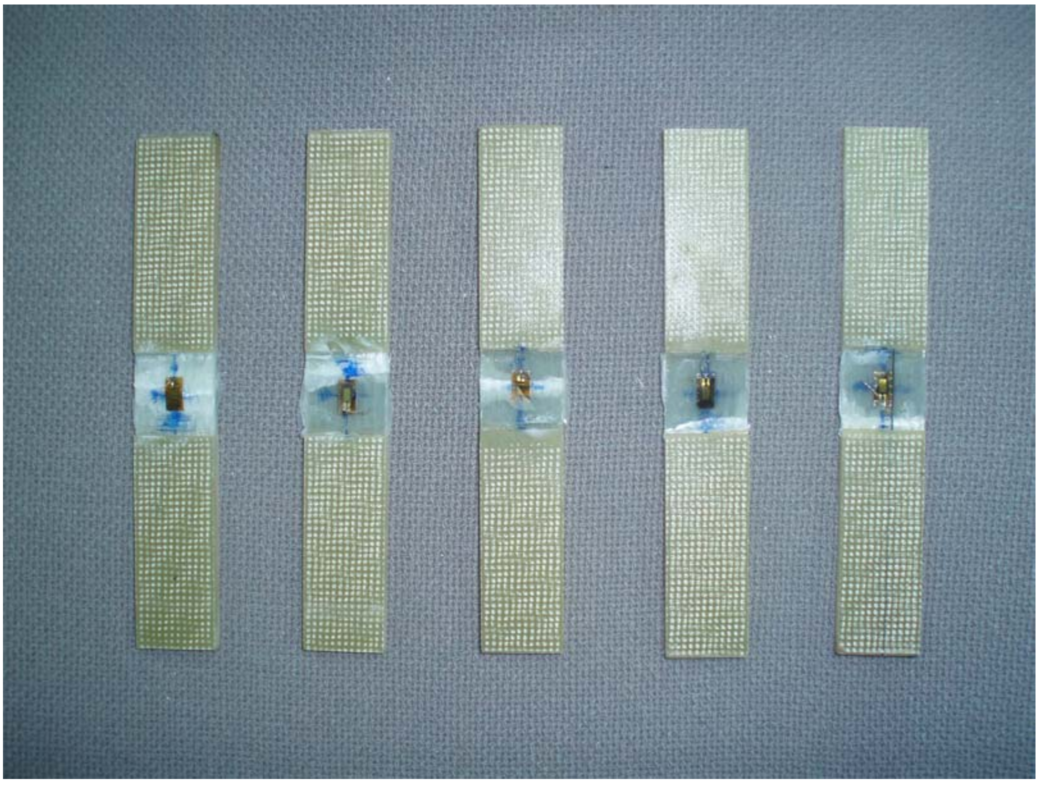

Fig. 52: Photo of the tested coupons CB10R08, CB12R08, CB26R08, CB28R08 and CB30R08 (from left to right)

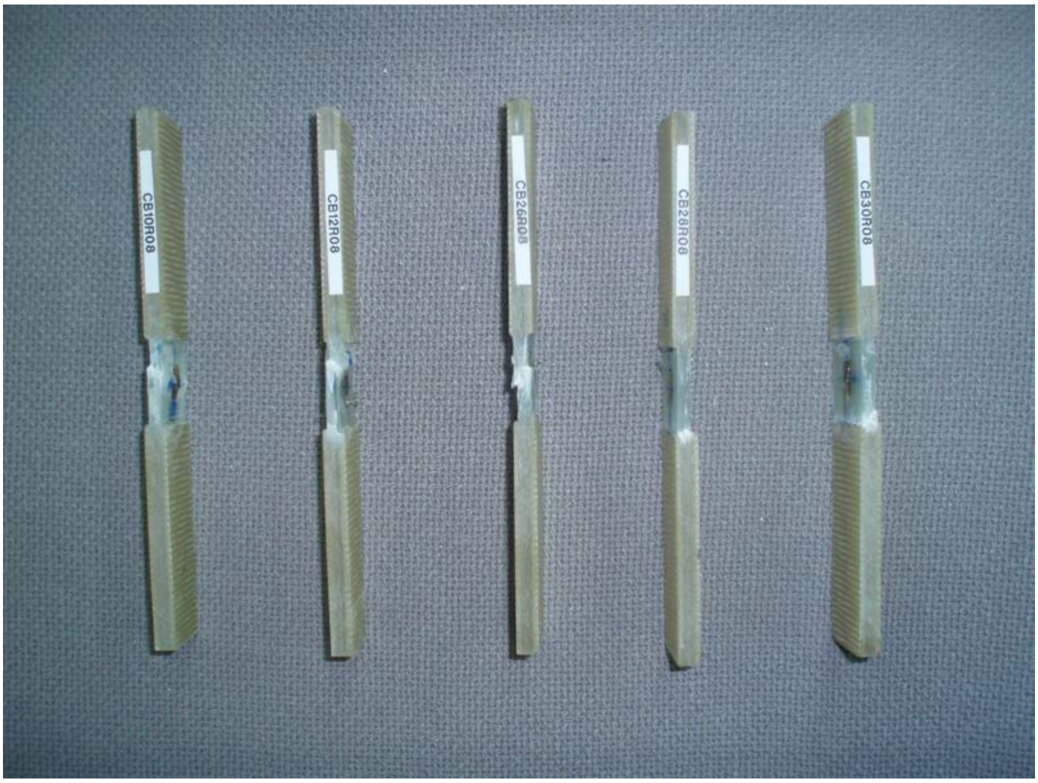

Fig. 53: Photo of the tested coupons CB10R08, CB12R08, CB26R08, CB28R08 and CB30R08 (from left to right)

8.3. Tensile UD tests transversely to the fibres

8.3.1. Stress-strain graphs

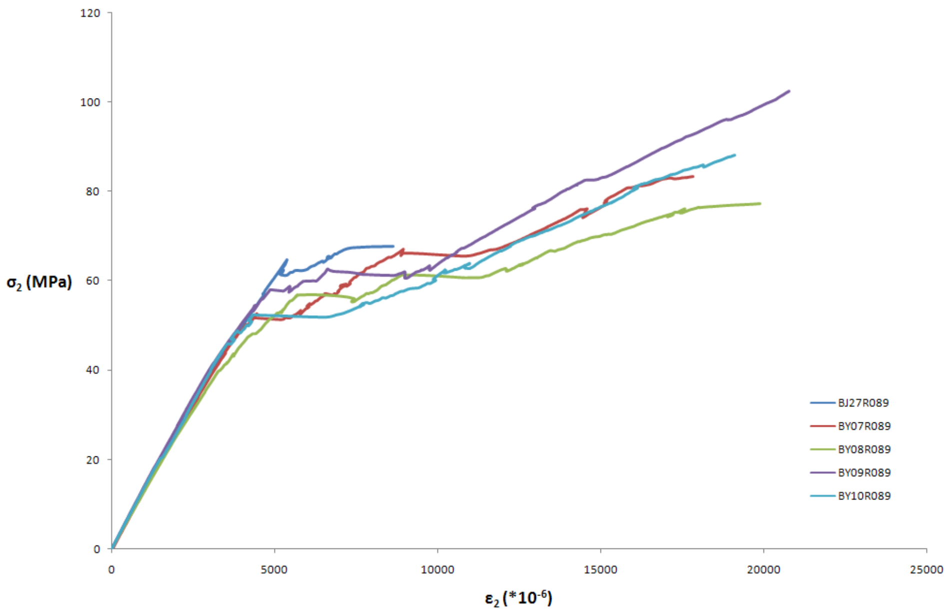

Fig. 54: Stress-strain curve of 5 coupons tested in tension in the transverse to the fibres direction: BJ27R089, BY07R089, BY08R089, BY09R089 and BY10R089

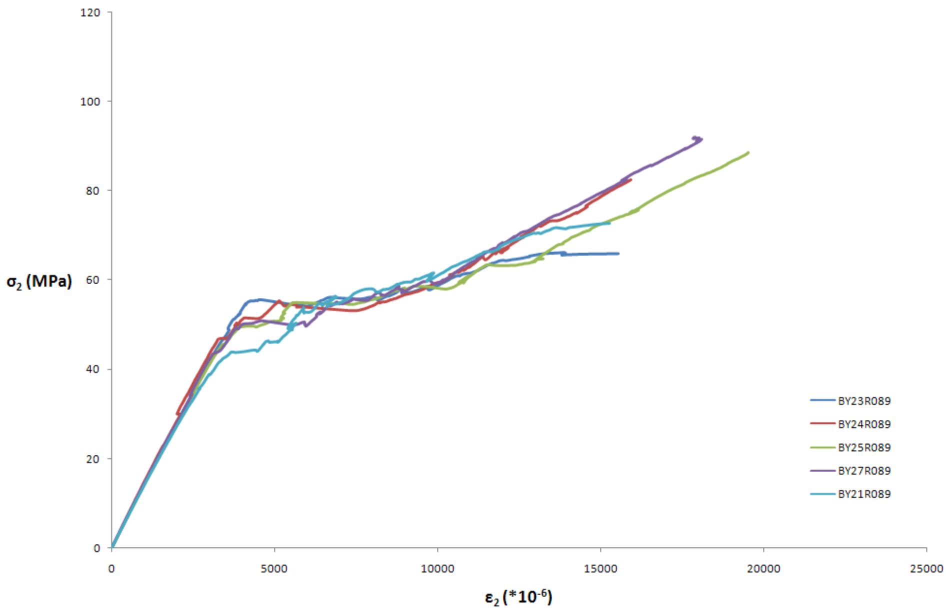

Fig. 55: Stress-strain curve of 5 coupons tested in tension in the transverse to the fibres direction: BY23R089, BY24R089, BY25R089, BY27R089 and BY21R089

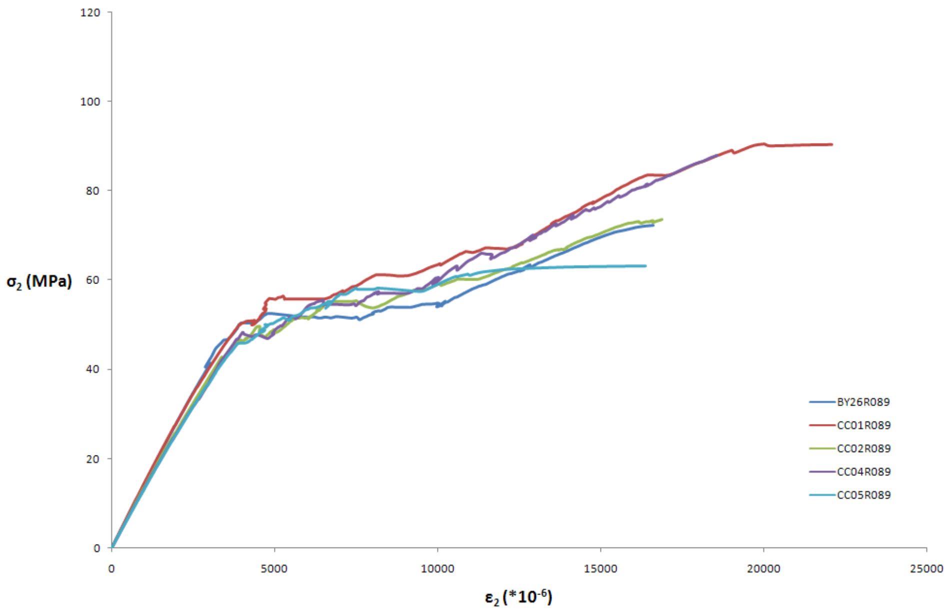

Fig. 56: Stress-strain curve of 5 coupons tested in tension in the transverse to the fibres direction: BY26R089, CC01R089, CC02R089, CC04R089 and CC05R089

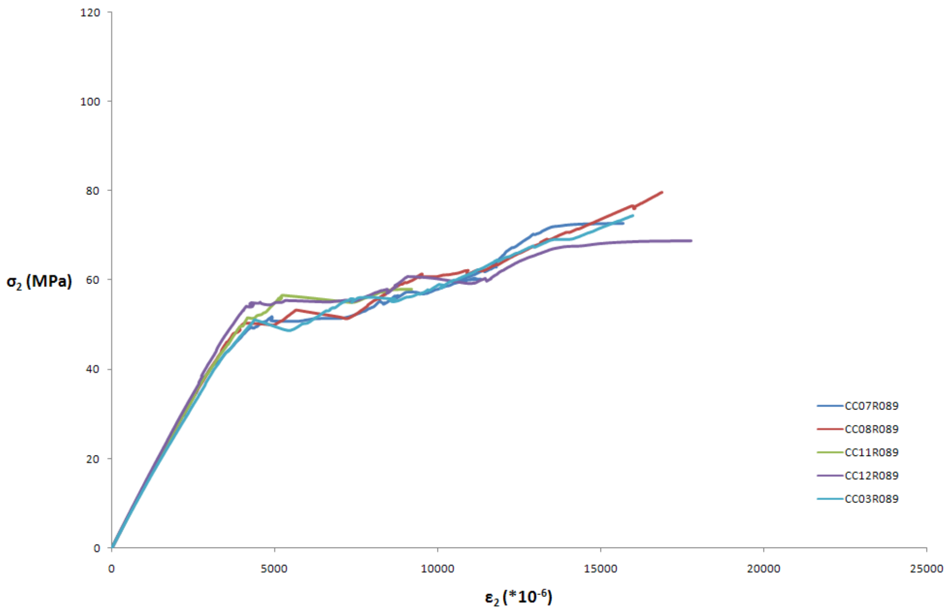

Fig. 57: Stress-strain curve of 5 coupons tested in tension in the transverse to the fibres direction: CC07R089, CC08R089, CC11R089, CC12R089 and CC03R089

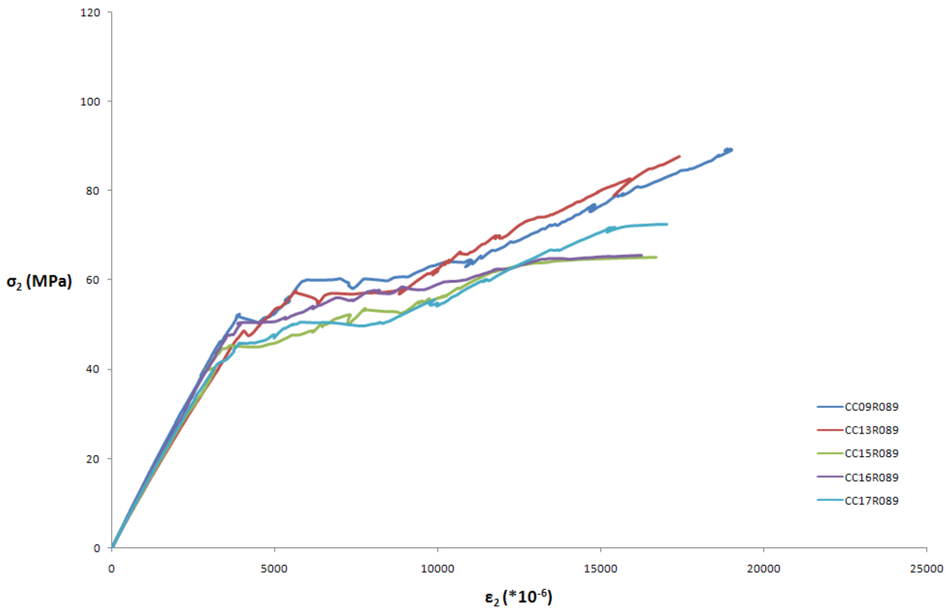

Fig. 58: Stress-strain curve of 5 coupons tested in tension in the transverse to the fibres direction: CC09R089, CC13R089, CC15R089, CC16R089 and CC17R089

8.3.2. Stress-strain graphs (500-2500 με)

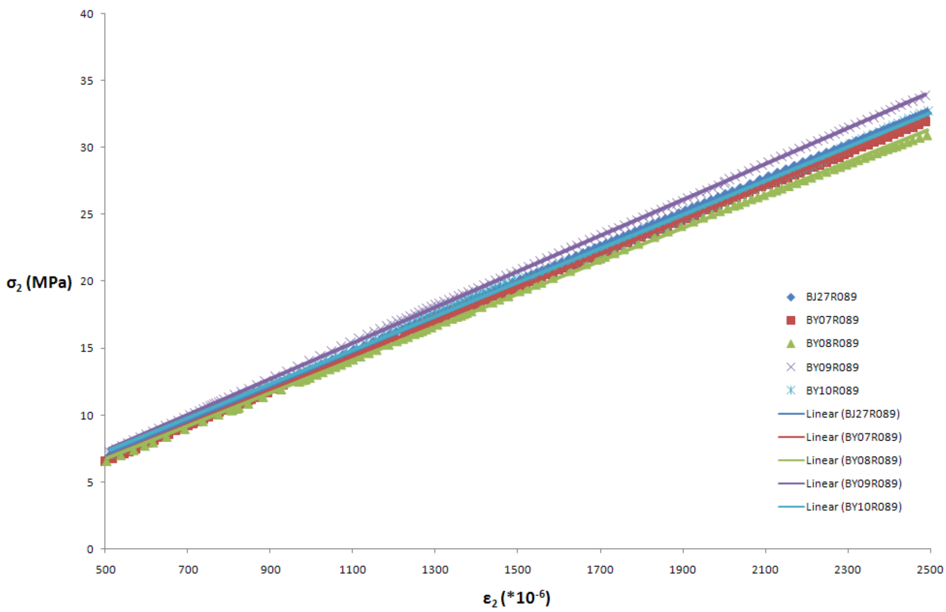

Fig. 59: Stress-strain curve of 5 coupons tested in tension in the transverse to the fibres direction and linear curve fit: BJ27R089, BY07R089, BY08R089, BY09R089 and BY10R089

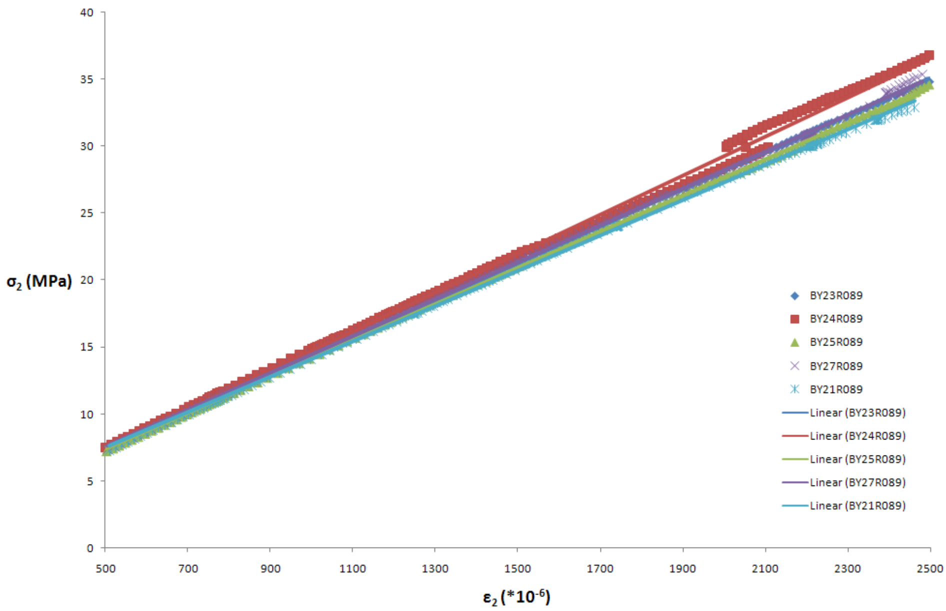

Fig. 60: Stress-strain curve of 5 coupons tested in tension in the transverse to the fibres direction and linear curve fit: BY23R089, BY24R089, BY25R089, BY27R089 and BY21R089

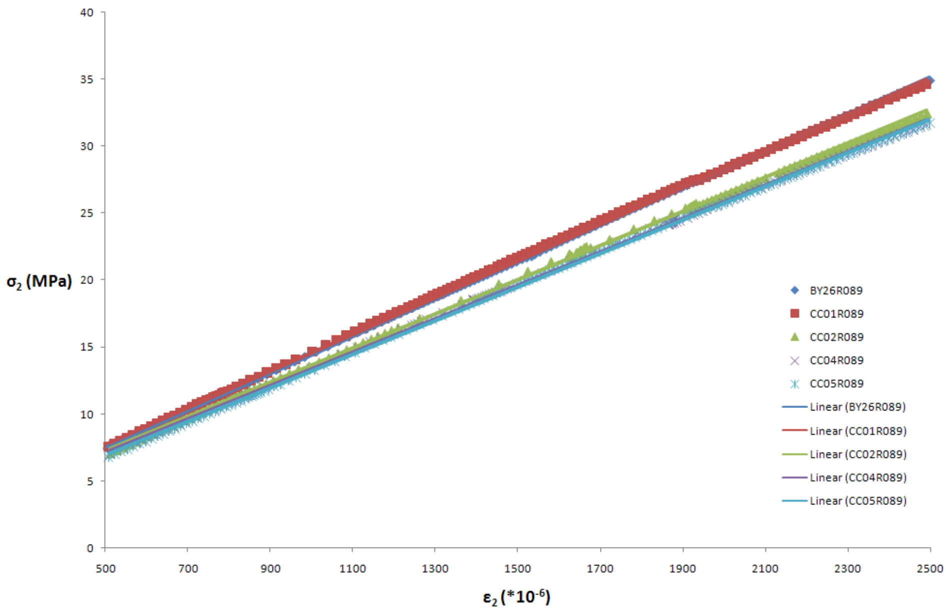

Fig. 61: Stress-strain curve of 5 coupons tested in tension in the transverse to the fibres direction and linear curve fit: BY26R089, CC01R089, CC02R089, CC04R089 and CC05R089

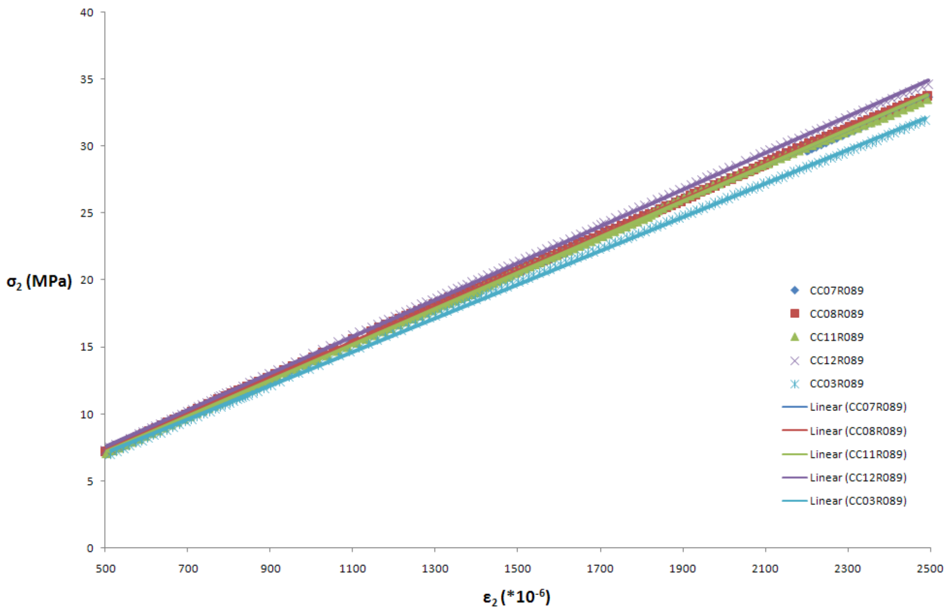

Fig. 62: Stress-strain curve of 5 coupons tested in tension in the transverse to the fibres direction and linear curve fit: CC07R089, CC08R089, CC11R089, CC12R089 and CC03R089

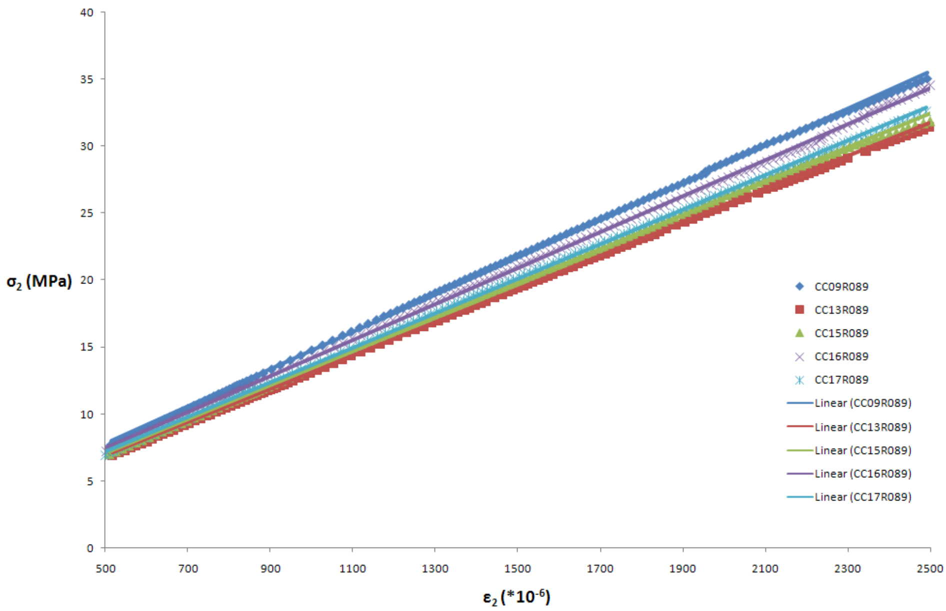

Fig. 63: Stress-strain curve of 5 coupons tested in tension in the transverse to the fibres direction and linear curve fit: CC09R089, CC13R089, CC15R089, CC16R089 and CC17R089

8.3.3. Transverse strain-Axial strain graphs (500-2500 με)

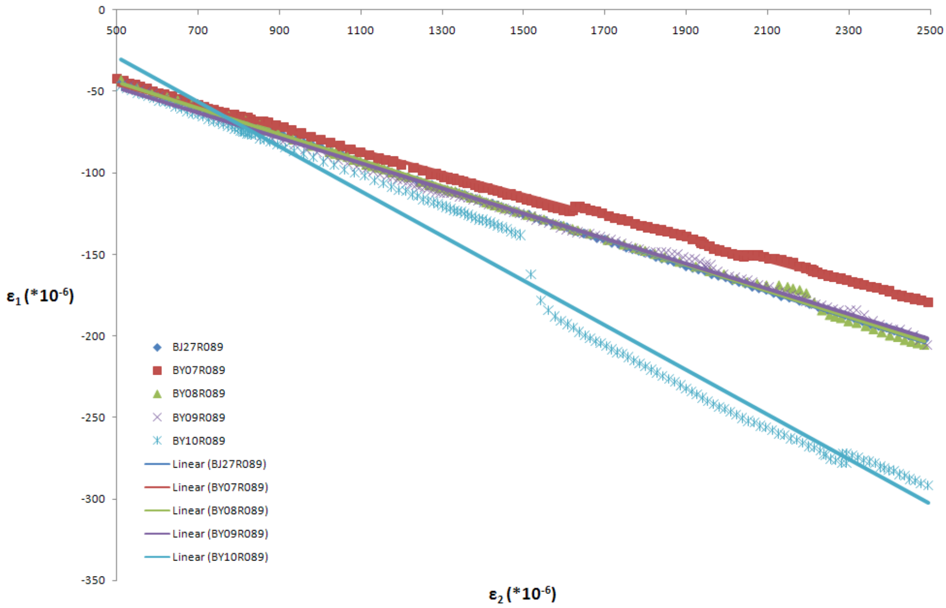

Fig. 64: Transverse strain-Axial strain curve of 5 coupons tested in tension in the transverse to the fibres direction and linear curve fit: BJ27R089, BY07R089, BY08R089, BY09R089 and BY10R089

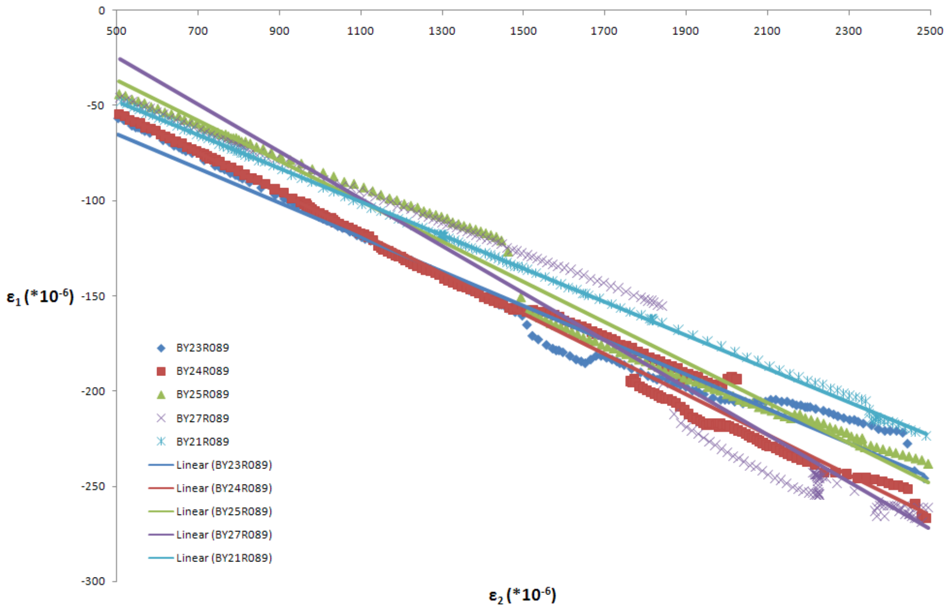

Fig. 65: Transverse strain-Axial strain curve of 5 coupons tested in tension in the transverse to the fibres direction and linear curve fit: BY23R089, BY24R089, BY25R089, BY27R089 and BY21R089

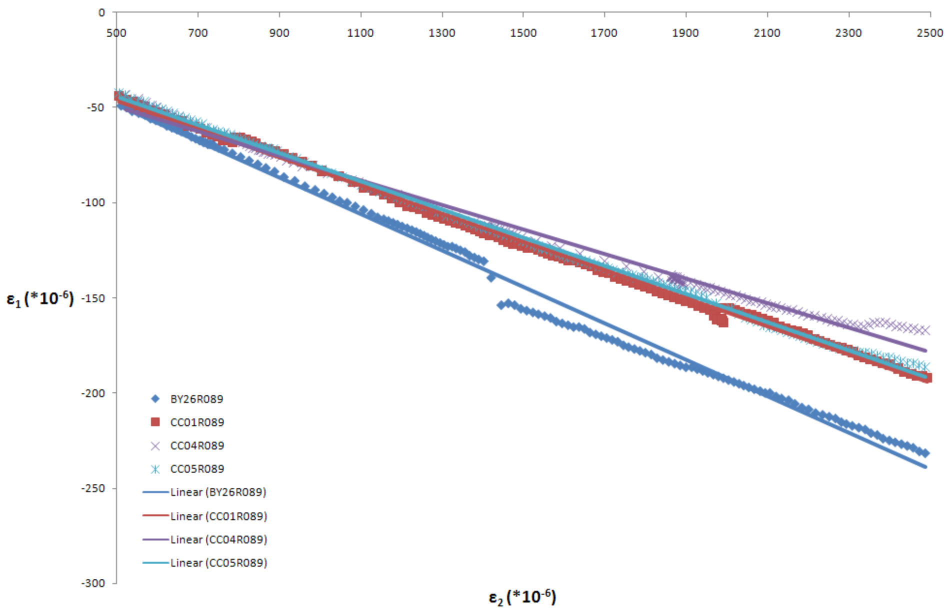

Fig. 66: Transverse strain-Axial strain curve of 4 coupons tested in tension in the transverse to the fibres direction and linear curve fit: BY26R089, CC01R089, CC04R089 and CC05R089

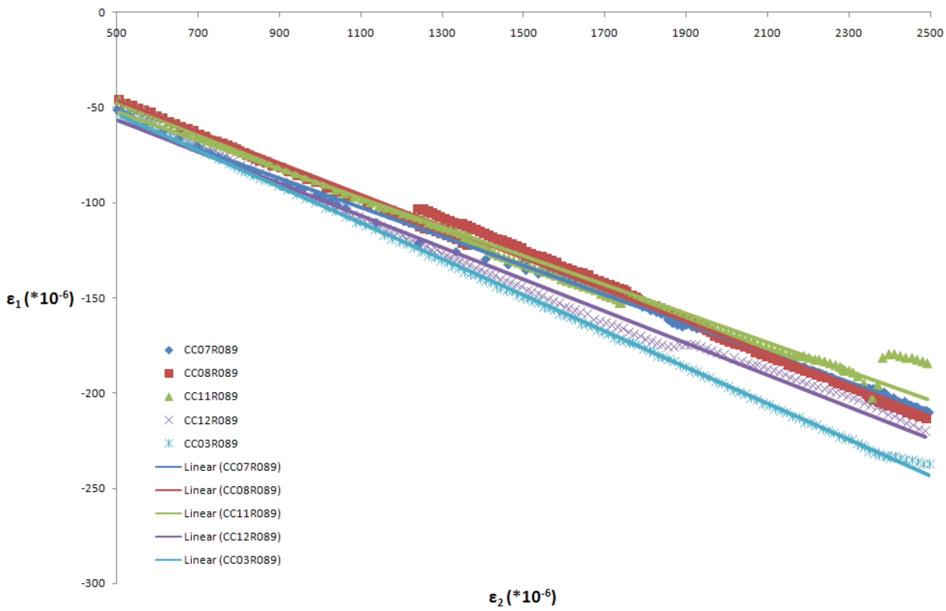

Fig. 67: Transverse strain-Axial strain curve of 5 coupons tested in tension in the transverse to the fibres direction and linear curve fit: CC07R089, CC08R089, CC11R089, CC12R089 and CC03R089

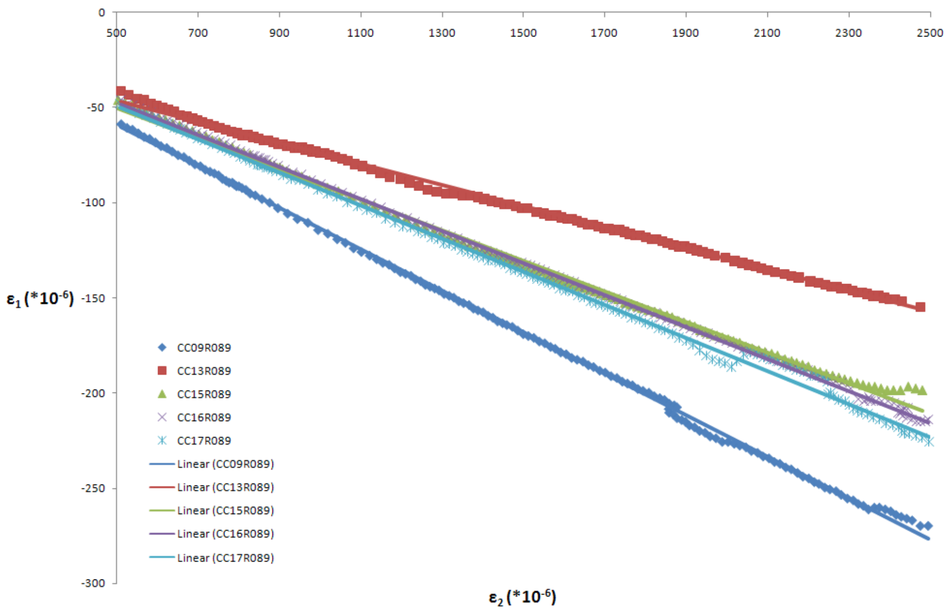

Fig. 68: Transverse strain-Axial strain curve of 5 coupons tested in tension in the transverse to the fibres direction and linear curve fit: CC09R089, CC13R089, CC15R089, CC16R089 and CC17R089

8.3.4. Photographs of tested coupons

Fig. 69: Photo of the tested coupons BJ27R089, BY07R089, BY08R089, BY09R089 and BY10R089 (from left to right)

Fig. 70: Photo of the tested coupons BJ27R089, BY07R089, BY08R089, BY09R089 and BY10R089 (from left to right)

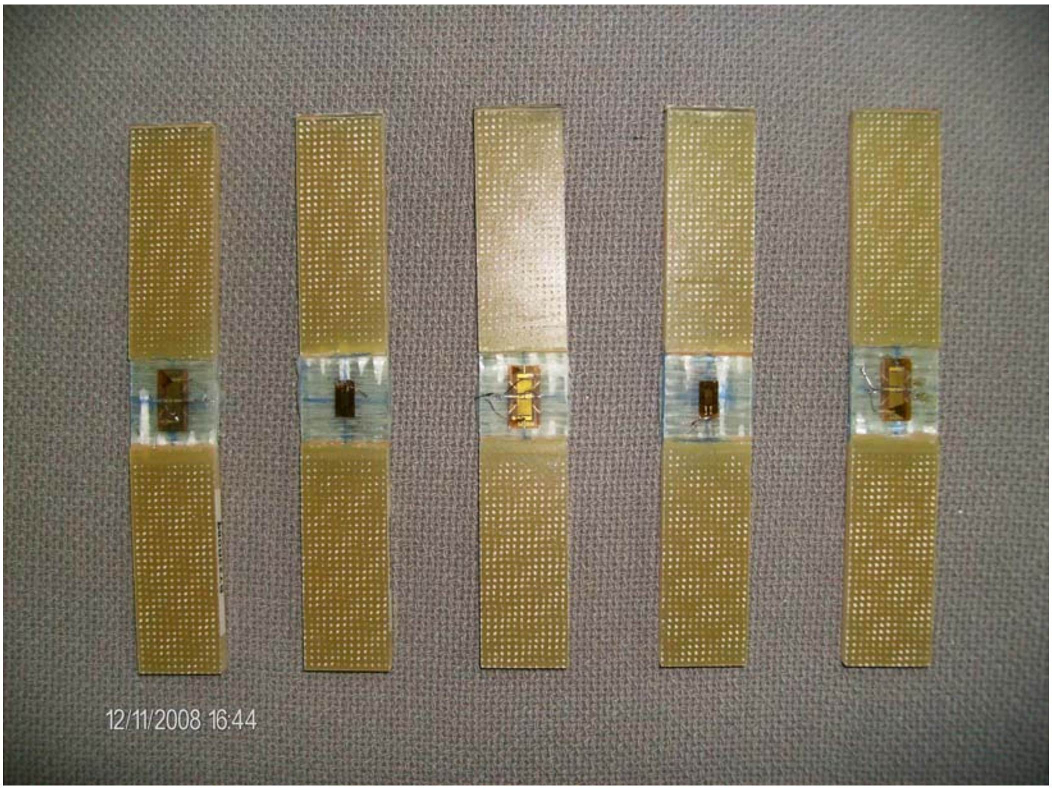

Fig. 71: Photo of the tested coupons BY23R089, BY24R089, BY25R089, BY27R089 and BY21R089 (from left to right)

Fig. 72: Photo of the tested coupons BY23R089, BY24R089, BY25R089, BY27R089 and BY21R089 (from left to right)

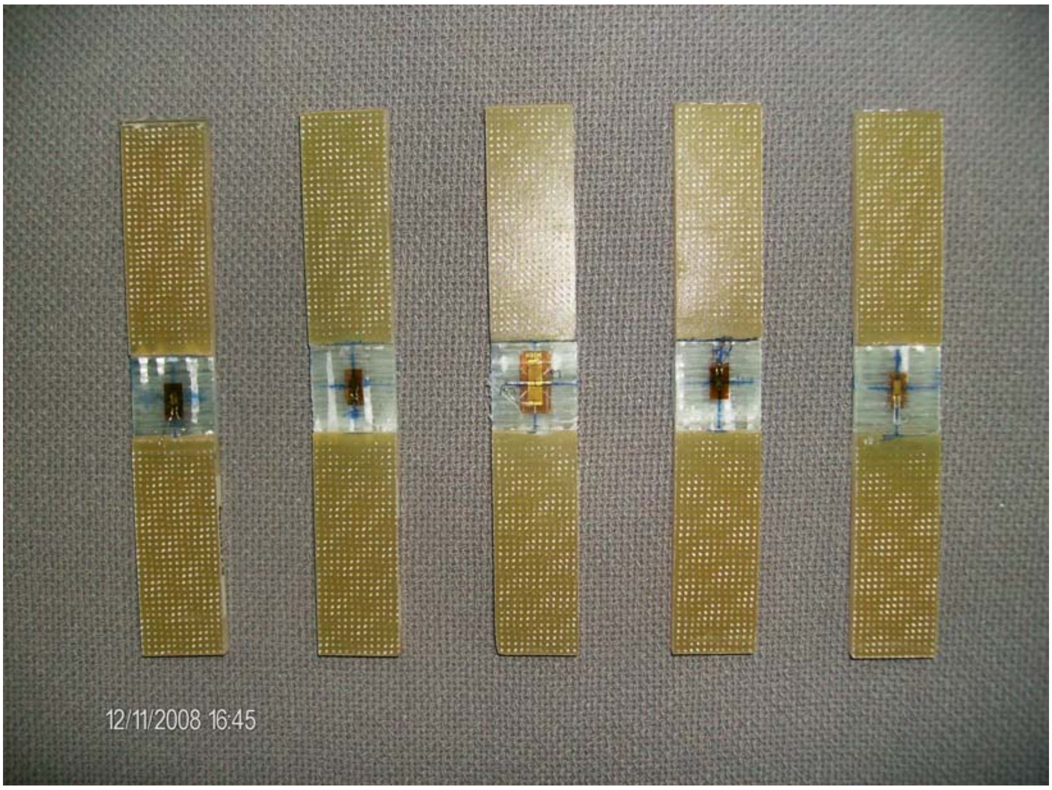

Fig. 73: Photo of the tested coupons BY26R089, CC01R089, CC02R089, CC04R089 and CC05R089 (from left to right)

Fig. 74: Photo of the tested coupons BY26R089, CC01R089, CC02R089, CC04R089 and CC05R089 (from left to right)

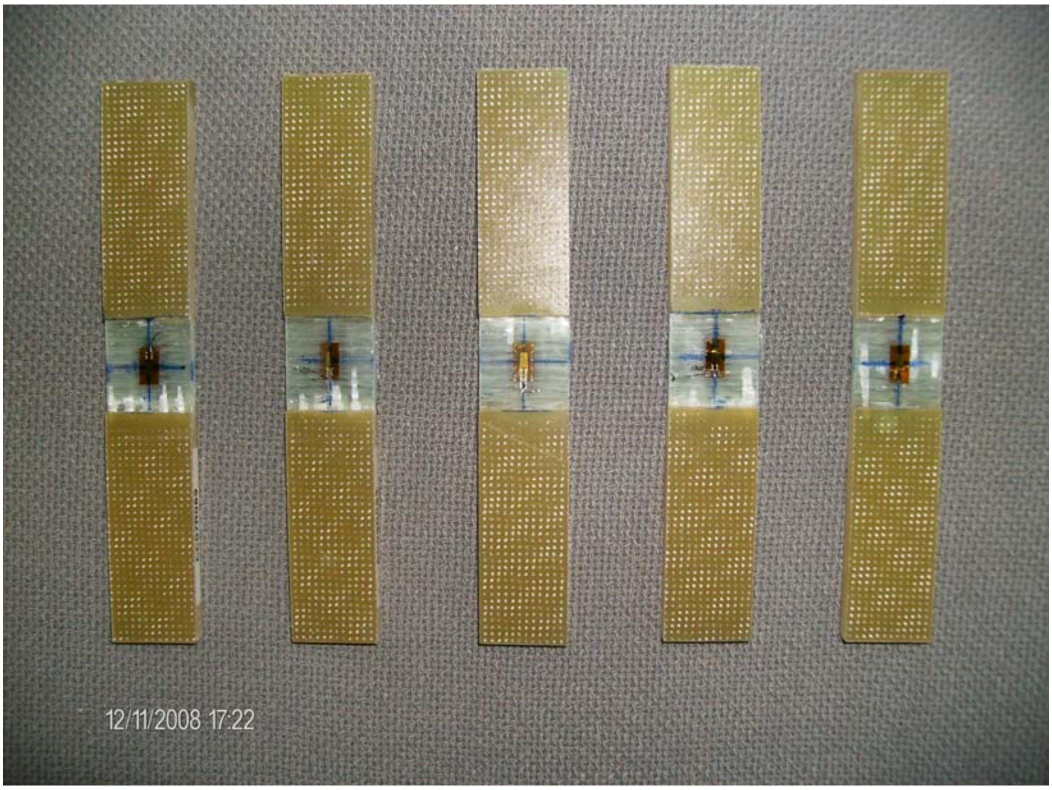

Fig. 75: Photo of the tested coupons CC07R089, CC08R089, CC11R089, CC12R089 and CC03R089 (from left to right)

Fig. 76: Photo of the tested coupons CC07R089, CC08R089, CC11R089, CC12R089 and CC03R089 (from left to right)

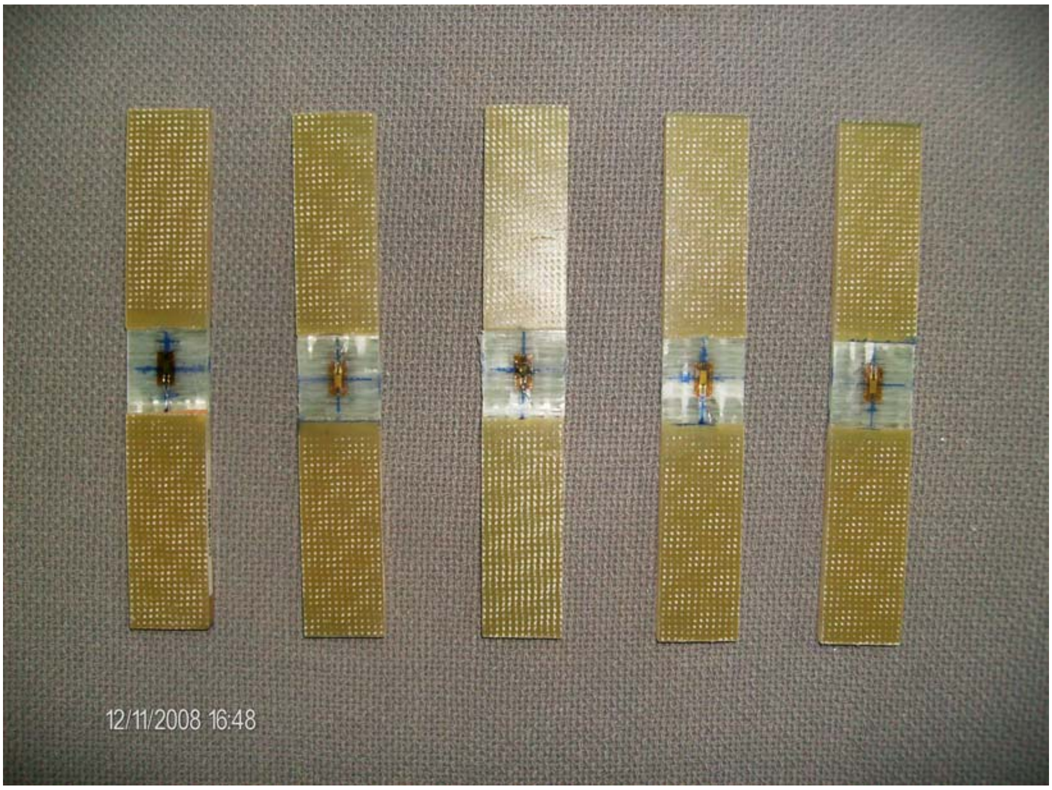

Fig. 77: Photo of the tested coupons CC09R089, CC13R089, CC15R089, CC16R089 and CC17R089 (from left to right)

Fig. 78: Photo of the tested coupons CC09R089, CC13R089, CC15R089, CC16R089 and CC17R089 (from left to right)

8.4. Compressive UD tests transversely to the fibres

8.4.1. Stress-strain graphs

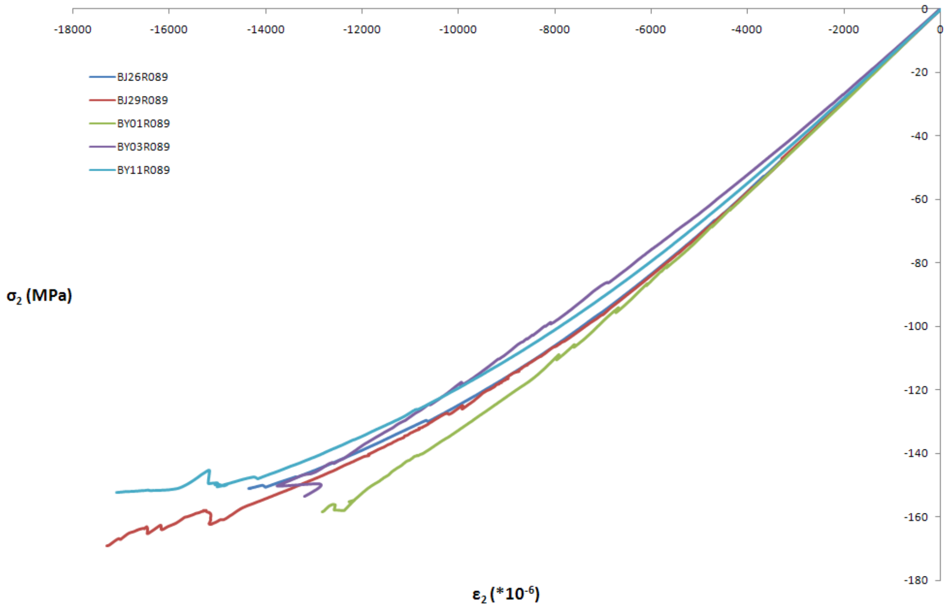

Fig. 79: Stress-strain curve of 5 coupons tested in compression in the transverse to the fibres direction: BJ26R089, BJ29R089, BY01R089, BY03R089 and BY11R089

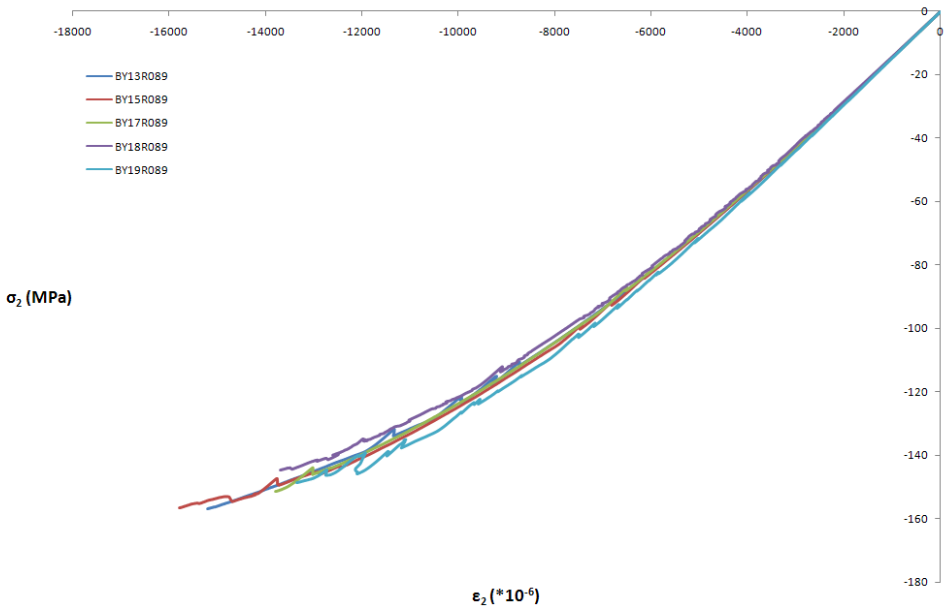

Fig. 80: Stress-strain curve of 5 coupons tested in compression in the transverse to the fibres direction: BY13R089, BY15R089, BY17R089, BY18R089 and BY19R089

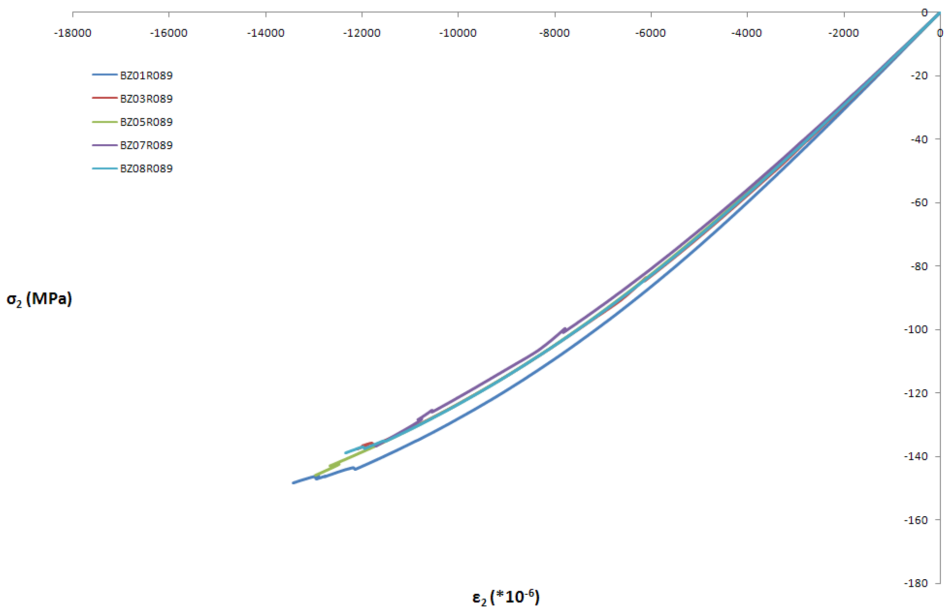

Fig. 81: Stress-strain curve of 5 coupons tested in compression in the transverse to the fibres direction: BZ01R089, BZ03R089, BZ05R089, BZ07R089 and BZ08R089

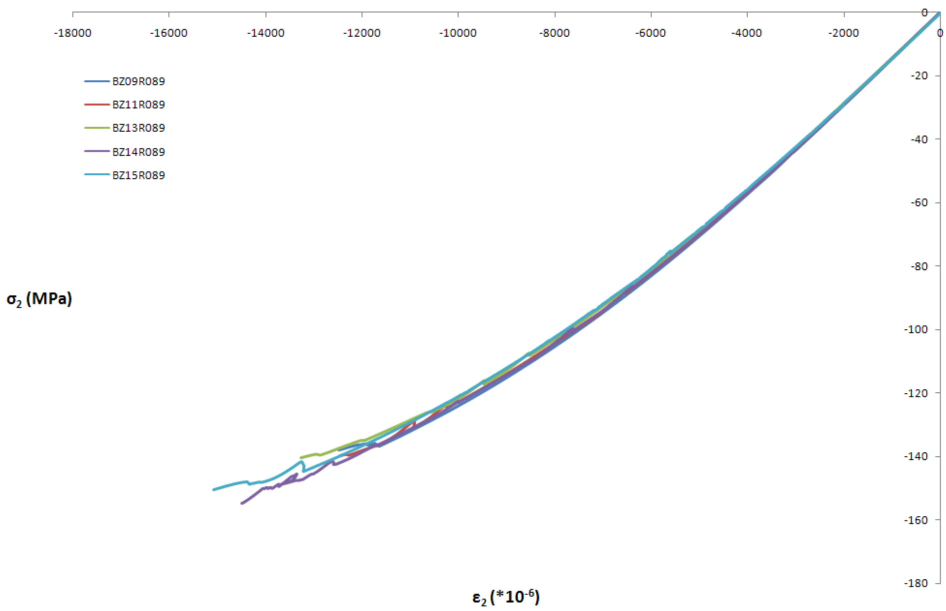

Fig. 82: Stress-strain curve of 5 coupons tested in compression in the transverse to the fibres direction: BZ09R089, BZ11R089, BZ13R089, BZ14R089 and BZ15R089

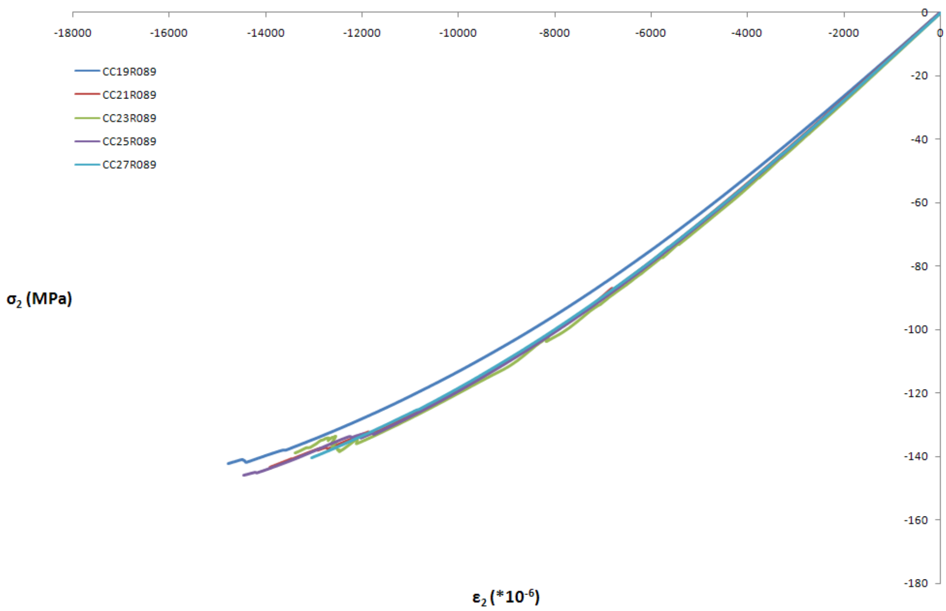

Fig. 83: Stress-strain curve of 5 coupons tested in compression in the transverse to the fibres direction: CC19R089, CC21R089, CC23R089, CC25R089 and CC27R089

8.4.2. Stress-strain graphs (500-2500 με)

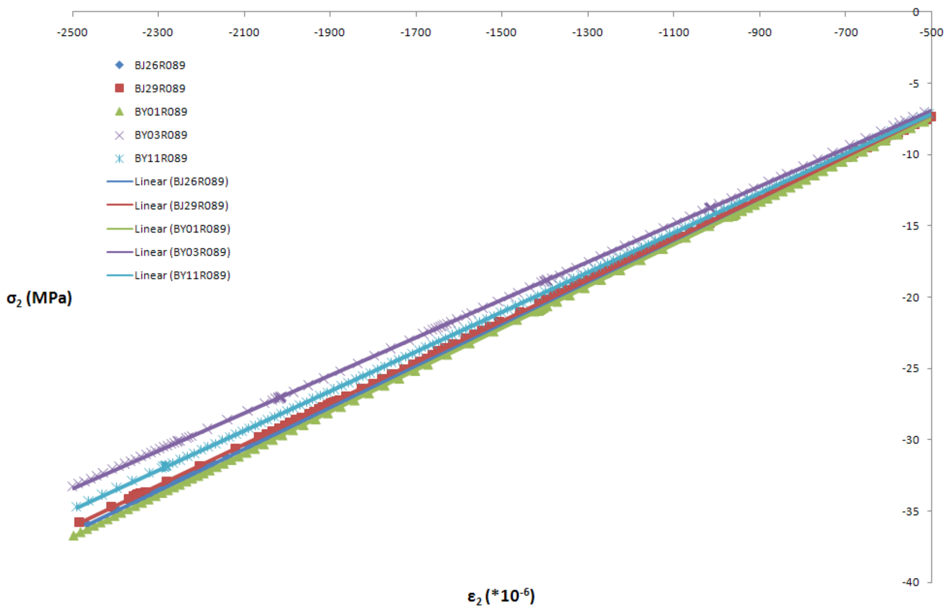

Fig. 84: Stress-strain curve of 5 coupons tested in compression in the transverse to the fibres direction and linear curve fit: BJ26R089, BJ29R089, BY01R089, BY03R089 and BY11R089

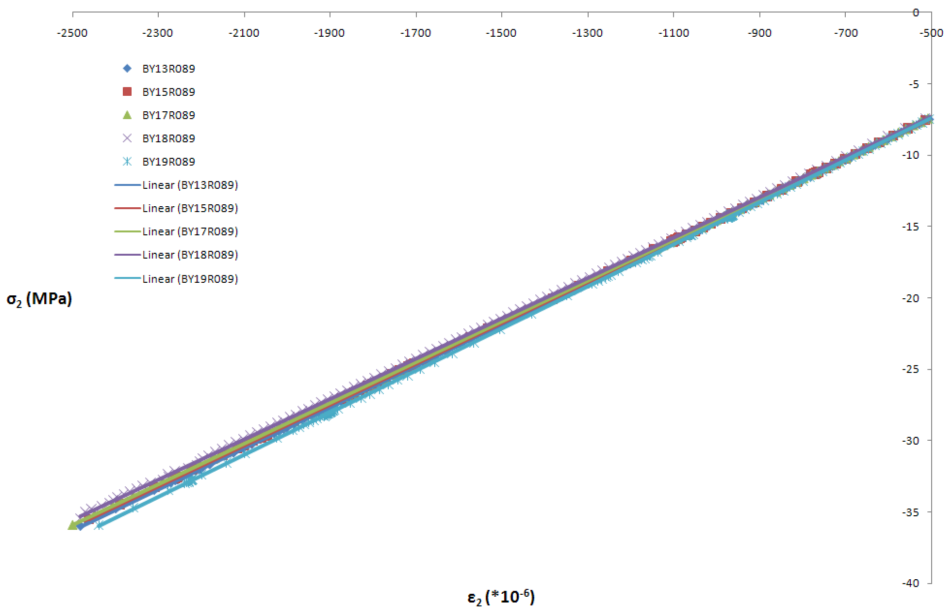

Fig. 85: Stress-strain curve of 5 coupons tested in compression in the transverse to the fibres direction and linear curve fit: BY13R089, BY15R089, BY17R089, BY18R089 and BY19R089

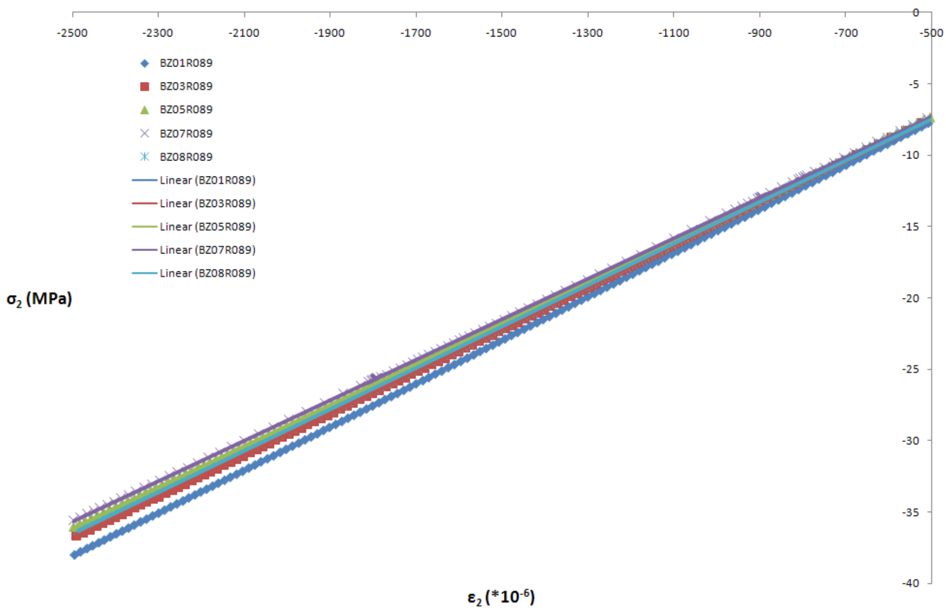

Fig. 86: Stress-strain curve of 5 coupons tested in compression in the transverse to the fibres direction and linear curve fit: BZ01R089, BZ03R089, BZ05R089, BZ07R089 and BZ08R089

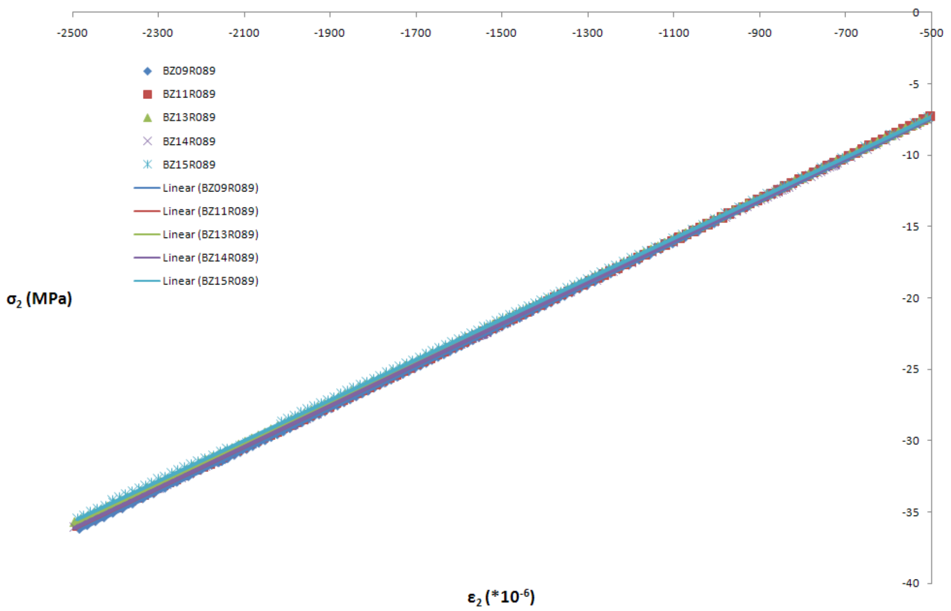

Fig. 87: Stress-strain curve of 5 coupons tested in compression in the transverse to the fibres direction and linear curve fit: BZ09R089, BZ11R089, BZ13R089, BZ14R089 and BZ15R089

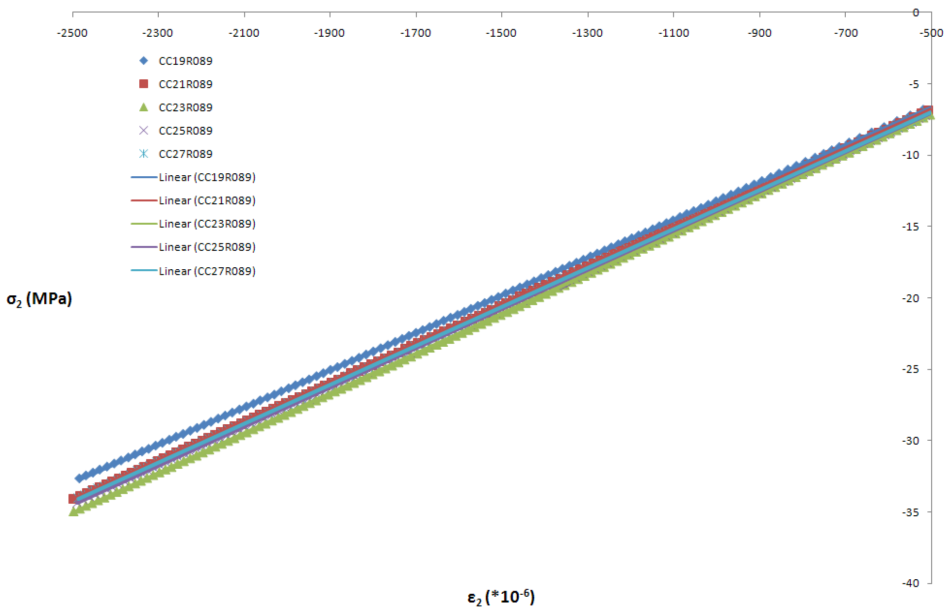

Fig. 88: Stress-strain curve of 5 coupons tested in compression in the transverse to the fibres direction and linear curve fit: CC19R089, CC21R089, CC23R089, CC25R089 and CC27R089

8.4.3. Bending strain-Axial stress graphs

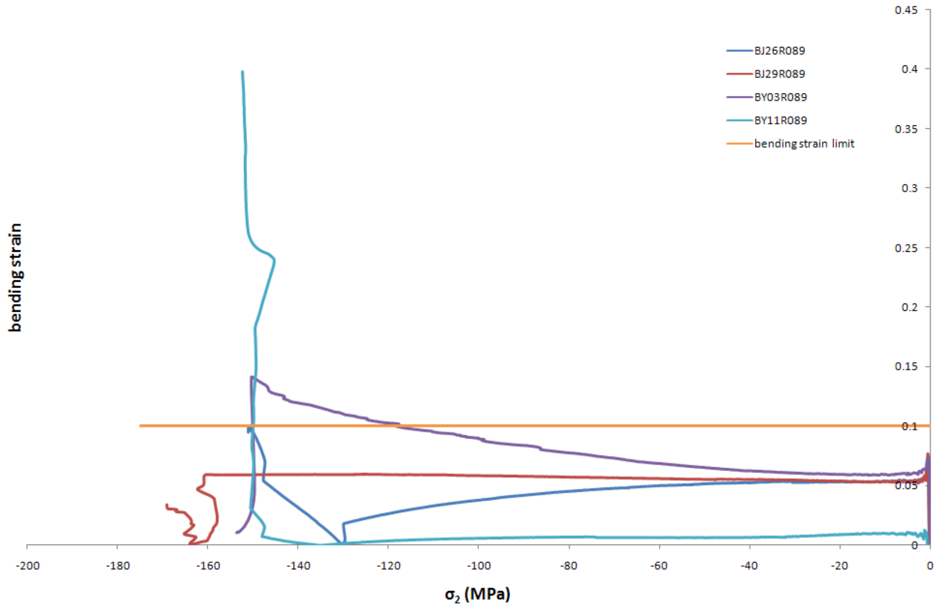

Fig. 89: Bending strain-Axial stress curve of 4 coupons tested in compression in the transverse to the fibres direction: BJ26R089, BJ29R089, BY03R089 and BY11R089

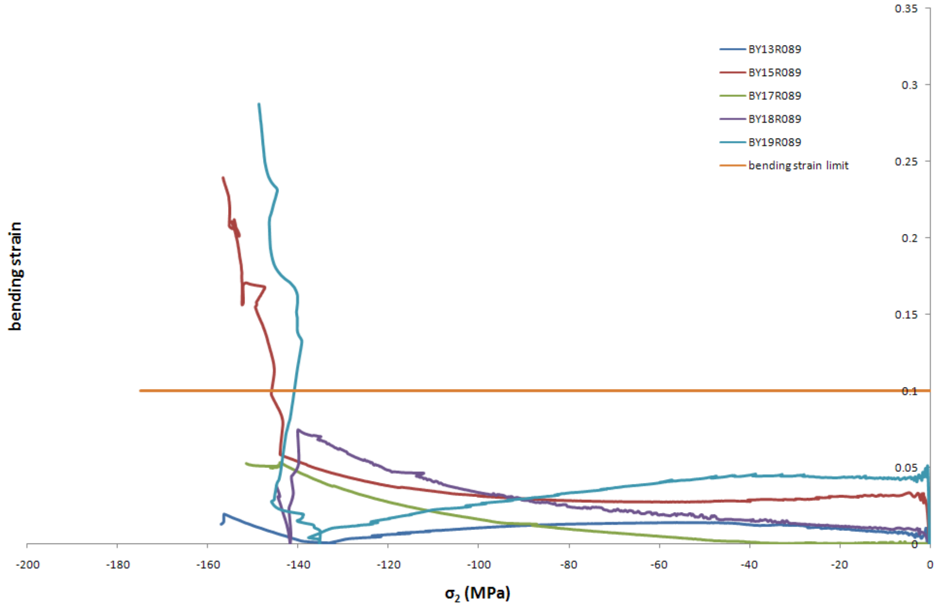

Fig. 90: Bending strain-Axial stress curve of 5 coupons tested in compression in the transverse to the fibres direction: BY13R089, BY15R089, BY17R089, BY18R089 and BY19R089

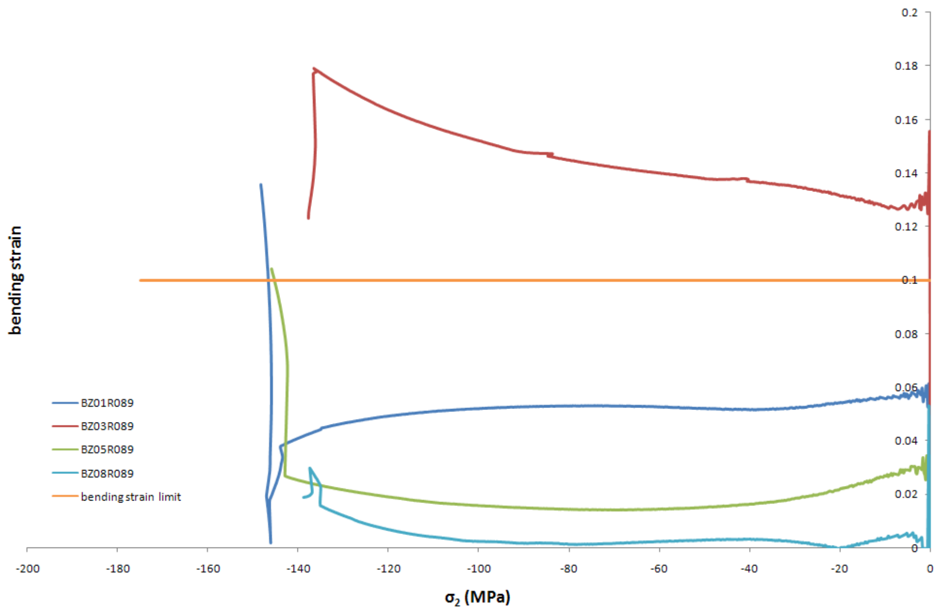

Fig. 91: Bending strain-Axial stress curve of 4 coupons tested in compression in the transverse to the fibres direction: BZ01R089, BZ03R089, BZ05R089 and BZ08R089

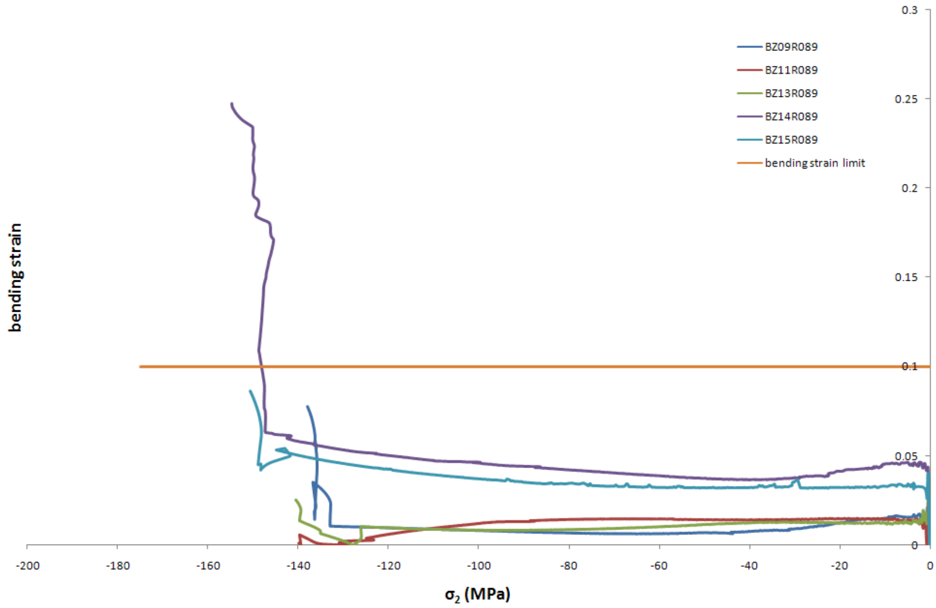

Fig. 92: Bending strain-Axial stress curve of 5 coupons tested in compression in the transverse to the fibres direction: BZ09R089, BZ11R089, BZ13R089, BZ14R089 and BZ15R089

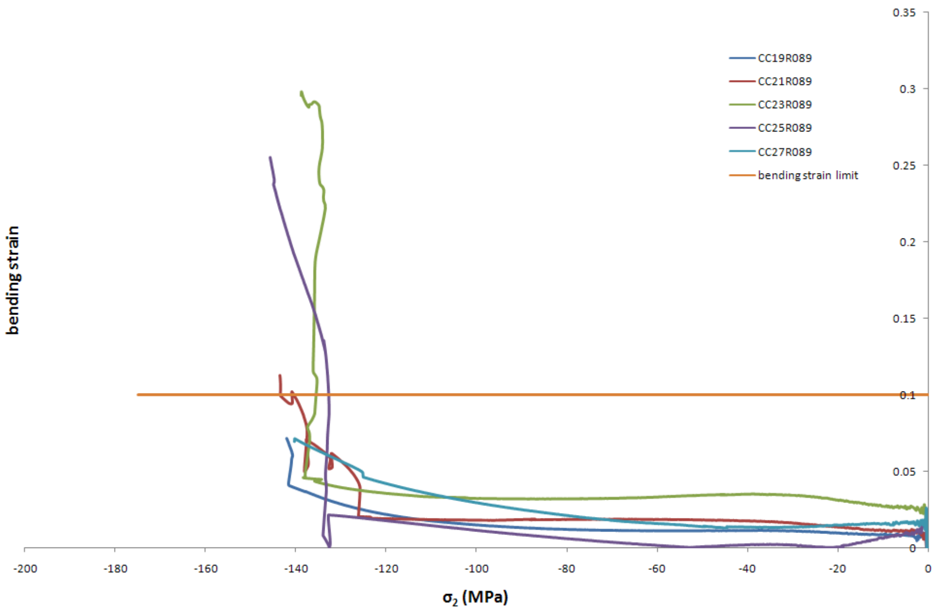

Fig. 93: Bending strain-Axial stress curve of 5 coupons tested in compression in the transverse to the fibres direction: CC19R089, CC21R089, CC23R089, CC25R089 and CC27R089

8.4.4. Photographs of tested coupons

Fig. 94: Photo of the tested coupons BJ26R089, BJ29R089, BY01R089, BY03R089 and BY11R089 (from left to right)

Fig. 95: Photo of the tested coupons BJ26R089, BJ29R089, BY01R089, BY03R089 and BY11R089 (from left to right)

Fig. 96: Photo of the tested coupons BY13R089, BY15R089, BY17R089, BY18R089 and BY19R089 (from left to right)

Fig. 97: Photo of the tested coupons BY13R089, BY15R089, BY17R089, BY18R089 and BY19R089 (from left to right)

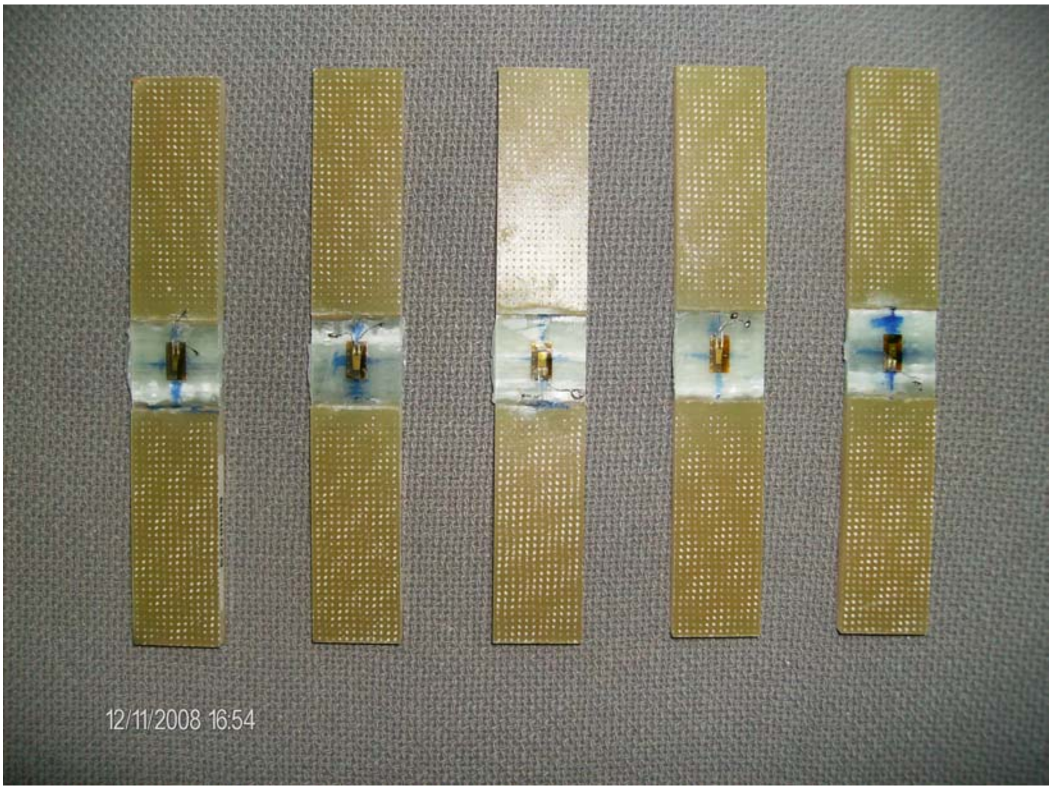

Fig. 98: Photo of the tested coupons BZ01R089, BZ03R089, BZ05R089, BZ07R089 and BZ08R089 (from left to right)

Fig. 99: Photo of the tested coupons BZ01R089, BZ03R089, BZ05R089, BZ07R089 and BZ08R089 (from left to right)

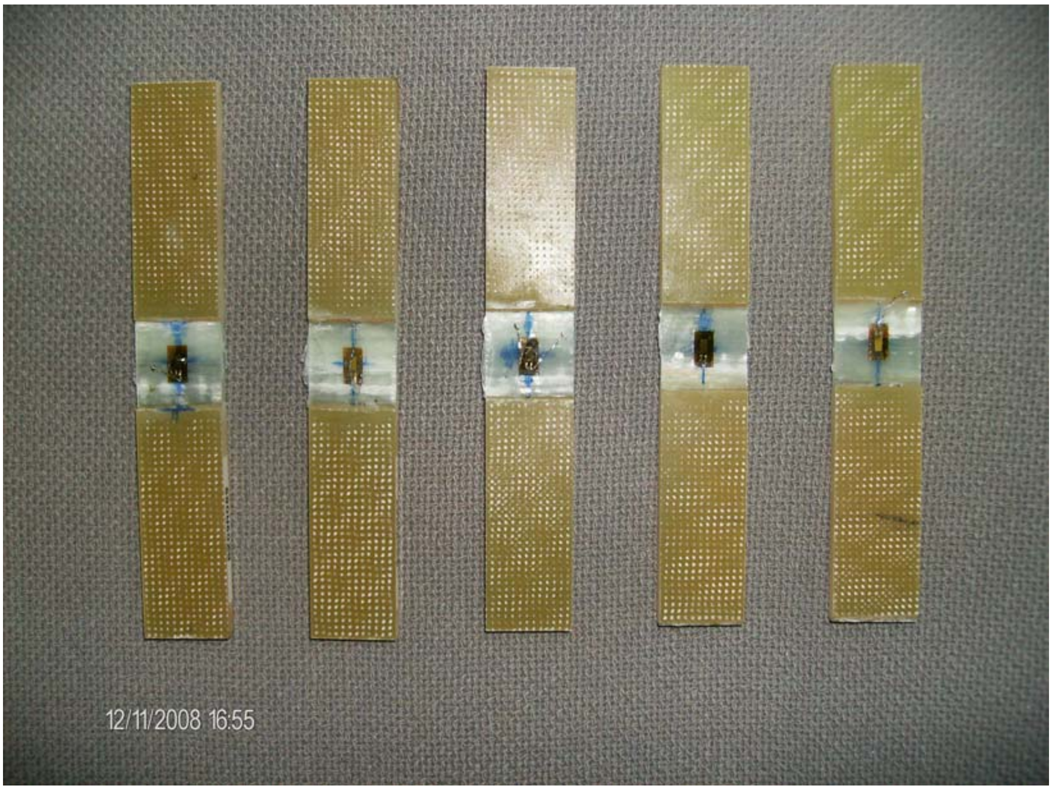

Fig. 100: Photo of the tested coupons BZ09R089, BZ11R089, BZ13R089, BZ14R089 and BZ15R089 (from left to right)

Fig. 101: Photo of the tested coupons BZ09R089, BZ11R089, BZ13R089, BZ14R089 and BZ15R089 (from left to right)

Fig. 102: Photo of the tested coupons CC19R089, CC21R089, CC23R089, CC25R089 and CC27R089 (from left to right)

Fig. 103: Photo of the tested coupons CC19R089, CC21R089, CC23R089, CC25R089 and CC27R089 (from left to right)

8.5. Tensile UD tests of ISO 14129 [±45]$_S$ coupons

8.5.1. Axial stress-strain graphs

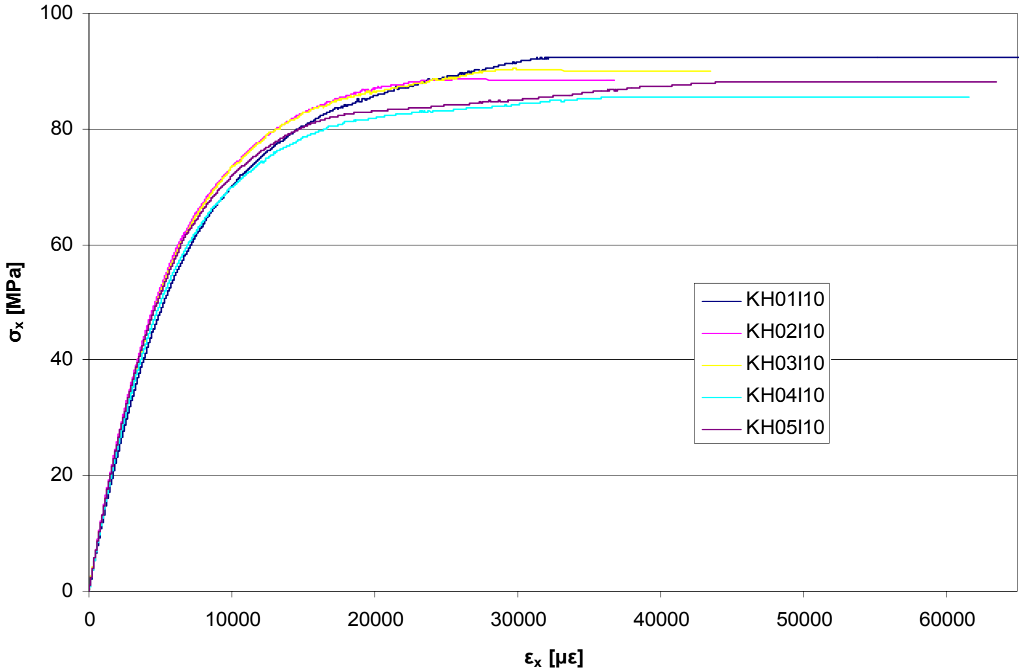

Fig. 104 Axial stress vs. axial strain for coupons KH01I10-KH05I10

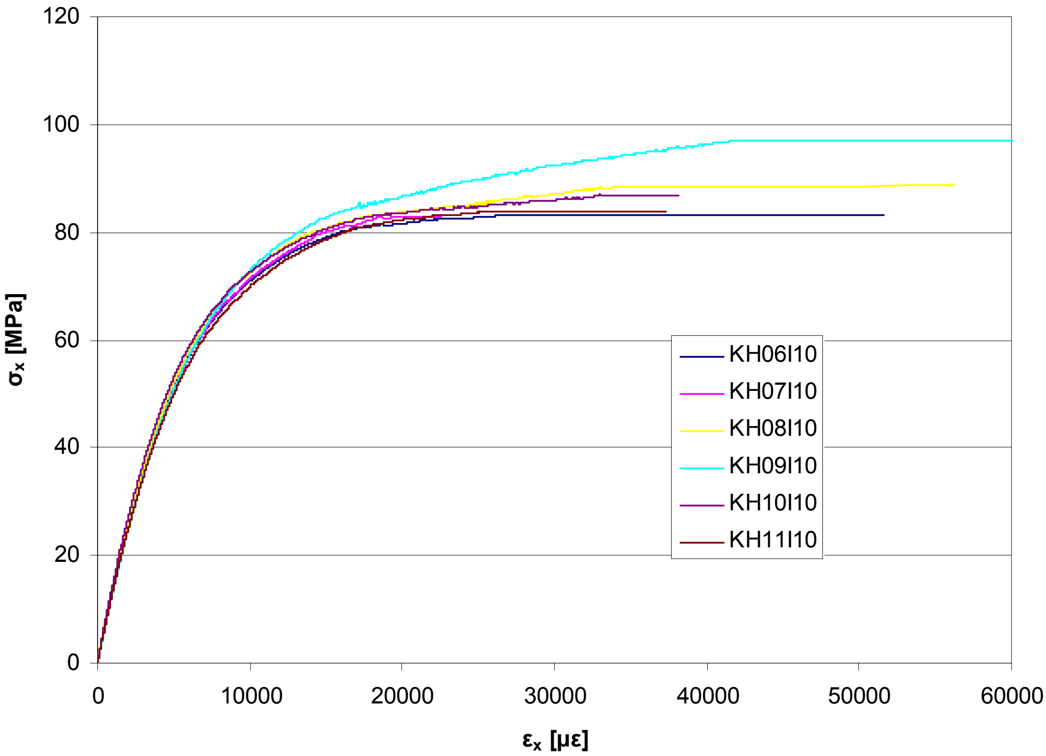

Fig. 105 Axial stress vs. axial strain for coupons KH06I10-KH11I10

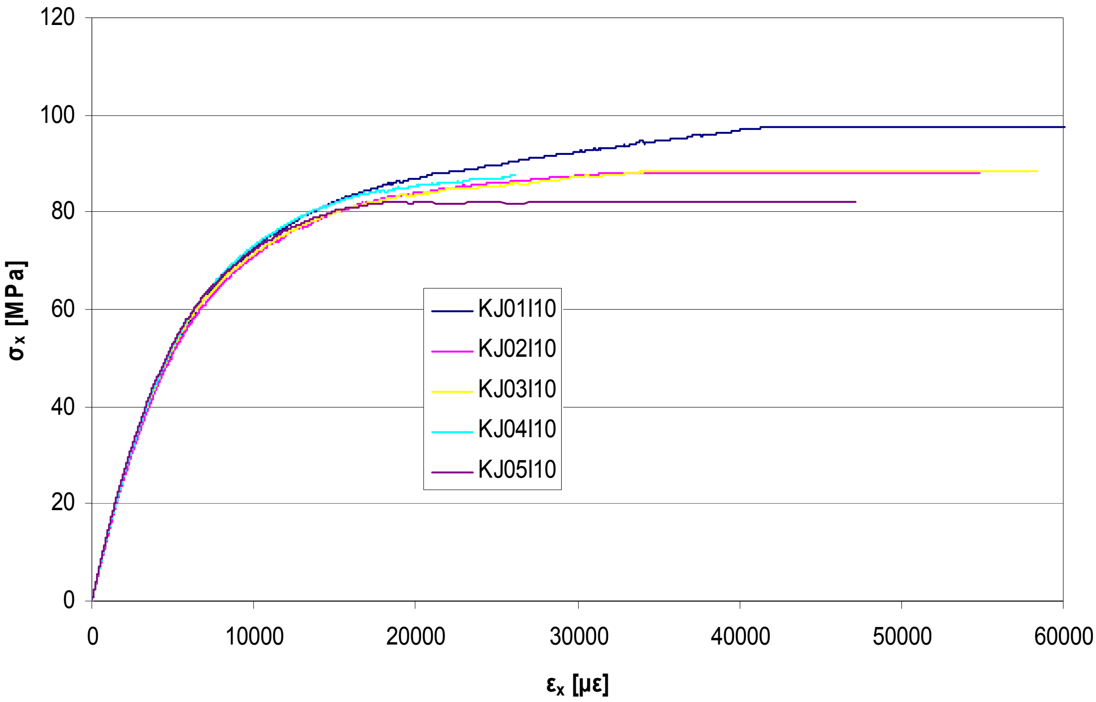

Fig. 106 Axial stress vs. axial strain for coupons KJ01I10-KJ05I10

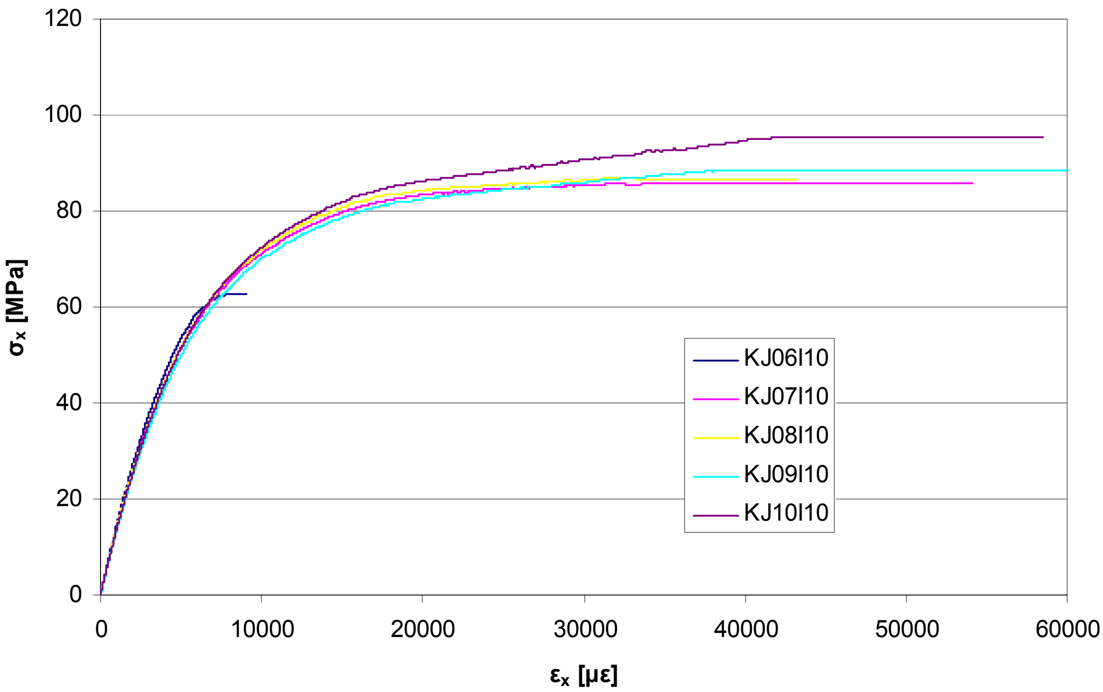

Fig. 107 Axial stress vs. axial strain for coupons KJ06I10-KJ10I10

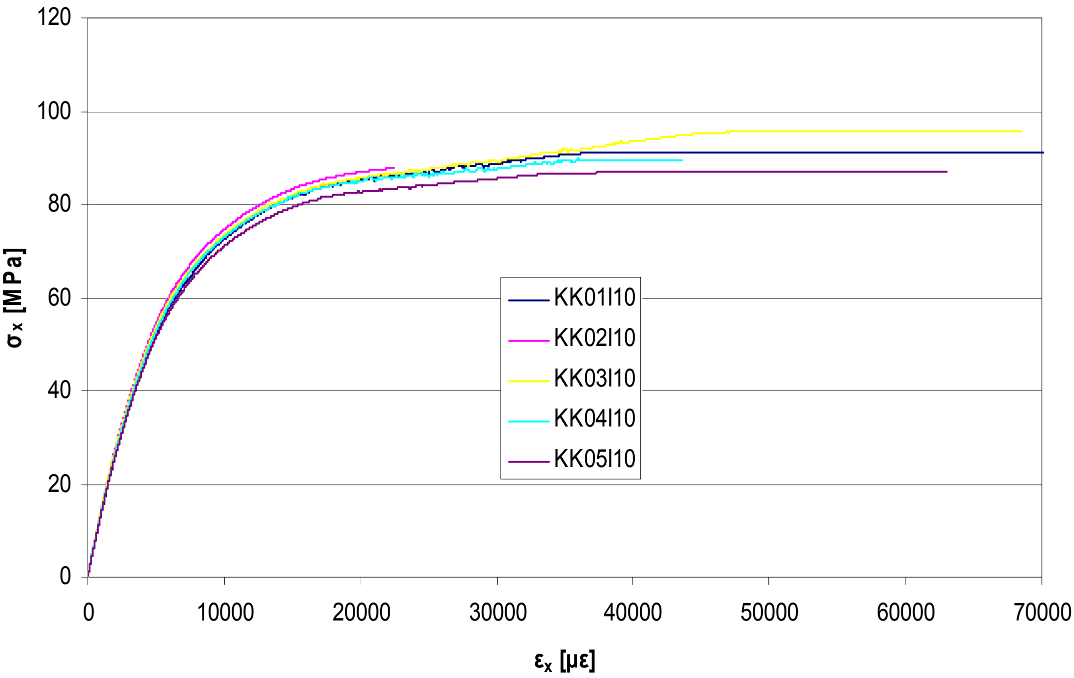

Fig. 108 Axial stress vs. axial strain for coupons KK01I10-KK05I10

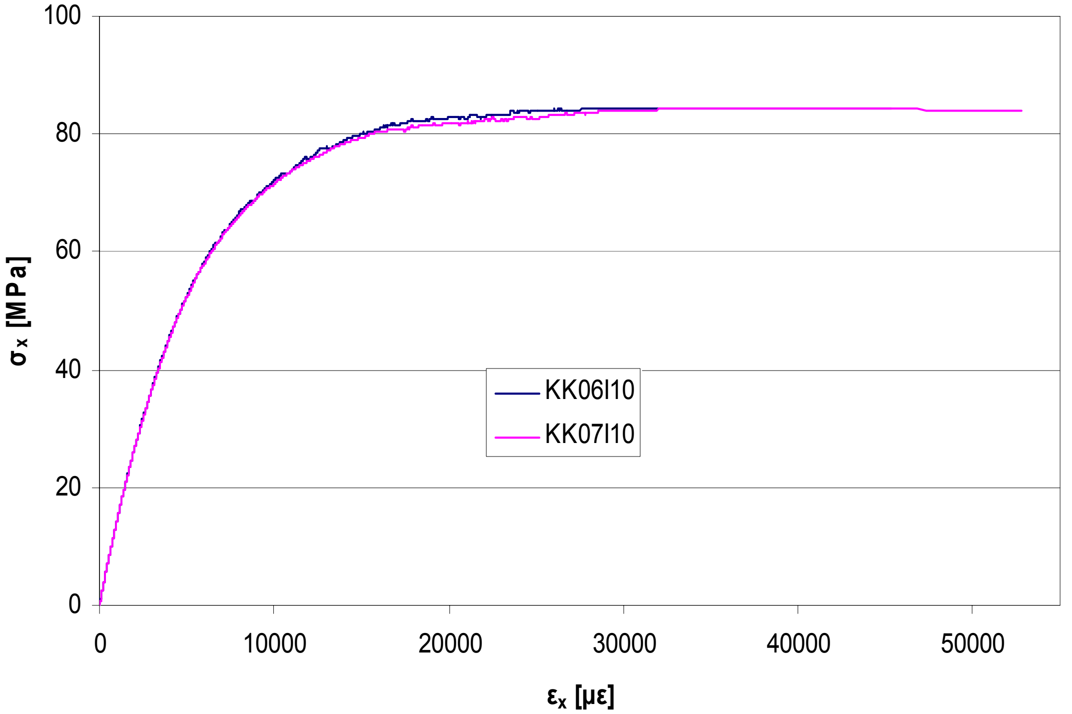

Fig. 109 Axial stress vs. axial strain for coupons KK06I10-KK07I10

8.5.2. Axial stress-strain graphs (500-2500 με)

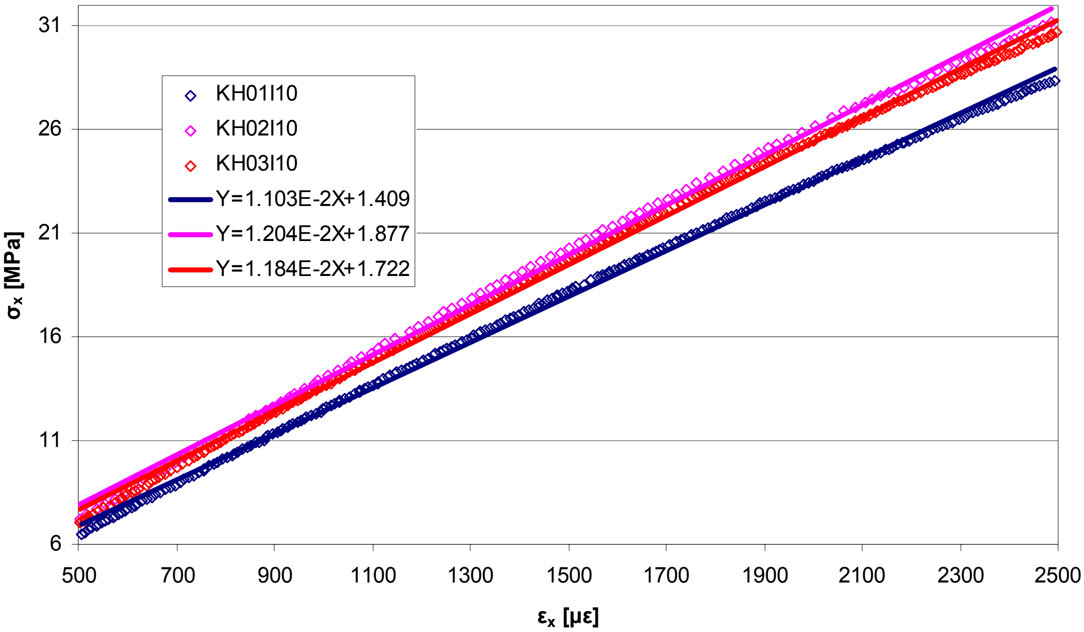

Fig. 110 Linear fits of axial stress vs. axial strain curves for coupons KH01I10-KH03I10

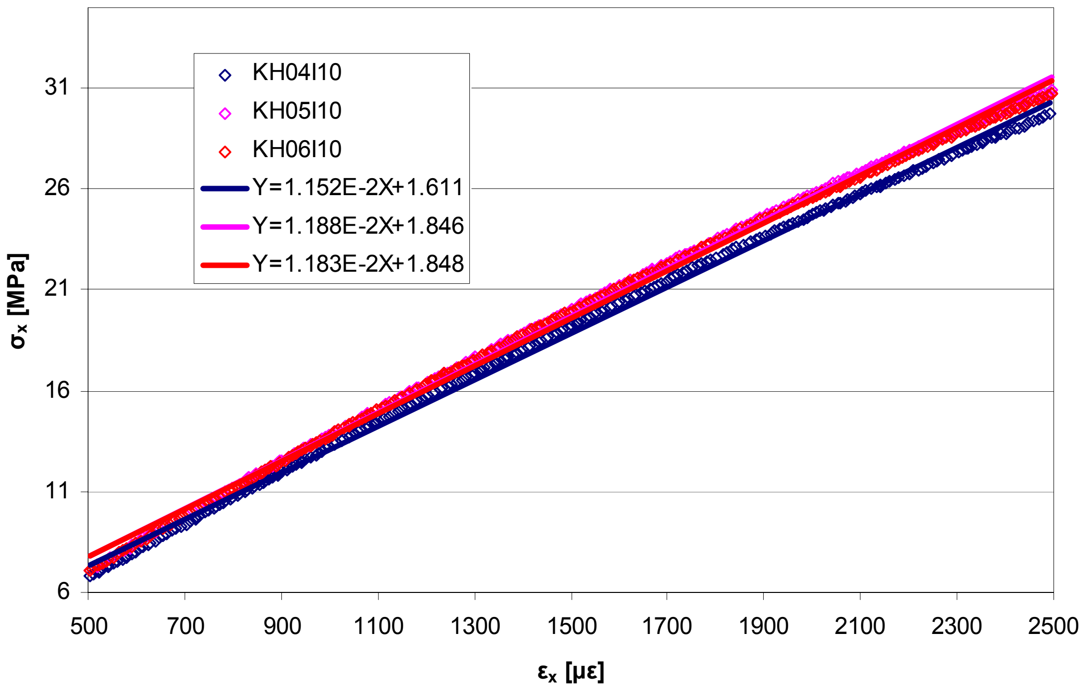

Fig. 111 Linear fits of axial stress vs. axial strain curves for coupons KH04I10-KH06I10

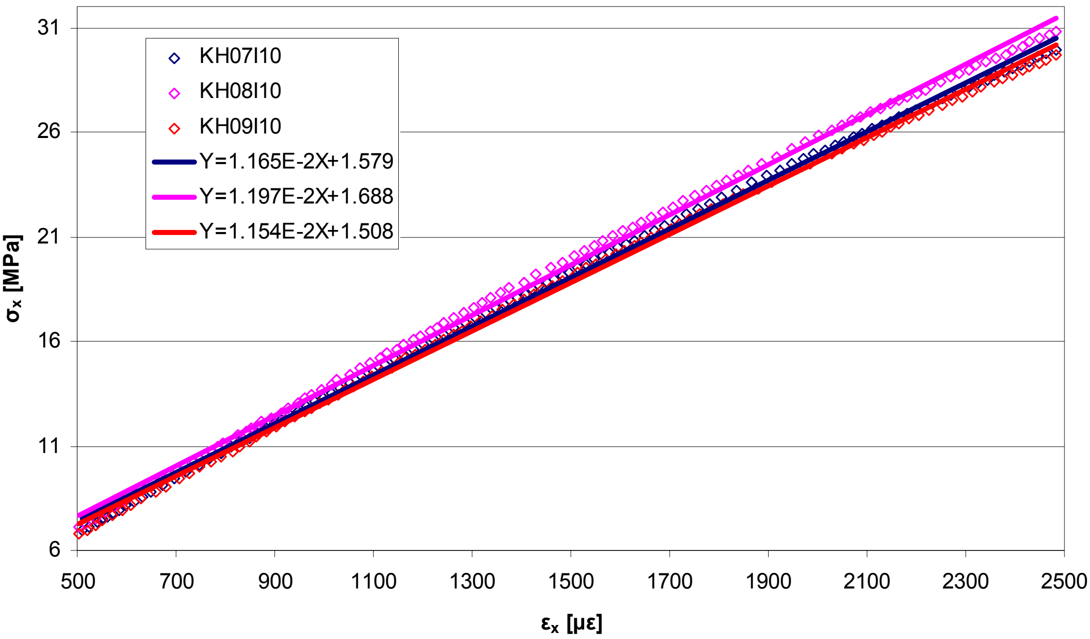

Fig. 112 Linear fits of axial stress vs. axial strain curves for coupons KH07I10-KH09I10

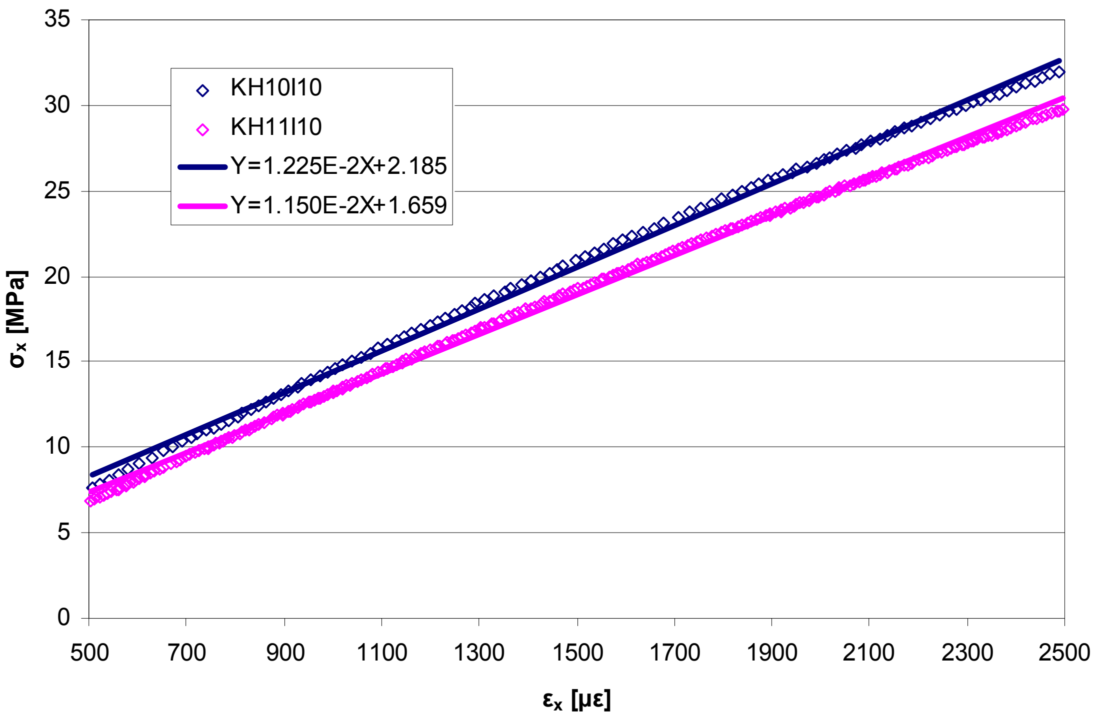

Fig. 113 Linear fits of axial stress vs. axial strain curves for coupons KH10I10-KH11I10

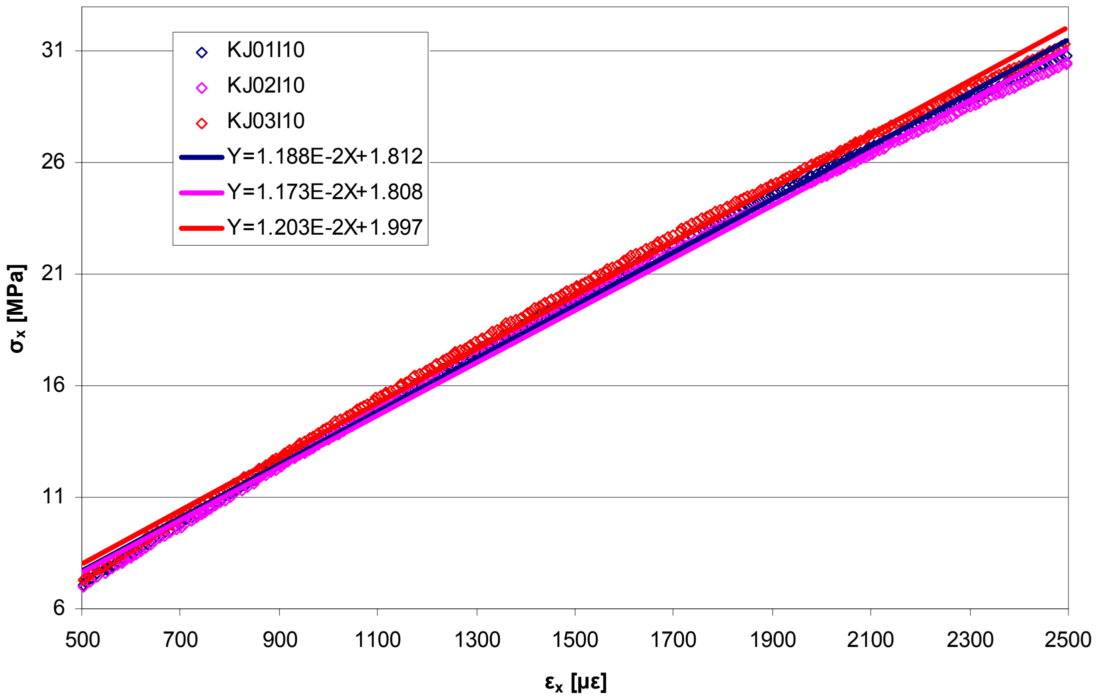

Fig. 114 Linear fits of axial stress vs. axial strain curves for coupons KJ01I10-KJ03I10

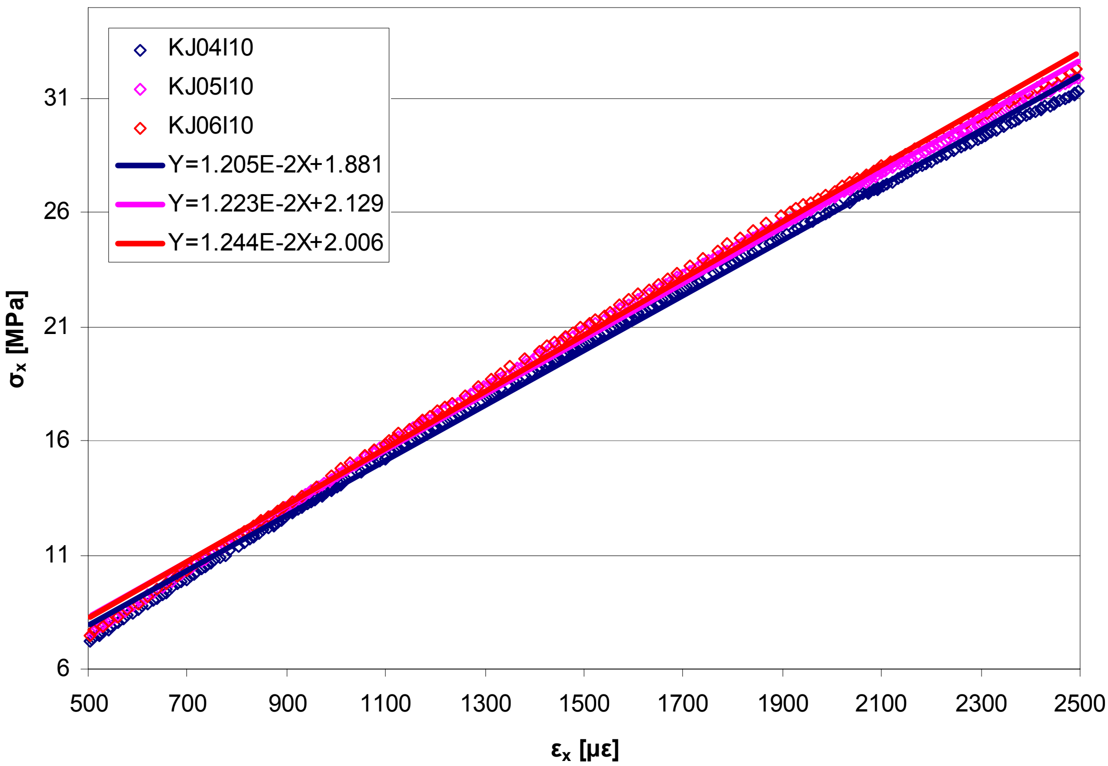

Fig. 115 Linear fits of axial stress vs. axial strain curves for coupons KJ04I10-KJ06I10

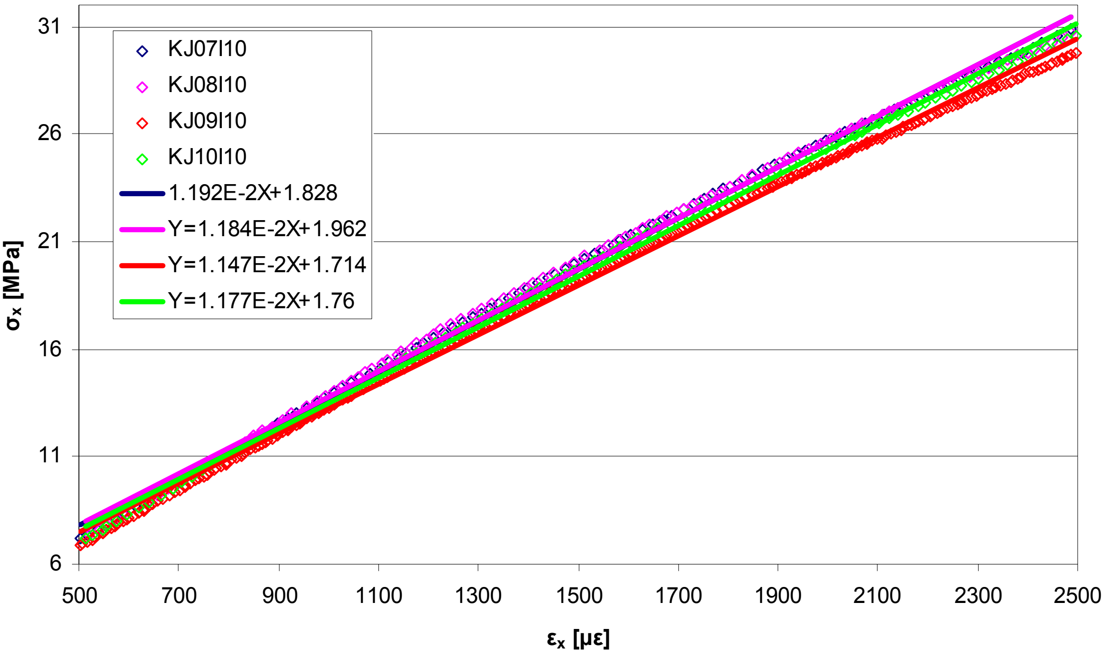

Fig. 116 Linear fits of axial stress vs. axial strain curves for coupons KJ07I10-KJ10I10

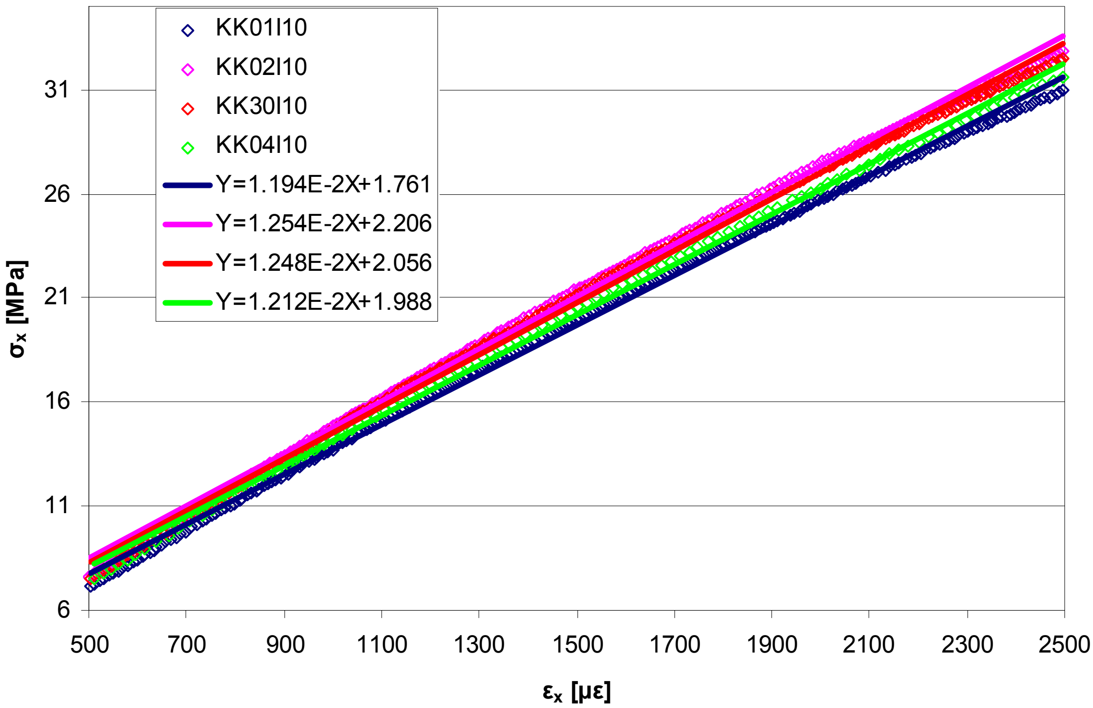

Fig. 117 Linear fits of axial stress vs. axial strain curves for coupons KK01I10-KK04I10

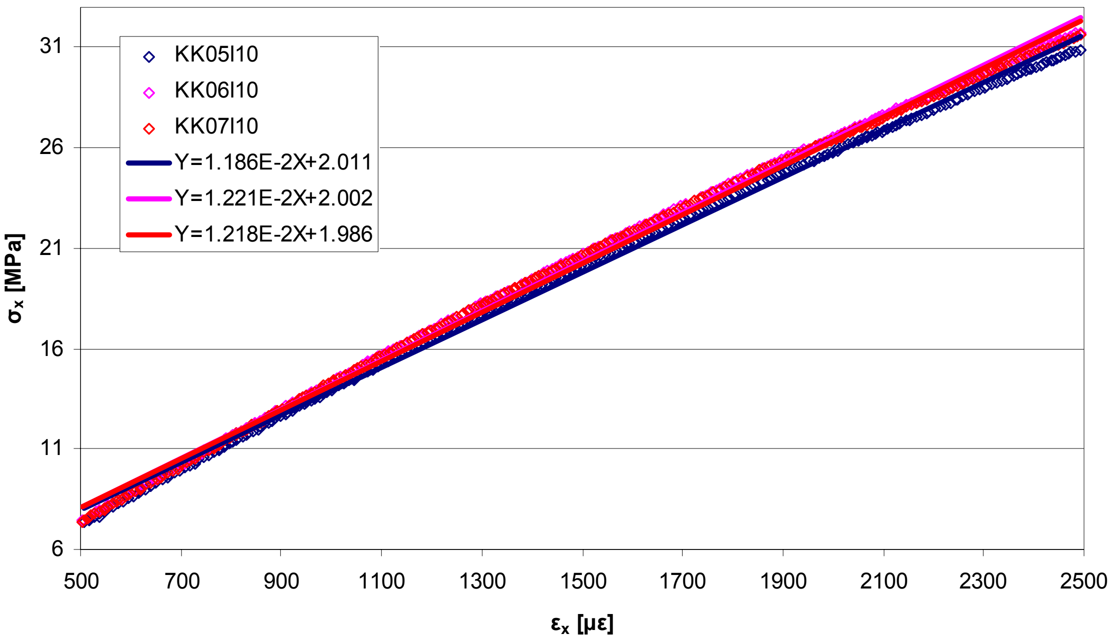

Fig. 118 Linear fits of axial stress vs. axial strain curves for coupons KK05I10-KK07I10

8.5.3. Transverse vs. axial strain graphs

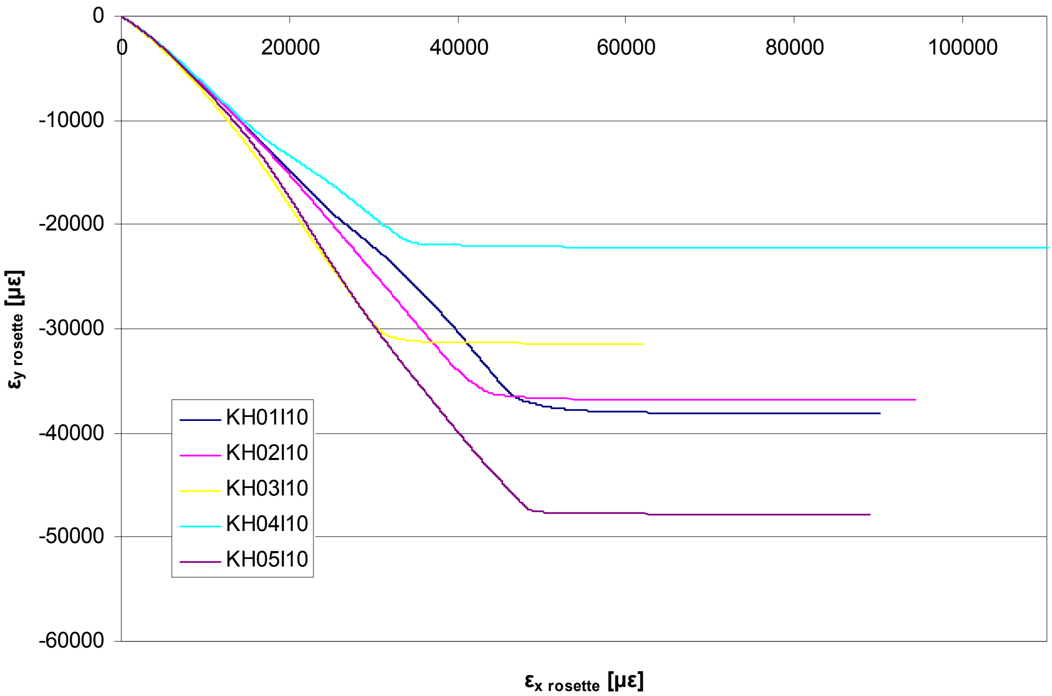

Fig. 119 Transverse vs. axial strain for coupons KH01I10-KH05I10

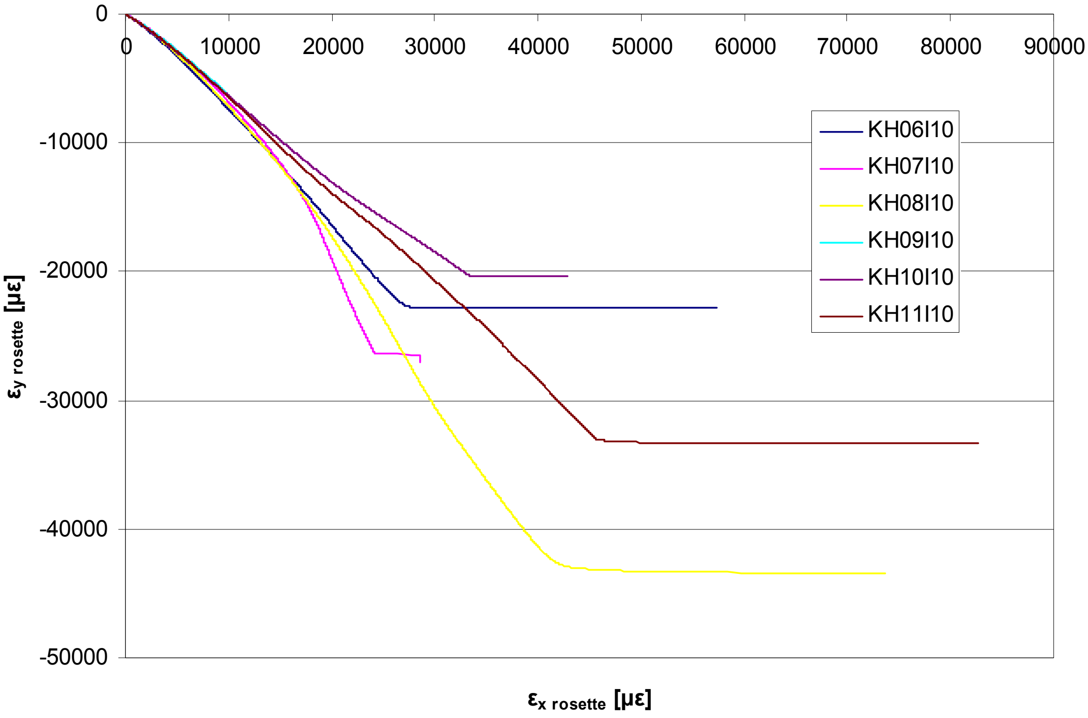

Fig. 120 Transverse vs. axial strain for coupons KH05I10-KH11I10

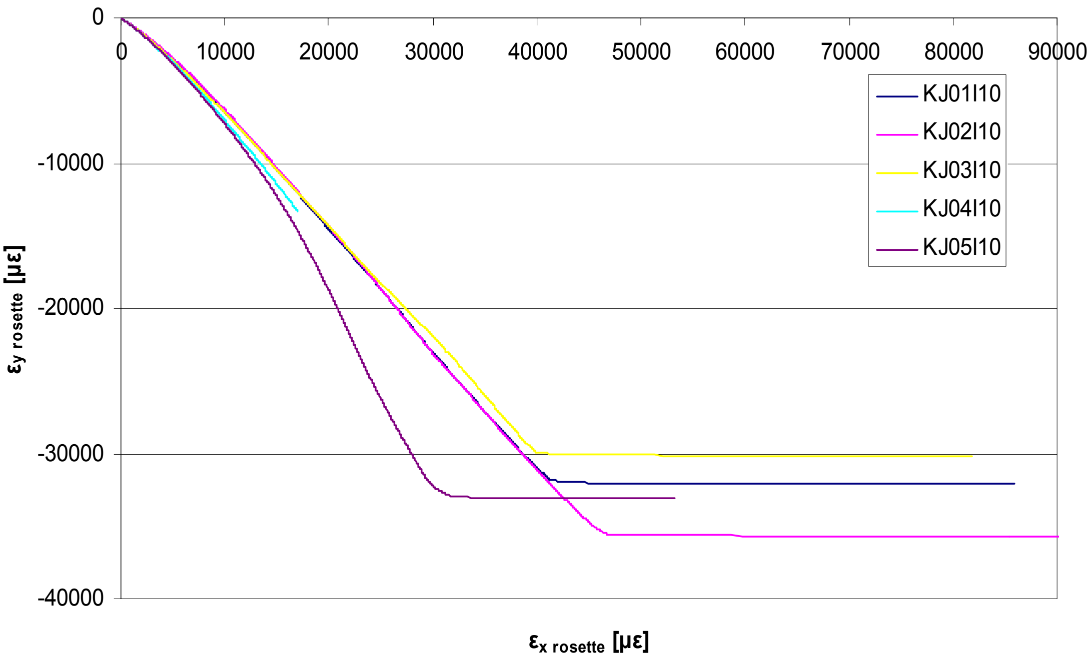

Fig. 121 Transverse vs. axial strain for coupons KJ01I10-KJ05I10

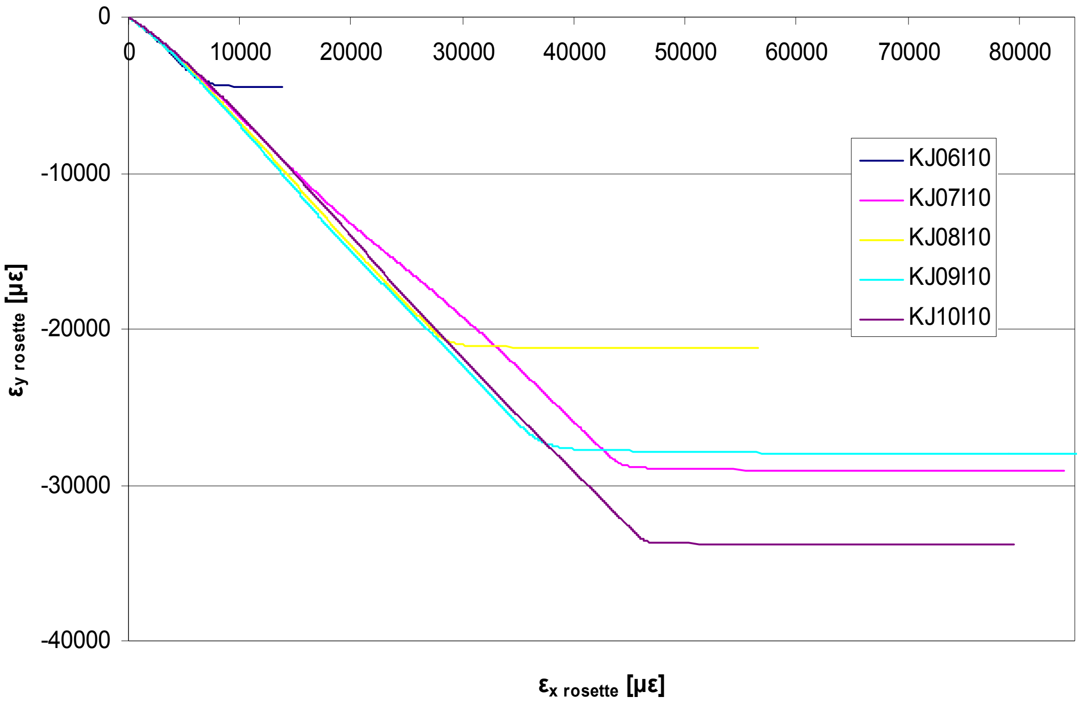

Fig. 122 Transverse vs. axial strain for coupons KJ06I10-KJ10I10

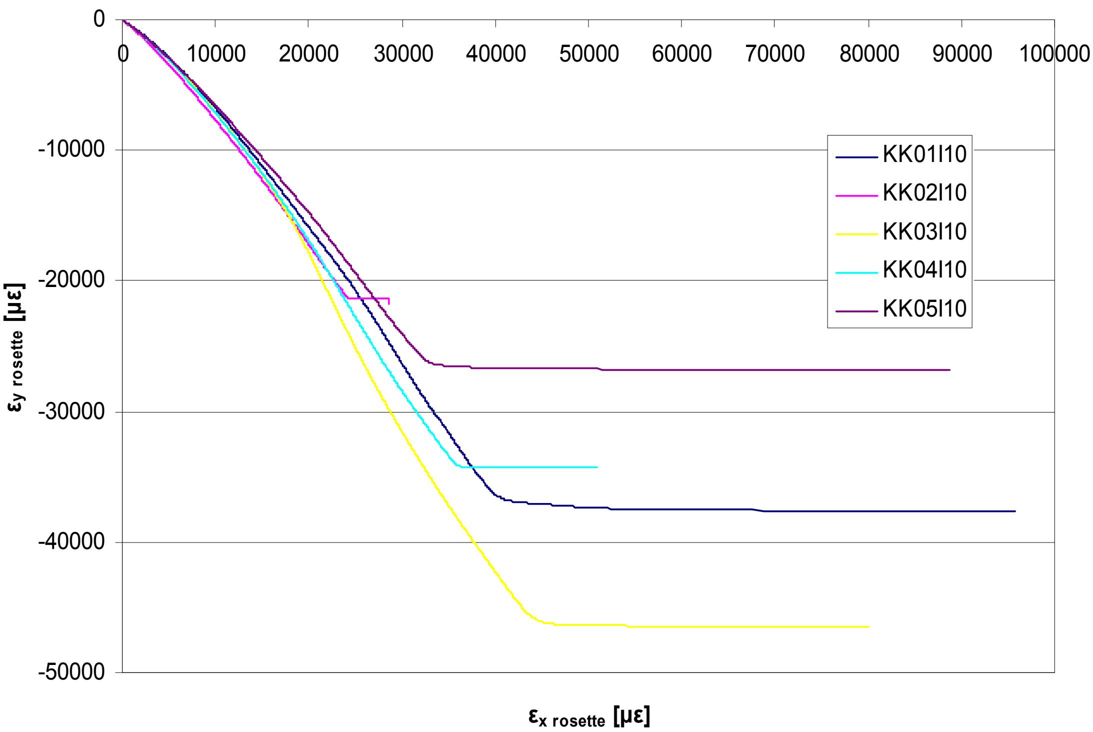

Fig. 123 Transverse vs. axial strain for coupons KK01I10-KK05I10

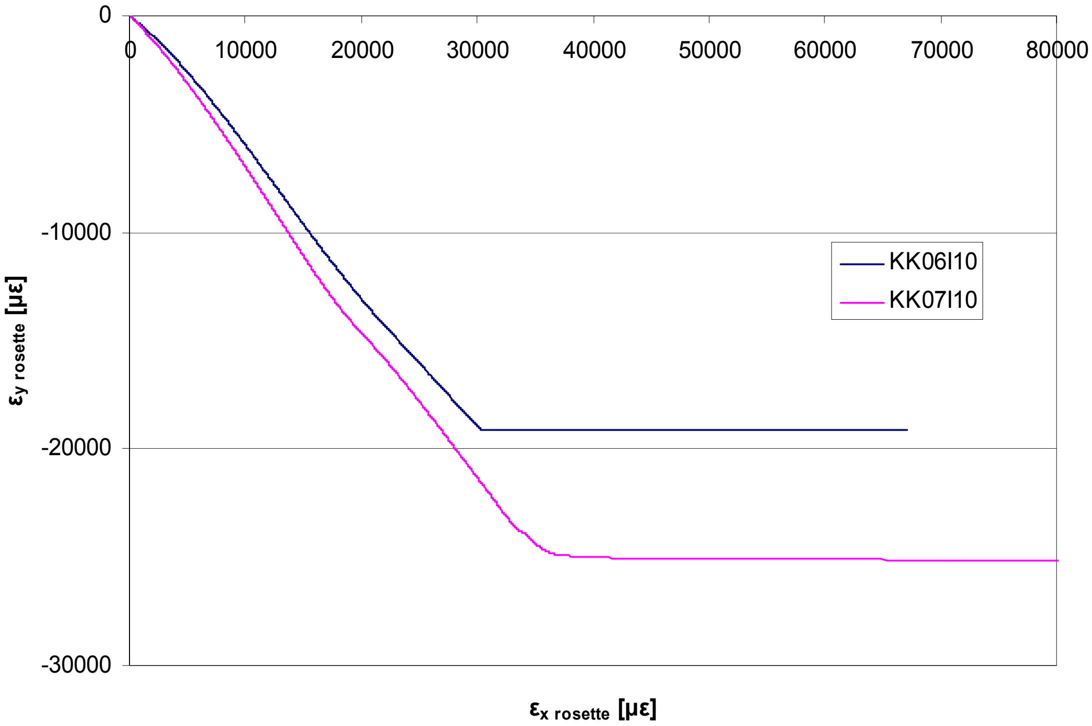

Fig. 124 Transverse vs. axial strain for coupons KK06I10-KK07I10

8.5.4. Transverse vs. axial strain graphs (500-2500 με)

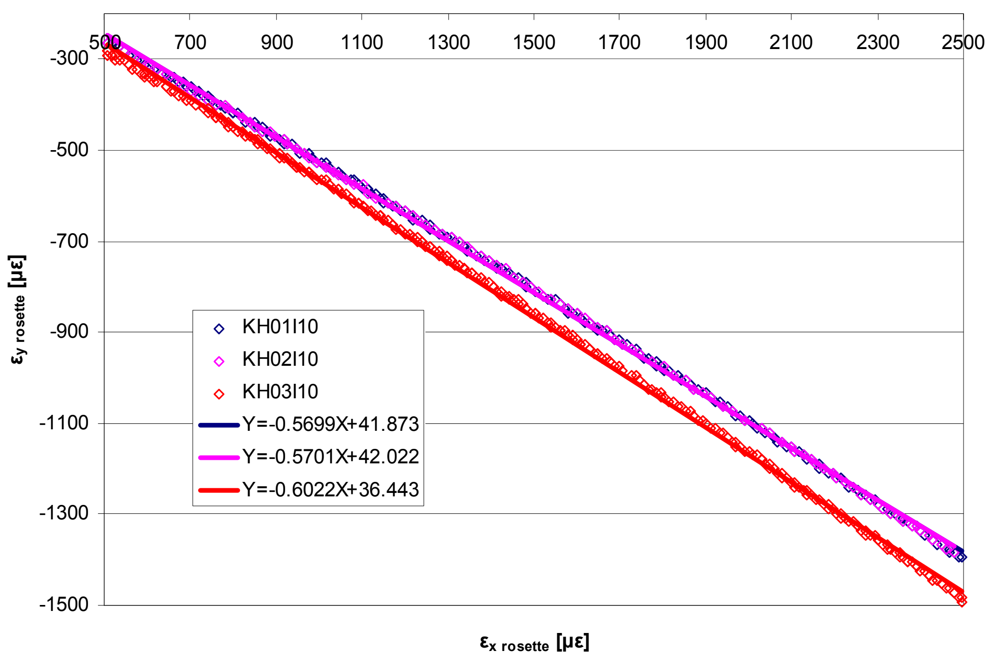

Fig. 125 Linear fits of the transverse vs. axial strain curves for coupons KH01I10-KH03I10

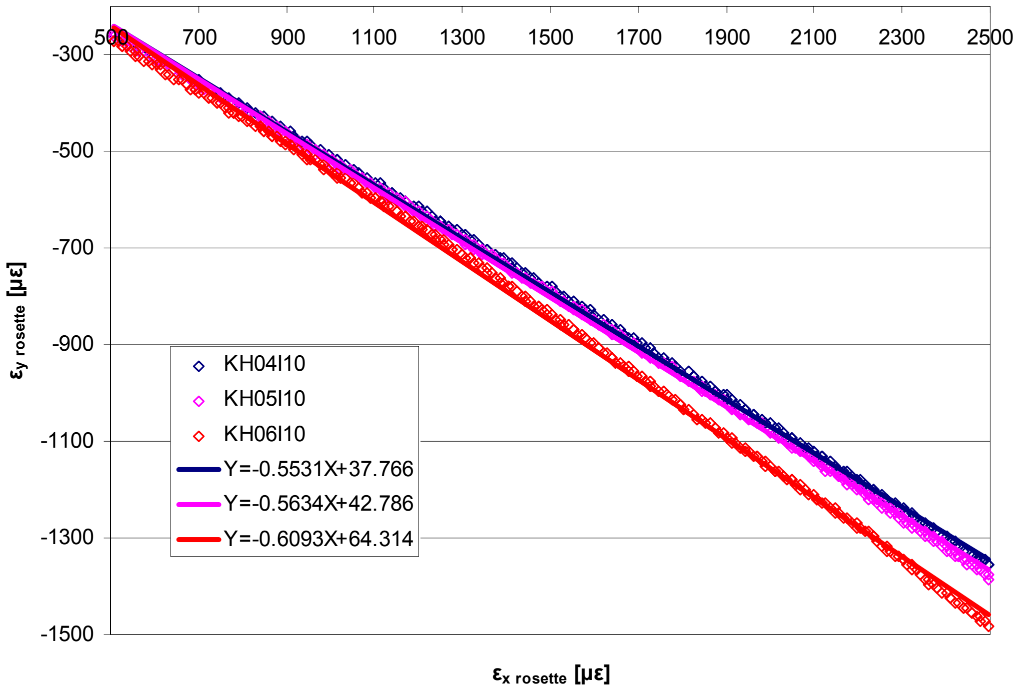

Fig. 126 Linear fits of the transverse vs. axial strain curves for coupons KH04I10-KH06I10

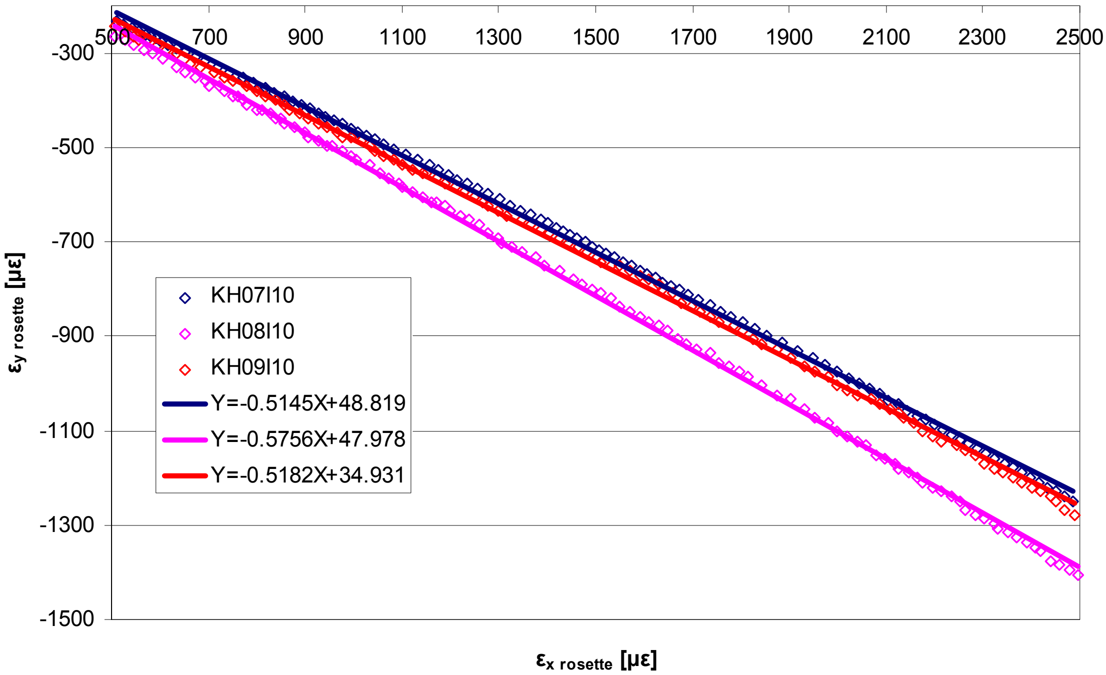

Fig. 127 Linear fits of the transverse vs. axial strain curves for coupons KH07I10-KH09I10

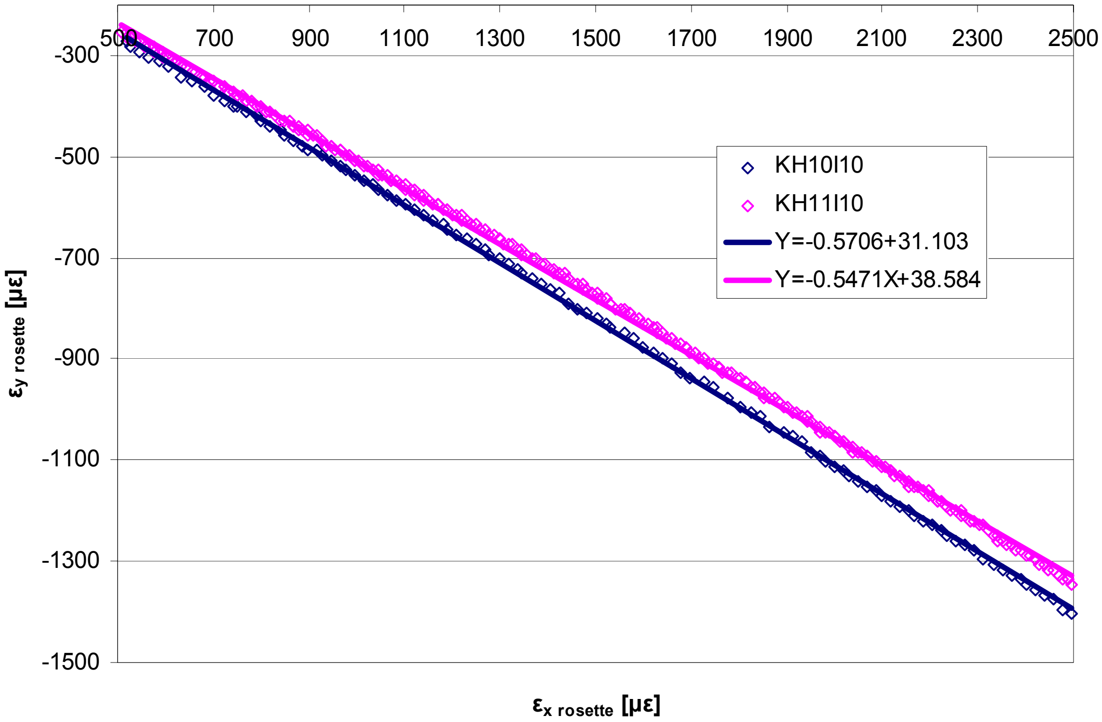

Fig. 128 Linear fits of the transverse vs. axial strain curves for coupons KH10I10-KH11I10

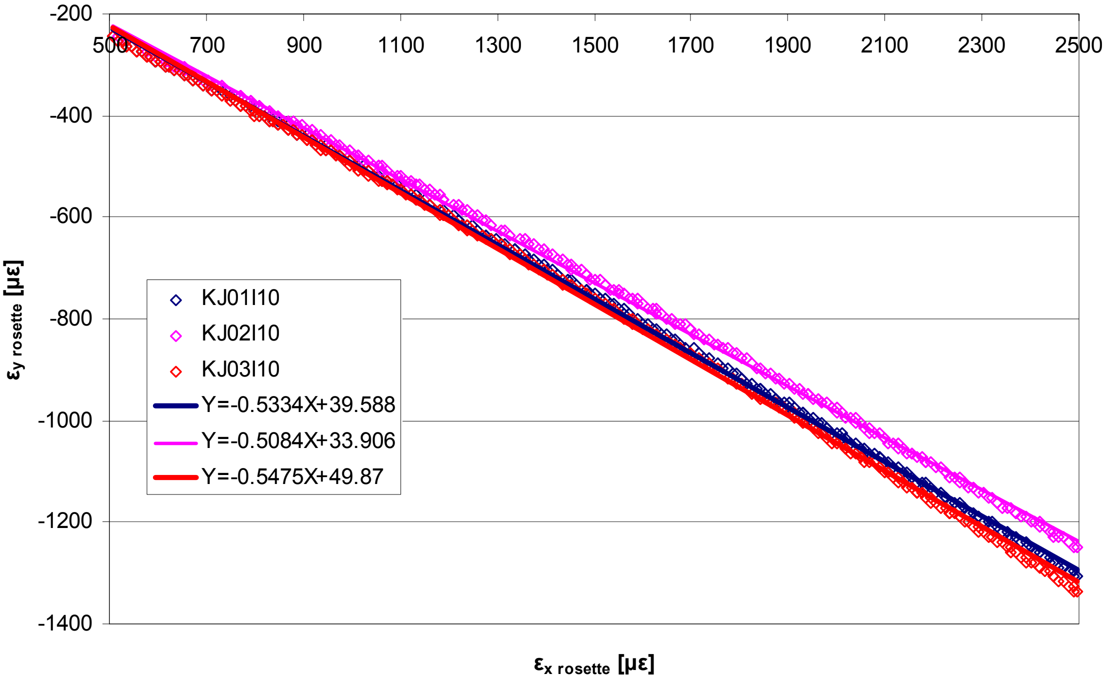

Fig. 129 Linear fits of the transverse vs. axial strain curves for coupons KJ01I10-KJ03I10

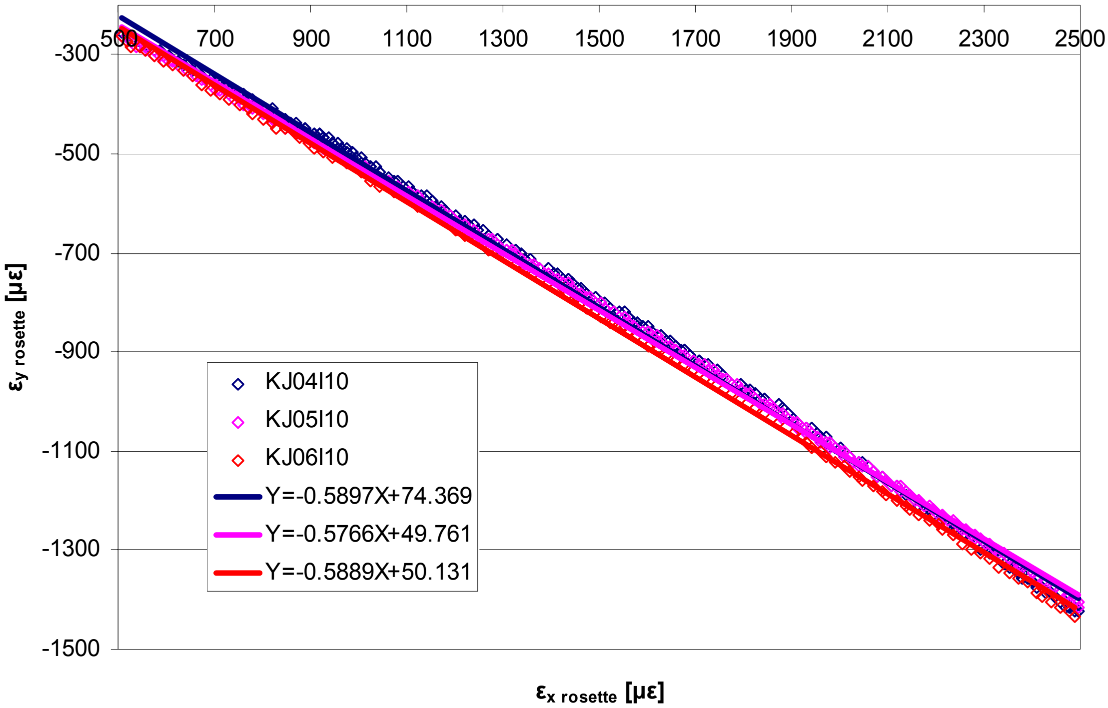

Fig. 130 Linear fits of the transverse vs. axial strain curves for coupons KJ04I10-KJ06I10

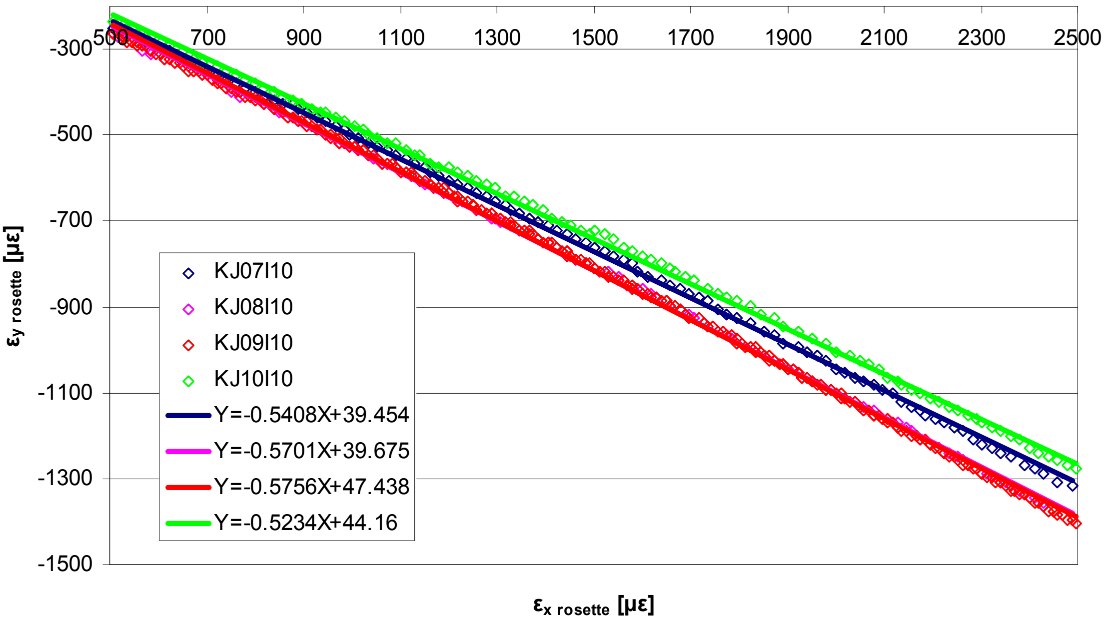

Fig. 131 Linear fits of the transverse vs. axial strain curves for coupons KJ07I10-KJ10I10

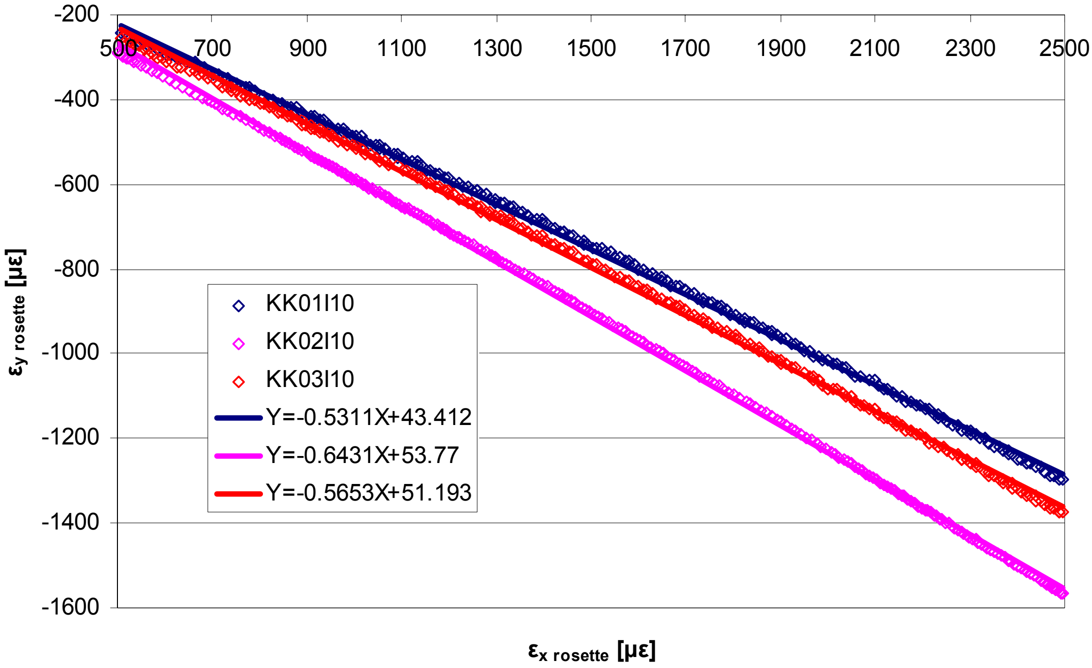

Fig. 132 Linear fits of the transverse vs. axial strain curves for coupons KK01I10-KK03I10

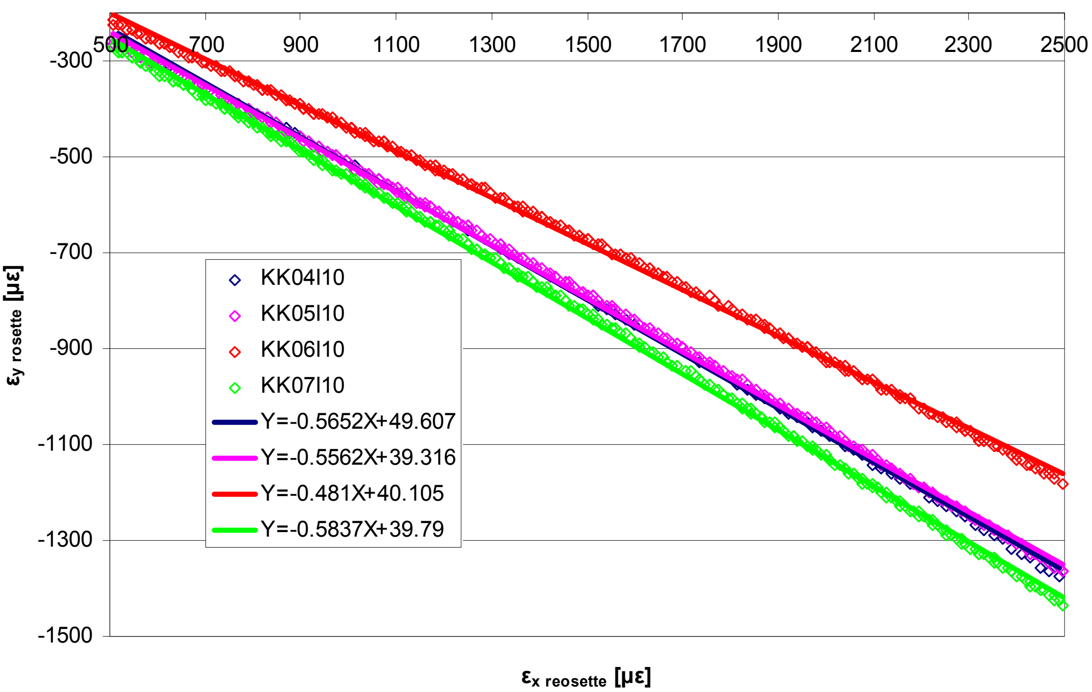

Fig. 133 Linear fits of the transverse vs. axial strain curves for coupons KK04I10-KK07I10

8.5.5. Shear stress-shear strain graphs

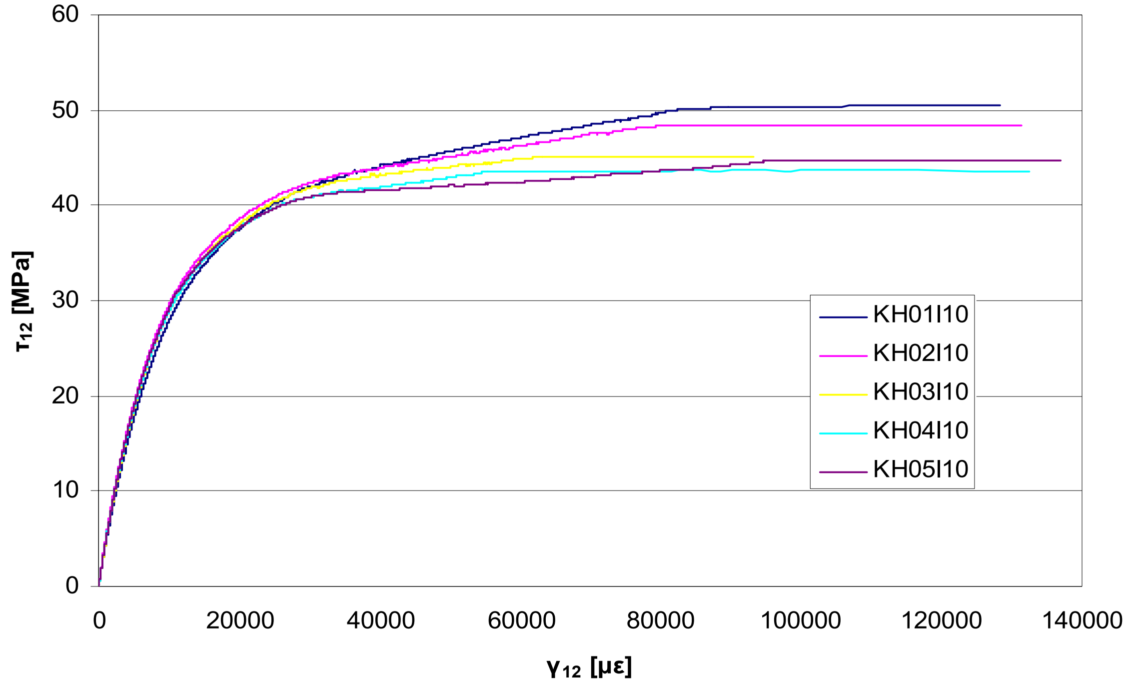

Fig. 134 Shear stress vs. shear strain for coupons KH01I10-KH05I10

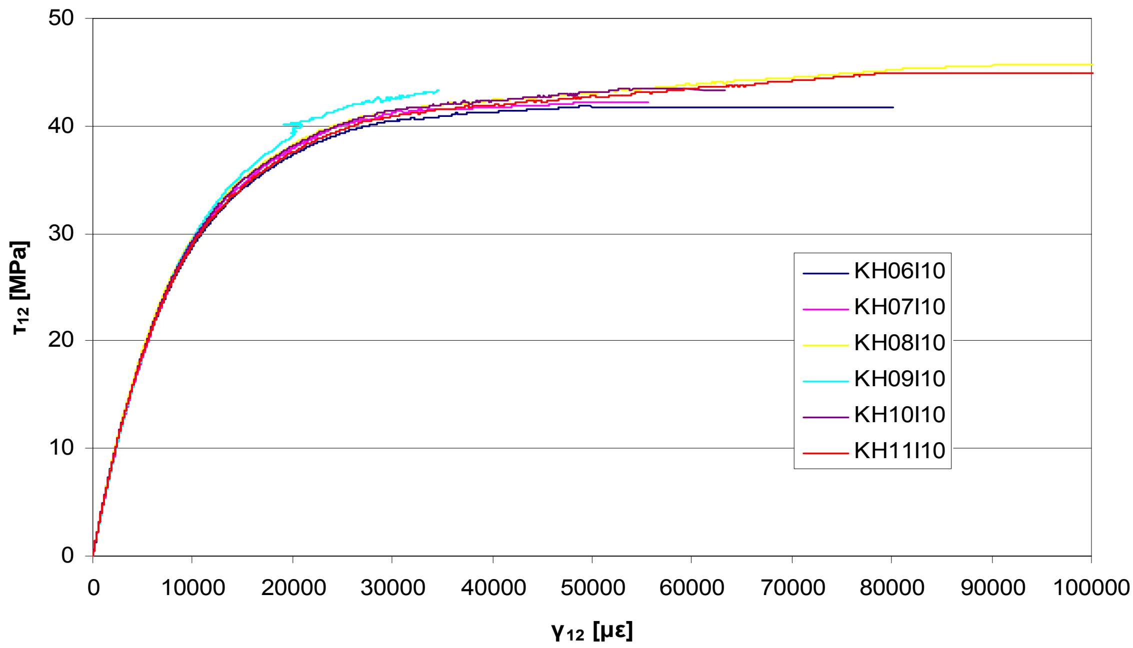

Fig. 135 Shear stress vs. shear strain for coupons KH06I10-KH11I10

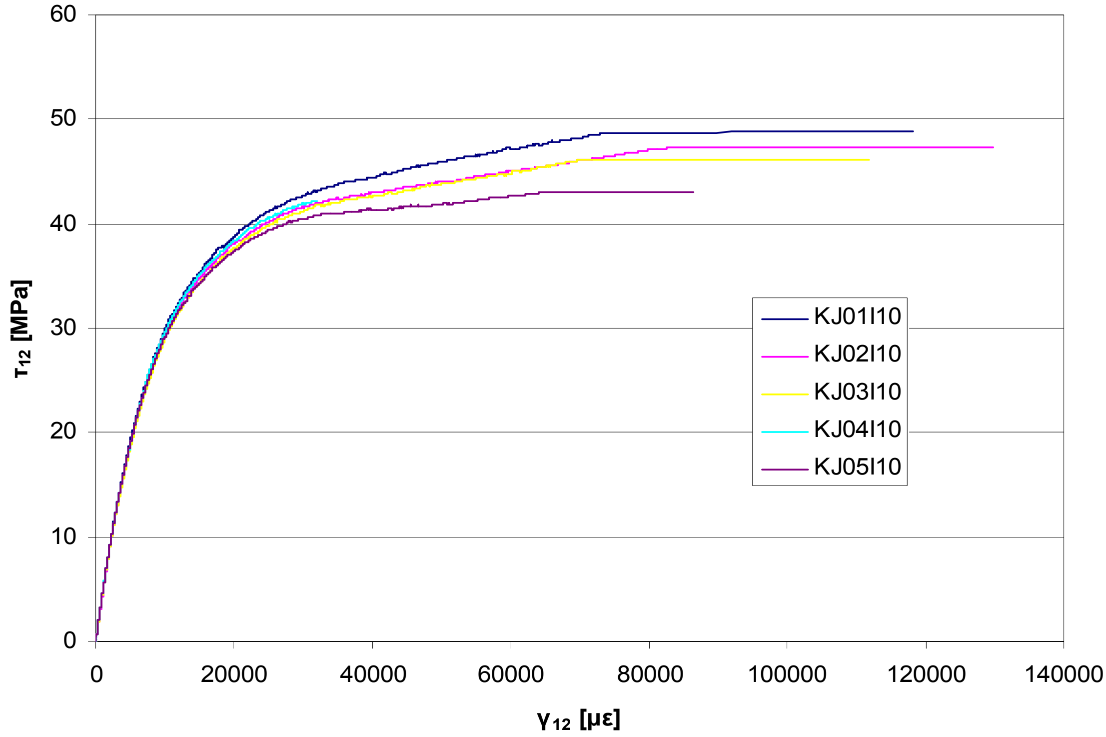

Fig. 136 Shear stress vs. shear strain for coupons KJ01I10-KJ05I10

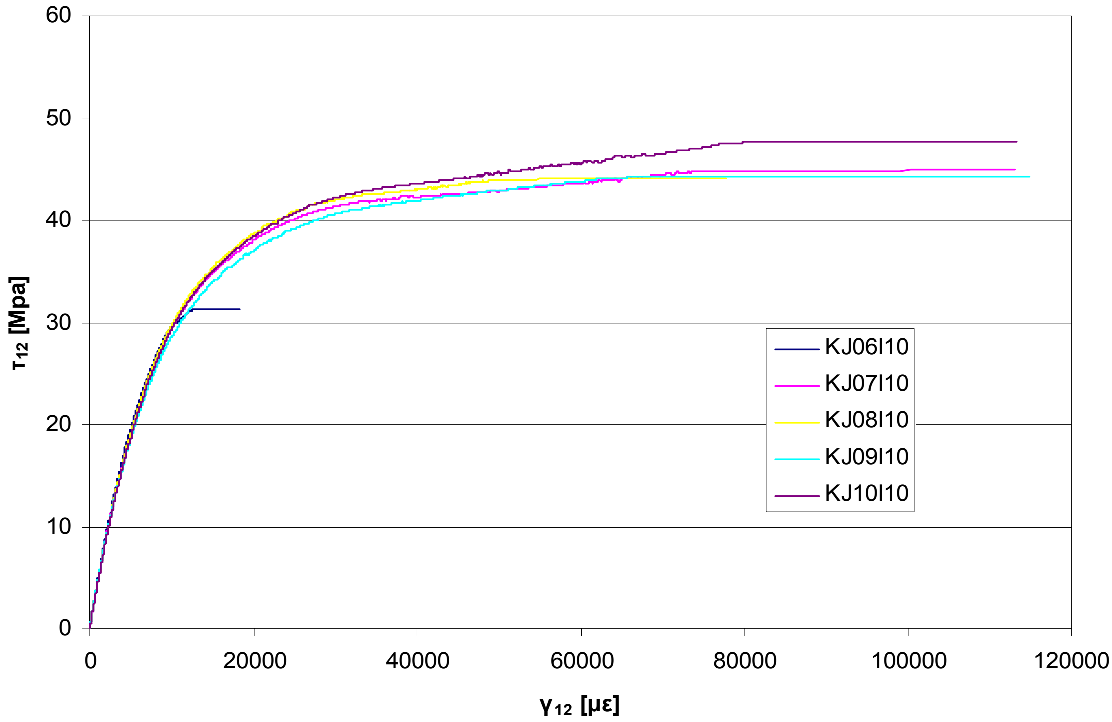

Fig. 137 Shear stress vs. shear strain for coupons KJ06I10-KJ10I10

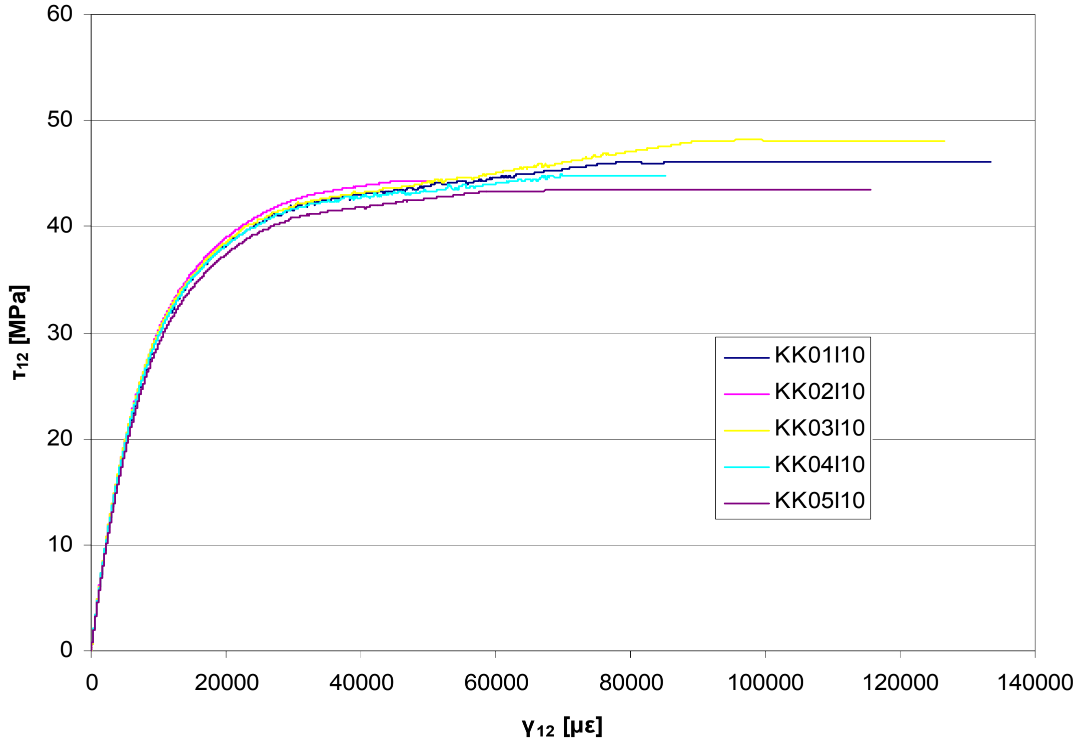

Fig. 138 Shear stress vs. shear strain for coupons KK01I10-KK05I10

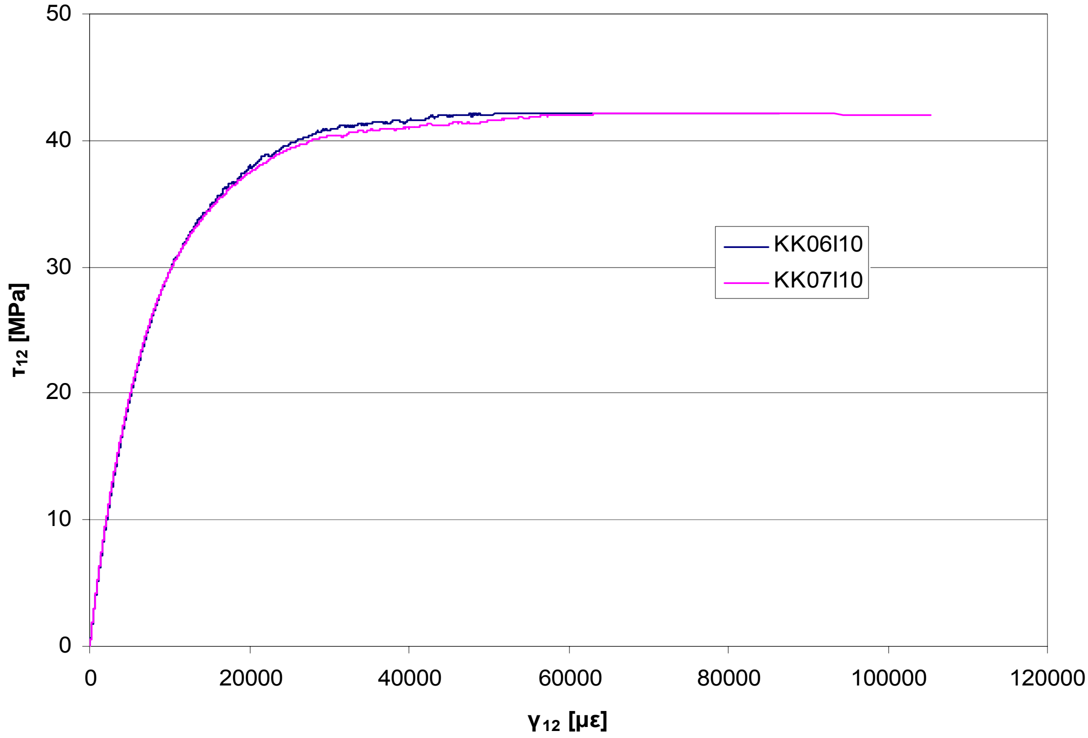

Fig. 139 Shear stress vs. shear strain for coupons KK06I10-KK07I10

8.5.6. Shear stress-shear strain graphs (1000-5000 με)

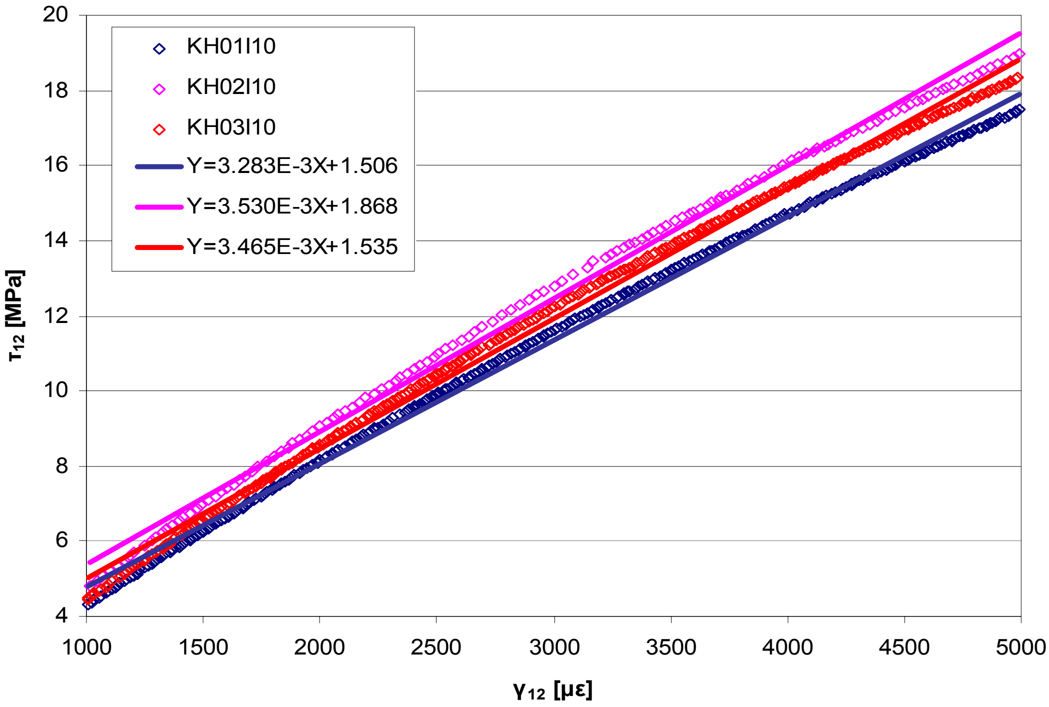

Fig. 140 Linear fits of shear stress vs. shear strain curves for coupons KH01I10-KH03I10

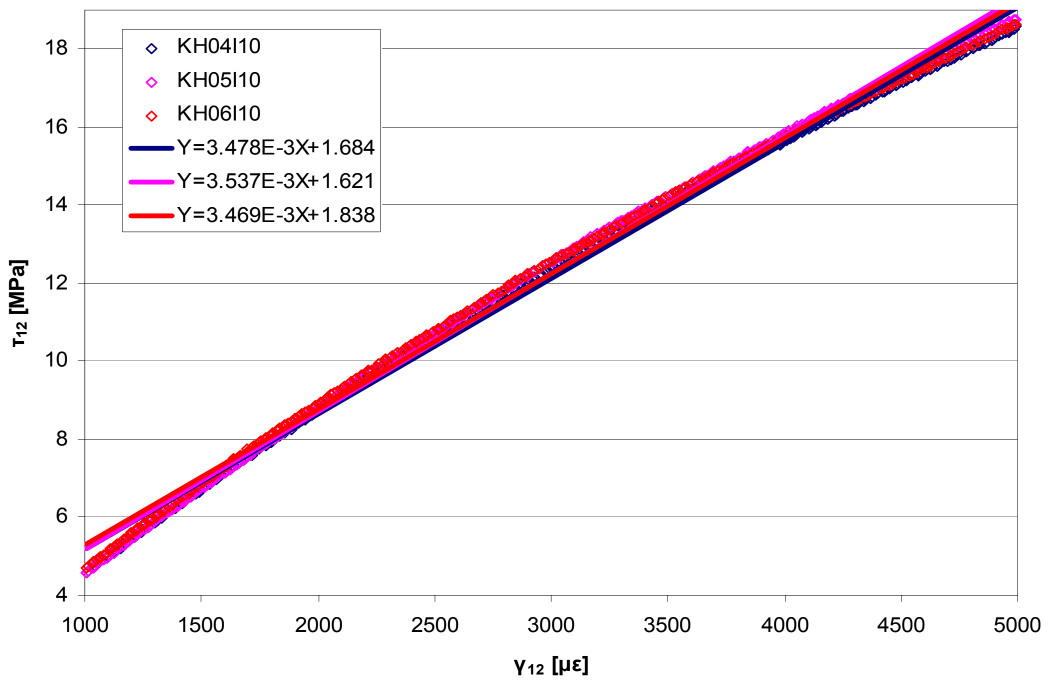

Fig. 141 Linear fits of shear stress vs. shear strain curves for coupons KH04I10-KH06I10

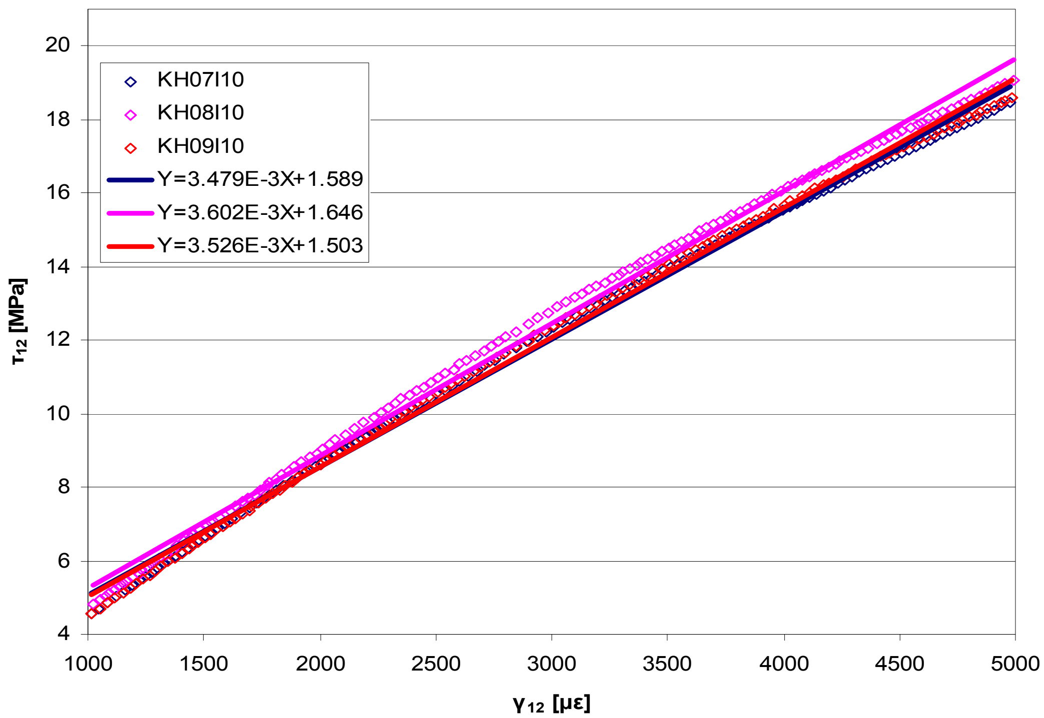

Fig. 142 Linear fits of shear stress vs. shear strain curves for coupons KH07I10-KH09I10

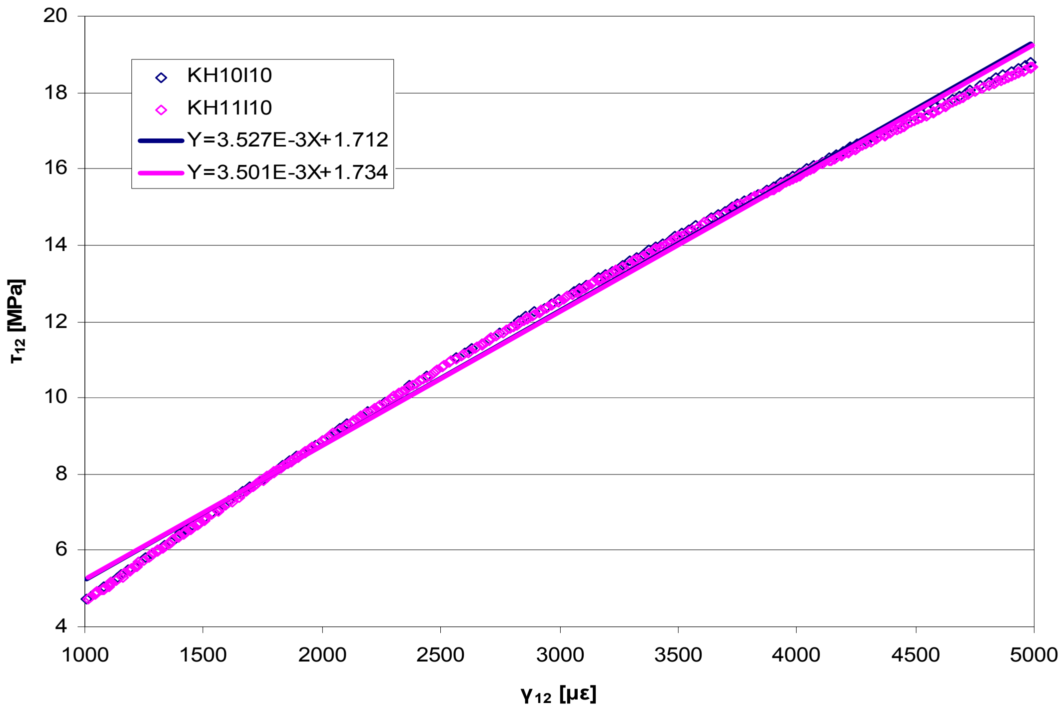

Fig. 143 Linear fits of shear stress vs. shear strain curves for coupons KH10I10-KH11I10

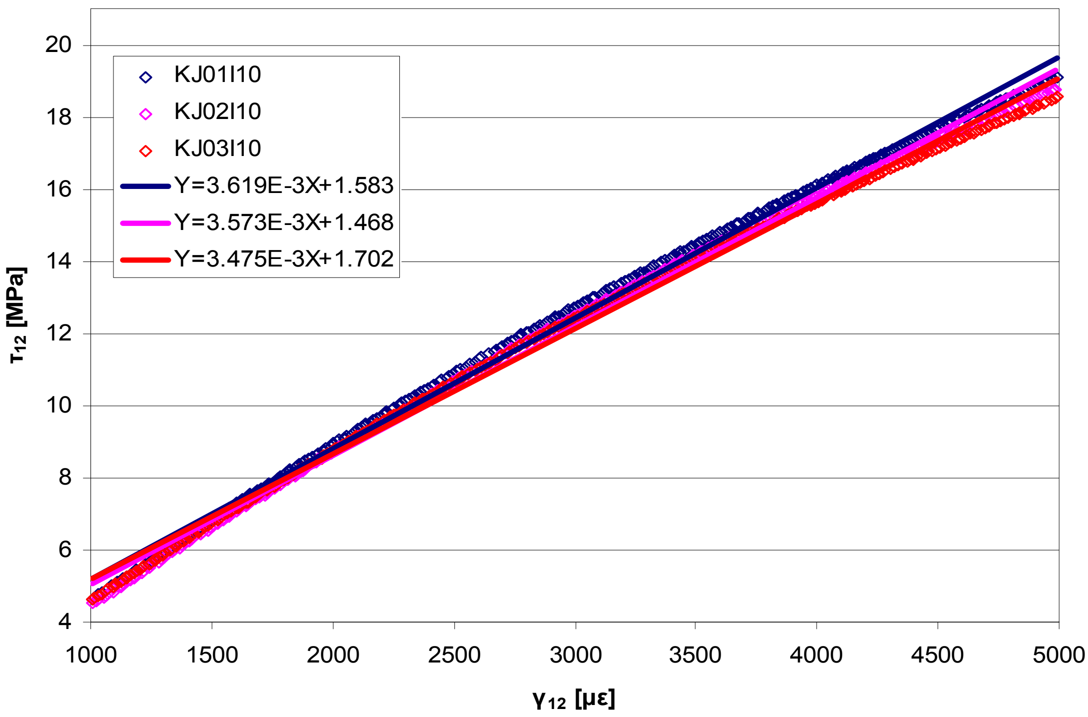

Fig. 144 Linear fits of shear stress vs. shear strain curves for coupons KJ01I10-KJ03I10

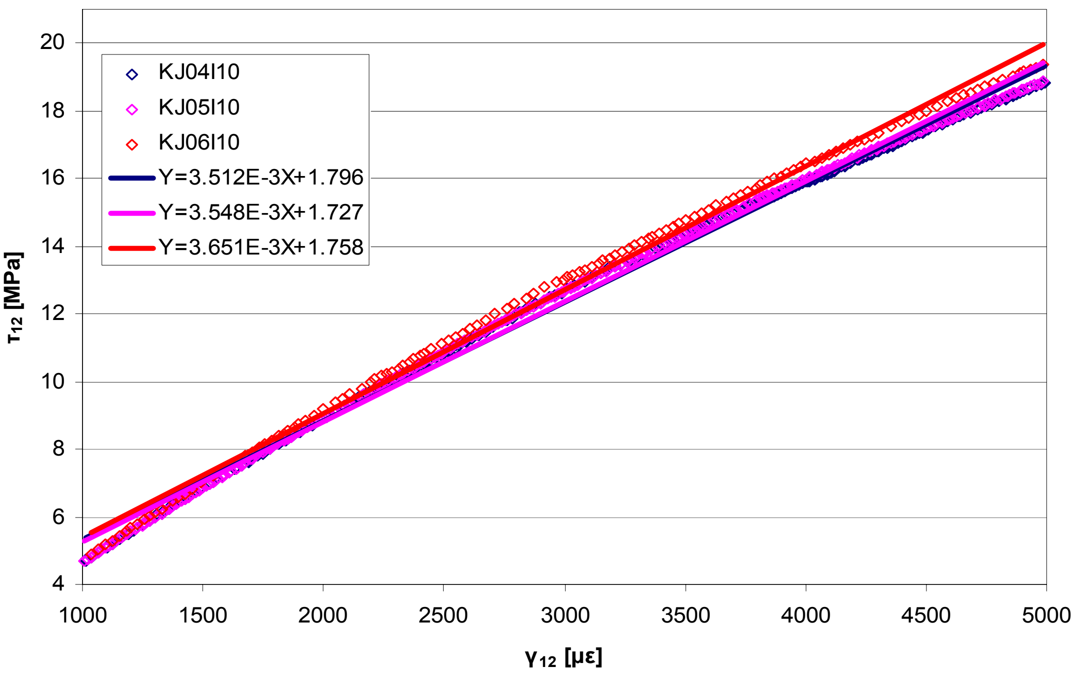

Fig. 145 Linear fits of shear stress vs. shear strain curves for coupons KJ04I10-KJ06I10

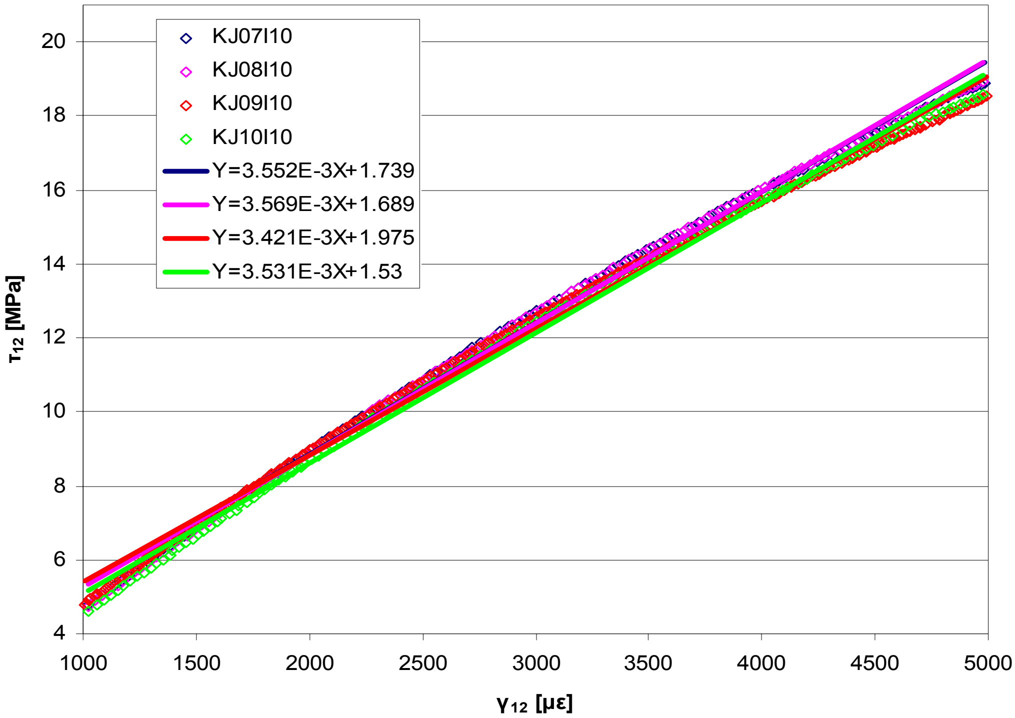

Fig. 146 Linear fits of shear stress vs. shear strain curves for coupons KJ07I10-KJ10I10

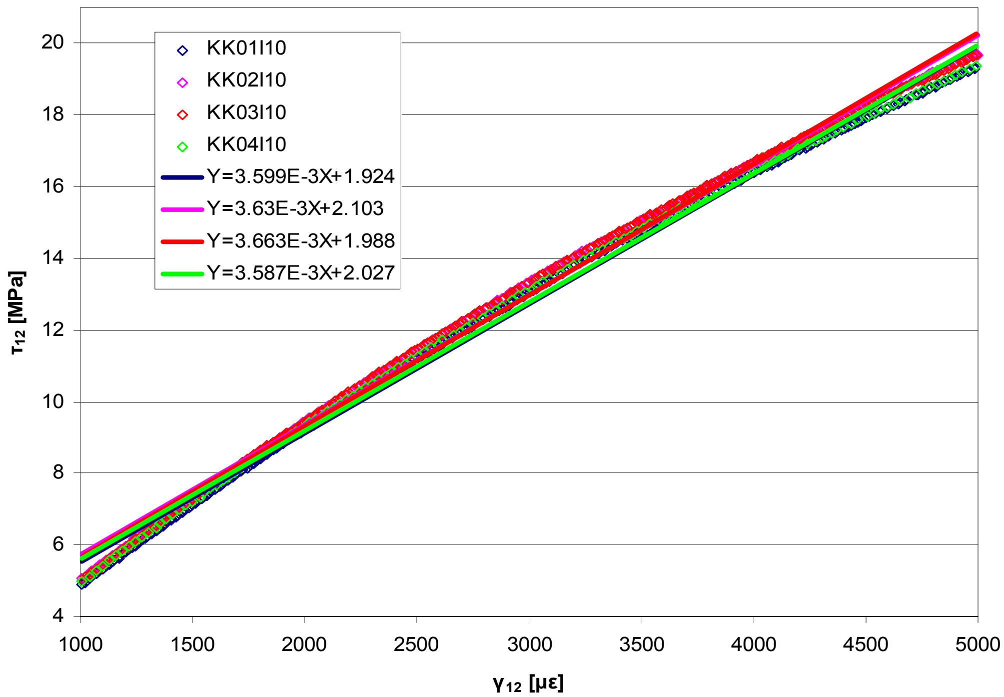

Fig. 147 Linear fits of shear stress vs. shear strain curves for coupons KK01I10-KK04I10

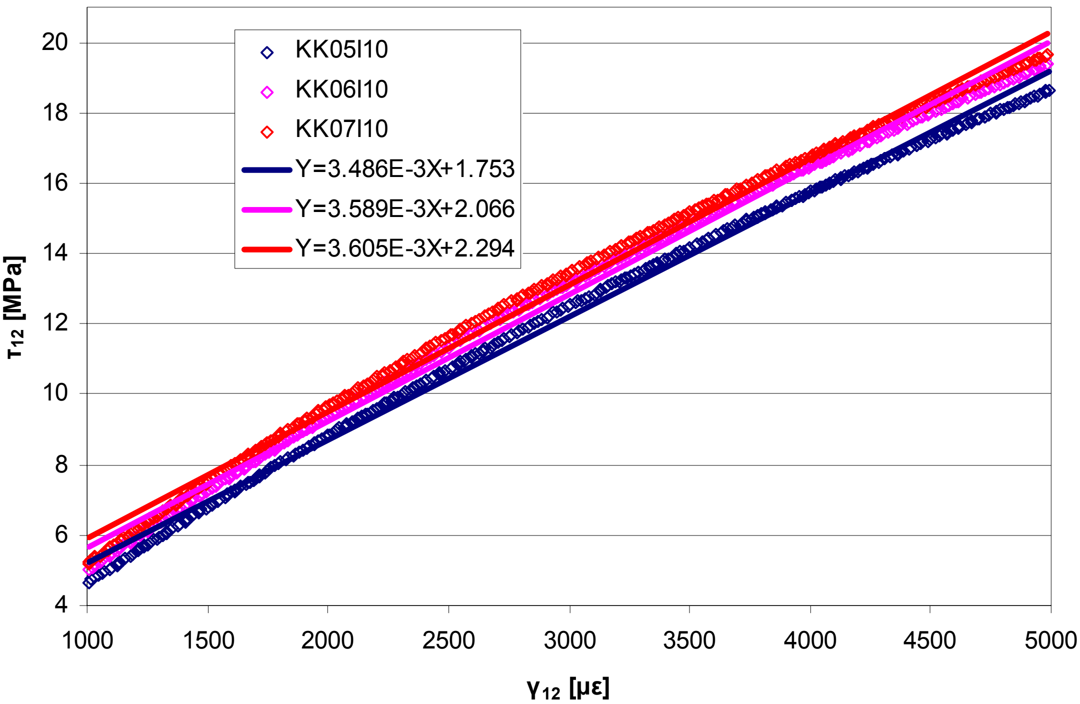

Fig. 148 Linear fits of shear stress vs. shear strain curves for coupons KK05I10-KK07I10

8.5.7. Photographs of tested coupons

Fig. 149 Photo of failed coupons KH01I10 to KH05I10 (bottom-up)

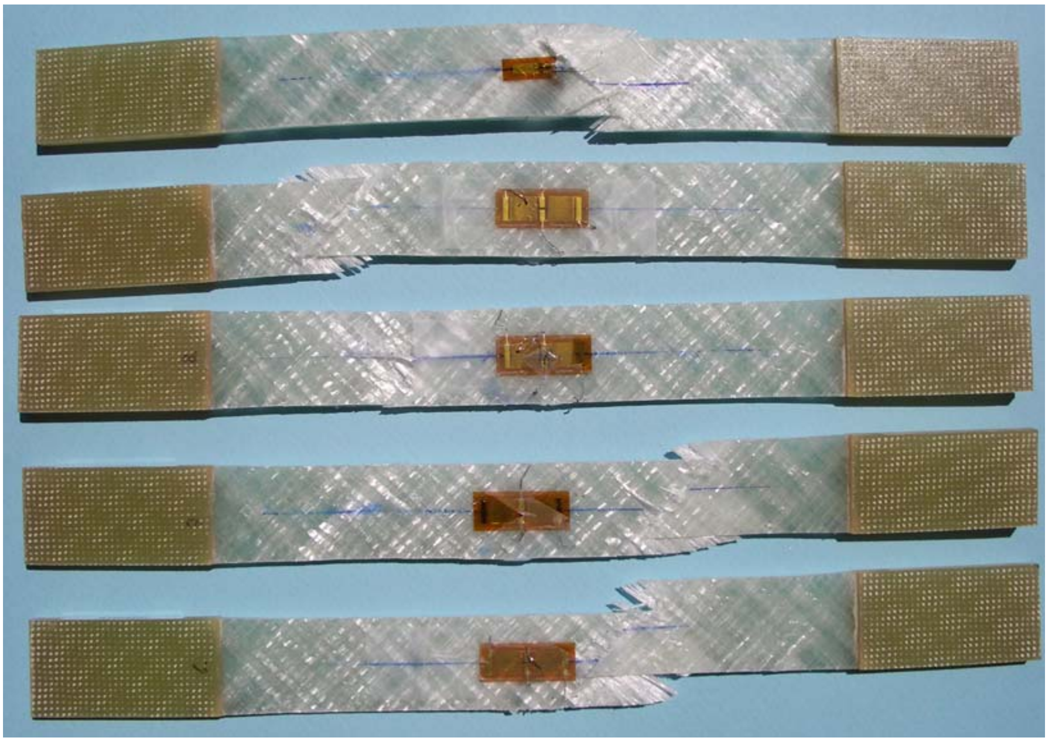

Fig. 150 Photo of failed coupons KH06I10 to KH10I10 (bottom-up)

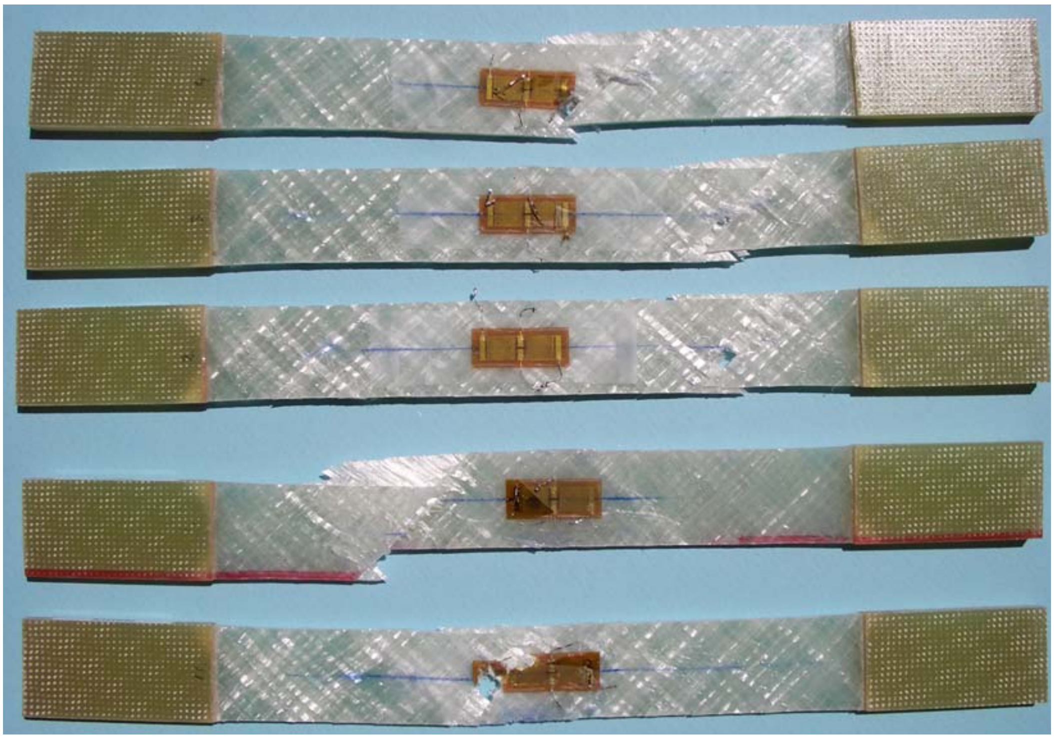

Fig. 151 Photo of failed coupons KH11I10 to KJ04I10 (bottom-up)

Fig. 152 Photo of failed coupons KJ05I10 to KJ09I10 (bottom-up)

Fig. 153 Photo of failed coupons KJ10I10 to KK04I10 (bottom-up)

Fig. 154 Photo of failed coupons KK05I10 to KK07I10 (bottom-up)

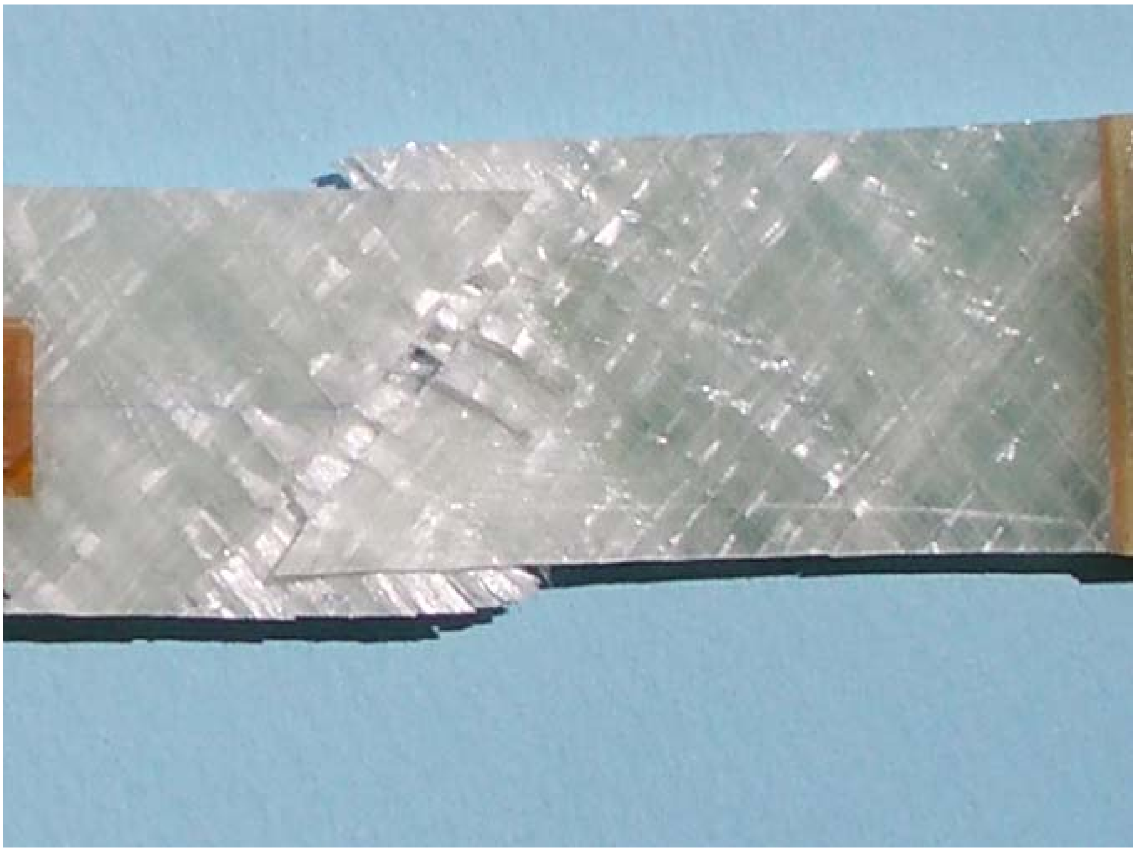

Fig. 155 Detail of failed coupon KK05I10